

VOLUME 81

AUGUST 11, 1977

NUMBER 16

JPCA_x

THE JOURNAL OF

PHYSICAL
CHEMISTRY



PUBLISHED BIWEEKLY BY THE AMERICAN CHEMICAL SOCIETY

THE JOURNAL OF PHYSICAL CHEMISTRY

BRYCE CRAWFORD, Jr., Editor
STEPHEN PRAGER, Associate Editor
ROBERT W. CARR, Jr., C. ALDEN MEAD, Assistant Editors

EDITORIAL BOARD: C. A. ANGELL (1973-1977), F. C. ANSON (1974-1978), V. A. BLOOMFIELD (1974-1978), J. R. BOLTON (1976-1980), L. M. DORFMAN (1974-1978), W. E. FALCONER (1977-1978), H. L. FRIEDMAN (1975-1979), H. L. FRISCH (1976-1980), W. A. GODDARD (1976-1980), E. J. HART (1975-1979), W. J. KAUZMANN (1974-1978), R. L. KAY (1977-1981), D. W. McCLURE (1974-1978), K. MYSELS (1977-1981), R. M. NOYES (1973-1977), R. G. PARR (1977-1979), W. B. PERSON (1976-1980), J. C. POLANYI (1976-1980), S. A. RICE (1976-1980), F. S. ROWLAND (1973-1977), R. L. SCOTT (1973-1977), W. A. STEELE (1976-1980), J. B. STOTHERS (1974-1978), F. A. VAN-CATLEDGE (1977-1981), B. WEINSTOCK (1977)

Published by the
AMERICAN CHEMICAL SOCIETY
BOOKS AND JOURNALS DIVISION

D. H. Michael Bowen, Director
Marjorie Laflin, Assistant to the Director

Editorial Department: Charles R. Bertsch,
Head; Marianne C. Brogan, Associate
Head; Celia B. McFarland, Joseph E.
Yurvati, Assistant Editors

Magazine and Production Department:
Bacil Guiley, Head
Research and Development Department:
Seldon W. Terrant, Head

Advertising Office: Centcom, Ltd., 25 Sylvan
Road South, Westport, Conn. 06880.

© Copyright, 1977, by the American
Chemical Society. No part of this publication
may be reproduced in any form without
permission in writing from the American
Chemical Society.

Published biweekly by the American
Chemical Society at 20th and Northampton
Sts., Easton, Pennsylvania 18042. Second
class postage paid at Washington, D.C. and
at additional mailing offices.

Editorial Information

Instructions for authors are printed in
the first issue of each volume. Please conform
to these instructions when submitting man-
uscripts.

Manuscripts for publication should be
submitted to *The Journal of Physical
Chemistry*, Department of Chemistry, Uni-
versity of Minnesota, Minneapolis, Minn.
55455. Correspondence regarding **accepted
papers and proofs** should be directed to the

Editorial Department at the ACS Easton
address.

Page charges of \$60.00 per page may be
paid for papers published in this journal.
Payment does not affect acceptance or
scheduling of papers.

Bulk reprints or photocopies of indi-
vidual articles are available. For information
write to Business Operations, Books and
Journals Division at the ACS Washington
address.

Requests for **permission to reprint**
should be directed to Permissions, Books and
Journals Division at the ACS Washington
address. The American Chemical Society and
its Editors assume no responsibility for the
statements and opinions advanced by con-
tributors.

Subscription and Business Information

1977 Subscription rates—including surface
postage

	U.S.	PUAS	Canada, Foreign
Member	\$24.00	\$33.00	\$34.00
Nonmember	96.00	105.00	106.00
Supplementary material	15.00	19.00	20.00

Air mail and air freight rates are avail-
able from Membership & Subscription Ser-
vices, at the ACS Columbus address.

New and renewal subscriptions should
be sent with payment to the Office of the
Controller at the ACS Washington address.

Changes of address must include both old
and new addresses with ZIP code and a recent
mailing label. Send all address changes to the
ACS Columbus address. Please allow six
weeks for change to become effective. **Claims
for missing numbers** will not be allowed if
loss was due to failure of notice of change of
address to be received in the time specified:

if claim is dated (a) North America—more
than 90 days beyond issue date, (b) all other
foreign—more than 1 year beyond issue date;
or if the reason given is "missing from files".
Hard copy claims are handled at the ACS
Columbus address.

Microfiche subscriptions are available
at the same rates but are mailed first class to
U.S. subscribers, air mail to the rest of the
world. Direct all inquiries to Special Issues
Sales, at the ACS Washington address or call
(202) 872-4554. **Single issues** in hard copy
and/or microfiche are available from Special
Issues Sales at the ACS Washington address.
Current year \$4.75. Back issue rates available
from Special Issues Sales. **Back volumes** are
available in hard copy and/or microform.
Write to Special Issues Sales at the ACS
Washington address for further information.
Microfilm editions of ACS periodical pub-
lications are available from volume 1 to the
present. For further information, contact
Special Issues Sales at the ACS Washington
address. **Supplementary material** men-
tioned in the journal appears in the microfilm
edition. Single copies may be ordered directly
from Business Operations, Books and Jour-
nals Division, at the ACS Washington ad-
dress.

	U.S.	PUAS, Canada	Other Foreign
Microfiche	\$2.50	\$3.00	\$3.50
Photocopy			
1-7 pages	4.00	5.50	7.00
8-20 pages	5.00	6.50	3.00

Orders over 20 pages are available only on
microfiche, 4 × 6 in., 24X, negative, silver
halide. Orders must state photocopy or mi-
crofiche if both are available. Full bibli-
ographic citation including names of all au-
thors and prepayment are required. Prices
are subject to change.

American Chemical Society
1155 16th Street, N.W.
Washington, D.C. 20036
(202) 872-4600

Member & Subscription Services
American Chemical Society
P.O. Box 3237
Columbus, Ohio 43210
(614) 421-7230

Editorial Department
American Chemical Society
20th and Northampton Sts.
Easton, Pennsylvania 18042
(215) 258-9111

THE JOURNAL OF
PHYSICAL CHEMISTRY

Volume 81, Number 16 August 11, 1977

JPCHAX 81(16) 1531-1606 (1977)

ISSN 0022-3654

Ion Photodissociation in the Two-Photon Region. Spectroscopy and Collisional Quenching of Bromobenzene Cations	Robert C. Dunbar* and Emil W. Fu	1531
Rare Gas Sensitized Radiolysis of Hydrogen Sulfide in the Presence of Butadiene	Antoni Jówko, Iwona Szamrej, and Mieczysław Forysta*	1537
Rate Constants for the Reaction of Hydrogen and Deuterium Atoms with Silane	D. Mihelcic, V. Schubert, R. N. Schindler, and P. Potzinger*	1543
Rate Constants for the Reactions of Hydrogen Atoms with Methylgermanes	E. R. Austin and F. W. Lampe*	1546
Oscillatory Evolution of Carbon Monoxide in the Dehydration of Formic Acid by Concentrated Sulfuric Acid	Peter G. Bowers* and Gulnar Rawji	1549
Cis-Trans Photoisomerization of β -Styrylnaphthalene and 3-Styrylquinoline	G. Gennari, G. Cauzzo,* and G. Galiazzo	1551
Size and Shape of Globular Micelles Formed in Aqueous Solution by <i>n</i> -Alkyl Polyoxyethylene Ethers	Charles Tanford,* Yasuhiko Nozaki, and Michael F. Rohde	1555
Light Scattering Study of Local Structures in Solutions. Chloroform-Cetyltrimethylammonium Chloride System	Tadashi Kato and Tsunetake Fujiyama*	1560
The Deconvolution of Photoluminescence Data	A. E. McKinnon, A. G. Szabo, and D. R. Miller*	1564 ■
Absorption and Fluorescence Spectra of the Intramolecular Dimer in Polyvinyl-naphthalene	Masahiro Irie,* Takao Kamiyo, Masayuki Aikawa, Takeshi Takemura, Koichiro Hayashi, and Hiroaki Baba	1571
Inorganic Ion Exchangers. 10. A Neutron Powder Diffraction Study of the Hydrogen Bond Geometry in α -Zr(HPO ₄) ₂ ·H ₂ O. A Model for the Ion Exchange	J. Albertsson,* Å. Oskarsson, R. Tellgren, and J. O. Thomas	1574
Surface Tension and Internal Pressure. A Simple Model	David R. Rosseinsky	1578
An Approximate Treatment of Long-Range Interactions in Proteins	Matthew R. Pincus and Harold A. Scheraga*	1579
Effect of Gallium Ions and of Preparation Methods on the Structural Properties of Cobalt-Molybdenum-Alumina Catalysts	M. Lo Jacono, M. Schiavello,* V. H. J. De Beer, and G. Minelli	1583
Analysis of Torsional Spectra of Molecules with Two Internal C _{3v} Rotors. 7. Far-Infrared and Low-Frequency Raman Spectra of the Gaseous Dimethylphosphine	J. R. Durig,* M. G. Griffin, and W. J. Natter	1588
The Fluorescent Level Inversion of Dual Fluorescences and the Motional Relaxation of Excited State Molecules in Solutions	Satoshi Suzuki,* Tsuneo Fujii, Akihiro Imai, and Hideo Akahori	1592
A Method for Calculating CNDO-MO Bonding Parameters. 1	Sankar Prasad Bhattacharyya and Mihir Chowdhury*	1598
A Method for Calculating CNDO-MO Bonding Parameters. 2. Preliminary Applications	Sankar Prasad Bhattacharyya and Mihir Chowdhury*	1602

COMMUNICATIONS TO THE EDITOR

The Photoperoxidation of Unsaturated Organic Molecules. 17. The Thermal
Regeneration of Acceptor B. Stevens* and R. D. Small, Jr. 1605

■ Supplementary and/or miniprint material for this paper is available separately (consult the masthead page for ordering information); it will also appear following the paper in the microfilm edition of this journal.

* In papers with more than one author, the asterisk indicates the name of the author to whom inquiries about the paper should be addressed.

AUTHOR INDEX

Aikawa, M., 1571	Foryś, M., 1537	Kato, T., 1560	Rawji, G., 1549
Akahori, H., 1592	Fu, E. W., 1531		Rohde, M. F., 1555
Albertsson, J., 1574	Fujii, T., 1592	Lampe, F. W., 1546	Rosseinsky, D. R., 1578
Austin, E. R., 1546	Fujiyama, T., 1560	Lo Jacono, M., 1583	
			Scheraga, H. A., 1579
Baba, H., 1571	Galiazzo, G., 1551	McKinnon, A. E., 1564	Schiavello, M., 1583
Bhattacharyya, S. P., 1598, 1602	Gennari, G., 1551	Mihelcic, D., 1543	Schindler, R. N., 1543
Bowers, P. G., 1549	Griffin, M. G., 1588	Miller, D. R., 1564	Schubert, V., 1543
		Minelli, G., 1583	Small, R. D., Jr., 1605
Cauzzo, G., 1551	Hayashi, K., 1571		Stevens, B., 1605
Chowdhury, M., 1598, 1602		Natter, W. J., 1588	Suzuki, S., 1592
	Imai, A., 1592	Nozaki, Y., 1555	Szabo, A. G., 1564
	Irie, M., 1571		Szamrej, I., 1537
		Oskarsson, Å., 1574	
De Beer, V. H. J., 1583	Jówko, A., 1537		Takemura, T., 1571
Dunbar, R. C., 1531		Pincus, M. R., 1579	Tanford, C., 1555
Durig, J. R., 1588	Kamijo, T., 1571	Potzinger, P., 1543	Tellgren, R., 1574
			Thomas, J. O., 1574

ANNOUNCEMENT

On the last two pages of this issue you will find reproduced the table of contents of the July 1977 issue of the *Journal of Chemical and Engineering Data*.

THE JOURNAL OF PHYSICAL CHEMISTRY

Registered in U. S. Patent Office © Copyright, 1977, by the American Chemical Society

VOLUME 81, NUMBER 16 AUGUST 11, 1977

Ion Photodissociation in the Two-Photon Region. Spectroscopy and Collisional Quenching of Bromobenzene Cations

Robert C. Dunbar*[†] and Emil W. Fu

Department of Chemistry, Case Western Reserve University, Cleveland, Ohio 44106 (Received March 1, 1977)

Publication costs assisted by the Petroleum Research Fund and the Air Force Geophysical Laboratory

It has been suggested recently by Freiser and Beauchamp that benzene cations undergo a sequential two-photon photodissociation process. In this study, the photodissociation spectroscopy of bromobenzene cations below the one-photon energetic threshold was undertaken first to provide a more substantial theoretical foundation and second to assess critically the extent to which the Freiser-Beauchamp picture of this process can serve as a framework for an exact quantitative analysis of two-photon data. The detailed treatment by three different methods of the time-resolved photodissociation data for bromobenzene cations confirmed the validity of the sequential two-photon mechanism; and also provided the methodology for reduction of two-photon data to cross sections which can be directly compared with the usual photodissociation cross section in the one-photon region. Careful analysis of two-photon photodissociation data also yields a direct measurement of the absolute rate of deactivation of the vibrationally excited ion. Deactivation occurs on nearly every collision of bromobenzene cations with bromobenzene neutrals. The values measured were as follows: σ_1 (first photon absorption) = 4.4×10^{-18} cm²; σ_2 (second photon absorption) = 7.9×10^{-18} cm²; K_3 (collisional deactivation) = 1.1×10^{-9} cm³/molecule s.

Introduction

In a rather extensive body of work investigating the photodissociation of gas-phase ions as a function of wavelength,¹⁻¹⁰ two principal kinds of information sought have been optical absorption information about the ions and thermochemical information about the dissociation process. An assumption underlying the thinking about these questions had been that photodissociation would be possible only at photon energies above the energy threshold for dissociation, so that a thermochemical dissociation threshold might be conveniently determined from threshold photodissociation, while spectroscopic studies would be automatically limited to wavelengths above threshold. In pointing out and demonstrating for benzene ion the possibility of two-photon dissociation in a sequential process at moderate light intensities, Freiser and Beauchamp¹¹ overturned these simple arguments. The newly recognized possibility of rapid photodissociation far

below the one-photon energetic threshold liberates the spectroscopic applicability of photodissociation from the constraints of thermochemical considerations, while it greatly complicates the analysis needed to obtain threshold thermochemical information from threshold photodissociation spectral line shapes.

The analysis of photodissociation curves in the transition region between one-photon and two-photon behavior has extraordinary potential for obtaining accurate thermochemical data concerning the dissociation reaction, and will be discussed and illustrated in a later publication. The new possibilities inherent in using two-photon photodissociation to investigate spectral properties have already been exploited in obtaining the photodissociation spectrum of methylnaphthalene cations,¹² and the obvious success in this case underscores the need for convincing quantitative understanding of the two-photon process and for reliable data reduction procedures. Neither Freiser and Beauchamp's treatment, nor our own earlier analysis,¹² seem to satisfy these needs fully, and the detailed

[†] Alfred P. Sloan Fellow, 1973-1975.

treatment of bromobenzene ion data given below was undertaken to provide a more substantial theoretical foundation, and to assess critically the extent to which the Freiser-Beauchamp picture of this process can serve as the framework for an exact quantitative analysis of two-photon data. The analysis presented here will be aimed first at providing a confirmation of the quantitative validity of the sequential two-photon mechanism, and second at clarifying and quantifying the methodology for reduction of two-photon data to cross sections which can be directly compared with the usual photodissociation cross sections in the one-photon region.

Following initial submission of this work, a paper appeared by Orłowski et al.¹³ concerned with two-photon photodissociation of cyanobenzene cation,¹³ which covers some of the theoretical development presented here. We have decided to retain these aspects here because of our somewhat more complete and perhaps useful development of the theory, and because it seems desirable to point out the erroneous nature of the treatment in ref 11 and to describe correct simple procedures for approximate data analysis.

Another aspect of the two-photon process which is of considerable interest is the dependence of the equations on the rate of collisional quenching of vibrationally excited ions, which leads to the possibility of direct measurement of this rate. Although extensive studies have been carried out to determine relative quenching efficiencies of various neutrals in ion-neutral collisions, there is little information about the absolute rate of quenching. As will be clear below, careful analysis of two-photon dissociation data yields a direct measurement of the rate of deactivation of the vibrationally excited ion. The present results point the way toward future quantitative collisional-quenching investigations, although in the present case the trivial possibility of resonant charge-transfer quenching makes the results less interesting in themselves.

Experimental Section

Photodissociation was followed by monitoring the decrease under illumination of the parent-ion signal in the ion cyclotron resonance (ICR) spectrometer. The UV portion of the photodissociation spectrum of Figure 1 was obtained by standard steady-state ICR photodissociation methods with a Hg-Xe light source and monochromator (132-Å fwhm), as in previously described work.⁷

The visible portion of this spectrum was also obtained using the Hg-Xe arc source, with appropriate filters used to isolate the strong Hg lines in the lamp spectrum. In the visible, the photon energy is clearly in the two-photon region, and also, with the low arc-lamp light intensity, the experiment is in the low-intensity limit. It has been shown appropriate under these conditions¹² to reduce the observed photodissociation rate K_{obsd} by the expression $\sigma_1 = (\text{constant})I^{-1}(PK_{\text{obsd}})^{1/2}$, where I is the light intensity and P the pressure, in order to obtain the relative cross section σ_1 for "effective" absorption of the first photon; σ_1 is then precisely comparable to the usual cross section for photodissociation in the one-photon region. The curve shape of the visible-region peak in Figure 1 was obtained by this simple normalization procedure. The absolute cross section calibration of this region was obtained from the detailed analysis of the laser data at 5145 Å described below. The absolute cross section of the UV peak is referenced back to the value¹³ $5 \times 10^{-18} \text{ cm}^2$ for the toluene ion at 4000 Å.

The quantitative 5145-Å laser data were obtained using the "time-resolved" mode of operation, in which the decay of the parent ion signal in a trapped sample of ions is

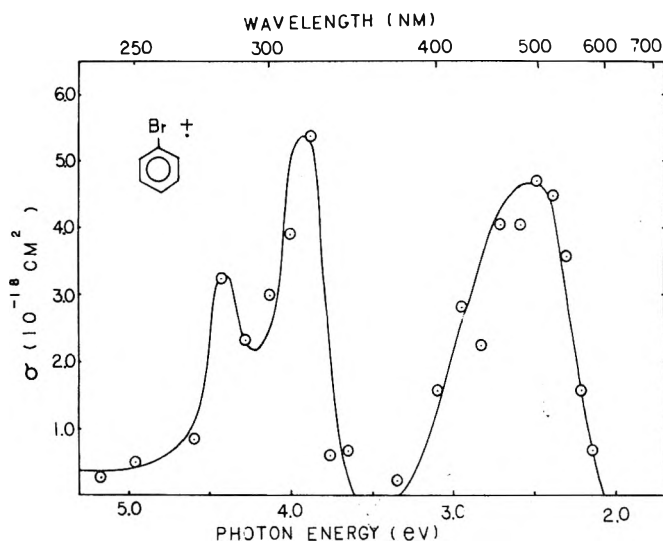


Figure 1. The photodissociation spectrum of bromobenzene cations in the visible and the UV spectral region. The cross section in the UV (one-photon) region was obtained by standard means, while the data in the visible (two-photon) region were treated as described in the text to provide cross section values (σ_1) corresponding to absorption of a single photon.

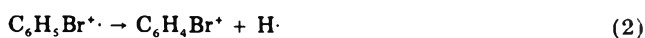
followed directly in real time after turning on the irradiating source. This experiment has been described in detail,⁹ and has the important advantages of allowing easy accurate quantitative measurements, and of revealing clearly potential problems such as ion rearrangement or interfering ion-molecule chemistry. We believe that considerable confidence can be placed in rate constants derived from clean, simply exponential photodissociation decay curves obtained by this approach. The laser source was a Coherent Radiation CR-12 argon-ion laser. Total power in the beam was measured with a thermopile, while the area of the beam, which was spread to a diameter of several centimeters to give flux uniformity over the ICR cell, was measured directly at a point corresponding to the source region of the ICR cell where the ions are believed to be concentrated in the ion trap used. Allowance was made for window transmission and back-reflection in the cell.¹⁴ Pressure was read from the ion pump gauge: calibration of the gauge against an MKS Baratron at higher pressures has indicated that for numerous aromatic compounds the indicated ion-pump pressure fortuitously agrees within 10–20% with the true pressure in the cell region (assuming linearity of the ion pump gauge). Ionizing energy was within 1–2 eV of the appearance potential for bromobenzene parent ions, and no significant fragment peaks were present in the absence of light.

Results and Discussion

The energetics of the bromobenzene photodissociation reaction



are well known,¹⁵ with the threshold lying at 3.52 eV (3500 Å). The next most facile reaction



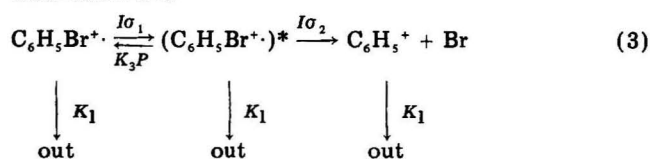
was not observed; it is probably more endothermic than (1) by about 1 eV, and would not be expected to compete significantly with reaction 1 at these ion excitation energies.

The observed photodissociation spectrum is shown in Figure 1. Not surprisingly, the spectrum is similar to that previously described for the bromotoluene cation.^{7,9} The UV peak can be plausibly assigned to either a $\pi \rightarrow \pi$ or

a $\pi \rightarrow \pi^*$ excitation, and this question will be considered in detail in subsequent work. The visible peak corresponds very clearly to an $n \rightarrow \pi$ electron promotion process; it involves the same excited cation electronic state as is observed in the photoelectron spectrum of bromobenzene,¹⁷ and which is commonly accepted to involve removal of an electron from the out-of-plane halogen lone-pair orbital. The optical transition to this state of the cation is strongly allowed.

The absolute cross sections of the photodissociation peaks are comparable to those which have been measured for other allowed photodissociation transitions in aromatic ions such as toluene. The "oscillator strengths" for photodissociation are of the order of 0.03 for both the visible peak and the UV peak, not unreasonable for allowed optical processes.

Two-Photon Photodissociation Kinetics. The sequential two-photon photodissociation scheme which Freiser and Beauchamp proposed for benzene cation,¹¹ and which we will apply to bromobenzene ion, may be written, for bromobenzene



where I is the light intensity (photon/cm² s), P is the density of neutral gas (molecules/cm³), σ_1 and σ_2 are cross sections for photon-induced processes, K_3 is a collisional deactivation rate constant, and K_1 is a rate constant for destruction of ions by processes other than photodissociation. The only significant loss of generality is the assumption that K_1 is equal for P^+ and P^{+*} (we use P^+ and P^{+*} to denote $\text{C}_6\text{H}_5\text{Br}^+$ and $(\text{C}_6\text{H}_5\text{Br}^+)^*$, respectively); this assumption will not lead to significant errors even if it is incorrect, since K_1 is very slow.

The nature of the $(\text{C}_6\text{H}_5\text{Br}^+)^*$ intermediate in (3) is of interest. In order for the kinetic scheme to be appropriate and for the effect to have the observed intensity, the internal energy of this species must be assumed to be retained until collisional deactivation (the K_3 process), implying a lifetime of the order of 1 s. Fluorescent excited electronic states are clearly excluded on this time scale, and the remaining possibilities are phosphorescent electronic states and excited vibrational states. Beauchamp et al.^{11,13} have argued that the excitation is vibrational, with the initially formed excited doublet electronic state undergoing rapid ($\ll 10^{-8}$ s) internal conversion to the vibrationally hot electronic ground state. Involvement of a phosphorescent (probably quartet) electronic state is conceivable, but for such a state to be formed and subsequently absorb the second photon with such high efficiency for the variety of molecules showing this behavior seems extremely improbable, and it seems nearly certain that the intermediate is in fact a hot ground state ion.

If fluorescence of the excited doublet electronic state competes with internal conversion, there will probably be little effect on the observed results: an event in which a photon is absorbed and then reradiated on a time scale of 10^{-8} s is unobservable in this experiment (except for a possible small amount of vibrational energy left behind), and such processes may safely be omitted from the kinetic scheme, and their cross sections omitted from σ_1 and σ_2 , which are properly the cross sections for "effective" photon absorption.¹²

The relevant kinetic equations for this experiment, in which the spectrometer monitors abundance of ions at the $\text{C}_6\text{H}_5\text{Br}^+$ mass, are

$$\begin{aligned} d[\text{P}^+]/dt &= (-I\sigma_1 - K_1)[\text{P}^+] + (K_3P)[\text{P}^{+*}] \\ d[\text{P}^{+*}]/dt &= (I\sigma_1)[\text{P}^+] + (-I\sigma_2 - K_3P - K_1)[\text{P}^{+*}] \end{aligned} \quad (4)$$

The exact integration of these equations yields

$$\frac{[\text{P}^+] + [\text{P}^{+*}]}{[\text{P}^+]_{\text{off}}} = \frac{\lambda_-}{\lambda_- - \lambda_+} e^{-\lambda_+ t} - \frac{\lambda_+}{\lambda_- - \lambda_+} e^{-\lambda_- t} \quad (5)$$

where $[\text{P}^+]_{\text{off}}$ is the P^+ concentration in the absence of light ($I = 0$), and λ_- and λ_+ are given by¹²

$$\lambda_{\pm} = 1/2 \{ I\sigma_1 + I\sigma_2 + K_3P \mp [(I\sigma_1 + I\sigma_2 + K_3P)^2 - 4I^2\sigma_1\sigma_2]^{1/2} \} \quad (6)$$

An important special case is the high-pressure low-intensity limit, defined by

$$I\sigma_1/K_3P \ll 1 \text{ and } I\sigma_2/K_3P \ll 1 \quad (7)$$

Expansion of (6) in terms of the small quantity $I^2\sigma_1\sigma_2/(I\sigma_1 + I\sigma_2 + K_3P)^2$ yields a result

$$\lambda_+ \approx \frac{I^2\sigma_1\sigma_2}{I\sigma_1 + I\sigma_2 + K_3P} + \Delta \quad (8)$$

$$\lambda_- \approx I\sigma_1 + I\sigma_2 + K_3P - \frac{I^2\sigma_1\sigma_2}{I\sigma_1 + I\sigma_2 + K_3P} - \Delta \quad (9)$$

where the correction term

$$\Delta = \frac{I^4\sigma_1^2\sigma_2^2}{(I\sigma_1 + I\sigma_2 + K_3P)^3} \quad (10)$$

is included for future reference, but will be ignored in most of the following. Finally, for times t long enough for the initial transient behavior to have died out ($t \gg 1/\lambda_-$), the ion decay curve becomes a simple exponential

$$\left(\frac{[\text{P}^+] + [\text{P}^{+*}]}{[\text{P}^+]_{\text{off}}} \right)_{\text{long time}} \approx \frac{\lambda_-}{\lambda_- - \lambda_+} e^{-\lambda_+ t} \quad (11)$$

so that

$$\ln \frac{[\text{P}^+] + [\text{P}^{+*}]}{[\text{P}^+]_{\text{off}}} \approx \ln \frac{\lambda_-}{\lambda_- - \lambda_+} - \lambda_+ t \quad (12)$$

This linear form is convenient for plotting time-resolved data, and yields directly the value of λ_+ for a given decay curve. Under high-pressure/low-intensity conditions it is clear from (8) that the quantities

$$\alpha = K_3/I^2\sigma_1\sigma_2 \quad (\text{slope}) \quad (13)$$

and

$$\beta = (\sigma_1 + \sigma_2)/I\sigma_1\sigma_2 \quad (\text{intercept}) \quad (14)$$

are obtained from the slope and intercept, respectively, of a plot of $1/\lambda_+$ vs. pressure. It is thus possible to determine only two of the three unknown quantities σ_1 , σ_2 , and K_3 by this analysis.

It may be noted that this result, specifically eq 14, differs from the result obtained by Freiser and Beauchamp¹¹ for the same limits, which gave $1/I\sigma_1$ as the intercept. Their steady-state-intermediate treatment is in fact not applicable, as shown by its disagreement with the complete solution. This is not unexpected since the steady-state approximation is strictly valid only in the limit where $I\sigma_1$ and $I\sigma_2$ are vanishingly small, and should not therefore be expected to yield expressions containing the correct dependence on σ_1 and σ_2 .

Assuming that the intensity-pressure regime of the present study can be approximated by the high-pressure

low-intensity limit for the bromobenzene ion, it is of interest to examine two questions: first, in this limit, exactly how much information can be obtained about σ_1 , σ_2 , and K_3 from the data; and second, whether the range of experimental conditions reaches a regime where deviations from this limit become observable and useful.

Manipulation of eq 13 and 14 reveals that σ_1 , σ_2 , and K_3 are more constrained than suggested by the discussion above. Rearranging (13) and (14) yields the equations

$$\sigma_1 = \frac{\sigma_2}{I\beta\sigma_2 - 1} \quad \sigma_2 = \frac{\sigma_1}{I\beta\sigma_1 - 1}$$

and

$$\sigma_1 = \frac{I\beta K_3 \pm [(I\beta)^2 K_3^2 - 4I^2\alpha K_3]^{1/2}}{2I^2\alpha}$$

It is seen that if the K 's are to be positive and finite, no solution is possible unless

$$\sigma_1 \text{ and } \sigma_2 > 1/I\beta \quad (15)$$

$$K_3 \geq K_{3\min} = 4I^2\alpha/(I\beta)^2$$

which are thus exact lower limits on the rate constants. Better limits can be written if an assumption is made about the relation of IK_1 and IK_2 . There seems no reason to suppose that the optical absorption cross section will be very different for P^+ and P^{++} , since P^{++} is assumed to be a vibrationally hot electronic ground state. As Freiser and Beauchamp¹¹ have noted, the chief difference is likely to arise because of spatial inhomogeneity of the light, and a consequent difference in the effective intensity between the σ_1 and σ_2 processes. It seems most unlikely that this effect could make $I\sigma_2$ as much as three times larger than $I\sigma_1$, and if we put the limits $1 \leq I\sigma_2/I\sigma_1 \leq 3$, we obtain the rather narrow set of limits

$$\frac{2}{I\beta} \geq \sigma_1 \geq \frac{4}{3I\beta} \quad (16)$$

$$\frac{4}{I\beta} \geq \sigma_2 \geq \frac{2}{I\beta} \quad (17)$$

$$5.3 \frac{I^2\alpha}{(I\beta)^2} \geq K_3 \geq 4 \frac{I^2\alpha}{(I\beta)^2} \quad (18)$$

Observable deviations from the limit represented by eq 7 can arise (see eq 5, 8, and 9) if one of the following conditions holds true:

(1) λ_- becomes small enough that the decay curve (12) intercepts at a value observably different from zero at $t = 0$; the actual intercept is given by

$$\begin{aligned} \ln \frac{\lambda_-}{\lambda_- - \lambda_+} &\approx \ln \left(1 + \frac{I^2\sigma_1\sigma_2}{K_3^2 P^2} \right) \\ &\approx \frac{I^2\sigma_1\sigma_2}{K_3^2 P^2} = \frac{1}{K_3 P^2 \alpha} \end{aligned} \quad (19)$$

so that deviation will be observable when the last term is greater than the uncertainty in intercept value. (The curvature in this plot due to the initial transient (second term on the right in eq 5) will also become observable at short times under similar conditions.)

(2) Δ becomes large enough to introduce curvature in the $1/\lambda_+$ vs. pressure plot. This may be checked by noting from (8) that to the next better approximation

$$\frac{1}{\lambda_+} \approx \alpha P + \beta - \frac{1}{I(\sigma_1 + \sigma_2) + K_3 P} \quad (20)$$

so that curvature or deviation will become important if the

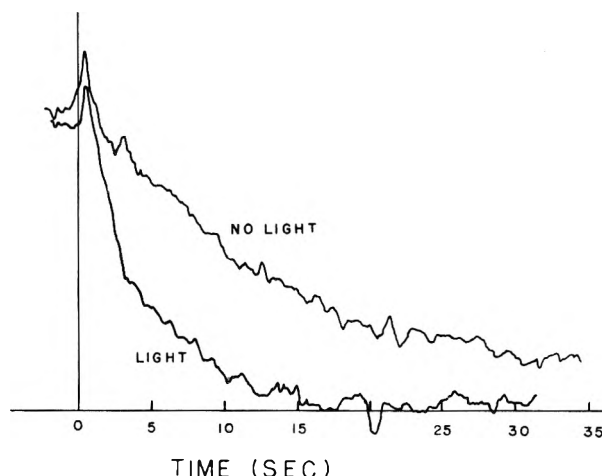


Figure 2. Time resolved ion decay curve for bromobenzene cation at 2.8×10^{-8} Torr pressure, 5145 Å, 0.1 W. At time zero the electron beam is switched off and (for the "light" trace) the laser is turned on. The curves then follow the decay of the parent ion signal due to photodissociation, leakage from the ion trap, and other loss mechanisms. The photodissociation effects are isolated by point-by-point division of the light-on decay curve by the light-off curve.²⁰

last term in (20) becomes significant compared with the uncertainty in the measured value of $1/\lambda_+$.

If one of the two situations described occurs, then the deviation from the high-pressure low-intensity limiting behavior gives an additional relation among σ_1 , σ_2 , and K_3 and the problem becomes fully determined.

To summarize the important results of this section: complete solution of the two-photon kinetic scheme gives calculated ICR signal decay curves as a function of pressure and intensity. In the high-pressure, low-intensity limit, data analysis can fix two of the three unknown rates σ_1 , σ_2 , and K_3 , and in addition set a lower limit on K_3 , while an assumption that $I\sigma_1$ is not very different from $I\sigma_2$ gives rather narrow limits on all three rates. Data at sufficiently high intensity and low pressure can give independent values to σ_1 , σ_2 , and K_3 and criteria have been noted for deciding when this is possible. We proceed now to examine the data for bromobenzene cation, with the objects, first, of establishing securely that the assumed two-photon mechanism (3) gives a quantitative description of this system, and second of obtaining accurate values for σ_1 , σ_2 , and K_3 .

Two-Photon Data Analysis. The data set analyzed consisted of time-resolved photodissociation decay curves at 5145 Å for 26 different combinations of pressure and intensity. A typical time-resolved decay curve is shown in Figure 2. The analysis above suggests several different approaches to data analysis; the three described below were tried for comparison.

1. **Graphical Analysis.** Complete graphical analysis based on eq 7-18 is probably the least accurate method, and most prone to distortion by errors in judgement, but it was performed because of the insight it yields into the behavior of the two-photon kinetic scheme as applied to this ion. Plotting $\ln \{([P^+] + [P^{++}])/[P^+]_{\text{off}}\}$ against time gave plots which were apparently linear within experimental uncertainties, and λ_+ values were measured from the slopes. A series of curves for one pressure is shown in Figure 3 (note that the solid lines are not those used to measure the slopes, but are the curves calculated from the fit described below in section 3). Assuming for the moment that the data are in the limit of eq 7, it is clear from (8) that λ_+ should be quadratic in light intensity at given pressure: this is found to be true to good accuracy. Further analysis depends on plotting $1/\lambda_+$ vs. pressure at

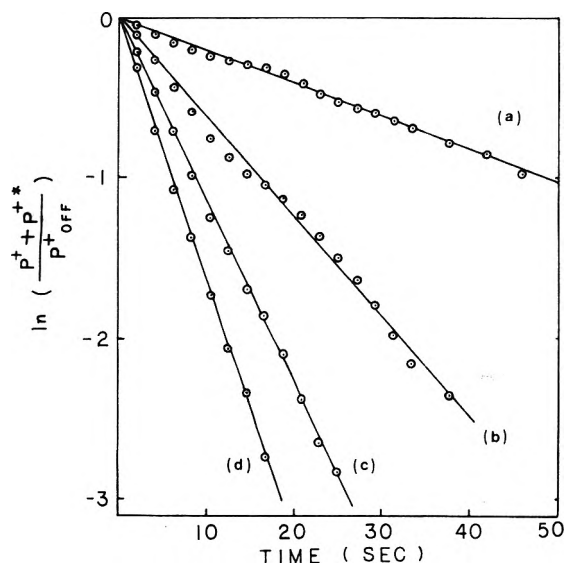


Figure 3. The $\ln \{([P^+] + [P^{*+}])/[P^+]_{\text{off}}\}$ values obtained from the time-resolved photodissociation decay curves at 5145 Å were plotted against time. This figure shows the results obtained at 2.8×10^{-8} Torr with four light intensities: (a) 2.9×10^{16} photon $\text{cm}^{-2} \text{s}^{-1}$, (b) 5.8×10^{16} photon $\text{cm}^{-2} \text{s}^{-1}$, (c) 8.7×10^{16} photon $\text{cm}^{-2} \text{s}^{-1}$, (d) 1.16×10^{17} photon $\text{cm}^{-2} \text{s}^{-1}$.

TABLE I: Parameter Values Obtained from Graphical Data Reduction

Intensity $\times 10^{17}$ $\text{cm}^{-2} \text{s}^{-1}$	$10^{25} I^2 \alpha$ $\text{s}^{-1} \text{cm}^{-1}$ molecule $^{-1}$	$10^{17} I \beta$ cm^{-2}
0.29 (0.05 W)	3.3	3.3
0.58 (0.1 W)	3.9	3.0
0.87 (0.15 W)	2.6	4.4
1.16 (0.2 W)	3.5	3.8
1.7 (0.3 W)	3.5	4.1

each intensity. These plots are found to be linear, as illustrated for one intensity in Figure 4. Slopes and intercepts of these lines yield values of the "constants" $I^2 \alpha$ and $I \beta$, which are tabulated in Table I. It is seen that both $I^2 \alpha$ and $I \beta$ are constant over the sixfold range of intensities (to within a degree of scatter which is reasonable in terms of the scatter in the data). The chief objections to this method are that the determination of K_3 depends on the square of the rather inaccurate β values, and that the measurement of these β values puts undue weight on the low-pressure points. The least-squares method of section 3 circumvents these problems.

The average values obtained from the above analysis are $I^2 \alpha = 3.3 \times 10^{25} \text{ s}^{-1} \text{ cm}^{-1} \text{ molecule}^{-1}$ and $I \beta = 3.7 \times 10^{17} \text{ cm}^{-2}$. (Standard deviations of the mean are $\pm 6\%$ for a $I^2 \alpha$, $\pm 8\%$ for $I \beta$. In the values given below, assumed uncertainties of $\pm 20\%$ in the pressure calibration constant and $\pm 30\%$ in the intensity calibration constant are combined with these.) The strict limit on K_3 obtained from (15) is then $K_3 \geq (1 \pm 0.3) \times 10^{-9} \text{ cm}^3/\text{molecule s}$. The realistic values obtained by combining experimental uncertainties with the ranges given by (16–18) are

$$\begin{aligned} \sigma_1 &= (4.7 \pm 2) \times 10^{-18} \text{ cm}^2 \\ \sigma_2 &= (8.8 \pm 3) \times 10^{-18} \text{ cm}^2 \\ K_3 &= (1.1 \pm .3) \times 10^{-9} \text{ cm}^3/\text{molecule s} \end{aligned} \quad (21)$$

It is calculated that deviations from the high-pressure, low-intensity limit, as manifested by the effects described by either eq 19 or 20, are of the same order as the scatter in the data. Further refinement of the graphical analysis to correct for these effects can be made, but the im-

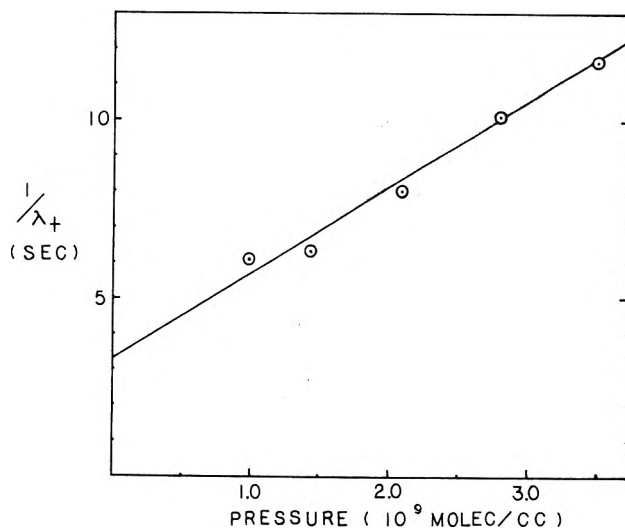


Figure 4. The slopes and intercepts of the $1/\lambda_+$ vs. pressure plots yield the values of α and β . The results illustrated in this figure were obtained at a light intensity of 1.16×10^{17} photon $\text{cm}^{-2} \text{s}^{-1}$.

provement is not large; in any case the more satisfactory methods described below are not high-pressure low-intensity approximations.

2. *Computer Fit to Eq 5.* In principle, generating simulated decay curves from eq 5 and direct comparison with the observed decay curves is the most satisfactory approach. This was done for a variety of choices of σ_1 , σ_2 , and K_3 . In practice, the agreement of these curves with the observed curves was reasonable for quite a wide range of parameter values, and there was considerable question about the most appropriate criterion to apply for deciding on the best fit. It was decided to require agreement between calculated and observed decay curves at 10 s for the greatest number of decay curves. Using this criterion, fits of essentially equal goodness were obtained for K_3 values ranging from 1.0×10^{-9} to $4.5 \times 10^{-9} \text{ cm}^3/\text{molecule s}$, σ_1 values between 3.8 and $7.6 \times 10^{-18} \text{ cm}^2$, and σ_2 such that $\sigma_1 \sigma_2 / (\sigma_1 + \sigma_2) \approx 2.7 \times 10^{-18} \text{ cm}^2$.

3. *Least-Squares Fit to Eq 6.* The slopes (at long t) of the decay curves of eq 12 could be measured with very good precision. The set of slope values was fitted to eq 6 using a non-linear least-squares routine¹⁸ which varied σ_1 and K_3 . (As expected from the discussion above, the ratio σ_2/σ_1 was not well defined by the data set, so calculations were made with σ_2 values from $\sigma_2 = \sigma_1$ to $\sigma_2 = 3\sigma_1$, with equally good fits in all cases, and this range of variation was included in the uncertainties in σ_1 and σ_2 .) The fits obtained were excellent and closely constrained (average deviation between computed and observed values $\sim 8\%$). The indication from the previous sections of excellent agreement of the results with the two-photon kinetic scheme was amply confirmed by the satisfactory fitting of all 26 slope values to the two-parameter model adopted. The fitted values of the parameters were $\sigma_1 = 4.4 \times 10^{-18}$, $\sigma_2 = 7.9 \times 10^{-18}$, and $K_3 = 1.05 \times 10^{-9}$. (The fitting errors in these are insignificant compared with the other experimental uncertainties discussed above, and realistic uncertainties are as given in (21).)

The agreement in parameter values obtained by all three analyses is satisfactory, and all three approaches support the validity of the assumed kinetic model. In this set of data, the accuracy of the results was not limited by the precision of the data analysis; in opposite circumstances, the approach of section 3 appears to have clear advantages over the other two in reliability, and should be preferred except when the convenience of the graphical approach outweighs its lower reliability.

Inserting the calculated rate constants into (7) shows that the high-pressure low-intensity limit is not well obeyed for the conditions of these experiments, with $I\sigma_2/K_3P$ being of the order of unity for some of the experimental points. In spite of this, the graphical treatment based on this limit gives results indistinguishable from the exact least-squares fit, indicating that if the limit (7) is not too severely violated, the two-photon kinetics may be considered in the high-pressure low-intensity approximation without major error.

The value of $1.1 \times 10^{-9} \text{ cm}^3/\text{molecule s}$ determined for collisional deactivation of the vibrationally excited bromobenzene ions represents very efficient quenching, and corresponds to quenching on nearly every orbiting collision. One should not attempt to interpret this as indicating rapid intermolecular energy transfer, however, since resonant charge transfer is also a highly effective process for quenching excited ions, and is likely to be as fast as or even faster than the rate of orbiting collisions.¹¹ Accordingly, we can only conclude that quenching is rapid, whether by means of energy transfer, charge transfer, or both. An important consequence of this observation is the fact that, in this system at least, the collisional quenching process must occur by a large transfer of excitation on most collisions; models in which the excited parent is quenched by a series of successive small energy-losing collisional events are entirely ruled out. It will be of considerable interest to see if this is still true in systems where symmetrical charge transfer is not a likely process.

Another very interesting question accessible to study through the two-photon process is the cooling by infrared radiation of the P^{+*} excited parent ion. Calculations suggest¹⁹ that for ions of this size with vibrational excitation of the order of 2 eV the rate constant for radiative cooling is likely to be about 1 s^{-1} , and it would be useful to test this prediction. Radiative cooling will appear in (3) as a pressure independent additive correction to the K_3P term, and should be experimentally accessible in two-photon experiments done at pressures low enough that $K_3P \lesssim 1 \text{ s}^{-1}$. The data reported here do in fact reach this

condition at the lowest pressures, but there is no indication of a consistent effect on the results from radiative deexcitation. Nevertheless, careful low-pressure studies offer a useful approach to this difficult problem.

Acknowledgment. Acknowledgment is made to the donors of the Petroleum Research Fund, administered by the American Chemical Society, to the National Science Foundation, and to the Air Force Geophysical Laboratory for support of this research.

References and Notes

- (1) R. C. Dunbar, *J. Am. Chem. Soc.*, **93**, 4354 (1971).
- (2) R. C. Dunbar, *J. Am. Chem. Soc.*, **95**, 472 (1973).
- (3) R. C. Dunbar, *J. Am. Chem. Soc.*, **95**, 6191 (1973).
- (4) R. C. Dunbar and E. W. Fu, *J. Am. Chem. Soc.*, **95**, 2716 (1973).
- (5) R. C. Dunbar and J. M. Kramer, *J. Chem. Phys.*, **58**, 1266 (1973).
- (6) J. M. Kramer and R. C. Dunbar, *J. Chem. Phys.*, **59**, 3092 (1973).
- (7) P. P. Dymerski, E. W. Fu, and R. C. Dunbar, *J. Am. Chem. Soc.*, **96**, 4109 (1974).
- (8) R. C. Dunbar in "Interactions between Ions and Molecules", P. Ausloos, Ed, Plenum Press, New York, N.Y., 1975.
- (9) E. W. Fu, P. P. Dymerski, and R. C. Dunbar, *J. Am. Chem. Soc.*, **98**, 337 (1976).
- (10) R. C. Dunbar, *Anal. Chem.*, **48**, 723 (1976).
- (11) B. S. Freiser and J. L. Beauchamp, *Chem. Phys. Lett.*, **35**, 35 (1975).
- (12) R. C. Dunbar and R. Klein, *J. Am. Chem. Soc.*, **98**, 7994 (1976).
- (13) T. E. Orłowski, B. S. Freiser, and J. L. Beauchamp, *Chem. Phys.*, **18**, 439 (1976).
- (14) M. T. Riggan and R. C. Dunbar, *Chem. Phys. Lett.*, **31**, 539 (1975).
- (15) As pointed out by a referee, interchange of σ_1 and σ_2 does not affect this expression, so that σ_1 and σ_2 cannot be separately determined from any analysis of the data. However, the procedures described below can yield unique σ_1 and σ_2 values subject *only* to the restriction that one does not know which is σ_1 and which is σ_2 . If, as discussed following eq 15, one makes the physically reasonable assumption $\sigma_1 \geq \sigma_2$, then the ambiguity is removed, and the determination is (in principle) unique.
- (16) J. L. Franklin et al., *Natl. Stand. Ref. Data Ser., Natl. Bur. Stands*, No. 26 (1969).
- (17) D. W. Turner et al. "Molecular Photoelectron Spectroscopy", Wiley-Interscience, New York, N.Y., 1970.
- (18) P. R. Bevington, "Data Reduction and Error Analysis for the Physical Sciences", McGraw-Hill, New York, N.Y., 1969.
- (19) R. C. Dunbar, *Spectrochim. Acta, Part A*, **31**, 797 (1975).
- (20) The decay curve of Figure 2 may be seen not to agree with that plotted in Figure 3, and was taken for illustration from a different data set with different expansion of the laser beam: its quality is comparable to the curves analyzed in this paper.

Rare Gas Sensitized Radiolysis of Hydrogen Sulfide in the Presence of Butadiene

Antoni Jówko, Iwona Szamrej, and Mieczysław Forýś*

Chemistry Department, University Teachers College, 08-110 Siedlce, Poland (Received November 7, 1975; Revised Manuscript Received December 15, 1976)

Hydrogen and sulfur yields have been measured from the argon, krypton, and xenon sensitized radiolysis of hydrogen sulfide in the presence of butadiene. A sharp decrease in the yield of elemental sulfur from 5–7 molecules/100 eV down to a very low value (ca. 0.1 atoms/100 eV) has been discovered even at the lowest added amounts of butadiene. Unlike the sulfur yields, the hydrogen yields diminished smoothly with $[C_4H_6]/[H_2S]$ ratio. A mechanism for the observed decrease in the sulfur and hydrogen yield has been discussed. It has been shown that elemental sulfur is produced via the HS⁺ ions and SH radicals and/or S atoms as intermediate products, each of them being scavenged by butadiene. The change in $G(H_2)$ with the $[C_4H_6]/[H_2S]$ ratio was ascribed to a competition between butadiene and hydrogen sulfide in an excitation transfer from the rare gas metastables, and hydrogen atom scavenging. The rate constant ratio $k_{H+H_2S}/k_{H+C_4H_6}$ has been calculated to be in the range of 0.22–0.28, 0.18–0.22, and 0.14–0.16 for Kr, Xe, and Ar, respectively. The observed increase in the rate constant ratio as compared to that for thermal H atoms (0.11) has been accounted for by a higher kinetic energy of hydrogen atoms produced in the system. The maximum values of G_{Xe} , G_{Kr} , and G_{Ar} have been found from energetic calculations to be equal to 3.1, 2.5, and 2.1, respectively. These have been compared with experimental results found under the supposition that primary radiolysis can be neglected. The discrepancy has been observed which has been ascribed to the significant decomposition of hydrogen sulfide by electrons subexcited with respect to rare gas atoms. The hydrogen yield due to the last process has been estimated to be ca. 1.4 for Ar and Xe.

Introduction

The effect of butadiene on $G(H_2)$ and $G(S)$ in the γ radiolysis^{1–3} and rare gas sensitized radiolysis⁴ of hydrogen sulfide has been recently investigated. It has been stated that addition of butadiene causes a slow decrease in $G(H_2)$ and drastically reduces $G(S)$ by $G \approx 6$ in the γ radiolysis of hydrogen sulfide. The rate constant ratio $k_{H+H_2S}/k_{H+C_4H_6}$ was reported to be twice as great as that for thermal hydrogen atoms (0.26 in ref 2 and 0.20 in ref 3). However, the data for the rare gas sensitized radiolysis⁴ included only $G(S)$ and were obtained mainly at high concentrations of hydrogen sulfide in mixtures (more than 20 mol %) thus involving a large part of the primary γ -radiolysis effect.

In this contribution we present detailed results on the influence of butadiene on both hydrogen and sulfur yields at small concentrations (below 10 mol %) of hydrogen sulfide in argon, krypton, and xenon. We discuss as well how these results bear on the energetics and kinetics of charge and excitation transfer from a rare gas to hydrogen sulfide and butadiene.

Experimental Section

The experimental procedure has been fully described earlier.^{3,5,6,8} In the present experiment irradiations were performed using a ⁶⁰Co γ source at a dose rate of 5.5×10^{15} eV g⁻¹ s⁻¹ in hydrogen sulfide, which was used as a dosimeter. The concentration of hydrogen in the mixture after radiolysis never exceeded 0.05 mol % to prevent the influence of the radiolysis products on the course of radiolysis. Hydrogen yields were measured as a function of hydrogen sulfide concentration in the mixture at several overall pressures and butadiene concentrations as noted in Figures 1–3.

Hydrogen was estimated gas chromatographically (Poropak Q column) and sulfur was determined spectrophotometrically after being extracted from ampoules and converted into a thiocyanate complex.⁵

Results

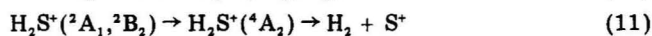
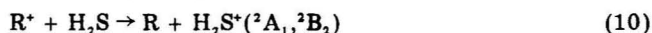
The addition of butadiene to a mixture of hydrogen sulfide and a rare gas has a very dramatic effect on the

sulfur yield: $G(S)$ decreases in all the mixtures below the limit of sensitivity of the analytical technique (ca. 0.2 atoms/100 eV). The experiment has been performed in which sulfur was extracted successively from several ampoules (of the same hydrogen sulfide and butadiene concentration) and the resulting extract was analyzed. The yield of sulfur of the order of 0.1 atoms/100 eV has been estimated in accordance with the expected $G(S)$ from a primary radiolysis of hydrogen sulfide in the presence of butadiene. The latter is equal to 0.8 ± 0.3 from previous experiments^{2,5} which should result in a value of 0.1 at a stopping power fraction of hydrogen sulfide in the mixture of 0.1 (this corresponds to 10, 17, and 25 mol % of H₂S in Ar, Kr, and Xe, respectively).

There is some disagreement between this result and those of ref 4. These authors have measured $G(S)$ for H₂S–C₄H₆–Xe and H₂S–C₄H₆–Ar mixtures and obtained $G(S)^{Xe} = 0.8$ at 22 mol % and $G(S)^{Ar} = 1.3$ at 2 mol % of hydrogen sulfide, the lowest concentration used (at butadiene concentrations of 1, 2, and 3 mol %). However, they also obtained a very large $G(S) \sim 20$ in the mixture H₂S–Ar as compared with $G(H_2) = 7.7,^8$ Meanwhile, the stoichiometry for hydrogen sulfide decomposition requires these two values to be equal. As yet, we can neither repeat their data, nor explain this discrepancy and thus we are forced to take into consideration only our results.

The dependence of $G(H_2)^t$ on the $[C_4H_6]/[H_2S]$ ratio is shown in Figures 1–3 for mixtures of hydrogen sulfide with argon, krypton, and xenon, respectively. Here $G(H_2)^t$ denotes the hydrogen yield calculated on the basis of energy absorbed by the mixture using stopping power ratios⁹ $S_{Ar}/S_{H_2S} = 0.96$, $S_{Kr}/S_{H_2S} = 1.74$, and $S_{Xe}/S_{H_2S} = 2.45$. The hydrogen yields from mixtures of butadiene with krypton and xenon have also been measured at 0.5 mol % of butadiene in each mixture. Values of 0.3 and 0.2 have been found in krypton and xenon, respectively. The hydrogen yield decreases smoothly with the $[C_4H_6]/[H_2S]$ ratio from a plateau value for a corresponding rare gas–hydrogen sulfide mixture⁸ to the $G(H_2)$ for the mixture rare gas–butadiene. No effect of the overall pressure used on $G(H_2)$ was observed.

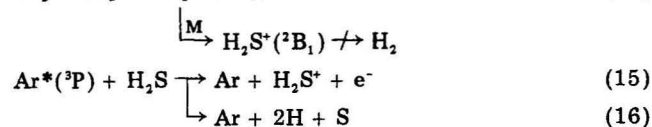
Recently, Laudenslager, Huntress, and Bowers¹⁴ have shown that charge transfer processes from the rare gas atoms to small molecules are fast when the resonance exists between RE(R⁺) and the energy required for Franck-Condon transition from the ground state molecule (AB) to the corresponding electronic state of the ion (AB⁺). It has been demonstrated in the preceding paper that the charge transfer processes in the system R-H₂S (R = Ar, Kr, and Xe) occur in accordance with this requirement. In particular, it follows from the analysis of the photoelectron spectra of hydrogen sulfide performed in ref 8 that there is a low probability for reaction 10 (R = Ar, Kr) followed by the predissociation, reaction 11.



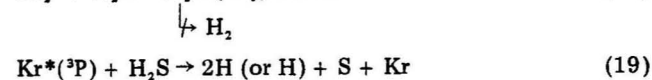
Our present finding that the S⁻ ion is not formed during a rare gas sensitized radiolysis of hydrogen sulfide supports this statement.

Xenon should be considered separately because the Xe⁺(²P_{1/2}) ion has RE = 13.44 eV, just above the AP(S⁺) = 13.40 eV produced from H₂S⁺(²A₁) via reaction 11 and thus reaction 10 should be expected to be fast. However, Dixon et al.¹⁵ concluded that between 13.40 and 13.55 eV predissociation lifetimes of the ²A₁ state are of the order of 10⁻⁸-10⁻⁶ s. Hence, at the radiolysis pressures reaction 11 can be replaced by the collisional deactivation of the H₂S⁺(²A₁) ion without giving the S⁺ ion, in accord with our experiment.

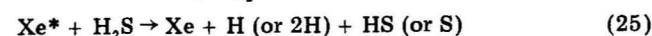
Hydrogen Formation. It has been demonstrated⁸ that the following charge and excitation transfer processes should occur in the rare gas-hydrogen sulfide mixtures: hydrogen sulfide-argon mixture



hydrogen sulfide-krypton mixture



xenon-hydrogen sulfide mixture



Reaction of the Kr⁺ ion is not shown here as it is slow compared to reaction 17 owing to a Franck-Condon gap (cf. above discussion on reaction 10 and ref 8). Reaction 22 does not lead to hydrogen formation. In the case of the

Xe⁺(²P_{3/2}) ion hydrogen formation is impossible on energetic grounds.⁸ The reaction of Xe⁺(²P_{1/2}) with hydrogen sulfide has been discussed above. Reactions 13 (followed by 14), 15, 17 (followed by 18), 22, and 23 (followed by 24) do not lead to formation of hydrogen from hydrogen sulfide¹⁶ and thus will not concern us. Reactions 20 (followed by 21) and 26 (followed by 27) are slow compared to competing reactions 19 and 25 but they become meaningful⁸ when the concentration of hydrogen sulfide in the mixture decreases below ca. 0.5 mol % (at near atmospheric pressures). Bourène and Le Calvé¹⁷ have measured the rate constants for the deexcitation of Ar(³P₂) metastable atoms by a number of molecules (the metastables R*(³P) alone take a part⁸ in the reactions listed in the above scheme). In particular, they determined the quenching rate constants for hydrogen sulfide $k_q = k_{15+16} = 8 \times 10^{-10} \text{ cm}^3 \text{ s}^{-1}$, as well as the rate constants for several hydrocarbons and have shown that the corresponding cross sections can be presented as a function of the polarizability of the molecule. Taking the proper polarizability for butadiene ($\alpha_{C_4H_6} = 8 \times 10^{-24} \text{ cm}^3$) we have found from their curve $k_{28} = 8 \times 10^{-10} \text{ cm}^3 \text{ s}^{-1}$, just the same value (within the range of the approximation used and their experimental error) as for hydrogen sulfide.



Unfortunately, the data for the deexcitation of Kr*(³P₂) and Xe*(³P₂) with hydrogen sulfide and butadiene are not available. However, Velazco and Setser¹⁸ measured the quenching cross sections for Xe*(³P₂) metastables with a set of molecules and demonstrated that the rate constants are similar to those for argon (the ratio $k_{Xe}/k_{Ar} = 0.9 + 1.6$). Therefore, it seems justified to suppose that butadiene also quenches xenon and krypton metastables with rate constants close to that for hydrogen sulfide. It was mentioned in the Experimental Section that the concentration of butadiene was kept constant through each series. It was equal 0.3 and 0.4 mol % for argon, 0.5 mol % for krypton, and 0.6 or 0.7 mol % for xenon containing mixtures. Moreover, for quantitative considerations, only points were used for which $[H_2S]/[C_4H_6] \geq 2$. Under these conditions, the overall concentration of hydrogen sulfide and butadiene was more than 1 mol %, just enough to prevent the occurrence of reactions 20 and 26.⁸ This means that metastable rare gas atoms decay solely by competitive quenching with hydrogen sulfide or butadiene in both the systems. The same is true for argon as the reaction of the formation of the excited molecule of argon, Ar₂^{*}, is even slower and was not taken into account in the scheme of reactions 12-16.

In the H₂S-C₄H₆-Ar mixture a charge transfer from the Ar⁺ ions to the H₂S molecule with the hydrogen atom formation, reaction 12, can additionally occur, being in ultimate competition with reaction 29. Reaction 12 has

been found⁸ to have a rate constant of $1.8 \times 10^{-9} \text{ cm}^3 \text{ s}^{-1}$. The rate constant for reaction 29 has not been measured as yet. The Langevin rate constant for this reaction can be calculated to be $2 \times 10^{-9} \text{ cm}^3 \text{ s}^{-1}$ if one takes $\alpha_{C_4H_6} = 8 \times 10^{-24} \text{ cm}^3$. Jones and Harrison¹⁹ determined the ratios of experimental and Langevin rate constants for the reactions of the Ar⁺ and Kr⁺ ions with methane, ethane, and ethylene. These are 0.87, 0.93, and 0.70 for the Kr⁺ ion and 0.69, 0.97, and 0.76 for Ar⁺, respectively. The number of accessible electronic states in butadiene should be larger than that in methane, ethane, or ethylene. Thus, it appears likely that in this case the value approaches even more closely to the Langevin one. Taking for reaction 29

that the dissociation of butadiene with formation of two hydrogen atoms occurs under photon impact with a relative yield equal to or 0.3 less (the quantum yield has not been measured). Thus, the relative yield of hydrogen atoms does not exceed 0.6. If this value is also accepted for energy transfer from rare gas atoms, then we obtain 0.6 or less hydrogen atoms produced in one excitation transfer event compared to ca. 1.5 atoms from hydrogen sulfide.

Reaction 35b with formation of one hydrogen atom is energetically possible for all the three rare gas ions as $AP(C_4H_5^+) = 11.6$ eV.²¹ However, the $C_3H_3^+$ ion is also produced at this energy ($AP = 11.7$ eV²¹) without formation of a hydrogen atom. Also, the parent butadiene ion, $C_4H_6^+$, ($IP(C_4H_6) = 9.2$ eV²¹) has several bonding states in the range of 11–15 eV which can be expected to be partially deactivated without decomposition of the ion. So, reaction 35b cannot be fully excluded but it can be supposed that it is not a major path for charge transfer from argon, krypton, and xenon ions to butadiene. Therefore it contributes to formation of hydrogen atoms with a yield significantly lower than the yield of the corresponding rare gas ions. On the other hand, reaction 36 is known to occur to a small extent ($k_{36}/k_2 = 0.02$) even with thermal hydrogen atoms in the photolysis experiments.²² Dzantiev et al.^{23,24} have also shown that hot hydrogen atoms produced photolytically with a kinetic energy of ca. 1 eV abstract hydrogen atoms from ethylene and propylene with a rate constant equal to that of reaction 1. Additionally, they demonstrated²⁵ that argon is very inefficient in thermalizing hot hydrogen atoms. On this basis, it may be inferred that reaction 36 proceeds under the conditions of the present experiments with a rate constant similar to that of reaction 1. To support this supposition, it should be emphasized that evidence has been recently obtained in this laboratory⁶ that hot hydrogen atoms are produced in the xenon sensitized radiolysis of hydrogen sulfide which effectively abstract halogen atoms from CCl_4 and SF_6 and an oxygen atom from N_2O molecules at conditions similar to those in the present experiment.

Thus, none of the reactions 34–36 may be fully excluded. It is not possible to make a kinetic analysis including all these reactions simultaneously. Therefore two extreme, simplified cases have been considered: (i) Reactions 34b and 35b compensate fully for a decrease in G_H from hydrogen sulfide caused by reaction 33, and reaction 36 does not occur. Then eq II is valid, and the k_1/k_2 ratio is equal to 0.22 and 0.18 for xenon and krypton, respectively. (ii) Reactions 34b and 35b can be neglected, and reaction 36 occurs with $k_{36} = k_1$ which compensates for a decrease in a hydrogen yield caused by reaction 33. Now we obtain eq III which has the same form as eq II. However, a sum

$$\frac{1}{G(H_2)^t} = \frac{1}{G_H^0} \left(1 + \frac{k_2 + k_{36} [C_4H_6]}{k_1 [H_2S]} \right) \quad (III)$$

$k_2 + k_{36}$ appears now instead of k_2 alone. The corresponding plots are shown in Figures 4 and 5 (closed circles). The intercept gives a value of $G_H^0 = 6.1$ for both xenon and krypton. This agrees fairly well with our previous results obtained directly from the plateau of $G(H_2)^R$ in the radiolysis of binary rare gas–hydrogen sulfide mixtures.⁸ These have been determined as 5.4 and 5.5 xenon and krypton, respectively.

From the slope and intercept of the lines the rate constant ratios $k_2 + k_{36}/k_1 = 4.6$ (for Kr) and 5.6 (for Xe) were determined. Keeping in mind that $k_1 = k_{36}$ we obtain $k_1/k_2 = 0.28$ for krypton and 0.22 for xenon. The actual

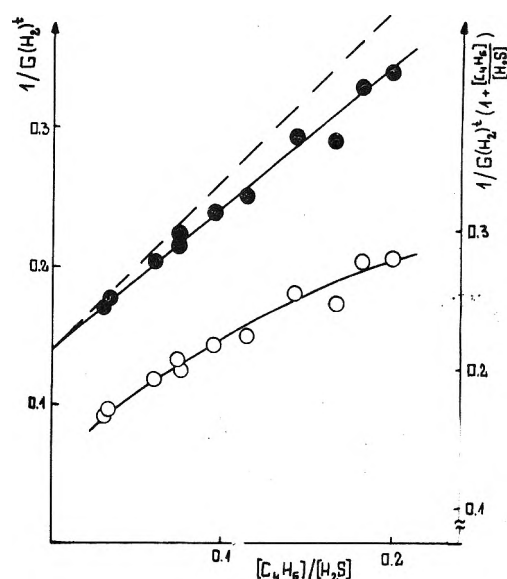


Figure 6. Experimental plots of eq I (right-hand ordinate, open circles) and eq III (left-hand ordinate, close circles) for irradiated H₂S–C₄H₆–Ar mixture. Broken line as in Figure 4.

TABLE I: Mean Excess Energy per One Hydrogen Atom Produced in Reactions 12, 16, and 32 (eV)

Reaction 32					
1 H atom produced		2 H atom produced		Reaction 12 Argon	Reaction 16 Argon
Xenon	Krypton	Xenon	Krypton		
4.4	6.0	0.4	1.2	0	1.9

values may be expected to lie between those obtained from eq II and III. Both sets of values are significantly larger than 0.11, the ratio found from experiments with thermal hydrogen atoms.²² However, they are just in the range of data from the γ radiolysis of hydrogen sulfide in the presence of butadiene (0.20^{1,3} and 0.26²) where a higher mean kinetic energy of hydrogen atoms was claimed. The higher value of k_1/k_2 for krypton is compatible with the higher energy for the $Kr^*(^3P_2)$ state reported as 9.91 eV compared to that for $Xe^*(^3P_2)$ equal to 8.31 eV,²⁶ provided that reaction 32 occurs via the same path in both the cases.

In the case of argon reaction 12 should be coupled to the set of reactions considered for xenon and krypton. If this is done and a ratio $[C_4H_6]/[H_2S] \leq 0.2$ is maintained, as discussed above, relationships identical with eq II or III can be obtained. However this time the intercept corresponds to G_H^0 produced in reactions 12, 16, and 31. A plot of $1/G(H_2)^t$ against the $[C_4H_6]/[H_2S]$ ratio presented in Figure 6 shows the expected linearity. The right-hand ordinate corresponds to eq I, exactly as for krypton and xenon. The intercept gives $G_H^0 = 7.2$, close to the one (7.0 atoms/100 eV) found from the plateau value of $G(H_2)^{Ar}$ in the radiolysis of the hydrogen sulfide–argon mixture.⁸ The rate constant ratio calculated from the slope (7.2) and intercept of the line in Figure 6 is $k_1/k_2 = 0.14$ (eq 5) and 0.16 (eq III). This is appreciably less than k_1/k_2 in krypton and xenon and should indicate that the mean kinetic energy of the hydrogen atom is significantly lower than that in krypton and xenon.

The mean excess energy per one hydrogen as found from the energetics²⁷ of reactions 12, 16, and 32 is shown in Table I. The assumption has been made that electronic and/or vibrational excitation of the products consumes only a small part of the excess energy as was shown for photochemical destruction of the hydrogen sulfide mol-

ecule.²⁸ It is seen from Table I that for the mean energy of hydrogen atoms in krypton and xenon to be appreciably higher than that in argon the supposition should be made that reaction 32 occurs to a large part with production of one hydrogen atom. This is in accord with the conclusion of ref 6, where the high kinetic energy of hydrogen atoms was assumed to explain the occurrence of halogen abstraction reactions from CCl_4 and SF_6 and oxygen abstraction from N_2O which effectively compete with reaction 1 in the xenon sensitized radiolysis of the corresponding mixtures.

On the other hand, it follows from ref 29 that the formation of the SH^+ ion occurs via predissociation of $^2\text{A}'$ state through the $^4\text{A}''$ state of the H_2S^+ ion. If SH^+ ion production in reaction 12 follows the same path, hydrogen atoms without an excess kinetic energy should be expected. It indicates that only reaction 16 actually leads to hot hydrogen atoms in argon.

Finally, it is well to note that an actual value of the coefficient before the H atom in reaction 32 (1 or 2) does not affect our kinetic equations. The only alteration appears in the value of G_{R^*} .

The foregoing discussion, as well as that in ref 8, has been based on the widely accepted supposition that the decomposition of an admixture in the rare gas sensitized radiolysis occurs mainly via charge and excitation transfer from the rare gas to the admixture molecule. If this assumption is valid, our estimation gives $2.7 < G_{\text{Xe}^*} < 5.4$, $2.8 < G_{\text{Kr}^*} < 5.5$, and $G_{\text{Ar}^*} = 3.5$.⁸ The higher and the lower limits for krypton and xenon correspond to the production of one and two hydrogen atoms, respectively, in reactions 19 and 25. Recently, Nagra and Armstrong³⁰ have measured $G(\text{H}_2)$ from a mixture of HBr (20 mol %) with Xe to equal 9.1. If we extract from this value the hydrogen yield from electron capture processes equal³⁰ to $G(e^-)^{\text{Xe}} = 4.6$, then we find $G_{\text{Xe}^*} = 4.5$, a value which lies well within our range of G_{Xe^*} .

These values can be compared with those possible on the grounds energetic considerations. If we take²⁶ $G_{\text{Kr}^*} = 4.2$, $G_{\text{Xe}^*} = 4.6$, the ratio $^2\text{P}_{3/2}/^2\text{P}_{1/2} = 2:1$, and the ionization potentials of $\text{Kr}^+(^2\text{P}_{3/2})$, $\text{Kr}^+(^2\text{P}_{1/2})$, $\text{Xe}^+(^2\text{P}_{3/2})$, and $\text{Xe}^+(^2\text{P}_{1/2})$ equal to 14.0, 14.7, 12.1, and 13.5 eV, respectively, then the energy required for ion formation should be at least 60 eV for Kr and 58 eV for Xe. Taking a mean excitation energy for the lowest four states of krypton and xenon equal to 10.3 and 9.0 eV, respectively, we find $G_{\text{Xe}^*}^{\text{max}} = 4.7$ and $G_{\text{Kr}^*}^{\text{max}} = 4.0$.

These calculations do not however take into account subexcitation electrons. Meanwhile the energy removed by subexcitation electrons may not be neglected. The mean energy of subexcitation electrons, $\bar{\varepsilon}$, can be estimated³¹ from

$$\bar{\varepsilon} = E_0 \left/ \left(2 + \frac{E_0}{\text{IP}} \right) \right. \quad (\text{IV})$$

where E_0 is the threshold energy of electronic excitation and IP is the ionization potential of the molecule involved. Using $\bar{\varepsilon}$ from eq IV and $G(e^-)$ we obtain for the total energy (per 100 eV absorbed) removed by subexcitation electrons 16.3, 15.9, and 14.7 eV in Ar, Kr, and Xe, respectively. This value may be estimated to be somewhat lower if we use $\bar{\varepsilon} = E_0/3$, as it was done by Willis and Boyd in a recent review.³² Then we obtain 14.8, 14.2, and 13.8 eV for Ar, Kr and Xe. Even if we use these lower values, we obtain the energy available for excitation $E_{\text{exc}} = 100 - (\text{IP} + \bar{\varepsilon})G(e^-)$ equal to 25, 26, and 28 eV for Ar, Kr, and Xe, respectively. Hence the corrected $G_{\text{R}^*}^{\text{max}}$ are equal to 2.1, 2.5, and 3.1 for argon, krypton, and xenon. These

values are well below the one necessary to be compatible with our and Woodward's results in argon,⁸ are less than the lower limit from our measurements for krypton, and are in our range of G_{Xe^*} , but well below the value evaluated above from the data of ref 28.

We believe that this discrepancy is not caused by experimental errors but rather that it demonstrates that in the binary systems the role of the electrons subexcited with respect to the main component should not be neglected because the energy of these electrons is deposited entirely in the second component. Thus, the low energy electrons should result in the primary decomposition of the low concentration component giving an additional significant yield of fragmentation. From the difference between the experimental estimation and the values calculated in the above discussion it seems to be ca. 1.4 for argon and xenon.

In ternary mixtures, a competition between hydrogen sulfide and butadiene for low energy electrons should be expected which leads to a similar effect as considered for excitation processes. Thus, the extreme case (i) discussed above actually includes not only reactions 33, 34b, and 35b but also (to a smaller extent) corresponding reactions with low energy electrons.

In spite of a large number of data on electron scattering by molecules,³³ there exist only few results on the dissociation of the molecules electronically excited by low energy electron impact. However, in a recent review Polak and Slovetsky³⁴ calculated cross sections for some simple molecules and have shown that there is a sharp increase in σ_{diss} immediately above threshold, $\sigma_{\text{diss}}^{\text{max}}$ reaching a value on the order of 10^{-16} cm^2 . This leads us to believe that the observed difference between the calculated and experimental values of G_{R^*} is due to the additional fragmentation of molecules of the second component by electrons with energy below the excitation threshold of a rare gas. This demonstrates a sizable role of subexcitation electrons in the irradiation of mixtures with rare gas as a main component, which has heretofore not been quantitatively established.

References and Notes

- (1) M. Foryś and E. Migdal, *Khim. Vys. En.*, **5**, 228 (1971).
- (2) D. W. Huyton and T. W. Woodward, *J. Chem. Soc., Faraday Trans.*, **1**, **69**, 467 (1973).
- (3) I. Szamrej, A. Jówko, and M. Foryś, *Radiat. Effects*, **25**, 191 (1975).
- (4) D. W. Huyton and T. W. Woodward, *J. Chem. Soc., Faraday Trans.*, **1**, **68**, 1857 (1972).
- (5) A. Jówko, I. Szamrej, and M. Foryś, *Radiochem. Radioanal. Lett.*, **15**, 353 (1973).
- (6) M. Foryś, *Radiat. Effects*, **25**, 111 (1975).
- (7) K. Jezierska and M. Foryś, *Nukleonika*, **17**, 23 (1972).
- (8) M. Foryś, A. Jówko, and I. Szamrej, *J. Phys. Chem.*, **80**, 1035 (1976).
- (9) D. W. Huyton and T. W. Woodward, *Radiat. Res. Rev.*, **2**, 205 (1969).
- (10) W. T. Huntress, Jr., and R. F. Pinizzotto, Jr., *J. Chem. Phys.*, **59**, 4742 (1973).
- (11) L. G. Christophorou and R. P. Blaunstein, *Chem. Phys. Lett.*, **12**, 173 (1971).
- (12) V. I. Vedeneyev, L. V. Gurvich, V. N. Kondrat'yev, V. A. Medvedev, and Y. L. Frankevich, "Bond Energies, Ionization Potentials and Electron Affinities" (in Russian), Academy of Sciences of the USSR, Moscow, 1962.
- (13) W. E. W. Ruska and I. L. Franklin, *Int. J. Mass Spectrom. Ion Phys.*, **3**, 221 (1969).
- (14) J. B. Laudenslager, W. T. Huntress, Jr., and M. T. Bowers, *J. Chem. Phys.*, **61**, 4600 (1974).
- (15) R. N. Dixon, G. Duxbury, M. Horani, and J. Rostas, *Mol. Phys.*, **22**, 977 (1971).
- (16) It has been shown before that hydrogen is not produced in the neutralization processes in hydrogen sulfide containing mixtures.^{3,5,8}
- (17) M. Bourène and J. Le Calvé, *J. Chem. Phys.*, **58**, 1452 (1973).
- (18) J. E. Velazco and D. W. Setser, *Chem. Phys. Lett.*, **25**, 197 (1974).
- (19) E. G. Jones and A. G. Harrison, *Int. J. Mass Spectrom. Ion Phys.*, **6**, 77 (1971).
- (20) R. D. Doepker, *J. Phys. Chem.*, **72**, 40 (1968).
- (21) "Ionization Potentials, Appearance Potentials, and Heats of Formation of Gaseous Positive Ions", *Natl. Stand. Ref. Data Ser., Natl. Bur. Stand.*, No. 28 (1969).

- (22) G. R. Wooley and R. J. Cvetanovic, *J. Chem. Phys.*, **50**, 4697 (1969).
 (23) B. G. Dzantiev, A. K. L'ubimova, and A. V. Shishkov, *Khim. Vys. En.*, **3**, 478 (1969).
 (24) B. G. Dzantiev, A. V. Shishkov, and M. S. Unukovitsch, *Khim. Vys. En.*, **2**, 571 (1968).
 (25) B. G. Dzantiev, O. S. Shirmschuk, and A. V. Shishkov, *Khim. Vys. En.*, **4**, 363 (1970).
 (26) B. Brocklehurst, *Radiat. Res. Rev.*, **1**, 223 (1968).
 (27) The following data were used for calculations: Xe(³P₂) 8.3 eV; Kr(³P₂) 9.9 eV; Ar(³P₂) 11.6 eV; RE(Ar⁺) = 15.8 eV;²⁶ D(H-SH) = 3.9 eV; D(S-H) = 3.6 eV;¹² AP(SH⁺) = 14.2 eV.²⁹
- (28) L. E. Compton, J. L. Gole, and R. M. Martin, *J. Phys. Chem.*, **73**, 1158 (1969).
 (29) F. Fiquet-Fayard and P. M. Guyon, *Mol. Phys.*, **11**, 17 (1966).
 (30) S. S. Nagra and D. A. Armstrong, *Can. J. Chem.*, **53**, 3305 (1975).
 (31) I. Santar and J. Bednar, *Collect. Czech. Chem. Commun.*, **34**, 1 (1969).
 (32) C. Willis and A. W. Boyd, *Int. J. Radiat. Phys. Chem.*, **8**, 71 (1976).
 (33) See, e.g., L. G. Christophorou, "Atomic and Molecular Radiation Physics", Wiley-Interscience, New York, N.Y., 1971.
 (34) L. S. Polak and D. J. Slovetsky, *Int. J. Radiat. Phys. Chem.*, **8**, 257 (1976).

Rate Constants for the Reaction of Hydrogen and Deuterium Atoms with Silane

D. Mihelcic, V. Schubert, R. N. Schindler,[†]

Institut für Physikalische Chemie der Kernforschungsanlage Jülich GmbH, Jülich, West Germany

and P. Potzinger*

Institut für Strahlenchemie im Max-Planck-Institut für Kohlenforschung, Mülheim a.d. Ruhr, West Germany (Received October 20, 1975; Revised Manuscript Received March 10, 1977)

Publication costs assisted by the Max-Planck-Institut für Kohlenforschung

The rate constants for the reaction of hydrogen and deuterium atoms with silane have been measured in a pulse radiolytic experiment. The values found for the rate constants were $k(\text{H} + \text{SiH}_4) = (4.6 \pm 0.3) \times 10^{-13} \text{ cm}^3 \text{ s}^{-1}$ and $k(\text{D} + \text{SiH}_4) = (3.4 \pm 0.3) \times 10^{-13} \text{ cm}^3 \text{ s}^{-1}$.

Introduction

A number of papers has appeared in the last few years concerning the rate of hydrogen abstraction from silane by hydrogen atoms.¹⁻⁸ Up to now, rate constants for hydrogen abstraction from SiH₄ by H and D atoms and from SiD₄ by H atoms have been reported.

The values of the measured or estimated rate constants for the reaction



show a large scatter differing by more than a power of ten. Niki and Mains⁹ estimated from scavenger experiments a value for the rate constant comparable with or larger than that for the hydrogen atom addition to ethylene. On the other hand, Hong,¹ from the same laboratory, using steady state photolysis with Lyman α photometry reported a much lower value. Moortgat,² using a flow technique, obtained a value very similar to that of Hong. In preliminary flow experiments aimed at the determination of the rate constant for the reaction



we also observed a very fast disappearance of D atoms, however, without a corresponding formation of HD.¹⁰ This led one of us to propose that a silane catalyzed D atom recombination was taking place involving the formation of the SiH₄D species.¹¹ A more thorough investigation showed that at low values for the ratio SiH₄/D₀ an effective heterogeneous wall recombination process was responsible for the D atom removal, and only for values of this ratio >50 was the disappearance of the D atoms mainly due to a homogeneous gas-phase abstraction reaction.⁴ Steady state photolysis was used by Strausz and co-workers³ and by one of us⁵ to determine the rate constant for reaction 2 relative to the rate constant for the addition of D atoms

to C₂D₄. If one uses the recently measured rate constant for $k(\text{D} + \text{C}_2\text{D}_4)$ ¹² one can convert these rate constants into absolute values. The agreement between these two values and the values from the flow experiments^{4,6} can be considered satisfactory.

Steady state photolyses was also used in two experiments^{5,8} to determine the rate constant for the reaction



Recently Michael⁶ and Gaspar⁷ reported on the determination of an absolute rate constant for the reaction of hydrogen atoms with silane, using a flow system. In ref 6, rate constants are also given for reaction 2 and for the reaction of H and D atoms with methylsilanes. The measured rate constants in ref 6 and 7 for H + SiH₄ were very much larger than one would have anticipated from the results of the isotopic reactions discussed above. The experiments were reportedly hampered by heterogeneous processes. On the other hand, the rate constant for (2) given in ref 6 is in good agreement with the other values mentioned above. If one would accept both values to be truly homogeneous gas phase values, one is left with explaining an enormously large isotope effect.

It is felt that for these reasons a redetermination of the rate constants for processes 1 and 2 is justified using experimental conditions which exclude wall effects and suppress secondary reactions.

Experimental Section

Our experimental setup was similar to that of Bishop and Dorfman¹³ with the exception that a 1-m Jarrel-Ash vacuum-ultraviolet monochromator with a dispersion of 8.3 Å/mm was used for the isolation of the resonance line instead of the unfiltered light from the discharge lamp (see Figure 1).

The following special features should be emphasized: (a) The analyzing light source was a windowless, differentially

[†] Present address: Institut für Physikalische Chemie, Universität Kiel, D 2300 Kiel, West Germany.

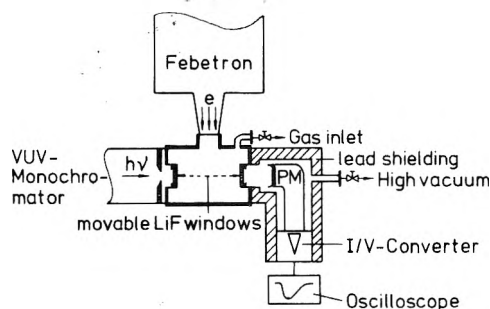


Figure 1. Apparatus.

pumped hydrogen or deuterium lamp with a pressure of 3 Torr in the discharge region. Due to the comparatively large distance between the lamp and Febetron, the stability of the light source was not affected by the electron pulse.

(b) The half-lifetime of H atoms in pure H_2 was ~ 95 ms at 800 Torr. The lifetime was reduced by more than two orders of magnitude when silane was present. Contributions from homogeneous three-body recombination or diffusion to the wall was thus considered unimportant in the time range of interest for the determination of the rate constants.

(c) The optical path length in the stainless steel absorption cell could be varied between 19, 31, and 65 mm. Good linearity was observed between optical density (OD) and hydrogen pressure with this arrangement under all experimental conditions for optical path lengths of 19 and 31 mm. For a 65-mm path length deviation was observed at pressures >1600 Torr for OD values >2 . Most kinetic measurements were carried out under experimental conditions to obtain an OD around 0.15.

(d) The recovery time of the electronic detection system was $\leq 7 \mu s$. The housing of the photomultiplier, Type 641 G 08-18 from EMR Photoelectric, was filled with lead to reduce the pick-up of signals induced by the electron pulse.

(e) All runs were conducted at hydrogen pressures between 800 and 1700 Torr with less than 1% SiH_4 added. For metering of silane a Baratron pressure meter was employed. The high total pressure in the reaction chamber together with a time resolution in the microsecond range ensured that in these static experiments wall effects could be entirely neglected. Furthermore, it was demonstrated that the reactions are observed in the pressure independent region.

Single electron pulses of 4-ns half-width from a Febetron 701 generator which entered the chamber through a 0.025-mm steel foil produced H or D atoms in the reaction cell at a concentration of roughly 10^{13} atoms cm^{-3} , depending on experimental settings. Thus, the substrate concentration was always in at least 1000-fold excess over the initial H or D atom concentration. Details are given elsewhere.¹²

Results and Discussion

The experimental results of our kinetic study are displayed in Figure 2. The error bars give the standard deviation of at least triplicate measurements. Within experimental scatter, no pressure dependence is observed in the range studied.

A pressure dependence in this system could only come from secondary reactions. A process which has to be considered is the recombination between hydrogen atoms and silyl radicals (reaction 4) giving rise to chemically activated silane.

$$H + SiH_3 \rightarrow SiH_4^* \quad (4)$$

The route of decomposition of a vibrationally excited silane, unfortunately, is not yet es-

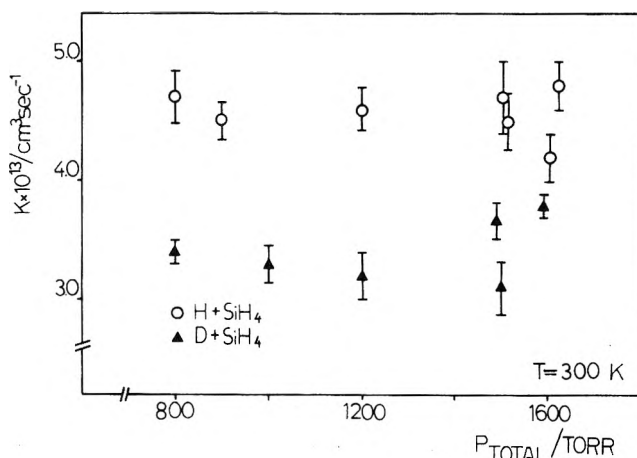


Figure 2. Pressure dependence of the rate constants for the reactions $H + SiH_4$ and $D + SiH_4$.

ablished. Purnell and Walsh¹⁴ favor a molecular hydrogen loss (reaction 5) while Ring and co-workers¹⁵ put forward



arguments in favor of Si-H bond rupture (reaction 6). If Purnell's mechanism is operating then there is no chance of stabilizing the activated silane due to the high exothermicity of process 5. No pressure dependence is expected, and the appearance of a secondary reaction would leave us with a higher apparent rate constant than expected for abstraction reaction 1 alone.

If, on the other hand, the silane decomposes back to the reactants (reaction 6) a rough estimate using the RRR theory seems to indicate that even in this case a stabilization is not possible, and the appearance of (4) would not falsify the rate constant for (1), but it would in the case of the rate constant for (2).

To estimate the extent of the secondary reaction 4, we solved the coupled differential equations for reactions 1, 4, and 7 assigning the following values to the rate constants:

$$2SiH_3 \rightarrow Si_2H_6 \quad (7)$$

$k_1 = 4.5 \times 10^{-13} cm^{-3} s^{-1}$, $k_4 = 5 \times 10^{-10} cm^{-3} s^{-1}$, and $k_7 = 3 \times 10^{-10} cm^{-3} s^{-1}$. k_7 has been taken to be the same as for the recombination of two trimethylsilyl radicals¹⁶ while k_4 is an estimate. After one half-life of the hydrogen atoms, 15% of them have disappeared by reaction 4. Decreasing k_4 by a factor of 2 brings the share of reaction 4 with respect to the hydrogen atom consumption down to well within our given error limits. The good agreement between our pulse radiolytic value for reaction 2 and a value obtained in a steady state photolysis system,⁵ where secondary reaction 4 is certainly excluded, lends further support to the unimportance of (4).

In Table I our experimental results are compared with published rate constants obtained using different experimental techniques. Our calculated values are also included.

The rate constant for $D + SiH_4$ is in good agreement with earlier determinations. For the reaction $H + SiH_4$ we find a value much lower than of Michael et al.⁶ and even lower yet than that found by Gaspar et al.⁷ One can only surmise that this difference is caused by wall effects and/or secondary reactions.

It was stated by several authors that the kinetic results are not in agreement with the known bond energies and that the BEBO method,¹⁷ for example, does not furnish values for the rate constants which agree with those found

TABLE I

Reaction	<i>p</i> , Torr	[SiH ₄] ₀ /[H] ₀	<i>T</i> , K	10 ¹³ <i>k</i> , cm ³ s ⁻¹		Remarks	Ref
				Expt	Calcd		
H + SiH ₄	800–1700 H ₂	<10 ³	300	4.6 ± 0.3	5,4	Pulse radiolyses/Lyman α	This work
			Room temp	2.5 ± 0.7		Steady state photolyses/Lyman α	1
		0.01	Room temp	>2.2		Flow reactor/mass spectrometer	2
	<5 He	Excess reactant	Room temp	26		Flow reactor/mass spectrometer	6
	20 He	<150 > 2	300	85 ± 7		Flow reactor/Lyman α	7
[SiH ₄] ₀ /[D] ₀							
D + SiH ₄	800–1600 D ₂	≥10 ³	Room temp	3.4 ± 0.3	(3.5)	Pulse radiolyses/Lyman α	This work
	4 Ar	<200	Room temp	3.0 ± 1		Flow reactor/EPR	4
	<5 He	0.03–0.013	Room temp	3.0 ± 0.7		Flow reactor/mass spectrometer	6
	3 He	5	Room temp	4.5 ± 0.5		Flow reactor/mass spectrometer	6
	<100		298	4.5		Steady state photolyses	3
	<150		298	3.7 ± 0.3		Steady state photolyses	5
[SiD ₄] ₀ /[H] ₀							
H + SiD ₄	<150		298	2.8	3.9	Steady state photolyses	This work
	<1280 He		Room temp	<3.0		Steady state photolyses	8
[SiD ₄] ₀ /[D] ₀							
D + SiD ₄				2.6			This work

experimentally for hydrogen abstraction from silane and trimethylsilane. Even changes representing the trends with methylation are not correctly exhibited.^{6,11,18} The experimental results were interpreted to indicate that hydrogen abstraction from silane and trimethylsilane proceed by different mechanisms, the silane proceeding by a SiH₅ intermediate as opposed to a direct mechanism in the trimethylsilane case.^{6,7,11} In the case of hydrogen abstraction by methyl radicals, no changes in the activation energy were observed going from silane to trimethylsilane and, in addition, the *A* factor for these two reactions is identical if one takes reaction path degeneracy into account.^{18–20} This finding does not support the hypothesis that there are two abstraction mechanisms operating.

From the data presented, it is concluded, that the apparent discrepancies between theory and experiment are due partly to wrong input data, particularly bond dissociation energies, and partly due to wrong experimental results.

A recent mass spectrometric determination of bond energies in silane and methylsilanes²¹ has shown that the Si–H bond energy is not as dependent on the degree of methylation, as earlier results suggested.^{22,23} Within rather large error limits, we found for the Si–H bond dissociation energy a value of $D(\text{Si–H}) = 89 \pm 4$ kcal/mol, independent of the extent of methylation. From kinetic experiments, this value is confirmed for trimethylsilane (Me₃SiH).^{24,25} For the bond energy in silane, upper limits of 90 and 87 kcal/mol are given.^{26,27} From the reaction of hot tritium atoms with silanes, Hosaka and Rowland²⁸ estimate that the bond energy changes only by 2–3 kcal/mol upon methylation.

For our BEBO calculation, we used the same input data as given earlier¹¹ except that for $D_e(\text{H}_3\text{Si–H})$ a value of 92 kcal/mol was chosen. The Sato parameter was adjusted such that there exists agreement between the calculated and now generally accepted experimental rate constant for $k(\text{D} + \text{SiH}_4)$. In this fashion we obtain the values for k_{calcd} given in Table I. Taking into account the new bond dissociation values of 89 kcal/mol independent of methylation the BEBO method furnishes values close to those obtained experimentally for the hydrogen abstraction by methyl radicals as well as by hydrogen atoms. For the reaction of H or D atoms respectively with Me₃SiH, we

calculate $k(\text{H} + \text{Me}_3\text{SiH}) = 3.2 \times 10^{-13} \text{ cm}^3 \text{ s}^{-1}$ and $k(\text{D} + \text{Me}_3\text{SiH}) = 2.1 \times 10^{-13} \text{ cm}^3 \text{ s}^{-1}$. These two values are also in good agreement with experiments.^{6,29}

In conclusion one can say that silanes behave quite “normally” with respect to H abstraction and no esoteric reaction model has to be assumed.

References and Notes

- (1) J.-H. Hong, Ph.D. Thesis, University of Detroit, 1972.
- (2) G. K. Moortgat, Ph.D. Thesis, University of Detroit, 1970.
- (3) K. Obi, H. S. Sandhu, H. E. Gunning, and O. P. Strausz, *J. Phys. Chem.*, **76**, 3911 (1972).
- (4) U. Mihelcic, P. Potzinger, and R. N. Schindler, *Ber. Bunsenges. Phys. Chem.*, **78**, 82 (1974).
- (5) P. Potzinger, L. C. Glasgow, and B. Reimann, *Z. Naturforsch. A*, **29**, 493 (1974).
- (6) J. A. Cowfer, K. P. Lynch, and J. V. Michael, *J. Phys. Chem.*, **79**, 1139 (1975).
- (7) K. Y. Choo, P. P. Gaspar, and A. P. Wolf, *J. Phys. Chem.*, **79**, 1752 (1975).
- (8) B. Reimann and P. Potzinger, *Ber. Bunsenges. Phys. Chem.*, **80**, 565 (1976).
- (9) H. Niki and G. J. Mains, *J. Phys. Chem.*, **68**, 304 (1964).
- (10) D. Mihelcic, P. Potzinger, and R. N. Schindler, unpublished results.
- (11) L. C. Glasgow, G. Olbrich, and P. Potzinger, *Chem. Phys. Lett.*, **14**, 466 (1972).
- (12) D. Mihelcic, V. Schubert, F. Höfler, and P. Potzinger, *Ber. Bunsenges. Phys. Chem.*, **79**, 1230 (1975).
- (13) W. P. Bishop and L. M. Dorfman, *J. Chem. Phys.*, **52**, 3210 (1970).
- (14) J. H. Purnell and R. Walsh, *Proc. R. Soc. London, Ser. A*, **543** (1966).
- (15) M. A. Ring, M. J. Puentes, and H. E. O'Neal, *J. Am. Chem. Soc.*, **92**, 4845 (1970); C. H. Haas and M. A. Ring, *Inorg. Chem.*, **14**, 2253 (1975).
- (16) P. Cadman, G. M. Tilsley, and A. F. Trotman-Dickenson, *J. Chem. Soc., Faraday Trans. 1*, **68**, 1849 (1972).
- (17) H. S. Johnston, “Gas-Phase Reaction Rate Theory”, Ronald Press, New York, N.Y., pp 339 ff.
- (18) E. R. Morris and J. C. J. Thynne, *J. Phys. Chem.*, **73**, 3294 (1969).
- (19) O. P. Strausz, E. Jakubowski, H. S. Sandhu, and H. E. Gunning, *J. Chem. Phys.*, **51**, 552 (1969).
- (20) I. A. Kerr, D. H. Slater, and J. C. Young, *J. Chem. Soc. A*, **134** (1968).
- (21) P. Potzinger, A. Ritter, and J. Krause, *Z. Naturforsch. A*, **30**, 347 (1975).
- (22) P. Potzinger and F. W. Lampe, *J. Phys. Chem.*, **73**, 3912 (1969).
- (23) I. M. T. Davidson and I. L. Stephenson, *J. Chem. Soc. A*, **282** (1968).
- (24) I. M. T. Davidson and A. V. Howard, *J. Chem. Soc., Faraday Trans. 1*, **71**, 69 (1975).
- (25) R. Walsh and I. M. Wells, *J. Chem. Soc., Chem. Commun.*, **513** (1973).
- (26) K. J. Reed and J. I. Brauman, *J. Chem. Phys.*, **61**, 4830 (1974).
- (27) W. H. Dueser and D. W. Setser, *J. Chem. Phys.*, **58**, 2310 (1973).
- (28) A. Hosaka and F. S. Rowland, *J. Phys. Chem.*, **77**, 705 (1973).
- (29) M. A. Contineanu, D. Mihelcic, R. N. Schindler, and P. Potzinger, *Ber. Bunsenges. Phys. Chem.*, **75**, 426 (1971).

Rate Constants for the Reactions of Hydrogen Atoms with Methylgermanes¹

E. R. Austin and F. W. Lampe*

Davey Laboratory, Department of Chemistry, The Pennsylvania State University, University Park, Pennsylvania 16802 (Received December 30, 1976)

Publication costs assisted by the U.S. Energy Research and Development Administration

Absolute rate constants for the reaction of H atoms, formed by mercury photosensitization of H₂-substrate mixtures at 32 °C, with (CH₃)_nGeH_{4-n} for n = 1, 2, 3 have been determined in experiments involving the competitive reaction of H atoms with Si₂H₆. Arrhenius parameters and bond dissociation energies have been estimated for this series of methylgermanes.

Introduction

While considerable kinetic information pertaining to the gas-phase reactions of radicals with various silanes and alkylsilanes has become available during the last 10 years,²⁻³³ very little kinetic data are available for radical reactions with germanes^{31,33} and no such information exists for methylgermanes containing Ge-H bonds. Recently we have developed a mass-spectrometric technique to measure rate constants for the reaction of hydrogen atoms with various silanes and mono- and digermane,³³ and it seemed worthwhile to apply this same technique to the methylgermanes.

We have conducted mass-spectrometric studies of the rates of hydrogen-atom induced decomposition of the methylgermanes relative to the rate of hydrogen-atom reaction with disilane at 32 °C. From these studies we have determined the specific reaction rates for hydrogen-atom attack on the methylgermanes, and this paper is a report of our results.

Experimental Section

Hydrogen atoms were generated by Hg(³P₁) photosensitization of hydrogen-substrate mixtures which contained about 98% hydrogen. Under these conditions more than 95% of the Hg(³P₁) atoms that are collisionally quenched react with hydrogen to yield hydrogen atoms. At the total pressures used in these experiments, namely 30-60 Torr, gas-phase recombination of hydrogen atoms and diffusion of hydrogen atoms to the walls are negligible when compared with the rates of reaction with substrate molecules^{21,33} (cf. Table I).

The reactions were carried out in a photolysis cell containing a pin-hole leak leading into the ionization region of a Bendix Model 14-101 time-of-flight mass spectrometer. The photolysis cell is connected via 1/4-in. stainless steel and 6-mm Pyrex tubing to large reservoirs (5-12 L) containing the reactants. Reactant gases thus flow continuously through the pin-hole leak into the mass spectrometer. The flow rates are such that during the course of a single experiment (typically 2-3 min) the pressure decrease in the reservoir is of the order of 0.5% or less. The apparatus has been previously described in detail.²⁴

The source of 2537-Å radiation for generation of Hg(³P₁) atoms was a General Electric 4-W G4T4/1 germicidal lamp. Measurements of the initial rate of formation of n-C₄H₁₀ in H₂-C₂H₄ mixtures indicate that in our experiments the lower limit for the rate of formation of hydrogen atoms was 6.7 × 10¹³ atom/cm³ s.³³ The temperature of the photolysis cell was measured using a chromel-alumel thermocouple and was found to be 32 ± 2 °C.

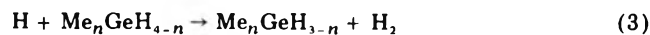
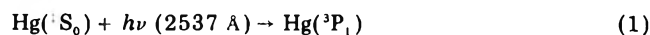
TABLE I: Rate Constants for H-Atom Induced Decomposition at 32 °C

Substrate	m/e	No. of runs	k ₃ (k ₄ + k ₅)	k ₃ (cm ³ /s) × 10 ¹²
CH ₃ GeH ₃	74	11	0.84 ± 0.08	3.1 ± 0.6
(CH ₃) ₂ GeH ₂	90	11	0.90 ± 0.06	3.3 ± 0.6
(CH ₃) ₃ GeH	105	11	1.22 ± 0.07	4.5 ± 0.7
(CH ₃) ₄ Si	88	1		< 0.01
(CH ₃) ₄ Ge				< 0.01
(CH ₃) ₄ Sn	165	2		< 0.01

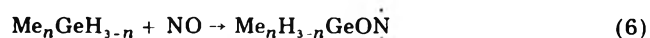
Hydrogen and nitric oxide were obtained from Matheson Gas Products. Methylgermane, dimethylgermane, and trimethylgermane were prepared by the reduction of trichloromethylgermane, dichlorodimethylgermane, and chlorotrimethylgermane, respectively, with lithium aluminum hydride. Disilane was prepared by the reduction of hexachlorodisilane with lithium aluminum hydride. Tetramethyltin was obtained from Alfa Inorganics.

Results and Discussion

Consider a gaseous system containing Si₂H₆, a methylgermane, Hg vapor, and an excess of H₂. Assume that H₂ is in such great excess that electronically excited Hg(³P₁) atoms are collisionally deactivated only by H₂. Irradiation of this gaseous mixture by 2537-Å radiation initiates the following reaction sequence:



The rates of reaction 3 and of reactions 4 + 5 can be determined from the time dependencies of the concentrations of Me_nGeH_{4-n} and Si₂H₆ provided the free-radical products of these reactions are intercepted and thereby prevented from reacting with Si₂H₆, Me_nGeH_{4-n}, and each other. It has been demonstrated^{19,33,34} that nitric oxide is an efficient interceptor for silyl-type radicals. With NO present we must add to the above reaction sequence the following:



The rate constants of reactions 3-5 are so large that at the total pressures used H atoms will not react with NO to any

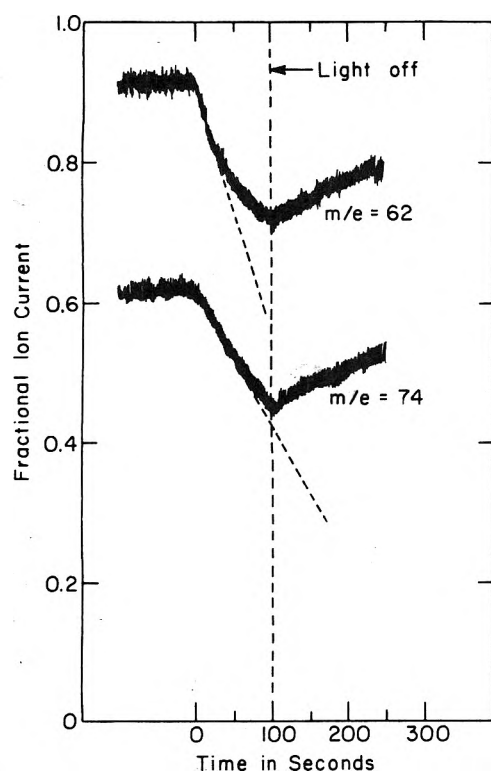


Figure 1. Typical competitive rate curves for CH_3GeH_3 (m/e 74) vs. Si_2H_6 (m/e 62).

significant extent. In reactions 6-8 addition of the radicals to the oxygen atom is indicated because silyl radicals have been shown^{19,34} to add to NO in this manner, and by analogy we think it is likely that germyl radicals will add the same way. The radical products of (7) and (8) react further with NO and produce intermediates that attack silanes^{19,34} and presumably the same will apply for the radical produced in (6). However, such reactions will be observed as secondary processes³⁴ in our experiments and will not affect our results,³³ provided we measure initial rates of depletion of Si_2H_6 and $\text{Me}_n\text{GeH}_{4-n}$.

The initial rates of disappearance of reactants are

$$-(d[\text{Me}_n\text{GeH}_{4-n}]/dt)_0 = k_3[\text{H}][\text{Me}_n\text{GeH}_{4-n}]_0 \quad (9)$$

$$-(d[\text{Si}_2\text{H}_6]/dt)_0 = (k_4 + k_5)[\text{H}][\text{Si}_2\text{H}_6]_0 \quad (10)$$

where the subscript zero indicates initial values. If s is an ion of m/e that is unique to the mass spectrum of the standard, Si_2H_6 , and x is an ion of m/e that is unique to the mass spectrum of $\text{Me}_n\text{GeH}_{4-n}$, then the relationship between initial ion currents and those at some later time are given by

$$i_s/i_s^0 = [\text{Si}_2\text{H}_6]/[\text{Si}_2\text{H}_6]_0 \quad (11)$$

$$i_x/i_x^0 = [\text{Me}_n\text{GeH}_{4-n}]/[\text{Me}_n\text{GeH}_{4-n}]_0 \quad (12)$$

Substitution of these latter expressions into (9) and (10) followed by division of (9) by (10) yields the expression

$$\frac{i_s^0(di_x/dt)_0}{i_x^0(di_s/dt)_0} = \frac{k_3}{k_4 + k_5} \quad (13)$$

Therefore, according to (13) we may determine the ratio $k_3/(k_4 + k_5)$ simply from measurements of the initial ion currents of s and x and their initial rates of decrease during irradiation. Typical recording tracings of such experiments are shown in Figure 1; from such curves sufficiently precise ($\pm 5\%$) initial slopes can be obtained and $k_3/(k_4 + k_5)$ calculated.

The simple expression in (13) was derived with the assumption that $\text{Hg}(^3\text{P}_1)$ atoms are collisionally deactivated

only in collisions with H_2 . This is only approximately true because, as pointed out in the Experimental Section, the gases Si_2H_6 and $\text{Me}_n\text{GeH}_{4-n}$ contribute up to about 5% of the total quenching of $\text{Hg}(^3\text{P}_1)$.³⁵ It is easy to show that inclusion of $\text{Hg}(^3\text{P}_1)$ quenching by $\text{Me}_n\text{GeH}_{4-n}$ and Si_2H_6 , with rates constants k_2^x and k_2^s , respectively, transforms (13) to (14), for our conditions of $[\text{H}_2]/[\text{Me}_n\text{GeH}_{4-n}] =$

$$\frac{i_s^0(di_x/dt)_0}{i_x^0(di_s/dt)_0} = \frac{k_3}{(k_4 + k_5)} \times \left\{ \frac{\left[196 + \frac{k_2^s}{k_2} + \frac{k_2^x}{k_2} \left(2 + \frac{k_4 + k_5}{k_3} \right) \right]}{\left[196 + \frac{k_2^s}{k_2} \left(2 + \frac{k_3}{k_4 + k_5} \right) + \frac{k_2^x}{k_2} \right]} \right\} \quad (14)$$

$[\text{H}_2]/[\text{Si}_2\text{H}_6] = 98$. Comparison of values of $k_3/(k_4 + k_5)$ calculated from (13) with those calculated from (14) assuming $k_2^s \approx k_2^x \approx 10k_2$ shows that the maximum error introduced in the ratio by using the simple expression is 2% or less. Since this lies within the precision of our measurement of initial slopes, we have calculated the rate constant ratios by the simpler expression in (13). Conversion of $k_3/(k_4 + k_5)$ to absolute values of k_3 is based on the value of $k_4 + k_5 = 3.7 \pm 0.6 \times 10^{-12} \text{ cm}^3/\text{s}$ previously determined.³³

The results of our measurements are given in Table I in terms of the relative value from (13) and the absolute value determined using $k_4 + k_5 = 3.7 \pm 0.6 \times 10^{-12} \text{ cm}^3/\text{s}$. Also given in Table I are the m/e values of the ions used in the mass spectrometric monitoring of the $\text{Me}_n\text{GeH}_{4-n}$ concentration and the number of replicate measurements involved in determining each value. The ion of m/e 62 was used to monitor Si_2H_6 concentration. The upper limit to the value for Me_4Ge was not determined experimentally, but is assumed on the basis of the experimental studies made on Me_4Si ³³ and Me_4Sn , i.e., there was no measurable reaction within the uncertainty of our measurements. Since Ge lies between Si and Sn in group 4 of the periodic table, it would be very surprising if Me_4Ge reacted at a measurable rate.

There exist no literature values with which to compare our rate constants for H-atom reactions with methylgermanes. However, they will be compared to the rate constants for H-atom reactions with the corresponding methylsilanes.³³ This is shown in Figure 2. It is clear that H atoms react faster with the germanes than with the corresponding silanes by factors of ~ 5 -6. Also, while methyl-substituted silanes and germanes react faster than monosilane or monogermane, respectively, the effect of methyl substitution in reactivity is greater in germanes than in silanes. Trimethylgermane reacts faster than any of the germanes while there is little difference in reactivity of monomethyl-, dimethyl-, and trimethylsilanes.

Unfortunately, it was not feasible to vary the temperature significantly in our experiments because of the design of the apparatus. Therefore, Arrhenius parameters cannot be calculated from our data alone. These parameters have been estimated by making the following assumptions:

(1) It is assumed that the preexponential factor for H-atom reaction with GeH_4 is the same as that for H-atom reaction with SiH_4 . This assumption is supported by the similarity of the bond lengths in these two molecules, i.e., 1.48 Å³⁶ for the Si-H bond length in SiH_4 and 1.52 Å³⁶ for the Ge-H bond length in GeH_4 .

(2) It is assumed that the preexponential factors per Ge-H bond are constant over the series $(\text{CH}_3)_n\text{GeH}_{4-n}$ with $n = 0, 1, 2, 3$. This assumption is supported by the ob-

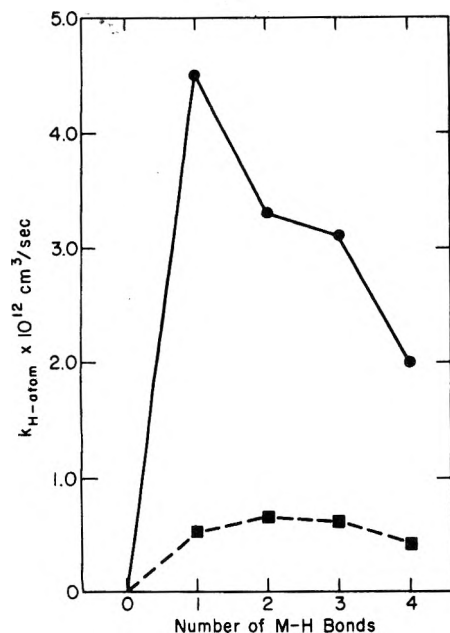


Figure 2. Comparison of the reactivity of alkylgermanes and alkylsilanes³³ expressed in terms of the number of Ge-H or Si-H bonds: (●) H + (CH₃)_{4-n}GeH_n; (■) H + (CH₃)_{4-n}SiH_n. The value for GeH₄ is from the previous paper.³³

TABLE II: Arrhenius Parameters for H-Atom Induced Decomposition of Germanes and Dissociation Energies of Germanium-Hydrogen Bonds

Molecule	10 ¹¹ A, cm ³ /s	E, kcal/mol	D(≡Ge-H), kcal/mol
GeH ₄ ^a	2.7	1.6	89
CH ₃ GeH ₃	2.0	1.1	83
(CH ₃) ₂ GeH ₂	1.4	0.86	79
(CH ₃) ₃ GeH	0.7	0.26	63

^a The values given for GeH₄ are from ref 33.

servation that for the reaction of CH₃ radicals with (CH₃)_nSiH_{4-n} with *n* = 0, 1, 2, 3 the preexponential factors per Si-H bond are remarkably constant at $9.0 \pm 1.1 \times 10^{-13}$ cm³/s.^{5,10} We expect the germanes to be analogous to the silanes.

The Arrhenius parameters *A* and *E* ($k = Ae^{-E/RT}$) that are obtained for the series of germanes by this admittedly crude approximation are given in Table II. It is to be noted from Table II that the activation energies fall off slowly as the Ge-H bonds in GeH₄ are successively replaced by Ge-CH₃ bonds.

The continuous lowering of the activation energy by successive replacement of the first three H atoms with alkyl groups is also observed in the silane series³³ and paraffin series. For the reaction of H atoms with the molecules, R_nCH_{4-n}, where R is an alkyl radical, it is well known that the activation energy parallels smoothly the dissociation energy of the ≡C-H bond as *n* changes from 0 to 3. The same trend in activation energies for the reaction of H atoms with (CH₃)_nGeH_{4-n}, seen in Table II, suggests that there should exist an analogous decrease in the dissociation energy of the Ge-H bond in the series (CH₃)_nGeH_{4-n} as *n* changes from 0 to 3. Confirmation of this suggestion by direct comparison with the literature is not possible because these bond dissociation energies have not been determined.

Because of this lack of thermochemical information in the literature, we have estimated the Ge-H bond dissociation energies for the series (CH₃)_nGeH_{4-n} for *n* = 0, 1, 2, 3. The most successful semiempirical technique of relating activation energies for H-atom abstraction to bond

dissociation energies is the bond-energy-bond-order (BEBO) method.³⁷ We have used this method employing the same value for the Sato parameter, i.e., 0.20, that we used in a similar calculation on the analogous silane series³³ to calculate the bond dissociation energies of the Ge-H bond in the series (CH₃)_nGeH_{4-n}. The results are shown in Table II. The estimated dissociation energy of the Ge-H bond in GeH₄, 89 kcal/mol, is in good agreement with the values of Saalfeld and Svec³⁸ (87.2 kcal/mol) and Reed and Brauman³⁹ ($\leq 92.3 \pm 4.6$ kcal/mol) while being 11 kcal/mol higher than the estimated value of Kim, Setser, and Bogan⁴⁰ (≤ 78 kcal/mol). The magnitude and trend of these crudely estimated dissociation energies compare reasonably with the better known values for the silanes,⁴¹⁻⁴³ with the exception of that for the (CH₃)₃Ge-H bond, which seems very low. If indeed it is not as small as indicated, some effect other than activation energy must operate to account for the very high reactivity toward H atoms.

Acknowledgment. This work was supported by the U.S. Energy Research and Development Administration under Contract No. EY-76-S-02-3416.

References and Notes

- U.S. Energy Research and Development Administration Document No. EY-76-S-02-3416-2.
- J. A. Kerr, D. H. Slater, and J. C. Young, *J. Chem. Soc. A*, 104 (1966).
- J. A. Kerr, D. H. Slater, and J. C. Young, *J. Chem. Soc. A*, 134 (1967).
- J. A. Kerr, A. Stephens, and J. C. Young, *Int. J. Chem. Kinet.*, 1, 339, 371 (1969).
- O. P. Strausz, E. Jakubowski, H. S. Sandhu, and H. E. Gunning, *J. Chem. Phys.*, 51, 552 (1969).
- E. R. Morris and J. C. J. Thynne, *J. Phys. Chem.*, 73, 3294 (1969).
- A. U. Chaudhry and B. G. Gowenlock, *J. Organometal. Chem.*, 16, 221 (1969).
- T. N. Bell and A. E. Platt, *J. Phys. Chem.*, 75, 603 (1971).
- H. E. O'Neal, S. Pavlou, T. Lubin, M. A. Ring, and L. Batt, *J. Phys. Chem.*, 75, 3945 (1971).
- R. E. Berkley, I. Safarik, H. E. Gunning, and O. P. Strausz, *J. Phys. Chem.*, 77, 1734 (1973).
- R. E. Berkley, I. Safarik, O. P. Strausz, and H. E. Gunning, *J. Phys. Chem.*, 77, 1741 (1973).
- T. N. Bell and B. B. Johnson, *Aust. J. Chem.*, 20, 1545 (1967).
- W. J. Cheng and M. Szwarc, *J. Phys. Chem.*, 72, 494 (1968).
- E. Jakubowski, H. S. Sandhu, H. E. Gunning, and O. P. Strausz, *J. Chem. Phys.*, 52, 4242 (1970).
- T. N. Bell and U. F. Zucker, *J. Phys. Chem.*, 74, 979 (1970).
- T. N. Bell and U. F. Zucker, *Can. J. Chem.*, 48, 1209 (1970).
- E. R. Morris and J. C. J. Thynne, *Trans. Faraday Soc.*, 66, 183 (1970).
- J. A. Kerr and D. M. Timlin, *Int. J. Chem. Kinet.*, 3, 1, 69 (1971).
- M. A. Nay, G. N. C. Woodall, O. P. Strausz, and H. E. Gunning, *J. Am. Chem. Soc.*, 87, 179 (1965).
- P. Cadman, G. M. Tilsley, and A. F. Trotman-Dickenson, *J. Chem. Soc., Faraday Trans. 1*, 68, 1849 (1972).
- T. L. Pollock, H. S. Sandhu, A. Jodhan, and O. P. Strausz, *J. Am. Chem. Soc.*, 95, 1017 (1973).
- B. Reimann, R. Laupert, and P. Potzinger, *Ber. Bunsenges. Phys. Chem.*, 79, 1160 (1975).
- E. R. Austin and F. W. Lampe, *J. Photochem.*, 5, 155 (1976).
- E. R. Austin and F. W. Lampe, *J. Phys. Chem.*, 80, 2811 (1976).
- I. M. T. Davidson, "Reaction Kinetics", Vol. 1, Chemical Society Special Periodical Report, London, 1975, pp 214 ff.
- M. A. Contineanu, D. Mihelcic, R. N. Schindler, and P. Potzinger, *Ber. Bunsenges. Phys. Chem.*, 75, 426 (1971).
- K. Obi, H. S. Sandhu, H. E. Gunning, and O. P. Strausz, *J. Phys. Chem.*, 76, 3911 (1972).
- D. Mihelcic, P. Potzinger, and R. N. Schindler, *Ber. Bunsenges. Phys. Chem.*, 78, 82 (1974).
- P. Potzinger, L. C. Glasgow, and B. Reimann, *Z. Naturforsch. A*, 29, 493 (1974).
- J. A. Cowfer, K. P. Lynch, and J. V. Michael, *J. Phys. Chem.*, 79, 1139 (1975).
- K. Y. Choo, P. P. Gaspar, and A. P. Wolf, *J. Phys. Chem.*, 79, 1752 (1975).
- P. Potzinger, private communication, Dec 1975.
- E. R. Austin and F. W. Lampe, *J. Phys. Chem.*, 81, 1134 (1977).
- E. Kamaratos and F. W. Lampe, *J. Phys. Chem.*, 74, 2267 (1970).
- J. G. Calvert and J. N. Pitts, Jr., "Photochemistry", Wiley, New York, N.Y., 1966, pp 72 ff.
- E. A. V. Ebsworth, "Volatile Silicon Compounds", Pergamon Press, Oxford, 1963, p 16.

- (37) H. S. Johnston, "Gas-Phase Reaction Rate Theory", Ronald Press, New York, N.Y.
- (38) F. E. Saalfeld and H. J. Svec, *J. Phys. Chem.*, **70**, 1753 (1966).
- (39) K. J. Reed and J. I. Brauman, *J. Chem. Phys.*, **61**, 4830 (1974).
- (40) K. C. Kim, D. W. Setser, and C. M. Bogun, *J. Chem. Phys.*, **60**, 1837 (1974).
- (41) P. Potzinger, A. Ritter, and J. R. Krause, *Z. Naturforsch. A*, **30**, 347 (1975).
- (42) R. Walsh and J. M. Wells, *J. Chem. Soc., Chem. Commun.*, 513 (1973).
- (43) I. M. T. Davidson and A. V. Howard, *J. Chem. Soc., Faraday Trans. 1*, **71**, 69 (1975).

Oscillatory Evolution of Carbon Monoxide in the Dehydration of Formic Acid by Concentrated Sulfuric Acid

Peter G. Bowers* and Gulnar Rawji

Department of Chemistry, Simmons College, Boston, Massachusetts 02115 (Received March 14, 1977)

Publication costs assisted by Simmons College

The periodic evolution of carbon monoxide from mixtures of formic acid and concentrated sulfuric acid has been studied. Oscillations are only observed under conditions favorable to good foaming. The composition of the foam differs from that of the liquid phase. A qualitative explanation of the oscillations is given in physical (rather than chemical) terms.

Introduction

The periodic nature with which carbon monoxide is evolved in the well-known reaction between formic acid and concentrated sulfuric acid was first reported over 50 years ago by Morgan.¹ Under rather specific conditions of mixture and temperature, Morgan observed that CO was released in gusts, which at their peak caused the whole mixture to rise and foam vigorously. The gusts were separated by quiescent periods with slow gas evolution, and little or no foam. Morgan was able to observe up to about 20 damped oscillations, with a time period of approximately 1 min.

At that time, the unusual kinetics were attributed to physical effects involving supersaturation, and indeed in later kinetic studies² carried out under conditions designed to prevent supersaturation, the oscillatory nature of the reaction was ignored, if indeed it was observed at all.

Despite the upsurge of interest in oscillating reactions,³ there are still only two well-documented examples of true chemical oscillators (excluding biochemical systems and electrode phenomena). These are the Belousov-Zhabotinski type and the Bray-Liebhafsky reaction (iodate-peroxide). They are both redox processes. For this reason we undertook to reexamine the Morgan reaction, which superficially at least, appears to involve no redox process, and to be stoichiometrically simple.

Experimental Section

Chemicals were reagent grade and used without further purification. Batches of concentrated sulfuric acid and 88% formic acid from several different manufacturers gave substantially the same results.

The best oscillations were obtained by cooling the two acids separately in ice before mixing in a large test tube immersed in a thermostat bath at 38 °C (11 mL of H₂SO₄-3 mL of HCO₂H). The acids were mixed vigorously for 30 s and subsequently agitated by gentle magnetic stirring. The test tube was connected to an adjustable capillary leak to the atmosphere, and to a U-tube manometer containing copper sulfate solution. By suitable adjustment of the capillary, periodic evolution of gas was reflected in oscillation of the levels of liquid in the manometer. A He-Ne laser beam was directed through the

length of Cu²⁺ solution in the open arm of the manometer, and the oscillatory transmittance recorded via a conventional photocell-recorder arrangement. In a similar way, with the capillary leak completely closed it was possible to follow stepwise build up in the pressure of evolved gas.

Analysis for formic acid was accomplished by measuring the absorbance (235 nm) of small samples which had been quenched with water, weighed, and appropriately diluted, after removal from the reacting mixture.

Results

General Course of the Reaction. A typical curve obtained by the differential method described above is shown in Figure 1. Steady oscillations begin after an initial period of vigorous gas evolution, and during the first few of them the mixture foams to an extent that no separate liquid phase is visible. At each maximum the foam ruptures quite suddenly, just after the maximum rate of gas evolution, and drains back to form an almost quiescent liquid, before gas evolution builds up again. The periodic behavior damps away gradually, with the time period of the oscillation going through a maximum (Figure 2). Slow gas evolution continues for several hours after the oscillatory phase. When the reaction appears to be over, vigorous agitation (or pumping) results in the removal of much dissolved CO.

Reproducibility. Appearance of oscillations in this system depend on a suitable choice of at least three critical variables—temperature, composition, and degree of agitation. Outside of fairly narrow limits for these, oscillations either do not occur at all, or are of low amplitude. Our composition and temperature are similar to that prescribed by Morgan. Mixtures too rich in either component react aperiodically, and without excessive foaming. Qualitatively, we observed oscillations in the temperature range 28–50 °C. At room temperature the mixture appears to be too viscous to foam well, while at high temperature gas evolution is too vigorous to permit the existence of a well-separated foam phase.

The sharpest oscillations occur when the reactants are gently agitated. With no agitation, other than that naturally inherent in gas evolution, the amplitude is less

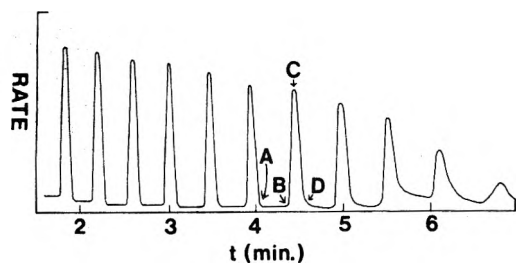


Figure 1. Oscillatory portion of differential rate curve for evolution of CO from 11 mL of concentrated H_2SO_4 -3 mL of HCO_2H at 38 °C. The ordinate is in relative nonlinear units.

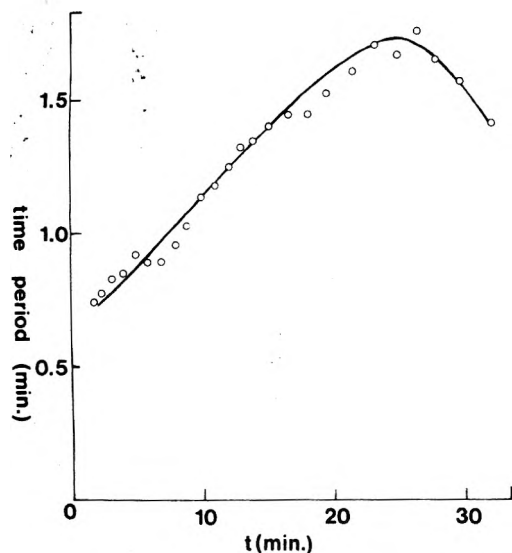


Figure 2. Variation of the time period of the oscillation with time.

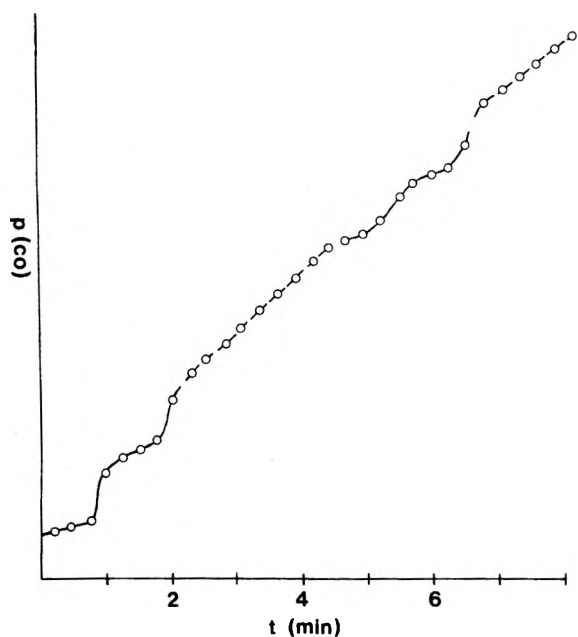


Figure 3. Integrated rate curve for CO evolution showing the effect of vigorous agitation (---) alternating with gentle agitation (—).

although the time period is little affected. Vigorous agitation results in smooth, nonoscillatory evolution of CO, and the mechanical production of foam. However, as Figure 3 shows, rapid agitation does not change the overall rate of gas evolution.

Effect of Detergent. Figure 4 shows the effect of a trace of detergent added at the start of the reaction. Detergent increases the time period of the oscillation significantly and lengthens the total time of the oscillatory phase.

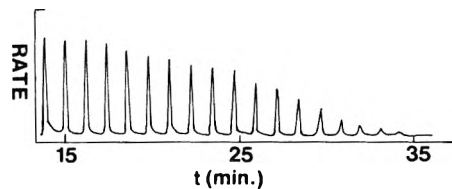


Figure 4. Oscillations in the presence of a trace of detergent, using same conditions as in Figure 1.

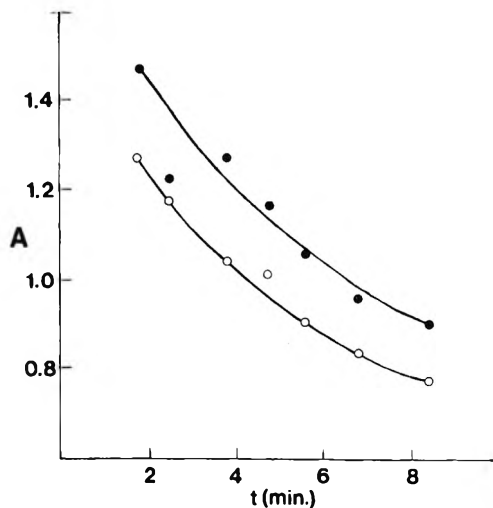


Figure 5. Relative absorbance (235 nm) of liquid (●) and foam (○) samples, taken at peaks of successive oscillations.

Antifoam has the reverse effect, giving a train of rapid oscillations of low amplitude.

Composition of Liquid and Foam Phases. The periodic behavior can be completely suppressed by removing most of the foam (by suction) just before it subsides. After several such removals during successive oscillations, the remaining liquid no longer oscillates.

In related experiments, small samples of both liquid and foam were removed simultaneously for analysis at the peaks of successive oscillations. The composition of each phase, as indicated from their UV absorption, is shown in Figure 5. Since neither water, sulfuric acid, or dissolved CO absorb at 235 nm, the foam, when it becomes unstable, is evidently deficient in formic acid as compared to the liquid below it. Although the precision of this analysis is not particularly high, the same relative position of the curves in Figure 5 was reproducibly found in several trials.

Similar analyses were carried out with mixtures in which the formic acid was replaced by either glacial acetic acid or formaldehyde. In these experiments, foam was produced using a stream of nitrogen through a fritted bubbler. Even after several separations and "refractionations", no difference in composition between liquid and foam fractions could be detected.

Discussion

The results described above indicate the critical part played by foam production in this reaction. In particular, differences in kinetic behavior and in composition, between bulk liquid and liquid separated by removal as foam, suggest a basis upon which an explanation of the oscillations can be made.

At the beginning of a cycle (time A in Figure 1), CO is being produced, but is supersaturating the solution, and not much escapes. Vigorous evolution begins at point B, resulting in the production of a foam phase in which the reaction proceeds more rapidly due to (I) significant foam fractionation, with a mole ratio in the foam more favorable

to reaction, and/or (II) inherent kinetic effects possibly involving more advantageous orientation and juxtaposition of the reactants at a surface than in bulk. At point C gas evolution ceases and almost simultaneously the foam ruptures. Factors influencing the rupture point might include (a) natural drainage of the foam, (b) instability of foam caused by composition changes due to reaction, (c) excessive CO pressure in the bubbles, and (d) depletion of reactants in foam causing cessation of gas evolution.

In any case, at C, on the basis of our experiments, there is a composition difference between the foam and bulk liquid. Between points C and D the foam drainage liquid runs back into the bulk. The drainage liquid is probably not, at this stage, supersaturated with gas, because of its history as foam with a high surface area. Thus the newly re-formed bulk liquid is less than supersaturated, and the cycle begins again.

It is difficult to decide which of the factors I or II above is the more important in producing a composition difference between the two phases at maximum amplitude. The fact that foam is produced at all indicates a surface excess of one of the components, and intuitively we would expect this to be the organic acid. However the reverse is observed. This, together with the fact that little, if any, fractionation occurs on foaming similar but nonreacting mixtures, leads us to favor explanation II as the predominant cause of the composition difference. That is, the acids react more rapidly at an interface than in bulk, and this results in faster depletion of formic acid in the foam.

Gentle agitation, by promoting good mixing between supersaturated bulk liquid, and the less saturated foam-drainage liquid, helps to produce sharp oscillations by making the slow stage more marked. Indeed, were it not for the composition and kinetic differences seen on separating the foam, a simple saturation-desaturation sequence could explain the periodicity, with the foam acting to "catalyze" the desaturation. Vigorous agitation, on the other hand, prevents natural periodic separation of the two phases; rapid mechanical interconversion of the mixture between foam and liquid, with an approximately constant amount of each, results in constant average rate.

Changes which are noted under different conditions (notably temperature, composition, and the presence of detergent or antifoam) are all explicable qualitatively in terms of the adverse or favorable effect they have on the stability of the foam. The pertinent physical factors which determine this stability are viscosity (relating to the drainage rate) and surface tension (relating to rupture of the bubbles).⁴

The maximum exhibited by the time period of the oscillation (Figure 2) is also understandable in terms of two opposing factors. As the reaction proceeds, the formic acid concentration decreases. This at first results in a decrease in the rate of gas production and hence in the formation and rupture of foam, which therefore increases the time period for a cycle. Eventually, depletion of the organic component adversely affects the stability of the foam for physical reasons, and the cycle speeds up before oscillations damp away entirely.

Concluding Remarks

Perhaps the chief point we wish to make from this work is that carbon monoxide evolution in the Morgan reaction is periodic in nature for reasons we believe to be physical in nature, and associated with the production of foam. The fact that it may not be a true chemical oscillator does not make it any the less interesting, and we are at present studying a number of other gas-evolution reactions which might, under the proper conditions, show periodicity for the same reasons.

Acknowledgment. One of us (P.G.B.) wishes to thank Professors C. A. McDowell and G. B. Porter of the Chemistry Department, University of British Columbia, where part of this research was carried out. The work was also supported in part by NSF Grant SMI76-03651.

References and Notes

- (1) J. S. Morgan, *J. Chem. Soc. Trans.*, **109**, 274 (1916).
- (2) G. A. Ropp, A. J. Weinberger, and O. K. Neville, *J. Am. Chem. Soc.*, **73**, 5573 (1951), and references cited therein.
- (3) G. Nicolis and J. Portnow, *Chem. Rev.*, **73**, 4 (1973).
- (4) Varying the external pressure also changes the frequency of the oscillations in a regular way (R. M. Noyes and K. Showalter, personal communication). This interesting effect constitutes a rapid and reversible method of "tuning" the frequency of gas evolution.

Cis-Trans Photoisomerization of β -Styrylnaphthalene and 3-Styrylquinoline

G. Gennari, G. Cauzzo,* and G. Gallazzo

Institutes of Physical Chemistry and Organic Chemistry, University of Padova, 35100 Padova, Italy (Received January 21, 1977)

Publication costs assisted by the Consiglio Nazionale delle Ricerche (CNR)

The direct and anthraquinone-sensitized cis-trans photoisomerization of β -styrylnaphthalene and 3-styrylquinoline has been investigated in benzene at 25 °C. The effect of azulene on the photostationary states is consistent with a triplet mechanism for direct photoisomerization. The influence of oxygen and of the substrate concentration on the reaction pathway is also discussed.

Introduction

Whereas the photosensitized cis-trans isomerization of ethylenic compounds in solution was shown to proceed by a triplet mechanism,¹ singlet or triplet pathways have been proposed for their isomerization induced by direct irradiation. For stilbene, quenching experiments of Saltiel and

co-workers² led to the conclusion that the direct cis-trans photoisomerization occurs via a single route. Recently, the singlet mechanism of stilbene has been confirmed by both theoretical calculations³ and photophysical measurements.⁴ A theoretical state model for the singlet mechanism has been proposed⁵ where a S_2 ($^1A_g^*$) excited singlet has a

TABLE I: Quantum Yields and Photostationary States for the Anthraquinone-Sensitized Photoisomerization of 5×10^{-2} M β -StN and 3-StQ in Deaerated Benzene at 25 °C^a

	ϕ_c	ϕ_t	$([t]/[c])_{ss}$	ϕ_c/ϕ_t	$\phi_c + \phi_t$
β -StN	0.46	0.45	1.00	1.02	0.91
3-StQ	0.43	0.42	0.90	1.02	0.85

^a[Anthraquinone] = 5×10^{-3} M.

minimum in the perpendicular configuration. A thermally activated radiationless transition thus occurs from S_1 (1B_u) to the perpendicular S_2 , from which internal conversion to S_0 is efficient because of the small S_2 - S_0 energy gap. This is the major process leading to cis isomerization at room temperature, whereas at low temperatures a triplet mechanism may predominate.⁶ On the other hand, in the photochemical trans \rightarrow cis isomerization of nitrostilbene a triplet mechanism was proposed,⁷ and long-lived triplet intermediates have also been detected.⁸ The nature of the substituents at the double bond thus appears to play a fundamental role in determining the route of the photochemical isomerization and a "mixed" singlet and triplet mechanism is probable in some cases. This was found, for instance, for some azastilbenes from the study of the excitation wavelength effect on the photoreaction.⁹

In a previous work,¹⁰ we studied the effect of azulene on the direct and sensitized photoisomerization of 3-styrylquinoline. In this paper we discuss the results of a more detailed investigation on the photoisomerization of 3-styrylquinoline (3-StQ) and β -styrylnaphthalene (β -StN).

Experimental Section

Benzene (Uvasol Merck), thiophene free, was used as solvent. Anthraquinone (RP Carlo Erba) and azulene (Fluka) were used without further purification. The synthesis of 3-StQ was previously reported;¹⁰ β -StN was obtained by decarboxylation of the corresponding phenylacrylic acid, as described by Bortolus and Galiazzo.¹¹

The irradiation procedure was the same as described elsewhere.¹⁰ In the direct isomerization, irradiations were performed at 313 nm with total absorption of the incident light. The extinction coefficients of the cis, ϵ_c , and trans, ϵ_t , isomers were determined from measurements of their absorbance using the same light source as in the irradiation experiments. In the anthraquinone-sensitized photoisomerization, the solutions were irradiated with 400-nm light, which is absorbed exclusively by the sensitizer. The anthraquinone and azulene absorption spectra in their long wavelength region are unaffected by the presence of 3-StQ and β -StN up to 5×10^{-2} M.

The percentage of the two isomers in the irradiation solutions was determined by GLC ($1/8$ -in. column, 5% SE 30 on Chromosorb G). In the experiments at low (10^{-4} M) substrate concentration (see Results) the chromatographic analysis proved to be unsuitable owing to the overlap of the peaks of the cis isomer with the solvent tail; in this case spectrophotometric analysis was employed.

Photostationary compositions in the photosensitized process were determined starting with pure cis or trans isomers, whereas in direct photoisomerization, owing to the concomitant photocyclization of the cis isomer, cis-

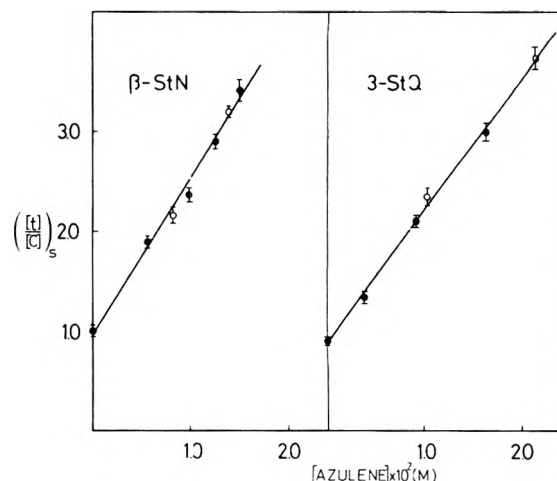


Figure 1. Effect of azulene on the anthraquinone-sensitized photoisomerization of β -StN and 3-StQ in benzene at 25 °C: (●) deaerated; (○) air saturated.

trans mixtures which bracketed the expected photostationary states were irradiated for short times. For the determination of quantum yields the percentages of isomerization, which in any case did not exceed 15%, were corrected for the contribution of the back reaction by the formula of Lamola and Hammond¹² applied to the experimental photostationary compositions. The quantum yields were obtained as a mean of at least two series of runs. The reproducibility was $\pm 3\%$ for sensitized, and $\pm 5\%$ for direct photoisomerization.

Fluorescence measurements were accomplished with a Perkin-Elmer MPF 44 spectrofluorimeter. For the determination of fluorescence quantum yields of trans isomers, ϕ_F , 2-(1-naphthyl)-5-phenyl-1,3,4-oxadiazole (α -NPD) in deaerated cyclohexane solution ($\phi_F = 0.58$)¹³ was used as standard, allowance being made for the refractive index difference with respect to benzene.

Results

Sensitized Photoisomerization. The quantum yields of the anthraquinone-sensitized cis \rightarrow trans, ϕ_c , and trans \rightarrow cis, ϕ_t , photoisomerization are reported in Table I along with the photostationary compositions $([t]/[c])_{ss}$. The anthraquinone and substrate concentrations were 5×10^{-3} and 5×10^{-2} M, respectively. The data refer to deaerated benzene solutions. However, the same results were obtained in air-saturated solutions. At lower substrate concentrations ($\sim 10^{-3}$ M) the presence of oxygen lowers the values of both ϕ_c and ϕ_t , even if the photostationary composition remains unaffected. This effect can be reasonably ascribed to a quenching of the triplet sensitizer by oxygen. The data in Table I fit quite well the relation $\phi_c/\phi_t = ([t]/[c])_{ss}$, which holds for high-energy sensitizers; the sum $\phi_c + \phi_t$ is near 0.9, the reported value for the singlet \rightarrow triplet intersystem crossing of anthraquinone,¹² and this fact indicates that the substrate concentration is high enough to intercept nearly all the triplets of the sensitizer.

The effect of azulene on the photostationary states is shown in Figure 1; the intercepts, i , and the slope/intercept ratios, s/i , of the azulene plots are reported in Table III. As shown in Figure 1, the azulene effect is the same in

TABLE II: Quantum Yields and Photostationary States for the Direct Photoisomerization of 5×10^{-3} M β -StN and 3-StQ in Deaerated Benzene at 25 °C

	ϕ_c	ϕ_t	$([t]/[c])_{ss}$	ϵ_c/ϵ_t	ϕ_F	$10^9 \tau_F, s$	ϕ_{15}^t	ϕ_{15}^c
β -StN	0.30	0.22	0.61	0.43	0.45	7 ± 0.5	0.44	0.60
3-StQ	0.32	0.17	0.75	0.37	0.33 _s	1.8	0.32	0.67

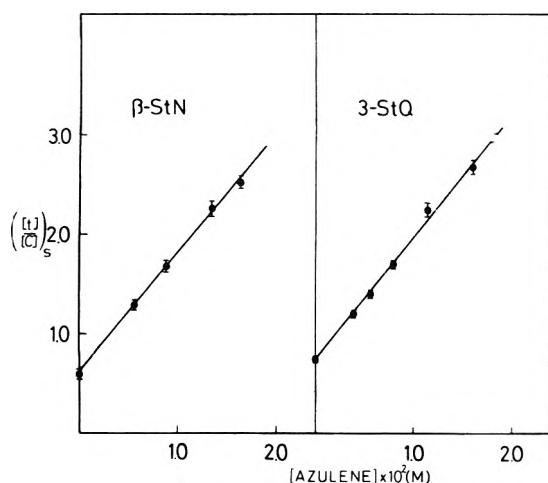


Figure 2. Effect of azulene on the direct photoisomerization of β -StN and 3-StQ in deaerated benzene at 25 °C.

TABLE III: Azulene Effect on the Direct and Anthraquinone-Sensitized Photoisomerization of β -StN and 3-StQ in Deaerated Benzene at 25 °C

	Direct		Sensitized	
	i	$s/i, M^{-1}$	i	$s/i, M^{-1}$
β -StN	0.61	190	1.00	165
3-StQ	0.75	165	0.90	150

TABLE IV: Effect of Oxygen and Substrate Concentration on the Quantum Yield of Direct $\text{trans} \rightarrow \text{cis}$ Photoisomerization of β -StN and the Oxygen Effect on the Fluorescence Quantum Yield and Lifetime of $\text{trans} \beta$ -StN in Benzene at 25 °C

	[β -StN] = $5 \times 10^{-3} M$		[β -StN] = $10^{-4} M$		$10^9 \tau_F, s$
	ϕ_t	$([t]/[c])_{ss}$	ϕ_t	ϕ_F	
Deaerated	0.22	0.61	0.11 (0.08) ^a	0.45	7 ± 0.5
Air saturated	0.27	0.47	0.19 (0.18) ^a	0.35	4.8 ± 0.5

^a Reference 8.

deaerated and in air-saturated solutions.

Direct Photoisomerization. The quantum yields as well as the photostationary states for the direct isomerization of β -StN and 3-StQ in deaerated solution are collected in Table II; the fluorescence quantum yields, ϕ_F , of the trans isomers are also reported. For both β -StN and 3-StQ, the consistency of the data with the relation $([t]/[c])_{ss} = (\phi_c/\phi_t)(\epsilon_c/\epsilon_t)$ is satisfactory. The azulene effect on the photostationary states for deaerated $5 \times 10^{-3} M$ β -StN and 3-StQ solutions is shown in Figure 2; the intercepts and the slope/intercept values for the azulene plots are reported in Table III. The effect of oxygen on the photoisomerization and on the fluorescence of β -StN is shown in Table IV. As may be seen, the behavior of β -StN is oxygen dependent. In particular, the decrease of the fluorescence quantum yield of $\text{trans} \beta$ -StN in the presence of oxygen is accompanied by an increase of ϕ_t and by a shift of the photostationary composition toward the cis isomer. On the other hand, both fluorescence and photoisomerization of 3-StQ appear to be oxygen insensitive, at least in the range of oxygen concentration investigated. In Table IV the quantum yields of $\text{trans} \rightarrow \text{cis}$ photoisomerization at low substrate concentration ($10^{-4} M$) are also reported. Under these conditions, no reliable values of ϕ_c and $([t]/[c])_{ss}$ could be obtained by spectrophotometric analysis because of the spectral disturbance of the

photocyclization products. Whereas, in agreement with what found by Bortolus and Galiazzi,¹¹ the ϕ_t for β -StN is concentration dependent, such a dependence was not observed for 3-StQ.

Discussion

The effect of triplet quenchers such as azulene on the direct and sensitized $\text{cis} \rightarrow \text{trans}$ photoisomerization of olefins has been extensively investigated, mainly for stilbene.^{1,2} Azulene strongly affects the position of the photostationary state in the triplet-sensitized isomerization of stilbene, whereas its influence is rather small in the direct photoisomerization for which a singlet mechanism was proposed. As shown by Saltiel and Megarity,¹⁴ if a triplet mechanism is operative in both the direct and sensitized photoprocesses, identical slope/intercept ratios are expected in the photostationary composition vs. [azulene] plots, provided the fluorescence quenching of the trans isomer by azulene is negligible. A comparison of the azulene plots in Figures 1 and 2 and of the data in Table III strongly indicates that the $\text{cis} \rightarrow \text{trans}$ isomerization induced by direct irradiation of both 3-StQ and β -StN occurs in the triplet state, which is populated by intersystem crossing from the initially formed excited singlet state. The enrichment in the trans isomer of the photostationary compositions in the presence of azulene can be explained in terms of a quenching by azulene of the phantom triplet, 3p , of the olefin leading to a preferred formation of the trans form.¹⁵

In a previous paper¹⁰ we have shown that the quenching of the fluorescence of $\text{trans} \beta$ -StQ by azulene is small compared to the effect on the quantum yield of the direct $\text{trans} \rightarrow \text{cis}$ photoisomerization and this fact, reported also for the photostationary states of nitrostilbenes,⁸ is in agreement with the triplet mechanism. The fluorescence quenching by azulene also explains the observed difference between the s/i values for the direct and sensitized photoisomerization. Unfortunately, these measurements cannot be made for β -StN because of the spectral overlap of the azulene and β -StN absorptions.

The data for direct photoisomerization (Table II) can be compared with those concerning sensitized photoisomerization (Table I) on the assumption that in both cases the geometrical interconversion occurs in the triplet manifold. Taking the values of $([t]/[c])_{ss}$ in Table II as equal to the triplet decay ratios, $\alpha/1 - \alpha$, where α is the fraction of triplets which are converted to the ground state trans isomer, the quantum yields of the direct photoisomerization can be expressed as $\phi_c = \alpha\phi_{is}^c$ and $\phi_t = (1 - \alpha)\phi_{is}^t$, where ϕ_{is}^c and ϕ_{is}^t are the singlet \rightarrow triplet intersystem crossing quantum yields for the cis and trans isomers, respectively. The values of ϕ_{is}^c and ϕ_{is}^t so calculated are reported in the last two columns of Table II. Since the cis isomer of β -StN and 3-StQ do not have detectable fluorescence, the excited singlet \rightarrow ground state, $S_1 \rightarrow S_0$ internal conversion must compete efficiently with intersystem crossing. For trans isomer, radiative and nonradiative deactivations of the excited singlet state, in addition to intersystem crossing, are involved.

The effect of oxygen on the photostationary states is rather puzzling in some aspects. The photostationary states in the triplet-sensitized isomerizations are the same in the presence and in the absence of oxygen and this fact can be explained since oxygen, as found for stilbene,¹⁵ can deactivate the phantom triplet without affecting the decay ratio. However, the slopes of the azulene plots are also the same in deaerated and in air-saturated solutions (see Figure 1); this result implies that oxygen, a well-known triplet quencher, exerts a negligible quenching on the

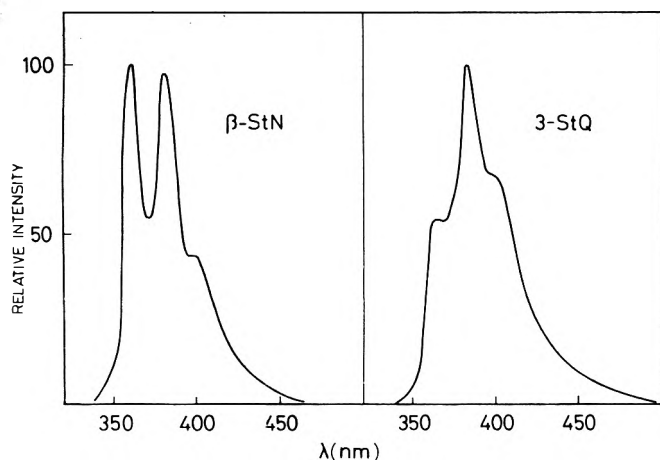


Figure 3. Fluorescence spectra of β -StN and 3-StQ in deaerated benzene at 25 °C excited with 313-nm light.

triplet olefin compared to azulene. A possible explanation is as follows. Like stilbene triplets,² almost all β -StN and 3-StQ triplets are probably in a 3p twisted configuration, which is converted by a radiationless deactivation to either ground state isomers. 3p states of β -StN and 3-StQ may not be quenchable by oxygen because their energies are lower than the 22 kcal/mol excitation energy of the O_2 $^1\Delta_g$ state. On the other hand, the excitation transfer to azulene, for which a larger energy gap is required, may occur via exciplexes or encounter complexes formation, as proposed by Saltiel and Thomas.¹⁵

As previously observed (see Results), oxygen has a noticeable influence on the fluorescence and on the direct photoisomerization of β -StN, whereas such effects are not observed for 3-StQ. The different behavior of β -StN and 3-StQ with respect to oxygen can be related to the lifetimes of their lowest excited singlet, S_1 , states. Measurements of fluorescence lifetimes¹⁶ in deaerated benzene solution gave for trans β -StN a value of about 7 ns, which drops to about 5 ns in air-saturated solution. On the other hand, the fluorescence lifetime of 3-StQ was found to be about 2 ns both in the presence and in the absence of oxygen. As shown in Table IV, the decrease of the fluorescence quantum yield of trans β -StN in the presence of oxygen is accompanied by an increase of ϕ_t and by a shift of the photostationary composition toward the cis isomer. If a triplet mechanism is involved in direct photoisomerization, the above effect can be ascribed to an enhancement of singlet \rightarrow triplet intersystem crossing of trans β -StN induced by oxygen.

As shown in Table IV, the quantum yield of direct trans \rightarrow cis photoisomerization of β -StN is concentration dependent. This fact was previously observed by Bortolus and Galiazzo,¹¹ who related it with the possibility of an excimer formation between the trans β -StN in the excited S_1 state and ground state molecules. On the other hand, ϕ_t for the shorter living 3-StQ is the same in 10^{-4} and 5×10^{-3} M solutions; if the above interpretation is correct, such a concentration independence for 3-StQ can be ascribed to the absence of excimer formation in this compound because of the shorter lifetime of its S_1 state.

The presence of heterocyclic nitrogen in 3-StQ may suggest an involvement of n, π^* states in the deactivation process. The weak n, π^* transition is not detectable in the absorption spectrum of 3-StQ; furthermore, the fluorescence of trans β -StN is of a comparable intensity with that of 3-StQ and the band positions in the two spectra (Figure 3) are about the same, indicating a π, π^* nature of the lowest emitting singlet state in both cases.

As shown in Table II, in 5×10^{-3} M solutions the intersystem crossing quantum yields of 3-StQ are not very different from those of the parent hydrocarbon. However, this comparison is unreliable because of the concentration effect on the ϕ_t of β -StN. In fact, at lower substrate concentration (10^{-4} M) the calculated ϕ_{is}^t for β -StN is considerably lower than the corresponding value for 3-StQ. If a triplet mechanism is still operative for direct photoisomerization under these conditions, the above findings can be interpreted in terms of an enhanced intersystem crossing in 3-StQ due to a n, π^* and π, π^* coupling.

Acknowledgment. This work was supported by the Consiglio Nazionale delle Ricerche (C.N.R.) through Contract No. CT 75.01.194.03, for which we are grateful.

References and Notes

- (1) G. S. Hammond et al., *J. Am. Chem. Soc.*, **86**, 3197 (1964).
- (2) J. Saltiel et al., *Org. Photochem.*, **3**, 1-113 (1972), and references therein.
- (3) G. Orlandi, private communication.
- (4) D. J. S. Birch and J. B. Birks, *Chem. Phys. Lett.*, **38**, 432 (1976).
- (5) G. Orlandi and W. Siebrand, *Chem. Phys. Lett.*, **30**, 352 (1975).
- (6) J. B. Birks, *Chem. Phys. Lett.*, **38**, 437 (1976).
- (7) D. V. Bent and D. Schulte-Frohlinde, *J. Phys. Chem.*, **78**, 451 (1974).
- (8) D. V. Bent and D. Schulte-Frohlinde, *J. Phys. Chem.*, **78**, 446 (1974).
- (9) U. Mazzucato, private communication.
- (10) G. Gennari, G. Cauzzo, and G. Galiazzo, *J. Photochem.*, **5**, 409 (1976).
- (11) P. Bortolus and G. Galiazzo, *J. Photochem.*, **2**, 361 (1973-1974).
- (12) A. A. Lamola and G. S. Hammond, *J. Chem. Phys.*, **43**, 2129 (1965).
- (13) J. B. Birks, "Photophysics of Aromatic Molecules", Wiley-Interscience, New York, N.Y., 1970, p 124.
- (14) J. Saltiel and E. D. Megarity, *J. Am. Chem. Soc.*, **94**, 2742 (1972).
- (15) J. Saltiel and B. Thomas, *J. Am. Chem. Soc.*, **96**, 5660 (1974).
- (16) F. Massettil, private communication.

Size and Shape of Globular Micelles Formed in Aqueous Solution by *n*-Alkyl Polyoxyethylene Ethers^{1a}

Charles Tanford,*^{1b} Yasuhiko Nozaki, and Michael F. Rohde

Department of Biochemistry, Duke University Medical Center, Durham, North Carolina 27710 (Received March 17, 1977)

Publication costs assisted by the National Science Foundation

Micelle molecular weights have been determined by sedimentation equilibrium for one homogeneous and one heterogeneous *n*-alkyl polyoxyethylene glycol monoether. Average dimensions were obtained from measurements of sedimentation velocity and intrinsic viscosity. Results are in good agreement with literature data for similar compounds. Comparison between calculated and observed Stokes radii and intrinsic viscosities shows that the micelles must have a disklike shape and that the polyoxyethylene chains in the outer mantle of the micelle must be in randomly coiled conformation. Previous results showing that large aggregates are formed by detergents of this type when the number of ethylene oxide units in the polyoxyethylene chain falls below a critical value have been confirmed. The available data support the likelihood that these aggregates arise by secondary association of small micelles.

Water-soluble nonionic detergents containing polyoxyethylene chains as hydrophilic moieties are being used extensively for solubilization of proteins from biological membranes.^{2,3} There is evidence to suggest that the solubilized protein may often be inserted into or through the detergent micelle, without large alteration in the size and shape of the micelle.³ Characterization of the pure detergent micelle thus has a practical importance for biochemists, as well as being of general interest from a physicochemical point of view. Robson and Dennis⁴ have recently discussed the size and shape of the micelles of Triton X-100, an alkylphenyl polyoxyethylene glycol monoether that has seen wide use in biochemistry. We present here some experimental results for one homogeneous and one heterogeneous *n*-alkyl polyoxyethylene glycol monoether. The results are used, together with data previously obtained in other laboratories, as a basis for general conclusions about the micelles formed by water-soluble detergents in this category.

Experimental Section

n-Dodecyl octaethylene glycol monoether (C₁₂E₈)⁵ was a homogeneous product from Nikko Chemicals Co., Tokyo, Japan. The homologue with six oxyethylene units (C₁₂E₆) was obtained from the same source. Homogeneity of both products was confirmed by thin layer chromatography on silica gels. C₁₂E₈ can be crystallized from hexane, and recrystallization from that solvent has no observable effects. Lubrol WX was a heterogeneous product manufactured by ICI United States Inc., and purchased from Sigma Chemical Co., St. Louis, Mo. According to the manufacturer it is the monoether formed from a close to equimolar mixture of hexadecyl and octadecyl alcohols, with an average content of 16.4 oxyethylene units per molecule, i.e., its average composition may be designated as C₁₇E_{16.4}. The detergent was used as received, apart from the removal of insoluble material.

Molecular weight measurements were based on sedimentation equilibrium measurements in a Beckman Model E analytical ultracentrifuge, using Rayleigh interference optics. Partial specific volumes of the detergents (above the critical micelle concentration) were measured using an Anton Paar precision densimeter, Model DMA 02C, as previously described.⁶ Sedimentation velocity measurements also utilized the analytical ultracentrifuge. When

the molecular weight and partial specific volume are known, they yield directly the frictional constant (*f*), which may be used to define an equivalent radius, generally called the Stokes radius (*R_s*), i.e., $f = 6\pi\eta R_s$, where η is the solvent viscosity.⁶ Measurements of intrinsic viscosity were made using Cannon-Fenske viscometers with a flow time for water at 25 °C near 300 s. Detergent solutions at the critical micelle concentration were used as "solvent" in the calculation of intrinsic viscosities from the data. Gel exclusion chromatography, using Sepharose 4B, was carried out as previously described.⁷

Some of the sedimentation studies were made with detergent dissolved in D₂O (99.84 mol %), obtained from Bio-Rad Laboratories. Densities and viscosities of solutions in D₂O were calculated with the aid of appropriate tabulated data.^{8,9} Most of the densities were checked experimentally and found to agree with the tabulated data within experimental error.

Results

Micelles in these measurements were dissolved in 0.1 M NaCl in H₂O or D₂O. The solvent for the micellar particles includes monomeric detergent at a concentration close to the critical micelle concentration. The concentrations of these solutes of low molecular weight are sufficiently small so that preferential hydration terms¹⁰ cannot be important and the experimental parameter yielded by sedimentation equilibrium results is thus $M(1 - \bar{v}\rho)$ where *M* is the average micelle molecular weight, \bar{v} the partial specific volume of the detergent in micellar form, and ρ the solvent density. This conclusion was checked for C₁₂E₈ by determining $M(1 - \bar{v}\rho)$ at several densities and interpolating to the density at which $M(1 - \bar{v}\rho) = 0$. The \bar{v} value obtained in this way was the same as that obtained directly by densimetry, $\bar{v} = 0.973 \text{ cm}^3/\text{g}$ in 0.1 M NaCl (in H₂O) at 25 °C. It should be noted that the H atom of the OH group of the detergent is exchangeable, and that \bar{v} will thereby be decreased in D₂O, in proportion to the D₂O content,^{11,12} to a minimal value of $0.971 \text{ cm}^3/\text{g}$ in pure D₂O. For Lubrol WX we measured $\bar{v} = 0.929 \text{ cm}^3/\text{g}$ in 0.1 M NaCl (in H₂O) at 25 °C, and the calculated value for pure D₂O is $0.928 \text{ cm}^3/\text{g}$.

Sedimentation equilibrium plots were linear, indicating no change in weight-average molecular weight with concentration (which reached maximal values of about 10

TABLE I: Results for $C_{12}E_8$ and Lubrol WX in 0.1 M NaCl

	$C_{12}E_8$	Lubrol WX
\bar{v} , cm ³ /g, in H ₂ O at 25 °C	0.973	0.929
Mol wt (15-25 °C)	65 000	92 000
Aggregation no.	120	94
$s_{20,w}^\circ \times 10^{13}$, 20 °C	0.46	<i>a</i>
R_s , Å	36	
$[\eta]$, cm ³ /g	4.2	6.2
R_s from $[\eta]$, Å	35	45

^a A single determination made in 1975 gave a sedimentation coefficient of about 1.2 S, corresponding to a Stokes radius of 50 Å. Because of the inherently better accuracy of the viscosity results and their good agreement with literature data, this measurement has not been repeated.

mg/mL), which in turn shows that the micelles have a relatively narrow size distribution, in which number and weight averages are closely similar.¹³ Results obtained for $C_{12}E_8$ were 63 000 in 0.1 M NaCl (H₂O) at 20 °C, and 68 500 in 0.1 M NaCl (D₂O) at 25 °C. Although a small effect of temperature on the molecular weight is to be expected (in the observed direction),^{14,15} we consider the difference between the results to be at the limit of experimental error, which is relatively large here because the factor $1 - \bar{v}\rho$ is very small (0.026 in H₂O and -0.076 in D₂O) so that an uncertainty of only 1 part per 1000 in \bar{v} or ρ can affect the molecular weight estimation by several percent. For Lubrol WX we determined molecular weights of 92 500 in 0.1 M NaCl (H₂O) at 20 °C and 91 500 in 0.1 M NaCl (D₂O) at 15 °C. The best values (estimated precision about ± 4000) and the corresponding aggregation numbers are given in Table I.

Both sedimentation velocity and intrinsic viscosity data have been used for estimating micelle dimensions. The viscosity data are much more reliable because they do not involve the buoyancy factor $1 - \bar{v}\rho$. We obtained $[\eta] = 4.2$ cm³/g for $C_{12}E_8$ in 0.1 M NaCl (H₂O) at 25 °C, with a Huggins constant of 2.0, which is the expected value for globular particles.¹⁶ For Lubrol WX $[\eta] = 6.2$ cm³/g in the same solvent, with a slightly smaller value for the Huggins constant. The intrinsic viscosity may be converted to an effective hydrodynamic radius (R_e) by the relation¹⁶

$$[\eta]M/N = (10\pi/3)R_e^3$$

where N is Avogadro's number. For globular particles the effective radius obtained this way should be indistinguishable from the Stokes radius, R_s . The latter can be determined directly from sedimentation velocity measurements,^{6,16} but as already noted, the experimental uncertainty is large. The results are shown in Table I. For $C_{12}E_8$ the two ways to estimate an equivalent radius are in excellent agreement.

Our molecular weight for $C_{12}E_8$ is in excellent agreement with light scattering measurements of Becher¹⁷ for heterogeneous compounds with dodecyl chains, as shown in Figure 1. The measurements were made at 25 °C in water, and additional data of Becher¹⁸ have shown that the presence of a low concentration of NaCl has no significant effect. Results obtained by other workers¹⁹ for heterogeneous $C_{12}E_x$ ($x > 8$) differ over a wide range.

Our molecular weight for $C_{12}E_8$ is in excellent agreement with light scattering measurements of Becher¹⁷ for heterogeneous compounds with dodecyl chains, as shown in Figure 1. The measurements were made at 25 °C in water, and additional data of Becher¹⁸ have shown that the presence of a low concentration of NaCl has no significant effect. Results obtained by other workers¹⁹ for heterogeneous $C_{12}E_x$ ($x > 8$) differ over a wide range.

Molecular weights measured at 25 °C for homogeneous $C_{16}E_x$ ($x > 8$) by Elworthy and Macfarlane²⁰ and for heterogeneous compounds of the same kind of El Eini et al.²¹ are also shown in Figure 1. The influence of heterogeneity appears to be small and both sets of data are in close accord with our result for Lubrol WX, which, as indicated above, is a mixture of $C_{16}E_x$ and $C_{18}E_x$, with

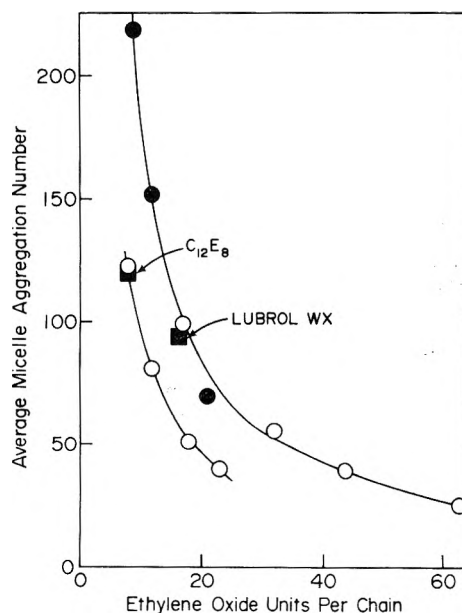


Figure 1. Micelle aggregation numbers for $C_{12}E_8$ and Lubrol WX compared with results from other laboratories (at 25 °C) for homogeneous $C_{16}E_x$ (filled circles, data of Elworthy and Macfarlane²⁰) and for heterogeneous $C_{12}E_x$ and $C_{16}E_x$ (open circles, data of Becher^{17,18} and El Eini et al.²¹).

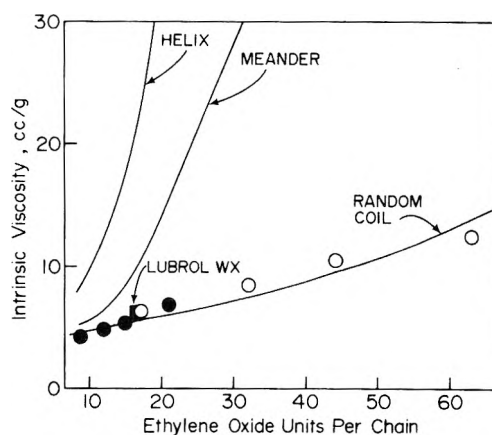


Figure 2. Intrinsic viscosity of Lubrol WX, compared with results of Elworthy and Macfarlane²⁰ for homogeneous $C_{16}E_x$ (filled circles) and of El Eini et al.²¹ for heterogeneous $C_{16}E_x$ (open circles). The three curves are calculated on the basis of different conformations for the polyoxyethylene chains, as outlined in the Discussion section.

average x equal to 16.4. (The heterogeneous detergents used by El Eini et al.,²¹ though not pure with respect to alkyl chain length, contain about 95% hexadecyl chains²².)

Figure 2 shows intrinsic viscosity results for both homogeneous and heterogeneous $C_{16}E_x$, and again our result for Lubrol WX fits well with these data. (The viscosity results of Elworthy and Macfarlane²⁰ were reported on the basis of detergent concentration expressed as volume fraction. The results in the figure have been corrected to the customary units of cm³/g.)

In making the comparisons of Figures 1 and 2, we have been careful to limit ourselves to results obtained (at 25 °C) for $C_{12}E_x$ and $C_{16}E_x$ with $x \geq 8$, because a distinctly different mode of association, generally believed to be the result of secondary aggregation,^{20,23} occurs at this temperature when $x < 8$. The phenomenon is characterized by a large effect of detergent concentration on molecular weight. There is a large increase in intrinsic viscosity with micelle size and an accompanying appearance of light scattering asymmetry, both indicating that large micelles, when formed, are asymmetric particles. Where $x > 8$, on

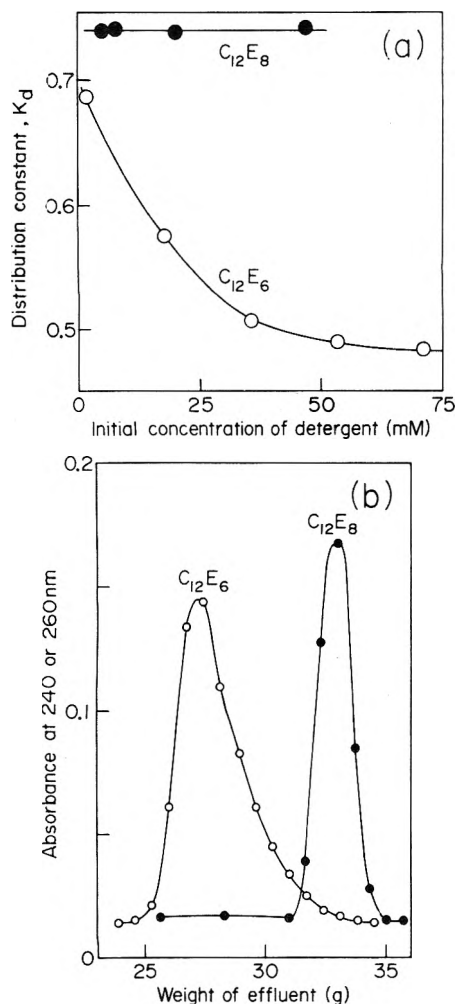


Figure 3. Gel chromatography on Sepharose 4B columns. Figure 3a shows the apparent equilibrium constant for distribution between the gel pores and the mobile eluting phase as a function of the concentration of detergent initially layered on the column. Figure 3b shows typical elution patterns. Initial concentrations were 35 mM in the experiment for $C_{12}E_8$ and 20 mM in the experiment for $C_{12}E_6$. Fractions eluting from the column were weighed and absorbance at 240 or 260 nm (arising from light scattering) was used as a measure of micelle concentration. Peak positions were used to calculate K_d . Essentially identical results were obtained when dye absorption methods were used to estimate micellar concentrations.

the other hand, the micelles are globular ($[\eta]$ small and no light scattering asymmetry) and there is no significant change in molecular weight with detergent concentration. The formation of large aggregates depends markedly on temperature as well as on the number of oxyethylene units. Thus, $C_{12}E_6$, which forms large aggregates at 25 °C or above,¹⁵ only forms well-behaved globular micelles at 5 °C.^{15,24}

We have confirmed this dividing line by comparing $C_{12}E_8$ and $C_{12}E_6$ at 25 °C, both by sedimentation equilibrium and by gel chromatography. As noted earlier, sedimentation equilibrium plots were linear throughout the cell for $C_{12}E_8$, but they were curved for $C_{12}E_6$ (in D_2O) with a continuous increase in weight-average molecular weight with increasing concentration. Gel chromatography results give a dramatic demonstration of the same effect, as shown in Figure 3. The equilibrium constant K_d for distribution of micelles between the gel pores and the mobile liquid phase remains the same for $C_{12}E_8$, independent of the initial concentration of detergent, whereas a sharp decrease occurs for $C_{12}E_6$ indicative of an increase in size. On the basis of calibration with globular proteins^{6,7} the K_d value of 0.74 observed for $C_{12}E_8$ corresponds to an

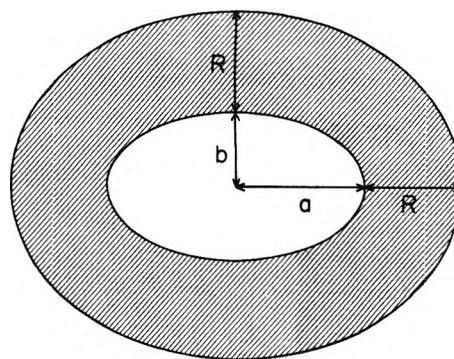


Figure 4. Micelle model used for calculations. The central cavity represents the hydrophobic core formed by the alkyl chains. The shaded portion is the solvent-permeated mantle formed by the polyoxyethylene chains.

R_s value of 35 ± 5 Å, in good agreement with the direct measurements of Table I. The K_d value of 0.45 observed for $C_{12}E_6$ at the highest concentrations employed corresponds to an R_s of about 75 Å.

Figure 3 also shows typical elution patterns for the two detergents. A sharp elution peak is obtained for $C_{12}E_8$, indicative of rapid equilibration between the micellar species of different size. The elution peak for $C_{12}E_6$ at the lowest concentration employed (not shown) had a similar appearance, but at the higher concentrations a peak with a steep front and a long trailing edge is observed. This indicates that the equilibration between the initially formed small micelles and the larger micelles existing at higher concentrations is a relatively slow process. The results strongly suggest therefore that the formation of large $C_{12}E_6$ micelles occurs by a mechanism differing from that of formation of the initial small micelles. The sedimentation velocity patterns observed for $C_{12}E_6$ at 25 and 35 °C by Ottewill et al.¹⁵ are skewed in the same direction, a result again indicating a chemical interconversion process that is slow in comparison with the rate of transport.

Discussion

The results presented here, including the earlier data we have cited, shed light on three aspects of the physical nature of *n*-alkyl polyoxyethylene micelles: (1) the micelle shape, (2) the conformation of polyoxyethylene chains, and (3) the mechanism of formation of large aggregates. These questions will be discussed in terms of the simplest possible micellar model,²⁵ illustrated by Figure 4. We assume that the alkyl chains form a central liquid hydrocarbon core, devoid of water, one dimension of which (b in the figure) is limited to the length of an alkyl chain in a liquidlike state.²⁶ The polyoxyethylene chains extend from the surface of the core to form a solvent-permeated mantle; the periphery of this mantle forms the surface of shear from the standpoint of hydrodynamic properties, and all solvent trapped within it is part of the hydrodynamic particle. A sharp demarcation line has been drawn between the hydrophobic core and the solvent-permeated mantle, ignoring the probable undulating nature of the core surface.^{27,28} The effect of undulations would be to increase micelle dimensions by 1 or 2 Å, a difference too small to be resolved in terms of a comparison between observed and calculated hydrodynamic data.

Micelle Shape. It is impossible for the $C_{12}E_8$ micelle to have a spherical core. Even if we assume that the entire dodecyl chain is hydrophobic and enters into formation of the core, and if we assume that the alkyl chain is fully extended, the maximal number of chains that could be accommodated is 55, less than half the observed degree of association. A spherical core with the radius of a fully

extended chain is in fact physically impossible because all chains would have to meet at the center of the sphere, and in any event thermodynamic considerations favor a flexible conformation for the chain. A realistic estimate for the maximal degree of association of a physically possible spherical micelle is thus even smaller. The maximal degree of association becomes 20 if we calculate the limiting dimension b as was done in a previous paper²⁶ (to be discussed further below), and in that case even the smallest of the micelles in the $C_{12}E_x$ series of Figure 1 ($C_{12}E_{23}$) could not have a spherical core. Similar considerations apply to the results for Lubrol WX and the $C_{12}E_x$ series.

There are only two truly distinct ways to increase the volume of the micelle core beyond the spherical volume while maintaining the restriction of a limiting value for the dimension b of Figure 4. One is to create a disklike shape, i.e., to keep only one dimension equal to b , allowing expansion along two perpendicular axes. The other is to create a rodlike shape, i.e., to keep two perpendicular dimensions equal to b and to allow extension along only one dimension, the rod axis. It is obvious that the asymmetry required to accommodate a given core volume must be greater for a rodlike than for a disklike shape, with a concomitantly greater increase in asymmetry-dependent parameters, such as the intrinsic viscosity. Rigorous equations relating shape to hydrodynamic properties exist for oblate and prolate ellipsoids of revolution and not for other possible detailed models that might fall within the general terms "disklike" and "rodlike", and we are therefore forced to use ellipsoidal models to make the distinction. Because any rodlike particle of given volume is more asymmetric than any disklike particle of the same volume, it is likely that conclusions based on an ellipsoidal model are valid regardless of the precise micelle shape. It may in fact be unrealistic to think of the micelle as having a precise shape such as a rigid body would have. The micelle is a small *liquid* droplet in a *liquid* solvent, subject to fluctuations in surface shape and extent. There may not be a more precise description than "disklike" and "rodlike".

It is appropriate to mention in this connection the recent theoretical discussion of micelle shape by Israelachvili et al.²⁹ They have pointed out that the micelle core is not simply a structureless continuum of hydrocarbon, but that it is a volume of space occupied by hydrocarbon chains that are geometrically constrained. Consideration of this factor leads to prediction of preferred shapes with more complex boundaries than those of ellipsoids of revolution. It is clear from the preceding paragraph that a comparison between calculated and experimental hydrodynamic properties cannot be sufficiently sensitive to permit an experimental test of their proposed models, especially in view of the probability that fluctuations in shape would have to be taken into account in interpreting the average micellar properties measured by hydrodynamic experiments.

Conformation of Polyoxyethylene Chains. Polyoxyethylenes in aqueous solution are typical randomly coiled polymers,^{30,31} and one would thus expect the polyoxyethylene chains extending from the micelle core to be likewise randomly coiled, with the distance R of Figure 3 approaching an approximately square-root dependence on the number of polyoxyethylene units as that number becomes large. However, the parallel alignment of the chains in the micelle mantle may affect the preferred conformation and three possible rigid conformations, with R directly proportional to the number of polyoxyethylene units, have been considered in the literature: the fully extended (zig-zig) conformation,³² with a length of 3.5 Å

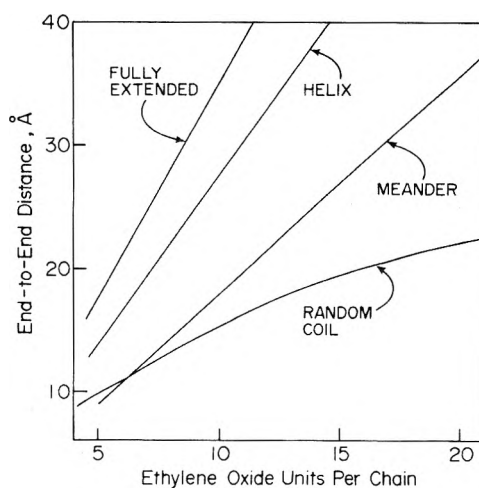


Figure 5. Length of polyoxyethylene segment as a function of ethylene oxide units per chain for several alternative conformations.

per monomer; the helical conformation seen in polyoxyethylene crystals,^{33,34} with a length of 2.76 Å per monomer; and the hypothetical "meander" conformation,³² with a length of 1.8 to 2 Å per monomer. Kalyanasundaram and Thomas³⁵ have recently interpreted Raman spectral data as indicating the presence of a helical structure in some micelles formed by detergents with long polyoxyethylene chains.

End-to-end distances of polyoxyethylene chains in the random coil conformation can be obtained from parameters calculated by the statistical mechanical methods of Flory.³⁰ These calculations give results in agreement with experiment for the limiting behavior of long-chain polymers, but also permit calculation of the deviations from limiting behavior for short chains. The dimensions yielded by the calculations are "unperturbed" dimensions and are directly applicable only when the polymer is dissolved in an ideal θ solvent. Water or 0.1 M NaCl is a nonideal solvent in which the dimensions are somewhat larger than in a θ solvent, but the effect for short chains should not be significant; the experimentally observed expansion falls rapidly with decreasing molecular weight and is only about 10% of the end-to-end distance (in water at 35 °C) for a degree of polymerization of about 1000.³¹ Expected end-to-end distances for all models are plotted as a function of the number of oxyethylene units in Figure 5. For the meander conformation the smallest possible value (1.8 Å per monomer) has been used.

Theoretical hydrodynamic properties of the micelles depend only on the overall size and shape of the hydrodynamic particle, and are thus under the influence of both the factors we have discussed. Calculations were made using standard equations for the frictional coefficient and intrinsic viscosity of oblate and prolate ellipsoids,^{16,36} with semiaxes $a + R$ and $b + R$, values of R being based on the data of Figure 5. The results for $C_{12}E_8$ are shown in Table II.

The parameters a and b are determined as was done in a previous paper on this subject.²⁶ The aggregation number and hydrocarbon density determine the core volume, b is estimated from the hydrocarbon chain length, and the value of a then follows automatically from the equation for the volume of an ellipsoid. In the absence of direct information to the contrary it is reasonable to assume that the parameter b of Figure 4 corresponds in length to a segment of a polymethylene chain with the same number of carbon atoms, and that it can be estimated from the statistical mechanical calculations of Flory.³⁰ For a dodecyl chain this means that b is about 75% of the fully

TABLE II: Theoretical Hydrodynamic Parameters^a for C₁₂E₈

n _c	b/l _{max}	Polyoxyethylene chain conformation					
		Random coil		Meander		Helical	
		R _s	[η]	R _s	[η]	R _s	[η]
Oblate Ellipsoidal Core							
11 ^b	0.75 ^b	37.0	5.0	39.8	6.2	45.9	9.5
11	0.85	36.4	4.8	39.2	5.9	45.4	9.2
12	0.73	36.2	4.7	39.0	5.9	45.2	9.1
12	0.85	35.6	4.4	38.4	5.6	44.5	8.6
Prolate Ellipsoidal Core							
11	0.75	43.3	8.5	46.3	10.3	52.6	14.9
11	0.85	40.2	6.6	43.0	8.0	49.3	12.0
12	0.73	42.0	7.8	45.0	9.4	51.3	13.8
12	0.85	38.5	5.7	41.3	7.1	47.5	10.7

^a R_s in Å and [η] in cm³/g. Experimental values are given in Table I. ^b n_c is the number of carbon atoms of the alkyl chain assumed to participate in formation of the micelle core; b/l_{max} is the ratio of the assumed length to the fully extended length of the alkyl chain, the smaller value in each pair representing the most probable value for a randomly coiled segment of a polymethylene chain.

extended length (l_{max}).²⁶ In the previous paper²⁶ we also assumed that the CH₂ group adjacent to the hydrophilic moiety of the detergent molecule would not enter the hydrophobic core because it probably lies within the solvation sphere of the polar groups, so that the number of carbon atoms of the embedded alkyl chain (n_c) is one less than the formula number, i.e., n_c = 11 for a dodecyl chain. When this is done, 1.25 Å is added to the dimension R to accommodate the extra CH₂ group in the micelle mantle. In the present context it is important to demonstrate that these assumptions are not critical for the conclusions, and this has been done by making alternate calculations with all 12 carbon atoms in the hydrophobic core and with b/l_{max} closer to unity. This factor is seen to have little influence, and the conclusion from the calculations is clear: the micelles must be disklike and the polyoxyethylene chains must be randomly coiled to obtain reasonable agreement between theory and the experimental results of Table I. Actual ellipsoid dimensions are listed in Table III.

The same result is obtained when similar calculations are made for the other micelles for which data were given above. The incompatibility between a prolate ellipsoid model and the observed data is most evident when the polyoxyethylene chain is short and the micelle size is large, e.g., for C₁₆E₉ (aggregation number 219), using n_c = 15 and b/l_{max} = 0.67 and the random coil dimensions for R, we calculate [η] = 4.7 cm³/g for an oblate shape and [η] = 11.1 cm³/g for a prolate shape. The experimental value is 4.85 cm³/g.

The fact that the polyoxyethylene chains must be randomly coiled is shown even more forcibly by comparing observed and calculated [η] values for micelles in the C₁₆E_x series with large x, where the dimension R becomes dominant and what is assumed about the shape of the hydrophobic core has less influence than it did in the case of C₁₂E₈ (Table II), especially since the micelles become smaller as x increases and the core correspondingly less asymmetric. Calculated and experimental viscosity data are compared in Figure 2, and ellipsoid dimensions for what we consider to be the optimal micelle model are shown in Table III.

The conclusion that the micelles considered in this study have a disklike rather than rodlike shape agrees with theoretical prediction.²⁶ A similar conclusion was reached previously from experimental data for sodium dodecyl

TABLE III: Calculated Dimensions for Oblate Ellipsoidal Micelles^a

C _x E _y	Aggregation no.	Dimensions defined by Figure 4, in Å		
		b	a	R
		C ₁₂ E ₈	120	11.6
		13.1	26.6	14.4
		12.2	28.7	13.2
		14.2	26.6	13.2
C ₁₂ E ₁₂	81	11.6	23.2	18.0
C ₁₂ E ₁₈	51	11.6	18.4	22.2
C ₁₂ E ₂₃	40	11.6	16.3	25.0
C ₁₆ E ₉	219	13.7	40.5	15.5
C ₁₆ E ₁₂	152	13.7	33.8	18.0
C ₁₆ E ₁₇	99	13.7	27.2	21.4
C ₁₆ E ₂₁	70	13.7	22.9	24.0
C ₁₆ E ₃₂	56	13.7	20.5	29.5
C ₁₆ E ₄₄	39	13.7	17.1	35.0
C ₁₆ E ₆₃	25	13.7	13.7	41.2
Lubrol WX	94	14.2	27.0	20.8

^a The calculations are for single micelles with aggregation number equal to the observed average extent of aggregation. Lubrol WX has been treated as C₁₇E₁₆. The four entries for C₁₂E₈ corresponds to the four slightly different values of n_c and b/l_{max} in the first four lines of Table II. All other entries were based on n_c one less than the nominal alkyl chain length and b/l_{max} as given in ref 26 for randomly coiled alkyl chains. Values of R include allowance for the presence of the CH₂ group excluded from the hydrophobic core.

sulfate micelles at moderate ionic strength and for C₁₂E₆ and C₁₄E₆ micelles at 5 °C, where no secondary association occurs.²⁶ Robson and Dennis⁴ have shown by similar methods that an alkylphenyl polyoxyethylene micelle (Triton X-100) must have a disklike shape. They point out that a spherical micellar shape would be possible if one could remove restriction on the parameter b of Figure 4 by allowing oxyethylene units to become incorporated in the hydrophobic core, but this is a thermodynamically improbable event. When the micelle size becomes very small, as for C₁₆E₆₃, a spherical shape is predicted (a = b in Table III), and a spherical shape is possible for C₁₆E₃₂ and C₁₆E₄₄ if we allow the alkyl chains to be more nearly fully extended, as El Eini et al.²¹ have already pointed out. There is however no possibility of fitting the large micelles formed by C₁₆E_x with the smaller values of x by a spherical model.

Micelle hydration numbers are frequently reported, but have usually been based on an assumed spherical shape. They are readily calculated for the ellipsoidal model used here by subtracting the volume occupied by the detergent molecules (using the measured \bar{v} values) from the total ellipsoid volume. For C₁₂E₈ one obtains 0.87 to 0.71 g of H₂O/g of detergent, depending on which of the four models is used. This corresponds to 3.3 to 2.7 water molecules per ethylene oxide group. For C₁₆E₉ the hydration is 0.65 g/g, corresponding to 2.6 water molecules per ethylene oxide group. Hydration increases with increasing polyoxyethylene chain length: in terms of water molecules per ethylene oxide group it is 4.2 for Lubrol WX and 12.4 for C₁₆E₆₃. The smallest values (about 2.5 water molecules per ethylene oxide group) may be significant in relation to the requirements for preventing secondary association. The larger numbers for longer chains simply represent the typical increase in the amount of solvent trapped by a randomly coiled polymer as the chain length is increased.

Formation of Large Aggregates. We have confirmed the phenomenon of concentration-dependent growth of particle size previously observed for *n*-alkyl polyoxyethylene

micelles when the polyoxyethylene chain length falls below a critical level. Elworthy and Macfarlane²⁰ and subsequently Attwood²³ ascribed this phenomenon to a secondary aggregation of small micelles into larger particles, but more recently Mukerjee²⁷ has shown that the data can be mathematically described in terms of a single continuous self-association process in which there is no distinction between the mode of growth (by addition of monomers) at the levels of small and large average micelle size. Our chromatographic data (Figure 3) provide very strong evidence that the growth to large size is in fact a different and slower process than the formation of small micelles from monomers, i.e., it supports the possibility of secondary association. Moreover, the strong dependence on temperature and on polyoxyethylene chain length suggest that hydrophobic forces are not the major factor in this phenomenon. Thus large particles might be formed from small micelles by association between polyoxyethylene groups, without alteration of the hydrophobic portion of the constituent micelles.

References and Notes

- (1) (a) This work was supported by Grant No. PCM76-15240 from the National Science Foundation. (b) Recipient of a Research Career Award from the National Institutes of Health, U.S. Public Health Service.
- (2) A. Helenius and K. Simons, *Biochim. Biophys. Acta*, **415**, 29 (1975).
- (3) C. Tanford and J. A. Reynolds, *Biochim. Biophys. Acta*, **457**, 133 (1976).
- (4) R. J. Robson and E. A. Dennis, *J. Phys. Chem.*, **81**, 1075 (1977).
- (5) We have abbreviated $C_nH_{2n+1}(OCH_2CH_2)_xOH$ as C_nE_x .
- (6) C. Tanford, Y. Nozaki, J. A. Reynolds, and S. Makino, *Biochemistry*, **13**, 2369 (1974).
- (7) Y. Nozaki, N. M. Schechter, J. A. Reynolds, and C. Tanford, *Biochemistry*, **15**, 3884 (1976).
- (8) Landolt-Börnstein Tabellen, Vol. II, 6th ed, Springer Verlag, Berlin, 1969-1971.
- (9) G. Jones and H. J. Fornwalt, *J. Chem. Phys.*, **4**, 30 (1936).
- (10) E. F. Casassa and H. Eisenberg, *Adv. Protein Chem.*, **19**, 287 (1964).
- (11) S. J. Edelstein and H. K. Schachman, *J. Biol. Chem.*, **242**, 306 (1967).
- (12) J. A. Reynolds and C. Tanford, *Proc. Natl. Acad. Sci. U.S.A.*, **73**, 4467 (1976).
- (13) D. G. Hall and B. A. Pethica in "Nonionic Surfactants", M. J. Schick, Ed., Marcel Dekker, New York, N.Y., 1967, Chapter 16.
- (14) M. Corti and V. Degiorgio, *Opt. Commun.*, **14**, 358 (1975).
- (15) R. H. Ottewill, C. C. Storer, and T. Walker, *Trans. Faraday Soc.*, **63**, 2796 (1967).
- (16) C. Tanford, "Physical Chemistry of Macromolecules", Wiley, New York, N.Y., 1961, Chapter 6.
- (17) P. Becher, *J. Colloid Sci.*, **16**, 49 (1961).
- (18) P. Becher, *J. Colloid Sci.*, **17**, 325 (1962).
- (19) Cited by P. Becher in "Nonionic Surfactants", M. J. Schick, Ed., Marcel Dekker, New York, N.Y., 1967, Chapter 15.
- (20) P. H. Elworthy and C. B. Macfarlane, *J. Chem. Soc.*, 907 (1963).
- (21) D. I. D. El Eini, B. W. Barry, and C. T. Rhodes, *J. Colloid Interface Sci.*, **54**, 348 (1976).
- (22) B. W. Barry and D. I. D. El Eini, *J. Colloid Interface Sci.*, **54**, 339 (1976).
- (23) D. Attwood, *J. Phys. Chem.*, **72**, 339 (1968).
- (24) J. M. Corkill and T. Walker, *J. Colloid Interface Sci.*, **39**, 621 (1972).
- (25) C. Tanford, "The Hydrophobic Effect", Wiley, New York, N.Y., 1973, Chapter 6.
- (26) C. Tanford, *J. Phys. Chem.*, **78**, 2469 (1974).
- (27) C. Tanford, *Proc. Natl. Acad. Sci. U.S.A.*, **71**, 1811 (1974).
- (28) D. Stigter and K. J. Mysels, *J. Phys. Chem.*, **59**, 45 (1955).
- (29) J. N. Israelachvili, D. J. Mitchell, and B. W. Ninham, *J. Chem. Soc., Faraday Trans. 2*, **72**, 1525 (1976).
- (30) P. J. Flory, "Statistical Mechanics of Chain Molecules", Wiley, New York, N.Y., 1969, Chapter V.
- (31) F. E. Bailey, Jr., and J. V. Koleske in "Nonionic Surfactants", M. J. Schick, Ed., Marcel Dekker, New York, N.Y., 1967, Chapter 23.
- (32) M. Rösch in "Nonionic Surfactants", M. J. Schick, Ed., Marcel Dekker, New York, N.Y., 1967, Chapter 22.
- (33) H. Tadokoro, Y. Chatani, T. Yoshihara, S. Tahara, and S. Murahashi, *Makromol. Chem.*, **73**, 109 (1964).
- (34) J. L. Koenig and A. C. Angood, *J. Polym. Sci.*, **A2**, **8**, 1787 (1970).
- (35) K. Kalyanasundaram and J. K. Thomas, *J. Phys. Chem.*, **80**, 1462 (1976).
- (36) H. L. Frisch and R. Simha in "Rheology", Vol. 1, F. R. Eirich, Ed., Academic Press, New York, N.Y., 1956, Chapter 14.
- (37) P. Mukerjee, *J. Phys. Chem.*, **76**, 565 (1972).

Light Scattering Study of Local Structures in Solutions. Chloroform-Cetyltrimethylammonium Chloride System

Tadashi Kato and Tsunetake Fujiyama*

Department of Chemistry, Faculty of Science, Tokyo Metropolitan University, Setagaya-ku, Tokyo 158, Japan (Received March 16, 1977)

Publication costs assisted by the Tokyo Metropolitan University

Light scattering spectra were observed for binary solutions of chloroform-cetyltrimethylammonium chloride (CTACl) at various concentrations (0-0.04 mole fractions). The Rayleigh intensities were reduced to concentration fluctuations. The observed concentration dependencies of the concentration fluctuation were explained well if we considered the existence of an aggregate which was composed of a few CTACl and about 60 chloroform molecules. Using the infrared data, the detailed structure of the aggregate was clarified as follows: (1) a few CTACl molecule make up the core of the aggregate; (2) about 15 chloroform molecules make up the first shell by forming direct hydrogen bonds with the core molecules; and (3) about 45 chloroform molecules envelop the first shell and form the second shell. A comparison of the present method and the Debye plotting method for determining the molecular weight of the solute molecule is given in the Appendix.

Introduction

In previous reports,^{1,2} quantitative analysis of the infrared absorption intensities of some water soluble surfactants in chloroform solutions has been reported. It has been concluded in these reports that those surfactants dissolve in chloroform by forming hydrogen bonds with several solvent chloroform molecules. As the hydrogen

bonds are not of the 1:1 type, we thought it important to study the structure of these complexes in more detail.

Recently, we presented a method for determining which local structures exist in binary solutions by observing the concentration fluctuation at various concentrations.³⁻⁶ In the present study, we applied the light scattering method to determine the local structures expected in the above

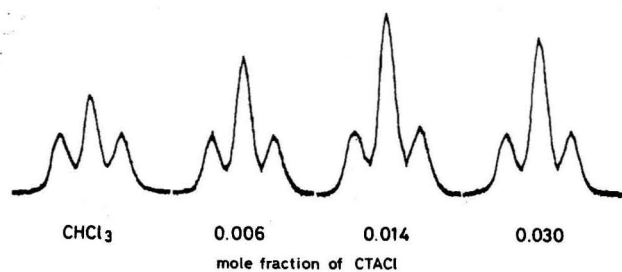


Figure 1. Observed light scattering spectra for the CTACl-chloroform system at 24 °C. The concentration is expressed in terms of the mole fraction of CTACl.

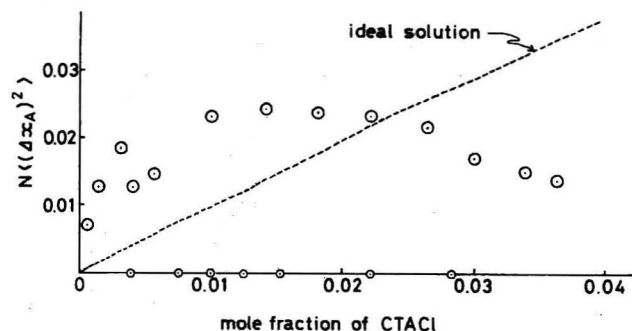


Figure 2. Observed concentration fluctuation for the CTACl-chloroform system at 24 °C.

chloroform solutions of the surfactants. Cetyltrimethylammonium chloride (CTACl) was chosen because the specific refractive index increment is large enough to obtain the concentration fluctuation accurately and because reliable infrared data are available for its chloroform solution.

Experimental Section

All chemicals used in the present study were commercial products. Chloroform was purified by column chromatography on alumina in order to eliminate water and ethanol. CTACl was dried over P_2O_5 under vacuum for several days. The sample solutions were made dust-free by the use of a millipore filter (FG) of 0.2- μ m pore size.

Light scattering spectra were observed at 24 ± 0.5 °C by the use of a spectrometer designed and constructed in our laboratory.³ The refractive indices of the sample solutions were measured by means of Shimadzu-Bausch & Lomb Abbe refractometer 3L.

Results and Discussion

Light Scattering Spectra and Concentration Fluctuation. Figure 1 shows the light scattering spectra observed at 24 °C for chloroform solutions of CTACl in the concentration range of 0–0.03 mole fraction. It is seen from the figure that the Rayleigh intensity takes a maximum value in this concentration range. After separating the Rayleigh part from the observed spectra, the Rayleigh intensity was expressed relative to the Rayleigh intensity of pure chloroform. Then, the concentration fluctuation of CTACl, $N\langle(\Delta x_A)^2\rangle$, was calculated from the equation of Iwasaki et al.,⁴ where N is total number of molecules in the field within which the concentration fluctuation is considered. In Figure 2, the concentration fluctuation thus obtained is plotted against the mole fraction, \bar{x}_A , of CTACl. The dashed line in Figure 2 corresponds to the concentration fluctuation expected for an ideal binary solution. It is seen from the figure that the observed concentration fluctuation takes a maximum value at $\bar{x}_A \approx 0.02$. In the region where \bar{x}_A is smaller than 0.02, the concentration fluctuation takes much larger values than those of an ideal solution. On the other hand, in the region where \bar{x}_A is

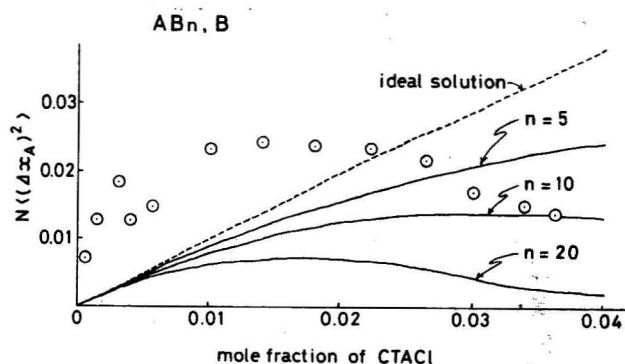


Figure 3. Theoretical values of the concentration fluctuation calculated from eq 3 for $n = 1, 5, 10, 20$.

larger than 0.02 the concentration fluctuation takes smaller values than those of an ideal solution. In the systems which we have reported so far,^{4–6} the concentration fluctuation has no maximum in at concentrations as low as $\bar{x}_A = 0.02$. The specific concentration dependence for the concentration fluctuation may arise from the existence of strong hydrogen bonding between CTACl and chloroform. The circles marked on the horizontal axis of Figure 1 indicate the concentrations at which the previous infrared intensity measurement was undertaken.

Analysis of $N\langle(\Delta x_A)^2\rangle$. In the analysis of the concentration fluctuation observed in the ethanol-chloroform system, an ideal associated complex model has been employed with reasonable success.⁶ As CTACl molecules form strong hydrogen bonds with chloroform molecules, it is assumed that a molecule of A and n molecules of B constitute an aggregate, AB_n , and that molecules of B and the aggregate AB_n behave as independent molecules in the solution, where A is CTACl and B is chloroform. Then, a probability, $f(n_A)$, of finding n_A molecules of A within the region which contains a constant number, N , of molecules is expressed as⁶

$$f(n_A) = \frac{(x+y)!}{x!y!} P^x (1-P)^y \quad (1)$$

where

$$x = n_A$$

$$y = N - (n+1)n_A \quad (2)$$

$$P = \bar{x}/(\bar{x} + \bar{y})$$

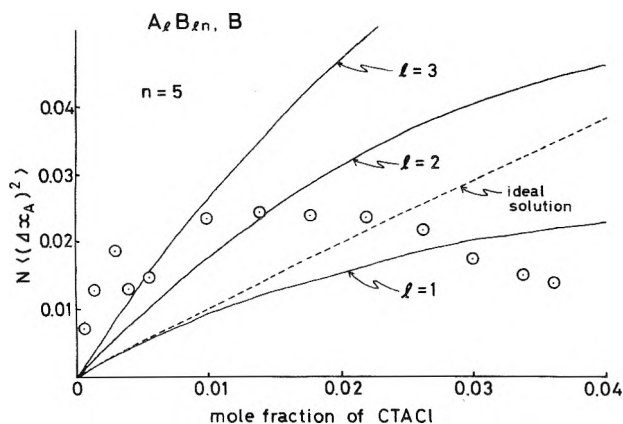
Therefore, the concentration fluctuation of molecule A is expressed in the form

$$N\langle(\Delta x_A)^2\rangle = -1/N [d^2 \ln f(n_A)/dn_A^2]_{n_A = \bar{n}_A} = \bar{x}_A(1 - n\bar{x}_A)[1 - (n+1)\bar{x}_A] \quad (3)$$

Figure 3 shows the concentration dependence of the concentration fluctuation calculated from eq 3 for various n values. It is seen from the figure that the concentration fluctuation decreases in magnitude as the solvation number, n , increases. Obviously these theoretical curves do not agree with the absolute values of the concentration fluctuation. However, the calculated curve for $n = 20$ can explain the experimental curve in the sense that concentration fluctuation takes a maximum value at $\bar{x}_A = 0.02$. We showed in the previous report^{5,6} that, when A molecules are mutually associated, the concentration fluctuation increases in magnitude as the association number increases. Therefore, the above discrepancy between the observed and calculated values of the concentration fluctuation may arise from the ignorance of the mutual association of CTACl molecules.

TABLE I: Results from Infrared Absorption Intensity Measurements for Various Cationic Surfactants^a

Surfactants		n	$n[\Gamma_B^{1/2} - \Gamma_C^{1/2}]$
Dodecyltrimethylammonium chloride	$C_{12}H_{25}N^+(CH_3)_3O^-$	5	160
Dodecyltrimethylammonium chloride	$C_{10}H_{21}N^+(CH_3)_3Cl^-$	4-4.5	130-150
Cetyltrimethylammonium chloride	$C_{16}H_{33}N^+(CH_3)_3Cl^-$	4-4.5	130-150
Cetylpyridinium chloride	$C_{16}H_{33}N^+C_{16}H_{33}Cl^-$	3-4	110-150
Trimethylamine oxide	$(CH_3)_3N^+O^-$	2.5	100
Tetraethylammonium chloride	$(C_2H_5)_4N^+Cl^-$	2-2.5	110-140
Tetra- <i>n</i> -butylammonium chloride	$(C_4H_9)_4N^+Cl^-$	2	130
<i>n</i> -Octylamine	$C_8H_{17}NH_2$	1	30
Pyridine	C_5H_5N	1	30
Pyridine 1-oxide	$C_5H_5N^+O^-$	2	60

^a Reference 1.Figure 4. Theoretical values of the concentration fluctuation calculated from eq 5 for $n = 5$ and $l = 1, 2, 3$.

Thus, it is assumed further that l AB_n molecules form an aggregate of the type A_lB_n and that A_lB_n type molecules and B molecules are mutually independent in solution. Then, the relation of x , y , and n_A corresponding to eq 1 are

$$\begin{aligned} x &= n_A/l \\ y &= N - (n + 1)n_A \end{aligned} \quad (4)$$

and the expression for the concentration fluctuation of A is modified as

$$N((\Delta x_A)^2) = \bar{x}_A [1 - (n + 1)\bar{x}_A] [l - \{l(n + 1) - 1\}\bar{x}_A] \quad (5)$$

The theoretical curves calculated from eq 5 are shown in Figure 4 ($n = 5$) and in Figure 5 ($n = 20$). The curve corresponding to $n = 20$ and $l = 3-4$ can explain the experimental results very well. The best fit between the calculated and observed concentration fluctuation was obtained by setting $l = 3.4$ and $n = 18$. The final result for the theoretical calculation is shown in Figure 6.

Local Structure in the Solutions. The present results may be summarized as follows. CTACl dissolves in chloroform by forming an aggregate which is made up of about three or four CTACl molecules and about 60 chloroform molecules. This conclusion is an apparent contrast to the conclusion drawn from the infrared absorption intensity analysis, that is, CTACl dissolves in chloroform by forming a complex which is made up of about four or five chloroform molecules and one CTACl molecule. The basic idea of the infrared intensity study was that the number ratio of free and bonded chloroform molecules can be determined from the intensities of the absorption bands corresponding to the free and bonded chloroform molecules. Therefore, the infrared result affords rigorous information about the number of chloroform molecules which are directly attached to a CTACl molecule

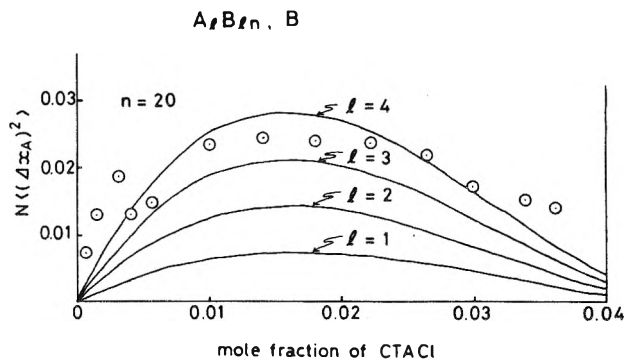
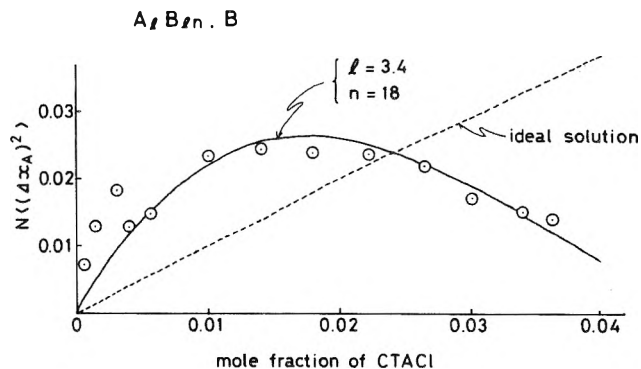
Figure 5. Theoretical values of the concentration fluctuation calculated from eq 5 for $n = 20$ and $l = 1, 2, 3, 4$.

Figure 6. Final results of the theoretical calculation.

by forming hydrogen bonds. In the light scattering study, however, the molecular aggregate which behaves as a single molecule in solution is important, because the concentration fluctuation is determined by the spacial distribution of component molecules in the solution.

Combining these two sets of results obtained from light scattering and infrared absorption studies, we may draw a picture for an aggregate formed in CTACl-chloroform solution. About four CTACl molecules make the core of the aggregate and the core is surrounded by about 60 chloroform molecules. Among the 60 chloroform molecules in one aggregate, about 15 chloroform molecules form hydrogen bonds directly with CTACl molecules and make the first shell. The remaining 45 chloroform molecules envelop the first shell by weak intermolecular interactions. In the above picture, we introduced implicitly the concept of two different types of chloroform molecules included in an aggregate. One is a chloroform molecule which forms a hydrogen bond with CTACl (chloroform A) and the other is with a chloroform (chloroform B). Since the chlorine atoms of the chloroform A molecule are more electronegative than those of usual chloroform molecules in the liquid phase, a weak hydrogen bond is expected between chloroform A and chloroform B molecules. The number of chloroform B molecules is expected to be three times

that of chloroform A molecules, because three molecules of chloroform B can attach to the three chlorine atoms of chloroform A molecules. In fact, the ratio of chloroform A to chloroform B molecules in one aggregate is observed to be 1:3.

Table I shows the number of chloroform molecules per one surfactant molecule, n , obtained from the infrared spectra for various cationic surfactants, where Γ_b and Γ_f are absolute intensities of the infrared absorption bands corresponding to the hydrogen bonded and free chloroforms, respectively. It has been shown that $[\Gamma_b^{1/2} - \Gamma_f^{1/2}]$ is proportional to the stabilization enthalpy originating from hydrogen bond formation between chloroform and surfactant molecules.⁷ Therefore, the product of n and $[\Gamma_b^{1/2} - \Gamma_f^{1/2}]$ is proportional to the overall stabilization enthalpy of one surfactant molecule due to hydrogen bond formation, ΔH , in solution. It is seen from the table that the $n[\Gamma_b^{1/2} - \Gamma_f^{1/2}]$ values of the surfactants whose n values are four or five are larger than those of the surfactants whose n values are one or two. This can reasonably be understood if we consider the entropy change due to the formation of an aggregate in solution. In case where an aggregate is formed in the solution, a decrease of the entropy value due to aggregate formation is expected. This, in turn, requires overall stabilization enthalpy for the surfactant molecule in order to dissolve in chloroform, which may actually be realized by hydrogen bond formation. In other words, in order to obtain much stabilization enthalpy, surfactant molecules such as CTACI associate mutually and form hydrogen bonds with many chloroform molecules. The stabilization enthalpy should overcome the decrease of entropy owing to association.

It is seen from Figure 6 that the experimental values where \bar{x}_A is smaller than 0.003 are larger than the theoretical values. We can obtain the l value to be $l = 6$ or 7 , in order to obtain the good agreement between the observed and calculated values in this concentration range, but cannot determine n value uniquely because the concentration fluctuation is rather insensitive to the n value in such low concentration range (see eq 10 or A5). In addition, we cannot know the number of chloroform A molecules because the information from infrared spectra is not available in this concentration range. However these experimental values may be of much importance, because it suggests the fact that the aggregation number in the low concentration range is larger than that in the high concentration range.

Appendix. Relation with Debye Plot

It will be shown below that, in the dilution limit, our method is identical with the Debye plotting method for determining the molecular weight of a solute molecule.

Debye presented an equation which is convenient to determine molecular weight of a solute molecule⁸⁻¹⁰

$$\frac{2\pi^2}{N_A \lambda^4} \left(n \frac{\partial n}{\partial c_1} \right)^2 \frac{c_1}{R_{90}} = \frac{1}{M_1'} + 2B_2 c_1 + 3B_3 c_1^2 + \dots \quad (\text{A1})$$

where n is the refractive index of solution, c_1 the concentration of solute (g mL^{-1}), N_A Avogadro's number, λ the wavelength of the incident light, R_{90} the Rayleigh ratio due to concentration fluctuation, M_1' the molecular weight of solute, and B_2 and B_3 are the virial coefficients. In case where an aggregate is expected even in the infinitely dilute solution, M_1' is equal to lM_1 , where M_1 is the true molecular weight and l is an average association number. In order to compare eq A1 with our method, we convert c_1 into mole fraction, \bar{x}_1 . Then, eq A1 becomes

$$\frac{K}{R_{90}} \bar{x}_1 = \frac{1}{l} + 2A_2 \bar{x}_1 + \dots$$

$$K = \frac{2\pi^2}{N_A \lambda^4} \left(n \frac{\partial n}{\partial x_1} \right)^2 \frac{M}{\rho}$$

$$A_2 = B_2 M_1^2 \frac{\rho}{M}$$

$$M = M_0(1 - \bar{x}_1) + M_1 \bar{x}_1 \quad (\text{A2})$$

where, ρ is the density of the solution and M_0 is the molecular weight of the solvent molecule. In our treatment, R_{90} is expressed as

$$R_{90} = \frac{2\pi^2}{\lambda^4} V \left(n \frac{\partial n}{\partial x_1} \right)^2 \langle (\Delta x_1)^2 \rangle \quad (\text{A3})$$

where V is the fluctuation volume. Modification of eq A3 leads to

$$\frac{K}{R_{90}} \bar{x}_1 = \frac{\bar{x}_1}{N \langle (\Delta x_1)^2 \rangle} \quad (\text{A4})$$

Substituting eq 4 into the right-hand side of eq A4, we obtain

$$\frac{K}{R_{90}} \bar{x}_1 = \frac{1}{l} + \left\{ \frac{2(n+1)}{l} - \frac{1}{l^2} \right\} \bar{x}_1 + \dots \quad (\text{A5})$$

Therefore, in the case of infinitely dilute solution, eq A5 is identical with eq A2 because the term higher than quadratic can be neglected. Comparing the coefficients of \bar{x}_1 in eq A2 and A5, it is seen that the virial coefficients are determined by only the association numbers, l and n , in our method.

References and Notes

- (1) M. Okazaki, I. Hara, and T. Fujiyama, *J. Phys. Chem.*, **80**, 64 (1976).
- (2) M. Okazaki, I. Hara, and T. Fujiyama, *J. Phys. Chem.*, **80**, 1586 (1976).
- (3) K. Iwasaki, M. Tanaka, and T. Fujiyama, *Bunko Kenkyu*, **25**, 134 (1976) (In Japanese).
- (4) K. Iwasaki, M. Tanaka, and T. Fujiyama, *Bull. Chem. Soc. Jpn.*, **49**, 2719 (1976).
- (5) K. Iwasaki, Y. Katayanagi, and T. Fujiyama, *Bull. Chem. Soc. Jpn.*, **49**, 2988 (1976).
- (6) T. Kato and T. Fujiyama, *J. Phys. Chem.*, **80**, 2771 (1976).
- (7) Y. Katayanagi and T. Fujiyama, to be published.
- (8) P. Debye, *J. Phys. Colloid. Chem.*, **51**, 18 (1947).
- (9) P. Debye, *J. Appl. Phys.*, **15**, 338 (1944).
- (10) P. Debye, *J. Phys. Colloid. Chem.*, **53**, 1 (1949).

The Deconvolution of Photoluminescence Data[†]

A. E. McKinnon,[‡] A. G. Szabo, and D. R. Miller*

Division of Biological Sciences, National Research Council of Canada, Ottawa, Canada K1A 0R6 (Received January 14, 1977)

Numerical techniques for deconvolution are many, and have rarely been compared for ease of use, accuracy of results, and resilience to noisy data. In this paper we report extensive computational tests using various artificial and real data sets and conclude that (i) several methods are satisfactory provided the structure of the observed data is simple, i.e., the lamp used has a sharp cutoff or the sample luminescence decay is accurately described by a single exponential process; (ii) if the decay is more complicated or the lamp has a long tail, a direct method of iterative convolution is more effective than any other; and (iii) artificial data may be generated which are indistinguishable from real observations. The problem of establishing confidence limits for the various parameters is discussed.

1. Introduction

Luminescence decay data produced by a short light stimulus have been used extensively in investigations of the excited state properties of many molecules,¹⁻⁷ particularly aromatic and biological molecules.⁸⁻¹⁰ The object is to interpret the luminescence data in terms of meaningful models of the physical processes which occur in the excited states. In most cases an exponential model for the luminescence decay is appropriate but others are sometimes used.¹¹

Deconvolution problems are important in a number of fields, and discussions have been presented in many places. Problems of this sort are important in communication theory¹² and in the general area of system identification.¹³ Recently, the deconvolution problem has also been studied in connection with measurement problems in the physical sciences,^{14,15} medicine,^{16,17} and applied optics.¹⁸⁻²²

All these problems share the feature that, if the stimulus may be regarded as instantaneous, the time course of the response (in our case luminescence) can be followed directly. Often, however, one wishes to study a response which occurs in a time comparable to that of the energy input itself; then, instead of observing the response directly, one can only observe the convolution integral of the response and the input. It is the problem of recapturing the "true" response that concerns us here.

In the specific case of fluorescence lifetime determinations using the single photon counting method¹⁰ or the sampling oscilloscope method²³ a repetitive lamp flash of nanosecond duration excites the sample and its fluorescence decay profile is measured. This decay profile is a convolution of the lamp intensity profile and the true fluorescence decay of the sample. The data may not indicate which of a variety of possible models and sets of parameter values is correct. In the more difficult situation where the width of the lamp pulse is comparable to the decay time of the sample emission, the problem of interpretation is aggravated by the need for a numerical deconvolution.¹¹

In theory, deconvolution is a mathematically well-defined problem. However, in fluorescence decay measurements the data are neither complete nor error-free, and in fact the functions are known only through an inherently noisy process of discrete observations over a finite time. Thus significant numerical difficulties exist, and a variety

of techniques have been developed to overcome them.

These techniques have not been subjected to exhaustive tests of comparative performance, especially tests distinguishing types of noise, distortions produced by the instrument itself, lamp characteristics, the differences between real and simulated data, and other factors. In this paper we report the results of such a study and recommend the use of iterative convolution as the technique of choice.

2. Problem Formulation

When excited by an energy input of a light flash that is not instantaneous, a sample fluoresces with a time distribution given by the convolution of the true excited state decay rate, say $g(t)$, and the lamp intensity function, say $f(t)$. The actual time-dependent emission thus has the form

$$h(t) = \int_0^t g(t - \tau) f(\tau) d\tau \quad (1)$$

The problem is simply to determine $g(t)$ when $f(t)$ and $h(t)$ are known, where $h(t)$ is the measured time intensity profile of the emission and $f(t)$ is that of the lamp. The difficulties are largely involved with the facts that, first, the functions $h(t)$ and $f(t)$ are known only at a limited number of discrete points and then with a certain numerical error; second, that regardless of the numerical difficulties the functions are measured by actual devices and are not directly observable.

The second point is often not really appreciated with the result that instrumental artifacts are often neglected. The functions $f(t)$ and $h(t)$ represent the "true" or undistorted response functions but what are actually observed or measured are the functions $F(t)$ and $H(t)$ which are functions that result from the former by convolutions with often unknown instrumental functions. However, if these latter convolutions are the same for both $F(t)$ and $H(t)$ then one can equally well use them to determine $g(t)$ in eq 1. Unfortunately this is not the case, for the lamp intensity profile, $F(t)$, must be measured at the wavelength of excitation of the sample since it is known that $f(t)$ varies with wavelength.²⁴

One of the important instrumental functions that is convolved in $F(t)$ and $H(t)$ is the time response of the detection photomultiplier. It is known that the time response of the photomultiplier varies with wavelength and recently it has been demonstrated that this variation, unless accounted for by a proper correction technique, will lead to inaccurate results in the deconvolution computations and a concomitant loss of confidence in the physical model chosen to represent the fluorescence decay.²⁵ In

[†] Issued as N.R.C.C. No. 16095.

[‡] Present address: Christchurch Clinical School, Christchurch Hospital, Christchurch, New Zealand.

TABLE I

Deconvolution method ^a	Function for the representation of $g(t)$	Reference to basic method	Treatment of difficulties	
			Effect of truncation of $h(t)$	Sensitivity to measurement error
1. Moments	Sum of decaying exponentials	Isenberg and Dyson ²⁶	Exponential weighting and iterative extrapolation ^b	Not explicitly treated
2. Modulating functions	Sum of decaying exponentials	Valeur and Moirez ²⁷	Not a theoretical limitation ^c	Not explicitly treated
3. Iterative convolution (weighted nonlinear least squares)	Representation of $g(t)$ is not restricted	Grinvald and Steinberg ²⁸	Not a theoretical limitation ^c	Dealt with by the least-squares process
4. Laplace transforms	Representation of $g(t)$ is not restricted	Gafni et al. ²⁹	Iterative extrapolation	Not explicitly treated
5. Exponential series	Series of decaying exponentials with fixed time constants	Ware et al. ¹⁰	Not a theoretical limitation ^c	Dealt with by least-squares estimation of exponential coefficients
6. Fourier transforms with high frequency filtering	Fourier series	Jones ³⁰	Exponential weighting ^b	Cosine bell filtering ^b
7. Fourier transforms with filtering to minimize second differences of $g(t)$	Fourier series	Hunt ¹⁴	Exponential weighting	Filtering to minimize second differences in $g(t)$

^a Methods 1-4 are intended for use when $g(t)$ is assumed to be the solution of a specific physical model for the luminescence decay. Of these methods, 1 and 2 may be used when the physical model includes only first-order kinetics (single exponential). Methods 5-7 are intended for use when it is desired to obtain a functional representation of the decay curve $g(t)$ without making assumptions as to the physical processes which may be occurring. ^b These represent additions or modifications to the published methods. ^c Although not a theoretical limitation in these methods, in practice, truncation of the measurement causes a loss of information because the data contain error.

what follows we assume that the functions which we deconvolve have been corrected for this effect and thus use $f(t)$ and $h(t)$ to represent correct observed data.

The solution of (1) for $g(t)$ is highly sensitive to numerical errors, and our task at this point is to minimize their effects. To do this many methods have been proposed and used, and one should examine the principal ones.

Generally, each method depends on the assumption that $g(t)$ can be represented as the sum of a (hopefully finite) number of functions of some specified family, so that the integral in (1) may be converted to a finite set of algebraic equations which may then be solved.

The functions chosen are generally either a mathematically complete set, infinite in number, which can represent a more-or-less general function but which have no physical or chemical basis, or else a very limited set chosen to correspond to the behavior expected for the system on physical or chemical grounds. Naturally, the latter allow more definite conclusions to be made, since the assumption of a certain process amounts to increased information. However, a priori physical models may be a hindrance if they are incorrect and, even if they are not, care must be taken when interpreting the results since other models might produce equally good results; one must not conclude that the presumed model is preferred simply because the fit is satisfactory. Although some authors have reported difficulty in fitting the leading edge of the decay curves, we know of no theoretical reason for this to be so. We have made no special allowances for such a phenomenon.

We have chosen seven deconvolution methods as being representative of what is done in the literature. These are

described in Table I, in which we also note the original references and give some indication about the characteristics of each. We assume the reader is familiar with the general nature of the methods, and refer to the supplementary material (see note at end of paper) for a precise description not only of the mathematical foundation of each approach, but also of the implementation in the present study.

3. Methods of Comparison

Initially one might plan to compare the various methods not only on the basis of their numerical features, specifically their ability to obtain correct answers in spite of noisy or limited data, but also for ease of programming and cost of the actual computation.

These latter points turn out, however, to be quite difficult to assess. Programming is in theory not a serious problem, since each of the methods discussed has been programmed by someone, and the program need only be adapted to a specified system. Concerning cost, both in terms of processing time and total storage requirements, we must observe that this is highly dependent on technique. As an example, the authors found that the first version of what is referred to here as the iterative convolution method, using a library Marquardt-type optimization program, occupied 118K bytes and was executed in 5.0 s of computer time. A second version programmed specifically for small storage requirements fitted into 11K bytes and was executed in 64.0 s. Such a range of values is typical when a selection of efficient library packages is available; while we have not verified it for each of the methods considered here, we surmise that each could be fitted into comparable storage.

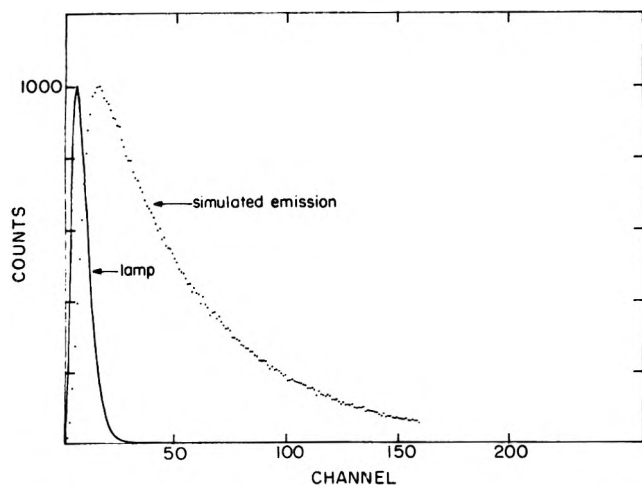


Figure 1. (a) Simulated sharp cutoff lamp (low tail) intensity profile according to the function $F(t) = 5.802t^2 \exp(0.4t)$: channel width corresponds to 0.12 ns, peak width at half-height ~ 1 ns. (b) Simulated fluorescence decay with $\alpha_1/\alpha_2 = 0.1$, $\beta_1 = 0.08 \text{ channel}^{-1}$, $\beta_2 = 0.02 \text{ channel}^{-1}$ convolved with simulated lamp intensity profile in (a) (case L in Table II).

We are left with consideration of the ability of the various methods to produce numerically good answers, and we see at once that several distinct difficulties may arise, and response to each needs to be investigated.

To begin with, determination of a decay curve (photoluminescence function) consisting of a single exponential term, the time constant of which is much larger than that of the lamp, ought not to present any difficulty, and it is reasonable to predict that any well-considered approach should work. However, the accuracy of a given method will decrease if (i) the signal-to-noise ratio is low (we have few counts per channel); (ii) the decay consists of more than one term, particularly if the constants involved are either very different or nearly identical; or (iii) the decay of the lamp is not particularly faster than that of the sample.

In practical terms, (i) may be thought of as an exact problem contaminated by various noise levels, (ii) is to be an experimentally investigated discriminatory ability, while (iii) amounts to very serious difficulty in analysis. Different methods may well be expected to react differently to each.

3.1. Nature of Test Data. In order to compare methods under controlled conditions, we prepared several artificial data sets. To begin with, we produced a "simulated lamp" by using a simple curve with the same general shape as a low-tail lamp (Figure 1). The actual function was

$$F(t) = 5.802t^2 \exp(-0.4t)$$

(In all the expressions to follow, t represents time, but is in units of channels of the multichannel analyzer which is used in single photon counting instrumentation. Since channel width is adjustable, time scales are not to be expected to be uniform.) Artificial sample data sets were obtained by convolving this function with

$$g(t) = \alpha_1 \exp(-\beta_1 t) + \alpha_2 \exp(-\beta_2 t)$$

for various values of α_i , β_i . Random error was added from a Poisson distribution, and relative error levels were made more severe by scaling down the data, adding noise, and renormalizing (Figure 1).

The details of these first test data sets are shown in Table II. Data sets A to D were designed to test the sensitivity of each method to measurement error. With

TABLE II: Parameter Values for Test Data Sets

Data set ^a	α_1/α_2	β_1 channel ⁻¹	β_2 channel ⁻¹
A	10.0	0.080	0.020
B	10.0	0.080	0.020
C	10.0	0.080	0.020
D	10.0	0.080	0.020
E	10.0	0.080	0.030
F	10.0	0.080	0.050
G	10.0	0.080	0.070
H	1.0	0.080	0.020
I	1.0	0.080	0.030
J	1.0	0.080	0.050
K	1.0	0.080	0.070
L	0.1	0.080	0.020
M	0.1	0.080	0.030
N	0.1	0.080	0.050
O	0.1	0.080	0.070
P	0.01	0.080	0.020
Q	0.01	0.080	0.030
R	0.01	0.080	0.050
S	0.01	0.080	0.070
T		1.25	

^a Peak counts in $h(t)$ equal to 10 000 in all cases except 1500 in A, 3000 in B, and 6000 in C.

a typical channel width of 0.12 ns the lamp specified above would have a half-peak width of about 1 ns, and exponents 0.08 and 0.02 would correspond to components with lifetimes of 1.5 and 6 ns, respectively. We set $0 \leq t \leq 159$ channels to give a realistic amount of data truncation for $h(t)$, so that $h(159)/h_{\max} = 0.008$. All methods were tested on data sets A to D.

Data sets E to S, all with 10 000 counts in the peak of $h(t)$, were used to test the ability of methods to discriminate between two exponentials with various ratios of lifetimes and coefficients. Only those methods (i.e., moments, modulating functions, Laplace transforms, and iterative convolution) intended for finding the parameters of decaying exponential functions were tested on these data sets. The final set, T, was designed to see how well each method could find the parameters of a very fast *single* component decay (lifetime of about 0.1 ns for the channel width of 0.12 ns).

All the above data sets represent cases where the simulated lamp decayed to a low value (short tail) over the time scale considered. This is not always the case in practice, since one must use narrow channels to observe a very rapid fluorescence decay or the very rapid component of a multiexponential decay process and equipment configuration limitations mean that the total time observed is short.

To test responses to these conditions further data sets were simulated using a real lamp decay profile which has a much slower decay (long tail) (Figure 2a). The various methods, now reduced to four in number because of earlier failures of the rest, were then tested for their ability to deconvolve this lamp in conjunction with (i) a simulated single-exponential decay profile (no noise), (ii) a simulated double-exponential decay profile (no noise) (Figure 2b), (iii) a simulated double-exponential decay profile with various levels of added noise (Figure 2c), and (iv) a real experimentally measured decay profile known to have double-exponential behavior (Figure 2d).

4. Results

The results are described in three ways: briefly in the paragraphs to follow, in somewhat more detail in Table III, and in full numerical detail in Tables IV–VI.

Essentially, the first four of the methods tested all work well for the simple case of a double-exponential decay

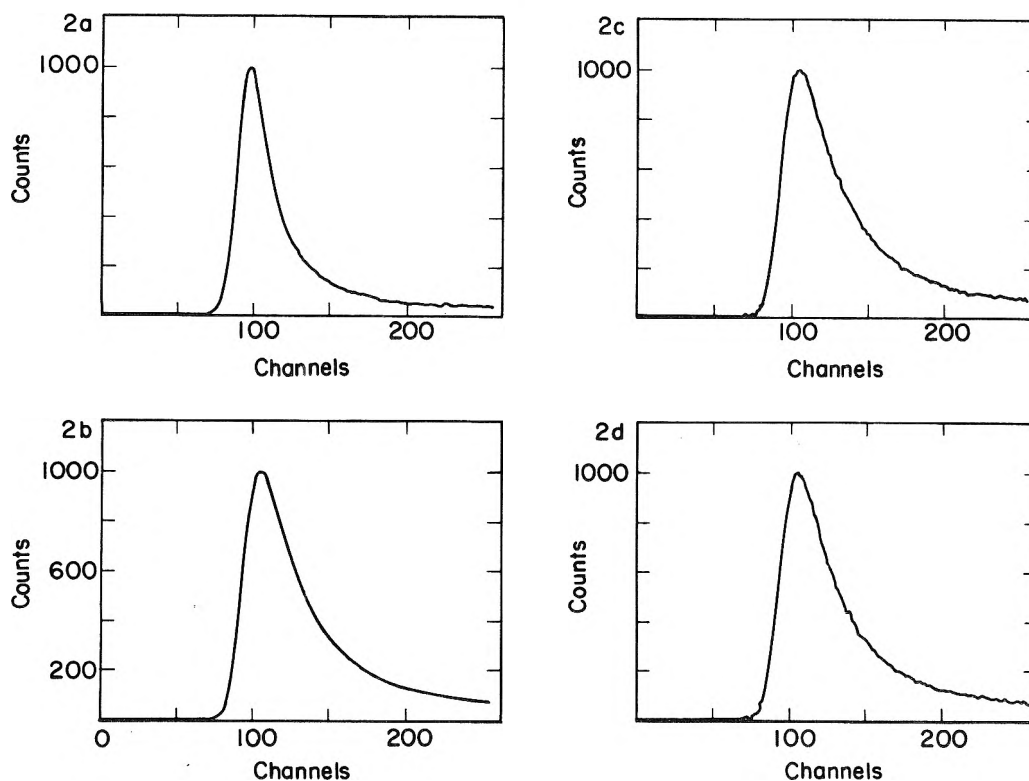


Figure 2. (a) Real lamp intensity profile having a long tail: channel width 0.12 ns, peak width at half-height ~ 3 ns. This lamp²⁵ was measured at 355 nm using a scattering solution. (b) Simulated measurement of a decay with a double exponential function with $\alpha_1 = 0.113$, $\beta_1 = 0.120$, $\alpha_2 = 0.0147$, $\beta_2 = 0.03$ convolved with real lamp in (a); no added noise. (c) As (b) but noise at level of real data added. (d) An actual observed decay of a system whose fluorescence is described by a double exponential function. In this case a cyclohexane solution of anthracene (2.1×10^{-5} M) and 2,2'-*p*-phenylenebis(5-phenyloxazole) (5×10^{-6} M); $\tau_1 = 4.89$ ns, $\tau_2 = 1.10$ ns. The lifetime values were the same as those measured for each component separately.

TABLE III: Summary of Results of Deconvolution Using Method of Moments, Laplace, Iterative Convolution, and Modulating Function Techniques

Case	Lamp $F(t)$	Sample $D(t)$	Result (four methods only)
1	Simulated (sharp cutoff)	Simulated (double exponential)	All methods successful
2	Simulated (sharp cutoff)	As in 1 with noise added	All methods successful, iterative convolutions slightly more accurate
3	Real (long tail)	Real (single exponential)	All methods successful
4	Real (long tail)	Simulated (double exponential, no error)	All successful except moments, which fails completely
5	Real (long tail)	As in 4 with added noise	Laplace fails; modulating functions inaccurate; iterative convolutions succeeds; moments unpredictable
6	Real (long tail)	Real (double exponential)	Identical with 5 (iterative convolutions is only reliable method)

convolved with a sharp cutoff lamp and a low noise level. Methods 6 and 7 gave unacceptable results in all cases and method 5 was unable to tolerate even low noise levels. Details of this performance are shown in Table IV; the final three methods were not tested further. The first four methods stood up more or less equally well to the case where the parameter values were varied in several different combinations, although the method of iterative convolutions performed slightly better and the method of moments not quite so well (Table V). The iterative convolution method was significantly more accurate in finding the fast decay in data set T.

In the simulated case of a long tailed lamp and a single-exponential decay, even with appropriate noise levels,

each of the four methods tested was quite acceptable (results omitted).

When the four methods were tested on a slow-decay real lamp and a double-exponential simulated data set with no noise (Figure 2b), the method of moments failed. When even slight amounts of noise were added to the artificial data sets, the method of modulating functions and the Laplace method failed (Table VI). When noise levels were reached corresponding to the noise levels in real data, only the method of iterative convolutions was satisfactory.

Finally, the test was repeated using real observed data, and all four methods behaved as they had for the simulated case with appropriate error levels (Table VI). We should point out that Ware et al.¹⁰ have reported that satisfactory

TABLE IV: Results of Tests on Data Sets A to D

Method	Data set	% errors in parameters			Mean sum of squares fit to $g(t) \times 10^7$
		α_1/α_2	β_1	β_2	
Moments	A	15.0	-3.9	-4.5	3.4
	B	11.0	-3.1	-4.0	1.2
	C	-14.0	3.0	8.5	1.2
	D	-19.0	3.5	11.0	0.6
Modulating functions	A	16.0	-1.3	-7.5	0.4
	B	-5.0	1.4	2.0	0.9
	C	-12.0	3.5	6.0	1.9
	D	5.0	-1.5	-2.5	0.4
Iterative convolution	A	-13.0	-3.0	-4.5	2.7
	B	-7.0	0.1	3.5	0.2
	C	2.0	0.3	0.0	0.3
	D	-2.0	0.6	1.0	0.2
Laplace transform	A	16.0	-3.9	-4.5	3.5
	B	-8.0	-0.1	4.0	0.4
	C	0.0	0.9	0.5	0.7
	D	-4.0	1.4	1.5	0.2
Exponential series ^a	A	70.0	-8.0	-23.0	11.1
	B	70.0	-7.8	-25.0	12.4
	C	-1.0	0.8	1.0	0.8
	D	-1.0	0.6	0.5	0.7
Fourier transforms with high-frequency filtering ^a	A	-50.0	3.7	45.0	20.6
	B	-33.0	0.1	25.5	51.7
	C	-36.7	2.9	28.5	23.5
	D	-2.0	0.9	0.5	12.7
Fourier transforms with filtering to minimize second differences of $g(t)$ ^a	A	964.0	-24.0	-100.0	41.0
	B	304.0	-17.4	-63.0	217.0
	C	154.0	-4.9	-100.0	1721.0
	D	129.0	-11.4	-40.0	186.0

^a For these methods the parameters α_1 , α_2 , β_1 , and β_2 were determined by fitting a sum of two exponentials to the $g(t)$ resulting from the deconvolution using the nonlinear least-squares program of Marquardt.³³ With the Fourier methods the first two and any negative points were eliminated before fitting.

TABLE V: Results of Tests of Four Methods on Data Sets E-T

Method	No. of parameters with greater than given error ^a				% error in exponent estimated for data set T
	2%	5%	10%	15%	
Moments	20	17	14	7	3.6
Modulating functions	13	10	6	6	22.0
Iterative convolution	11	7	6	5	0.3
Laplace transform	16	9	6	5	4.0

^a Only results from data sets E, F, H, I, J, L, and M were included in these figures because none of the methods could separate the two exponentials in data sets G, K, and N-S.

parameters were obtained by the exponential series method provided that a poor fit to the beginning or the end of the decay curve was ignored. We feel that making such allowances significantly reduces the confidence one has in the parameter values obtained and, for that matter, the accompanying physical model.

Several other observations are important. For example, a series of attempts were made to eliminate noise by some kind of Fourier smoothing process on either real data or artificial data to which Poisson noise had been added. In each case all methods responded to the smoothed data exactly as they had to the raw data.

An analysis of the form of the noise on real data was also made, and it was found that it was not of Poisson type, but had an added constant component. For comparability of results reported here to those generally reported,

however, noise added to simulated data was always Poisson. The analysis of noise characteristics will be reported elsewhere.

5. Discussion and Conclusions

From these observations we can determine which of the several deconvolution methods will provide values of kinetic parameters such that one can have a high degree of confidence both in their accuracy and in the validity of the associated physical model. First, the two Fourier series methods considered should not be recommended, as they provide substantial error even for "good" data sets. The method of exponential series, invariably at a disadvantage because of its preassigned discrete decay rates, fares somewhat better but is not competitive with the four methods which are specifically intended for finding the parameters of decaying exponentials.

Of the remaining four methods, the iterative convolution technique was marginally better in its sensitivity to noise and its ability to resolve exponentials when tested on the simulated data with a rapidly decaying lamp. This alone would be insufficient evidence on which to base a firm recommendation for its exclusive use; however, the tests using a long tailed lamp clearly demonstrate the superiority of this method.

Modulating functions is next best. Particularly for truncated data, this is mathematically reasonable since the moments method gives additional weight to points at large t values, and the Laplace transform method requires an artificial extrapolation which may be expected to be accurate only when truncation is insignificant.

In general, the method of modulating functions is restricted to the case where only simple exponential decays are expected, so that the iterative convolution procedure

TABLE VI: Total Percentage Errors in Four Parameters (Real Lamp, Simulated Two-Exponential Data with Varying Levels of Added Noise)

Run	Combination	Method			
		Iter convn	Moments	Mod functions	Laplace
1	A1-B1	0.0	9.11	17.59	1.85
2	A1-B2	6.95	28.04	59.25	9.11
3	A1-B3	5.05	212.43	340.13	29.27
4	A2-B1	1.01	8.25	10.17	1.36
5	A2-B2	2.86	177.69	129.98	28.97
6 ^a	A2-B3	10.49	153.98	234.21	10.21
7	A2-B4	5.73	453.72	<i>b</i>	54.53
8	A3-B2	0.68	273.30	469.41	29.31
9	A3-B3	2.18	135.93	286.73	10.35
10	A3-B4	17.78	416.08	<i>b</i>	38.48
11	A3-B5	27.32	250.06	1019.54	213.76
12	A4-B3	10.83	376.86	676.37	92.14
13	A4-B4	22.62	301.62	499.22	29.33
14	A4-B5	11.41	255.28	<i>b</i>	136.87
15	A5-B4	10.16	350.04	7336.20	29.46
16	A5-B5	21.55	255.38	1027.60	182.74
Example ^c		12.50	187.10	272.62	214.30

^a Chosen as most representative of real case. ^b Failure. ^c Example is performance on real data.

is even more reasonably preferred. Furthermore, this approach makes possible the testing of other physical models and the easy inclusion of additional constraints on the results since it is implemented by a nonlinear search procedure.

In any case it is clear that no matter which deconvolution method is used to find the parameters of an a priori model, careful interpretation of the parameter values is required. First it must be established that the model does adequately represent the data; second, error estimates for the fitted parameters must be obtained. These considerations appear to warrant far more discussion than they sometimes receive.

The question of model adequacy, specifically with regard to deciding whether one or two exponential functions are required, is of considerable interest, and can be investigated in several ways. To begin with, if the model is adequate the plot of the weighted residuals

$$r_e(k) = [w(k)]^{1/2} [h_e(k) - h_c(k)]$$

vs. k should appear to be randomly and uniformly distributed about zero. In this equation $h_e(k)$ is the number of counts of the luminescence measured in the k th channel, $h_c(k)$ is the value of the emission in the k th channel obtained from the derived model parameters after deconvolution and $w(k)$ is the weight assigned to the data in the k th channel (usually $w(k) = 1/h_e(k)$). In theory, the residuals cannot be entirely uncorrelated because the model parameters (usually no more than six) have been estimated from the data. However, as N is typically 150 or more, the weighted residuals have sufficient degrees of freedom (at least $N - 6$) so that this minor correlation cannot be observed. Attempts have been made³¹ to determine the statistical properties of the ratio

$$\frac{\sum_{k=2}^N [r_e(k) - r_e(k-1)]^2}{\sum_{k=1}^N r_e^2(k)}$$

with a view to using it as a quantitative measure of the randomness of the residuals, but the results are only approximate and cannot be used without also referring to the graph itself. Other authors^{28,29} calculate and plot the autocorrelation function of the weighted residuals. This approach offers no particular advantage and involves the same type of subjective decision as does the plot of the weighted residuals. It is evident that the adequacy of the model cannot be assessed satisfactorily from superimposed

graphs of $h_e(t)$ and $h_c(t)$ ¹⁰ because this display is not sufficiently sensitive. Similarly, criteria based on parameters such as the weighted sum of squares of residuals and the root mean square deviation³² should not be used by themselves because they may not detect significant correlation among the residuals.

When the adequacy of a model is being assessed, the performance of the whole instrument and its ability to conform to the convolution relation are actually being tested. Therefore, the failure of an adequacy test may mean a failure of the instrument or the model, or both.

Considerations such as these led us to the problem of the wavelength dependence of the time response of photomultiplier tubes (PMT). Like others we found that this problem has a marked effect on the results of deconvolution, making the parameter values for two exponential components virtually meaningless. We have developed and tested²⁵ a practical technique which enables the measured emission to be corrected for this time response variation with wavelength of the PMT.

Given that a model has been judged adequate there is no reason to assume that it is correct. Especially with exponential models it is impossible to be sure that there are not more components present than are required to explain the data.

The statistics of the model parameters are crucial in the interpretation of the deconvolution results. We use the iterative convolution method with the nonlinear least-squares algorithm due to Marquardt³³ because this algorithm includes calculation of a number of worthwhile parameter statistics. These statistics could be calculated after using any of the other deconvolution methods, however.

The principle of determining the confidence limits of the parameters is based on the sensitivity of the weighted sum of squares of residuals S to changes in the model parameters once it has been demonstrated that the model is adequate. Although $h_c(t)$ is unlikely to be linearly related to all the model parameters (e.g., in an exponential model $h_c(t)$ is linearly related to the α_j but nonlinearly related to the β_j) useful indicators of parameter accuracy (standard error estimates, parameter correlation matrix, conventional one-parameter confidence intervals, and support plane confidence intervals)^{33,34} can be obtained by assuming that, in the region of the best values of the parameters, the relation is linear. The support plane confidence interval for any particular parameter is the

maximum range of that parameter within which S is less than or equal to a value S_c which is usually a 95 or 99% confidence value. The other parameters are allowed to adjust to maximize this range. For the value S_c the parameters lie on an ellipsoid of m dimensions (in parameters) if $h_c(t)$ is linearly related to the parameters, but the shape of this surface is not known for a nonlinear model. Marquardt³³ suggests a method for determining a nonlinear confidence interval for each parameter, given that the other parameters remain at their best values, by incrementally increasing (or decreasing) the parameter value until S just exceeds S_c . However, the restriction placed on the other parameters means that the confidence interval obtained may be misleadingly narrow particularly if the parameters are highly correlated. At the expense of a great deal of computational effort the nonlinear support plane confidence interval for a particular parameter may be obtained by incrementally increasing (or decreasing) the parameter value and at each step minimizing S with respect to all the other parameters. When finally S just exceeds S_c one limit of the confidence interval for that parameter has been obtained.²⁸ Although undoubtedly the most rigorous approach, the extensive computations involved may not be worthwhile. As a compromise, we use the support plane confidence interval obtained using the linearity assumption, but at each parameter limit thus obtained we calculate S and compare it with S_c to get an indication of the extent to which the linearity assumption is valid.

The present work is not sufficient to answer all questions about optimization of the settings for various experimental parameters (such as channel width, effect of total counts, and minimum number of channels) for luminescence decay measurements. Neither have we answers to the important question as to what is the ultimate capability of the apparatus and under what conditions. Rather we have shown that the iterative convolution method is the most successful and reliable of the deconvolution methods tested and that it would be unwise to use the Fourier transform, moments, and exponential series methods. We have also pointed out that general use of the Laplace and modulating function techniques are limited and care must be taken in interpreting the results when using these methods. The question of the ultimate capability of the apparatus would require a much more extensive set of simulations than reported here.

Acknowledgment. The studies reported here required very substantial assistance in computer programming, equipment operation, and consulting on statistical

questions. The authors thank Lise Bramall, Dr. David Rayner, Mr. Peter Tolg, Dr. Peter Hackett, and Dr. Michael Zuker for help in these areas.

Supplementary Material Available: A precise description of the mathematical foundation of each deconvolution method studied (16 pages). Ordering information is available on any current masthead page.

References and Notes

- (1) V. W. F. Burns, *Arch. Biochem. Biophys.*, **133**, 420 (1969).
- (2) C. Yang and D. Soll, *Proc. Nat. Acad. Sci. U.S.A.*, **71**, 2838 (1974).
- (3) Y. Kubota, *Chem. Lett.*, 299 (1973).
- (4) B. Donzel, P. Gaudochon, and Ph. Wahl, *J. Am. Chem. Soc.*, **96**, 801 (1974).
- (5) Ph. Wahl, J. C. Auchet, A. J. W. G. Visser, and F. Miller, *FEBS Lett.*, **44**, 67 (1974).
- (6) M. R. Loken, J. W. Hayes, J. R. Gohlke, and L. Brand, *Biochemistry*, **11**, 4779 (1972).
- (7) A. A. Thaeer and M. Sernetz, Ed., "Fluorescence Techniques in Cell Biology", Springer-Verlag, New York, N.Y., 1973.
- (8) K. Salsbury in "Specialist Periodical Reports", Vol. 5, D. Bryce-Smith, Ed., The Chemical Society, London, 1974, pp 119-198.
- (9) M. H. Hul, P. De Mayo, R. Suau, and W. R. Ware, *Chem. Phys. Lett.*, **31**, 257 (1975).
- (10) W. R. Ware, L. J. Doemeny, and T. L. Nemzek, *J. Phys. Chem.*, **77**, 2038 (1973).
- (11) W. R. Ware in "Creation and Detection of the Excited State", Vol. 1, Part A, A. A. Lamola, Ed., Marcel Dekker, New York, N.Y., 1971, p 213.
- (12) D. Slepian and T. T. Kadota, *SIAM J. Appl. Math.*, **17**, 1102 (1968).
- (13) A. P. Sage and J. L. Melsa, "System Identification", Academic Press, New York, N.Y., 1971.
- (14) B. R. Hunt, *Math. Biosci.*, **10**, 215 (1971).
- (15) A. F. Jones and D. L. Misell, *Brit. J. Appl. Phys.*, **18**, 1479 (1967).
- (16) G. R. Neufeld, *J. Appl. Physiol.*, **31**, 148 (1971).
- (17) J. Szymendera, R. P. Heaney, and P. D. Saville, *J. Lab. Clin. Med.*, **79**, 570 (1972).
- (18) C. W. Barnes, *J. Opt. Soc. Am.*, **56**, 575 (1966).
- (19) G. Kunetz and J. M. Fourman, *Geophysics*, **33**, 412 (1968).
- (20) P. A. Jansson, *J. Opt. Soc. Am.*, **60**, 184 (1970).
- (21) W. C. Sauder, *J. Appl. Phys.*, **37**, 1495 (1966).
- (22) M. J. McDonnell and R. H. T. Bates, *Comput. Graphics Image Process.*, **4**, 25 (1975).
- (23) L. Hundley, T. Coburn, E. Garwin, and L. Stryer, *Rev. Sci. Instrum.*, **38**, 488 (1967).
- (24) Ph. Wahl, J. C. Auchet, and B. Donzel, *Rev. Sci. Instrum.*, **45**, 28 (1974).
- (25) D. M. Rayner, A. E. McKinnon, A. G. Szabo, and P. A. Hackett, *Can. J. Chem.*, **54**, 3246 (1976).
- (26) I. Isenberg and R. D. Dyson, *Biophys. J.*, **9**, 1337 (1969).
- (27) B. Valeur and J. Moirez, *J. Chim. Phys.*, **70**, 500 (1973).
- (28) A. Grinvald and I. Z. Steinberg, *Anal. Biochem.*, **59**, 583 (1974).
- (29) A. Gafni, R. L. Modlin, and L. Brand, *Biophys. J.*, **15**, 263 (1975).
- (30) R. E. Jones, Ph.D. Thesis, Stanford University (University Microfilms, Ann Arbor, Mich. 1976).
- (31) J. Durbin and G. S. Watson, *Biometrics*, **58**, 1 (1971).
- (32) E. Haas, M. Wilchek, E. Katchalskikatzir, and I. Z. Steinberg, *Proc. Nat. Acad. Sci. U.S.A.*, **72**, 1807 (1975).
- (33) D. W. Marquardt, *SIAM J.*, **11**, 431 (1963).
- (34) N. R. Draper and H. Smith, "Applied Regression Analysis", Wiley, New York, N.Y., 1966, p 265.

Absorption and Fluorescence Spectra of the Intramolecular Dimer in Polyvinyl-naphthalene

Masahiro Irie,* Takao Kamijo, Masayuki Akawa,¹ Takeshi Takemura,¹ Koichiro Hayashi, and Hiroaki Baba¹

The Institute of Scientific and Industrial Research, Osaka University, Suita, Osaka, Japan (Received April 5, 1976)

Solvent effects on the absorption and emission spectra of polyvinyl-naphthalenes were studied. In poor solvents, such as cyclohexane, new absorption and fluorescence spectra which are attributable to the dimer formed between naphthyl side groups of the polymer were observed in addition to normal spectra, though they are scarcely detected in good solvents. The dependence of the band intensity on solvent as well as on temperature indicates that dimer formation depends on the conformation of the polymer chain.

Introduction

Emission spectra of polymers with aromatic side groups have been studied extensively and it is now well established that the polymer emits fluorescence not only from the monomer but also from the excimer produced by intramolecular interaction between two chromophores.² Excimer formation in polystyrene³⁻⁵ and polyvinyl-naphthalene^{5,6} is attributed to the interaction of adjacent chromophores, while in polyacenaphthylene^{7,8} or poly-*N*-vinylcarbazole⁹ chain coiling is considered to play a role in producing geometries favorable to excimer formation between nonadjacent chromophores. In the case of poly-*N*-vinylcarbazole, the low temperature emission is composed of excimer and dimer fluorescence, and the dimer, which results from strong exciton coupling of neighboring chromophores, has a conformation different from that of the excimer.¹⁰

Although such emission characteristics are sensitive probes of the conformation of polymer, no extensive study on polymer emission spectra has been carried out as yet from this point of view. During the study of the photochemical reaction of polyvinyl-naphthalene,¹¹ we found that both its emission and absorption spectra were remarkably dependent on the solvent. In poor solvents new absorption and emission bands were observed in addition to the normal spectra. The purpose of this study is to identify these new bands and discuss the correlation of the bands to the conformation of the polymer in solution. The results are expected to contribute to the understanding of the primary process of the photochemical reaction of the long chain polymer.

Experimental Section

1-Vinyl-naphthalene and 2-vinyl-naphthalene were synthesized from the corresponding naphthaldehydes. The crude products were purified by column chromatography on silica gel with *n*-hexane as a solvent. They were polymerized in dilute benzene or cyclohexane solution ($\sim 10^{-1}$ mol/L) by the use of azobis(isobutyronitrile) as an initiator at 60 °C under degassed condition. The polymer yield was kept less than 5%. In order to eliminate the effect of double bonds at the polymer ends, they were saturated in tetrahydrofuran by palladium black in an atmosphere of hydrogen. The polymers were purified by repeated reprecipitation from methylene chloride solution with methanol and the soluble part of the product polymer in cyclohexane was used. The molecular weight distribution of the polymer used is shown in Figure 1. It was measured with a Tōyōsoda gel permeation chromatograph spectrometer (HLC-801). The viscosity average molecular weight is about 3000. The sample has no low molecular

weight impurity such as monomer or dimer.

Absorption and emission spectra were recorded by means of a Shimadzu UV-200 spectrometer and a Hitachi MPF-2A spectrofluorometer, respectively. The temperature of the sample was controlled by passing hot water around the sample holder and was monitored via thermocouples attached to the sample. A cell with a light pass of 10 cm was used for measurement of the temperature dependence of the absorption spectrum. All sample solutions were degassed by freeze-thaw cycles under a reduced pressure of less than 10^{-5} mmHg.

Results

(I) *Absorption Spectra.* Figure 2 shows the absorption spectra of poly-1-vinyl-naphthalene at room temperature in methylene chloride as well as in cyclohexane. The position and shape of the ${}^1L_a \leftarrow {}^1A$ band around 285 nm of the polymer in methylene chloride are similar to those of the model compound, 1,3-di- α -naphthylpropane, in solution at room temperature, though the vibrational structure in the polymer spectrum is not as clear as in the spectrum of the model compound. The shoulder observed at 315 nm in the polymer spectrum in methylene chloride can be assigned to the ${}^1L_b \leftarrow {}^1A$ band of the naphthalene nucleus. The spectrum of the polymer in methylene chloride (a good solvent) is thus attributed to a monomeric naphthyl side group, which will hereafter be called a monomer. The polymer spectrum in methylene chloride agrees with the spectrum obtained by Vala et al.⁵

The absorption spectrum of poly-1-vinyl-naphthalene in cyclohexane is, however, clearly different from that in methylene chloride and also from the corresponding spectrum of the model compound, especially in the region to the red of 330 nm. It has new bands at 339 and 331 nm, though the polymer in methylene chloride shows only an absorption tail at wavelengths longer than 330 nm. In addition to these longer wavelength absorption bands, new peaks appear at 253 and 243 nm. The bands around 340 and 250 nm are considered to result from a red shift or splitting of the ${}^1L_b \leftarrow {}^1A$ band at 315 nm and of the ${}^1B_b \leftarrow {}^1A$ band at wavelengths shorter than 240 nm, respectively. On the contrary, the ${}^1L_a \leftarrow {}^1A$ band around 285 nm shows a small blue shift in cyclohexane.

The new bands were observed not only in cyclohexane but also in other poor solvents such as *n*-hexane and tetrachloromethane. The absorption intensity, however, depends on the solvent used, the highest intensity being obtained in cyclohexane. By the addition of a good solvent to a cyclohexane solution, the intensity of the new band decreases. Figure 3 shows the dependence of the ratio of the intensity of the new band to that of the monomer band

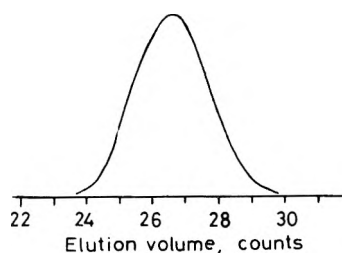


Figure 1. Gel permeation chromatograph of poly-1-vinylnaphthalene.

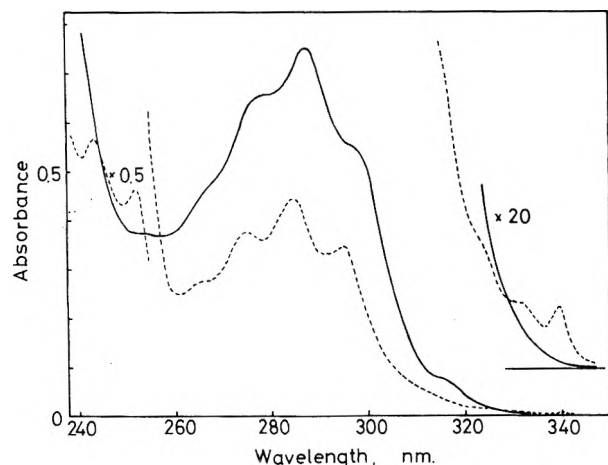


Figure 2. Absorption spectra of poly-1-vinylnaphthalene in methylene chloride (—) and in cyclohexane (---) at room temperature. The concentration of the polymer is the same in both samples and is 1.3×10^{-4} mol/L in monomer base unit. A cell with a light pass of 1 cm was used.

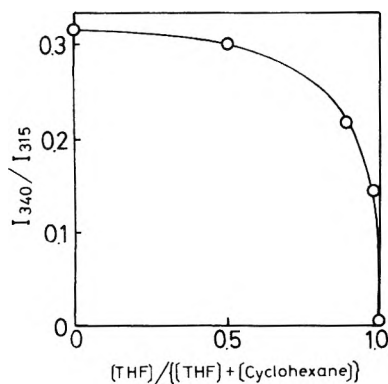


Figure 3. Solvent effect on the ratio of intensity of dimer absorption (340 nm) to that of monomer absorption (315 nm) for poly-1-vinylnaphthalene in mixed solvents of cyclohexane and tetrahydrofuran at room temperature.

on the content of tetrahydrofuran in the mixed solvent of cyclohexane and tetrahydrofuran. The intensity ratio decreases by the addition of tetrahydrofuran. The solvent effect suggests that the appearance of the new band is due to a conformational change of the polymer in a poor solvent, and the new spectrum is ascribed to a dimer formed by association of two naphthyl side groups; hereafter, this type of dimer will simply be called a dimer. The decrease in the interaction between polymer and solvent must cause a specific interaction between the naphthyl side groups to give the associated dimer conformation.

In a mixed solvent containing cyclohexane and tetrahydrofuran the intensity of the new band was found to depend on the temperature. The intensity of the new band decreased by raising the temperature, as shown in Figure 4. At 70 °C the shoulder due to the new band completely disappeared. When the sample was recooled to room

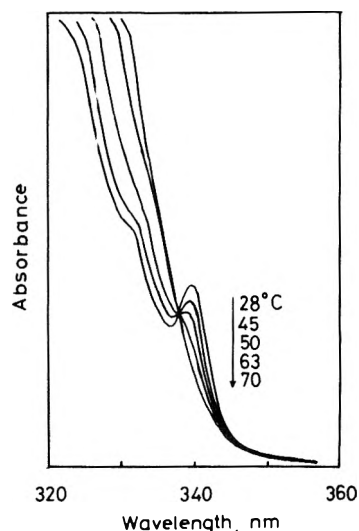


Figure 4. Temperature dependence of the absorption spectrum of poly-1-vinylnaphthalene in a mixed solvent of cyclohexane and tetrahydrofuran (volume ratio of 98:2). A cell with a light pass of 10 cm was used.

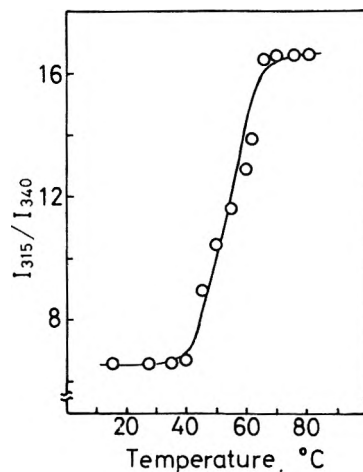


Figure 5. Temperature dependence of the ratio of the intensity of monomer absorption (315 nm) to that of dimer absorption (340 nm) for poly-1-vinylnaphthalene in a mixed solvent of cyclohexane and tetrahydrofuran (volume ratio of 98:2).

temperature, the shoulder reappeared, though it was not as clear as that in the initial sample. The ratio between the intensities at 315 and 340 nm indicates the recovery of about 50% of the initial content.

The dependence of the ratio between the intensities at 315 and 340 nm on the temperature is shown in Figure 5. The ratio increased remarkably in the region 40–65 °C, while no change was observed below 40 °C and above 65 °C even when the sample was allowed to stand for 30 h. The S-shape of the curve in Figure 5 suggests that the conversion from a rigid conformation to a normal one is a kind of phase transition. The transition occurs in a narrow temperature region between 40 and 60 °C. Above 65 °C, the mobility of the chain presumably becomes more important than the interaction between aromatic side groups of the polymer chain.

The specific conformation in poor solvents at lower temperatures is considered to be produced as a result of the decrease of the interaction between the polymer chain and solvent and the increase of the interaction between aromatic side groups of the polymer chain. It is expected that within the distribution of conformations there are geometries favorable to the formation of an associated dimer of the naphthyl side groups, which gives rise to a new absorption.

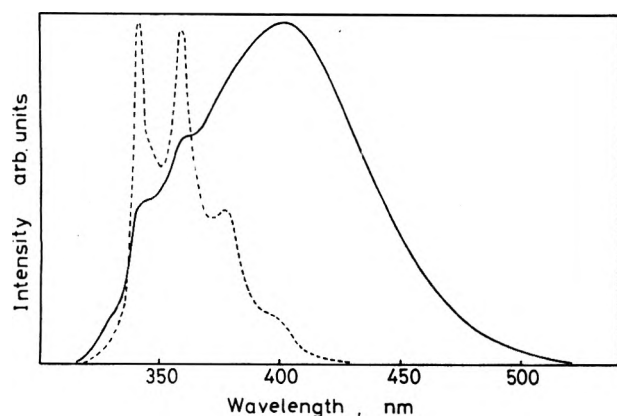


Figure 6. Fluorescence spectra of poly-1-vinylnaphthalene in methylene chloride (—) and in cyclohexane (---) at room temperature. The spectra are not corrected.

For poly-2-vinylnaphthalene in cyclohexane new absorption bands due to a dimer were observed at 339, 330, and 323 nm. The behavior of these bands is similar to the case of poly-1-vinylnaphthalene in both solvent effect and temperature dependence.

(II) *Fluorescence Spectra.* Fluorescence spectra of poly-1-vinylnaphthalene in methylene chloride as well as in cyclohexane are shown in Figure 6. The spectrum in methylene chloride has a maximum at 400 nm and shoulders around 325, 340, and 360 nm. This spectrum agrees with the result of Vala et al.⁵ and Fox et al.⁷ They attributed the band around 340 nm to monomer fluorescence and the structureless broad band at 400 nm to excimer fluorescence.

The fluorescence spectrum in cyclohexane has a clear vibrational structure with maxima at 342, 359, 378, and 397 nm. The positions of the former two bands are essentially the same as those observed in methylene chloride. The structureless broad band at 400 nm in methylene chloride, however, decreases remarkably in intensity and is scarcely observed in cyclohexane. The intensity of the emission band around 325 nm is also much smaller in cyclohexane.

The spectral difference between the two solvents suggests that there should exist three kinds of fluorescence emissions in poly-1-vinylnaphthalene. (1) The first emission is related to the band around 325 nm, which has a mirror symmetry with the absorption band at 315 nm due to the ${}^1L_b \leftarrow {}^1A$ transition of the naphthalene unit. The first emission is therefore ascribable to monomer fluorescence, with the 325-nm band being assigned to the 0-0 transition. (2) The second is related to the band at 342 nm, which has a mirror symmetry with the absorption band due to the associated dimer site at 339 nm. The second emission is assigned tentatively to dimer fluorescence, i.e., fluorescence emitted from an excited dimer which is produced by exciting the dimer with its conformation in the ground state essentially unchanged. The bands at 359, 378, and 397 nm behave similarly to 342-nm band, and all these bands are considered to be the members of a vibrational progression of dimer fluorescence. The spacing between successive bands of the progression is $0.14 \mu\text{m}^{-1}$. The difference in nature between the 325- and 342-nm bands is clearly evidenced by photoillumination. The band at 342 nm disappears with photoillumination to give a photoproduct, whereas the band at 325 nm increases in intensity.¹¹ (3) The last one is related to the broad band at 400 nm, and is unambiguously assigned to excimer fluorescence; here the excimer means a kind of excited dimer the conformation of which is suitable for strong interaction between constituent monomers and is

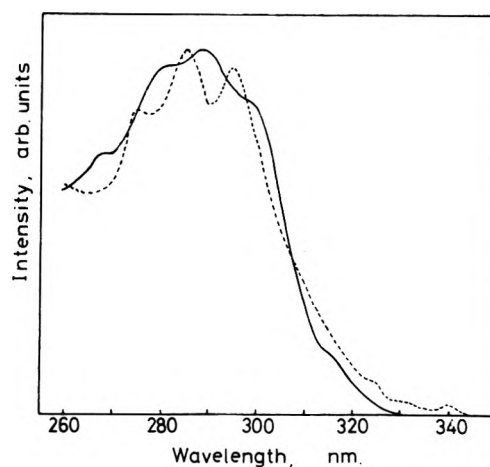


Figure 7. Excitation spectra of poly-1-vinylnaphthalene in methylene chloride at room temperature. The solid line spectrum is obtained when the fluorescence is monitored at 440 nm and at 330 nm, and dotted line spectrum at 360 nm. Both spectra are corrected.

clearly different from the conformation of the dimer formed in the ground state. By introduction of air, the dimer fluorescence is effectively quenched in comparison with the excimer. This quenching behavior suggests that the dimer lifetime is longer than that of the excimer.

Excitation spectra are shown in Figure 7 for the fluorescence of poly-1-vinylnaphthalene in methylene chloride. The excitation spectra obtained by monitoring the fluorescence at 330, 360, and 440 nm can be assigned, respectively, to the monomer, dimer, and excimer. These spectra will be referred to as excitation spectrum 1, 2, and 3, respectively.

Excitation spectrum 1 agrees with the absorption spectrum in methylene chloride (Figure 2), after correction for the spectral intensity distribution of the exciting light. Excitation spectrum 2 is obviously different from spectrum 1 and agrees with the absorption spectrum of the dimer. Furthermore, spectrum 2 resembles the corresponding excitation spectrum in cyclohexane monitored at 360 nm. It should be noted here that the absorption spectrum of poly-1-vinylnaphthalene in methylene chloride is considered to involve absorption due to the dimer to a small extent.

The disagreement between excitation spectra 1 and 2 confirms the view that the fluorescence bands at 325 and 359 nm originate from the monomer and dimer, respectively. Also, a comparison of excitation spectrum 2 with the absorption spectrum in methylene chloride reveals that the excited monomer is hardly responsible for the formation of the excited dimer; in other words, the excited dimer results mainly from excitation of the dimer itself.

Excitation spectrum 3 related to the excimer is essentially the same as excitation spectrum 1. This observation indicates that the excited monomer combines with the ground-state monomer during its lifetime to form the excimer or the energy absorbed by a monomer unit migrates to the excimer site.

In order to confirm further the above dimer assignment, the fluorescence spectrum of 1,3-di- α -naphthylpropane was also measured in cyclohexane in very diluted condition ($<10^{-6}$ M) at 77 K. If the fluorescence at 342 nm is due to the dimer, the spectrum is expected to be formed even in the bis(naphthalene) compound. The fluorescence spectrum measured at 77 K is very similar to that of the polymer in cyclohexane. It has peaks at 343 nm (maximum) and 358 nm. The similarity of the two spectra is unambiguous evidence of the formation of dimer in the polymer.

The fluorescence spectrum of poly-2-vinylnaphthalene in methylene chloride also involves three kinds of emissions; it shows a monomer emission band at 328 nm, dimer bands at 342, 359, and 379 nm, and an excimer band at 400 nm. The excitation spectrum of each emission component has the same characteristic as that of poly-1-vinylnaphthalene. The excitation spectrum of the dimer is evidently different from the excitation spectra of the monomer and excimer, though the latter spectra have the same character.

Discussion

It is generally supposed that the fluorescence in solution of a polymer with aromatic side groups is composed of monomer and excimer emissions, which give structured and structureless spectra, respectively. It is possible, however, that the fluorescence may contain another type of emission giving a structured spectrum. In fact, the results of the present investigations on the change of the excitation spectrum with the monitoring wavelength as well as on the solvent and temperature dependence of the absorption spectrum show that the structured part of the fluorescence spectrum of poly-1-vinylnaphthalene is composed of two kinds of emitting species, monomer and dimer.

The absorption spectrum of the dimer, which has a mirror symmetry relation with the dimer fluorescence, is clearly observed in cyclohexane solvent both at room temperature and at 77 K, but it is scarcely detected in methylene chloride or tetrahydrofuran. On the other hand, the fluorescence of the polymer in such good solvents gives structured bands at the same positions as the dimer fluorescence in cyclohexane. This fact means that the polymer chain involves a geometry favorable to the for-

mation of the dimer even in good solvents.

The well-defined vibrational structure of the absorption and emission spectra of the dimer and the relatively large spectral shift which occurs in passing from monomer to dimer suggest that two naphthyl groups are fixed in a specific geometry through strong interaction. The resulting dimer is so rigid in the polymer that it cannot be converted to the excimer even in the excited state, though the conformation of the excimer is more stable.

The absorption and emission characteristics of poly-2-vinylnaphthalene are very similar to those of poly-1-vinylnaphthalene. The argument made for poly-1-vinylnaphthalene is also applicable to poly-2-vinylnaphthalene.

Acknowledgment. The authors express their thanks to Professor F. De Schryver, University of Louvain, Belgium, for invaluable discussions and to Mr. P. Williams, University of Kent, England, for kindly reading the manuscript.

References and Notes

- (1) Research Institute of Applied Electricity, Hokkaido University, Sapporo, Japan.
- (2) W. Klöpffer in "Organic Molecular Photophysics", Vol. 1, J. B. Birks, Ed., Wiley, New York, N.Y., 1973.
- (3) S. S. Yanari, F. A. Bovey, and R. Lumry, *Nature (London)*, **200**, 242 (1963).
- (4) L. J. Basile, *J. Chem. Phys.*, **36**, 2204 (1962).
- (5) M. T. Vala, Jr., J. Haebig, and S. A. Rice, *J. Chem. Phys.*, **43**, 886 (1965).
- (6) L. A. Harrah, *J. Chem. Phys.*, **56**, 385 (1972).
- (7) R. B. Fox, T. R. Price, R. F. Cozzens, and J. R. McDonald, *J. Chem. Phys.*, **57**, 534 (1972).
- (8) C. David, M. Piens, and G. Gœuskens, *Europ. Polym. J.*, **8**, 1019 (1972).
- (9) P. C. Johnson and H. W. Offen, *J. Chem. Phys.*, **55**, 2945 (1971).
- (10) G. E. Johnson, *J. Chem. Phys.*, **62**, 4697 (1975).
- (11) M. Irie, T. Kamijo, and K. Hayashi, to be published.

Inorganic Ion Exchangers. 10.¹ A Neutron Powder Diffraction Study of the Hydrogen Bond Geometry in α -Zr(HPO₄)₂·H₂O. A Model for the Ion Exchange

J. Albertsson,* Å. Oskarsson,

Inorganic Chemistry, Chemical Center, University of Lund, P.O.B. 740, S-220 07 Lund 7, Sweden

R. Tellgren, and J. O. Thomas

Institute of Chemistry, University of Uppsala, P.O.B. 531, S-851 21 Uppsala 1, Sweden (Received February 25, 1977)

The hydrogen atom positions in the crystalline α phase of Zr(HPO₄)₂·H₂O (α -ZRP) were determined by profile refinement of powder neutron diffraction data. The structure is built up of zirconium phosphate layers which form cavities in which the water molecules are located. The monohydrogen phosphate groups donate hydrogen bonds to the water molecule which, in turn, donates one hydrogen bond to a phosphate oxygen atom. The other water hydrogen atom does not participate in hydrogen bonding. No hydrogen bonds occur between the zirconium phosphate layers; they are held together by van der Waals forces alone. Hydroxide ions must be added to an alkali metal halide solution before the metal ions enter α -ZRP. From this fact, an assumed small Donnan potential, and the location of the hydrogen atoms, a model for the ion exchange is suggested whereby hydroxide ions create sorption sites in α -ZRP by the reaction $\text{>O}_3\text{POH} + \text{OH}^- \rightarrow \text{>O}_3\text{PO}^- + \text{H}_2\text{O}$. This reaction should provide enough energy to move the zirconium phosphate layers apart, thus allowing hydrated metal ions to be sorbed at the phosphate groups.

Introduction

The ion exchange properties of crystalline α -zirconium bis(monohydrogen orthophosphate) monohydrate, Zr(HPO₄)₂·H₂O, denoted α -ZRP, have been studied extensively. No acceptable model has so far emerged for the

ion-exchange mechanism. This can be illustrated by the titration curves given in Figure 1, where the pH is shown as a function of the amount of base added per gram of α -ZRP. The uptake of Na⁺ and K⁺ occurs in two distinct steps, as if the two hydrogen phosphate groups in α -ZRP

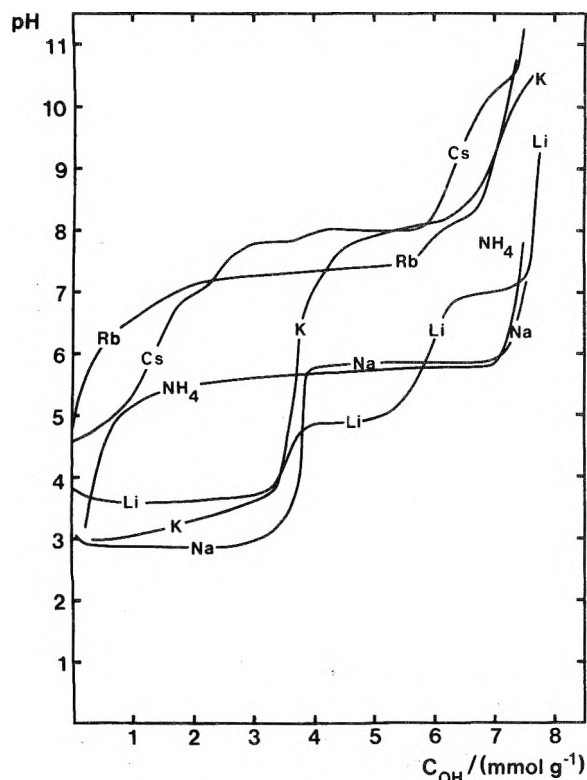


Figure 1. Potentiometric titration curves: pH vs. amount of base added per gram of α -ZRP for alkali metal and ammonium ions. Data are taken from ref 2-8.

TABLE I: Crystal Data for α -ZRP

Zr(HPO ₄) ₂ ·H ₂ O, mol wt 301.2
Monoclinic; space group $P2_1/c$
$a = 9.0610(10)$, $b = 5.2873(7)$, $c = 16.2481(31)$ Å
$\beta = 111.41(1)^\circ$; $V = 724.7$ Å ³
$Z = 4$; $D_x = 2.76$ g cm ⁻³

have different acidities.²⁻⁵ In contrast, only one step is found for NH₄⁺ while the Li⁺ curve has three.^{6,7} The Rb⁺ and Cs⁺ curves have anomalous shapes, but they may indicate only one step in the titration.^{2a,8}

In order to explain these and similar results, we must know the location of the sorption sites in solid α -ZRP, and the possibilities for various ions to reach these sites from the solution. The structure of the non-hydrogen atoms has been determined from x-ray intensity data by Clearfield and Smith.⁹ The crystal data are given in Table I. The structure comprises zirconium phosphate layers of pseudo-hexagonal symmetry (Figure 2). Any two adjacent layers are displaced relative to one another by $x = 1/3$, $y = 2/3$ (and by 7.54 Å in the z direction), so that cavities are formed between the layers. Each cavity contains one water molecule. Clearfield and co-workers⁴ have shown that if the phosphate oxygen atoms have a van der Waals radius of 1.4 Å, a spherical ion with a radius of less than 1.3 Å can enter the cavities along directions parallel to the zirconium phosphate layers. To enter the cavities in a perpendicular direction, the ion must have a radius less than 1.2 Å. Of the alkali metal ions only non-hydrated Li⁺, Na⁺, and K⁺ could possibly move through the α -ZRP structure, but not Rb⁺ and Cs⁺. The model of the M⁺/H⁺ exchange mechanism proposed in ref 4 requires a diffusion of unhydrated metal ions into the cavities through the small openings. This model is in conflict with the titration curves given in Figure 1.

A better understanding of the metal-ion sorption on α -ZRP would be possible if the positions of the hydrogen atoms were also known. The hydrogen-bond geometry

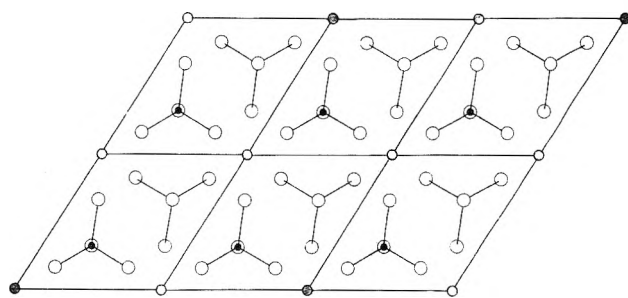


Figure 2. Idealized layer in the α -ZRP structure. Open circles represent oxygen, shaded zirconium, and black phosphorus. The axes a_h , b_h of this pseudo-hexagonal layer are related to the axes a_m and b_m of the monoclinic unit cell by $a_h = (a_m - b_m)/2$ and $b_h = b_m$.

determines the energy required to expand the entrances to the cavities. Since all attempts to make large single crystals of α -ZRP have failed, we turned to the powder neutron diffraction method (profile refinement) to locate the hydrogen atoms.

Experimental Section

A well-crystallized sample of α -ZRP was obtained by refluxing an amorphous preparation in 12 mol L⁻¹ H₃PO₄ for 300 h.³ The unit cell dimensions given in Table I were determined at 295(1) K with a Guinier-Hägg focusing camera as described previously.³ The neutron powder data were collected at about 295 K at the R2 reactor, Studsvik, Sweden. The instrument used was a four-circle diffractometer modified for powder work. The neutron beam was taken from a radial reactor channel and passed through a double monochromator system.¹⁰ The (200) planes in two copper crystals were used to give a wavelength of 1.56 Å and a neutron flux at the specimen of 10⁶ cm⁻² s⁻¹. The powder was packed lightly into a 12-mm diameter vanadium tube of length 40 mm. The range 10° < 2 θ < 108° was scanned in steps of 0.08°, and with a measuring time per step of about 8 min. Only the section 15-63° was used in the refinement. The data between 10 and 15° were omitted because of an electrical irregularity in the detector system, which was not discovered until after the measurements were completed. The profile above 63° was essentially featureless, so that this region too was omitted from the refinements. It was found experimentally that absorption could be neglected.

Structure Refinement

The programs used for data processing and structure refinement are local modifications¹¹ of the original Rietveld powder profile preparation and refinement programs.¹² The preparation program assigns to each point in the profile a set of contributing reflexions. They are calculated using the wavelength, cell dimensions, and a rough knowledge of the assumed Gaussian peak form. The refinement then proceeds to minimize the quantity $\sum w(y_o - k^{-1}y_c)^2$, where y_o is the number of counts at 2 θ after subtraction of the background contribution B ; k is a scale factor, and $w = (y_o + B)^{-1}$ the weighting function.

From the model of the heavy-atom structure (Table II) four possible hydrogen bond schemes could be proposed (Table III).⁹ A preliminary refinement of all four models immediately eliminated models 1 and 2. Noting model 3 to be an ordered form of model 4, a refinement of the hydrogen atom occupancies in model 4 clearly indicated that the correct structure was that defined by the ordered model 3 but with a significant shift applied to the suggested starting position for H(4). Further refinement of this latter model produced final R values $R_1 = 0.061$, R_{profile}

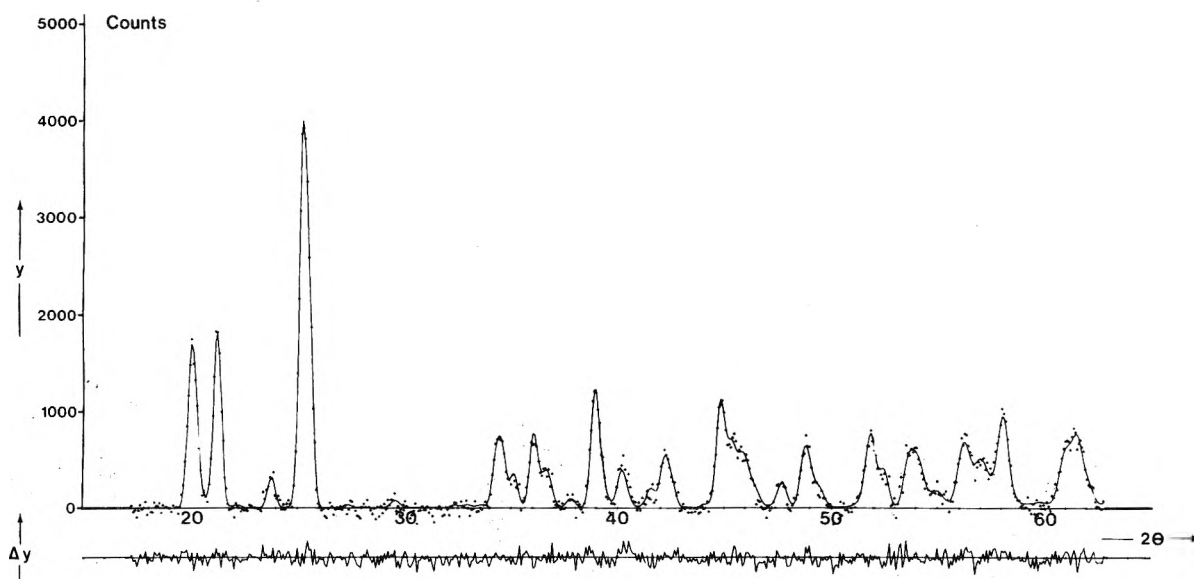


Figure 3. The neutron powder profile fit for α -ZRP. The points are the observed number of counts y_o at 2θ and the line is the calculated profile. The difference profile is on the same scale.

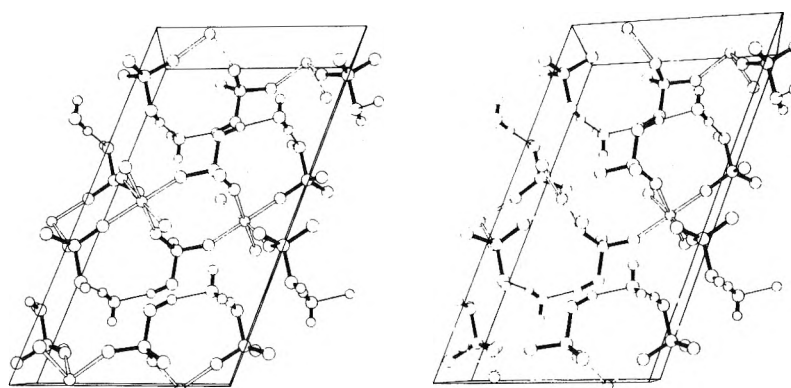


Figure 4. The structure of α -ZRP viewed along b .

TABLE II: The Heavy-Atom Positions (Fractional Coordinates) Used in the Refinement^a

Atom	x	y	z	$B, \text{Å}^2$
Zr	0.7606(2)	0.250(2)	0.5144(1)	0.67(2)
P(1) ^b	0.0008(6)	0.752(5)	0.6129(4)	1.13(8)
P(2)	0.4711(6)	0.245(5)	0.6044(4)	0.98(8)
O(1)	0.105(2)	0.806(5)	0.560(1)	1.7(3)
O(2)	-0.066(3)	0.486(6)	0.601(2)	2.6(4)
O(3)	-0.131(2)	0.941(5)	0.589(4)	1.6(4)
O(4)	0.104(2)	0.760(9)	0.716(1)	2.2(3)
O(5)	0.344(3)	0.443(5)	0.562(1)	2.0(4)
O(6)	0.418(2)	-0.014(5)	0.569(1)	1.6(3)
O(7)	0.625(2)	0.314(5)	0.590(1)	1.9(4)
O(8)	0.512(2)	0.243(9)	0.705(1)	2.3(3)
O(9)	0.254(2)	0.235(8)	0.759(1)	3.1(4)

^a The data are taken from ref 9. ^b P(2)-P(3) in ref 9 are changed to P(1)-P(2), O(4)-O(9) to O(1)-O(6), O(10) to O(8), O(11) to O(7), and O(12) to O(9). The coordinates of P(2), O(2), O(3), and O(5)-O(9) are transformed compared to ref 9.

$= 0.162$, and $R_{w,\text{profile}} = 0.134$. These R values are defined by $R_I = \sum |I_o - k^{-1} I_c| / \sum I_o$, $R_{\text{profile}} = \sum |y_o - k^{-1} y_c| / \sum |y_o|$, and $R_{w,\text{profile}} = \{ \sum w(y_o - k^{-1} y_c)^2 / \sum w \cdot y_c^2 \}^{1/2}$, respectively. I denotes the integrated intensity of a reflexion. At no stage were the original heavy-atom positions refined.

The final hydrogen atom positions are given in Table IV. The scattering lengths used in the refinements were 0.71, 0.51, 0.580, and -0.374×10^{-14} m for Zr, P, O, and H, respectively.¹³ The final profile fit is shown in Figure 3,

TABLE III: Four Possible Sets of Hydrogen-Atom Positions Suggested by the Heavy-Atom Structure of α -ZRP

	x	y	z	Occupancy
Model 1				
H(1)	0.17	0.92	0.73	1.0
H(2)	0.51	0.40	0.74	0.5
	0.51	0.09	0.74	0.5
H(3)	0.35	0.26	0.74	1.0
H(4)	0.18	0.40	0.74	1.0
Model 2				
H(1)	0.17	0.92	0.73	0.5
	0.17	0.60	0.73	0.5
H(2)	0.51	0.40	0.74	0.5
	0.51	0.09	0.74	0.5
H(3)	0.35	0.26	0.74	1.0
H(4)	0.18	0.40	0.74	0.5
	0.18	0.08	0.74	0.5
Model 3				
H(1)	0.17	0.92	0.73	1.0
H(2)	0.42	0.26	0.73	1.0
H(3)	0.18	0.40	0.74	1.0
H(4)	0.24	0.19	0.82	1.0
Model 4				
H(1)	0.17	0.92	0.73	0.5
	0.17	0.60	0.73	0.5
H(2)	0.42	0.26	0.73	1.0
H(3)	0.18	0.40	0.74	0.5
	0.18	0.08	0.74	0.5
H(4)	0.24	0.19	0.82	0.5
	0.26	0.25	0.82	0.5

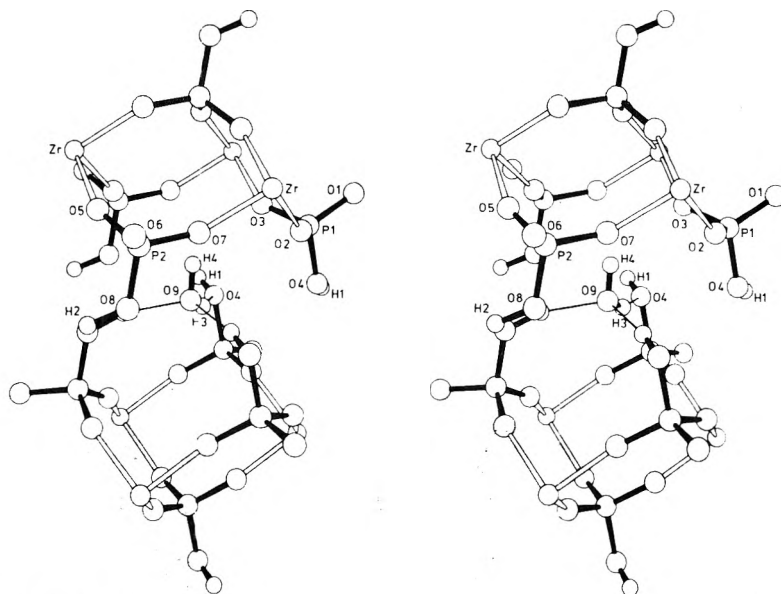


Figure 5. The cavity formed by two adjacent layers in α -ZRP.

TABLE IV: Final Positions of the Hydrogen Atoms in α -ZRP^a

Atom	x	y	z
H(1)	0.154(7)	0.908(11)	0.737(5)
H(2)	0.428(6)	0.275(12)	0.734(4)
H(3)	0.189(8)	0.375(9)	0.734(6)
H(4)	0.286(7)	0.273(12)	0.818(3)

^a The overall isotropic temperature factors B refined for Zr, P, O, and H were 0.8(3), 2.5(3), 1.9(2), and 6.9(8) Å², respectively.

a list of which can be obtained (from J.O.T.) on request.

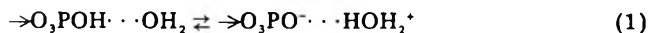
Structure Description

The unit cell content of α -ZRP is shown in Figure 4. Six phosphate oxygen atoms form a slightly distorted octahedron around each zirconium ion. There are two independent phosphate groups in the structure: P(1)O₄(1-4) and P(2)O₄(5-8). Each group is coordinated to three different zirconium ions forming layers of linked coordination polyhedra (Figure 2). The layers are parallel to the ab plane. In each layer the zirconium atoms are nearly coplanar with the phosphate groups located above and below this plane. Figure 5 shows the cavity formed by the relative displacement of adjacent layers. 24 phosphate oxygen atoms form the bounds of the cavity where the water molecule is located. The water molecule accepts the two hydrogen bonds O(4)-H(1)-O(9) and O(8)-H(2)-O(9) but donates only one bond, O(9)-H(3)-O(4). The second water hydrogen atom, H(4), points toward the top of the cavity, completing the approximately tetrahedral environment of the water molecule. Via the hydrogen bonds the water molecule participates in two ten-membered rings within the zirconium phosphate layer. There are no hydrogen bonds between the layers; they are held together

by van der Waals forces only. Table V gives a detailed description of the geometry of the water molecule, the hydrogen bonds, and the P-O-H angles.

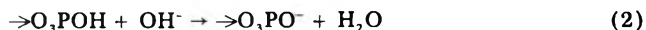
Discussion

The hydrogen bond geometry in α -ZRP shows no indication of disorder. This means that the hydrolysis reaction



within the cavities has a small equilibrium constant. The electrolytic conductivity in α -ZRP is about $9 \times 10^{-5} \text{ ohm}^{-1} \text{ cm}^{-1}$,¹⁴ which is a fairly large value but still compatible with a weak acidity of the monohydrogen phosphate groups. On the other hand, the bonding of each phosphate group to three zirconium(IV) atoms should greatly enhance the acidity compared to the acidity of HPO₄²⁻ in water solution ($\text{p}K_a = 12.32$). As the number of charged particles are small within solid α -ZRP, there should only be a small Donnan potential preventing negative ions from diffusing into the solid phase when α -ZRP is in contact with an electrolytic solution. Only negligible sorption of metal ions occurs when α -ZRP is brought to equilibrium with an alkali metal halide solution. Hydroxide ions have to be added before the metal ions enter the solid phase. On the basis of this fact, the presumably small Donnan potential, and the location of the acid hydrogen atoms in α -ZRP, we suggest the following stoichiometric mechanism for the sorption of an alkali metal ion.

Hydroxide ions accompanied by metal ions diffuse into the solid phase. In the following step a sorption site is created by the reaction



As can be seen in Figures 4 and 5, it is not necessary for

TABLE V: The Geometry of the Water Molecule and the Hydrogen Bonds^a

O(9)-H(3)	0.94(7) Å	O(4)-H(1)	0.91(7) Å
O(9)-H(4)	0.92(5) Å	H(1) ··· O(9) ⁱ	1.92(7) Å
H(3)-O(9)-H(4)	101(8)°	O(4)-H(1) ··· O(9)	169(7)°
		P(1)-O(4)-H(1)	116(5)°
O(9)-H(3)	0.94(7) Å	O(8)-H(2)	1.05(6) Å
H(3) ··· O(4)	2.16(7) Å	H(2) ··· O(9)	1.78(6) Å
O(9)-H(3) ··· O(4)	160(7)°	O(8)-H(2) ··· O(9)	159(6)°
		P(2)-O(8)-H(2)	123(4)°

^a The superscript i denotes the equivalent site $x, y + 1, z$ in the structure.

the hydroxide ion to enter the cavity before being close enough to a monohydrogen phosphate group to pick up its hydrogen atom.

If we divide the reaction in eq 2 into two steps



we can estimate the enthalpy change ΔH_2 in eq 2. ΔH for the dissociation $\text{HPO}_4^{2-} \rightarrow \text{H}^+ + \text{PO}_4^{3-}$ is about 15 kJ mol^{-1} .¹⁵ As the acidity of the monohydrogen phosphate group is larger in α -ZRP than in a "free" state, this is a maximum estimate of ΔH_3 . ΔH_4 is about -56 kJ mol^{-1} and we find

$$\Delta H_2 = \Delta H_3 + \Delta H_4 < -41 \text{ kJ mol}^{-1}$$

As the number of particles in eq 2 is unchanged, a rough estimate of $T\Delta S_2$ is zero resulting in $\Delta G_2 < -41 \text{ kJ mol}^{-1}$. The neutralization of the monohydrogen phosphate groups involves also the breaking and formation of hydrogen bonds inside the cavity. If we assume that the energy terms arising from these processes cancel each other, the energy ΔG_2 is available to move the zirconium phosphate layers apart. There is one O(7)...O(9) and one O(8)...O(8) van der Waals contact per cavity and two monohydrogen phosphate groups. Neutralization of only one of these should provide sufficient energy to move the layers apart, thus creating a transition state where hydrated alkali metal ions can reach the $\rightarrow\text{O}_3\text{PO}^-$ groups formed. The hydroxide ion acts as a wedge for the alkali metal ion. In the final steps of the sorption the zirconium phosphate layers, the alkali metal ions, and the water molecules inside α -ZRP rearrange themselves to obtain the energetically most favorable configuration.

Kinetic studies⁵ on the sorption of potassium ions are

in general agreement with the model we propose. When α -ZRP is brought in contact with a potassium hydroxide solution, its layers move apart as shown by a broad reflexion at low angle in the x-ray powder pattern.⁵ This reflexion was not present after the system had reached "equilibrium" (15 days). The neutralization and accompanying expansion of the cavities (the sorption of the hydrated metal ions) are thus fast processes, while the rearrangement to the less hydrated equilibrium phase is slow, since it involves diffusion of water molecules in the solid, metal-ion-loaded ZRP.

Acknowledgment. The Swedish Natural Science Research Council provided the financial support, which is hereby gratefully acknowledged.

References and Notes

- (1) For No. 9 in this series, see *J. Inorg. Nucl. Chem.*, **38**, 2377 (1974).
- (2) (a) J. Albertsson, *Acta Chem. Scand.*, **20**, 1689 (1966); (b) A. Clearfield and J. A. Stynes, *J. Inorg. Nucl. Chem.*, **26**, 117 (1964).
- (3) A. Clearfield, L. Kullberg, and Å. Oskarsson, *J. Phys. Chem.*, **78**, 1150 (1974).
- (4) A. Clearfield, W. L. Duax, A. S. Medina, G. D. Smith, and J. R. Thomas, *J. Phys. Chem.*, **73**, 3424 (1969).
- (5) A. Clearfield, W. L. Duax, J. M. Garces, and A. S. Medina, *J. Inorg. Nucl. Chem.*, **34**, 329 (1972).
- (6) A. Clearfield and R. Hunter, *J. Inorg. Nucl. Chem.*, **38**, 1085 (1976).
- (7) A. Clearfield and D. Tuhtar, *J. Phys. Chem.*, **80**, 1296 (1976).
- (8) G. Alberti, U. Costantino, S. Allulli, and M. A. Massucci, *J. Inorg. Nucl. Chem.*, **37**, 1779 (1975).
- (9) A. Clearfield and D. Smith, *Inorg. Chem.*, **8**, 431 (1969).
- (10) R. Stedman, L. Almqvist, G. Raunio, and G. Nilsson, *Rev. Sci. Instrum.*, **40**, 249 (1969).
- (11) J. O. Thomas, Institute of Chemistry, University of Uppsala, Sweden, Publication No. UUIC-B13-9 (1976).
- (12) H. M. Rietveld, *J. Appl. Crystallogr.*, **2**, 65 (1969).
- (13) G. E. Bacon, *Acta Crystallogr., Sect. A*, **28**, 357 (1972).
- (14) G. Alberti and U. Costantino, *J. Chromatogr.*, **102**, 5 (1974).
- (15) National Bureau of Standard Technical Note 270-3, Washington, D.C. 1968.

Surface Tension and Internal Pressure. A Simple Model

David R. Rosseinsky

Department of Chemistry, The University, Exeter, England (Received March 2, 1977)

A sphere in continuum model, with an internal surface, is used to relate surface tension and internal pressure. The results support the previous use of this model for polar interactions. The agreement of theory and experiment is close to that obtained with a recent lattice model.

The surface tension γ has been related¹ by means of a simple lattice model to the internal pressure $(\partial U/\partial V)_{T,N}$ and molecular number density n by

$$\gamma = \frac{1}{8n^{1/3}} \left(\frac{\partial U}{\partial V} \right)_{T,N} \quad (1)$$

For liquids with an r^{-6} pair potential the main approximation would introduce an inherent 11% error. The Onsager model² (polar molecules each assigned spherical volumes in continua having bulk-liquid permittivities) explains the perhaps surprising accord¹ of ether, among several nonpolar liquids: for ethers the dipole-dielectric interaction is demonstrably³ almost negligible, giving an observed vapor pressure close to that of the isostructural hydrocarbon, as predicted.³ The Onsager model implies a surface between sphere and surrounding dielectric, and it is of interest to examine whether explicitly defining this surface incurs any hitherto latent and unresolved complications.

TABLE I: Surface Tension Parameters of Several Liquids

Substance	T, K^a	3.22α	$(\partial U/\partial A)_{T,N}$ (eq 2 ^b), dyn cm ⁻¹	$(\partial U/\partial A)_{T,N}$ (expt ^c), dyn cm ⁻¹
Lattice model ¹		8		
Benzene	333	9.1	58.1	66.1
<i>n</i> -Heptane	303	8.0	47.6	47.9
Diethyl ether	286	7.8	45.2	43.0
Argon	87	8.8	20.0	34.3
Nitrogen	84	11.8	15.4	27.0
Oxygen	80	8.2	23.2	40.1
Methane	105	9.2	22.5	42.5
Carbon tetrachloride	315	8.4	53.5	63.3

^a Median value.¹ ^b From n and $(\partial U/\partial V)_{T,N}$ as in ref 1. ^c From¹ J. J. Jasper, *J. Phys. Chem. Ref. Data*, **1**, 841 (1972).

Changes in V implied in $(\partial U/\partial V)_{T,N}$ are assumed to occur essentially in the regions between molecules, each,

considered singly, filling a spherical volume $1/n$. Concomitant changes are imputed to the surface area A of the enclosing spherical cavity similarly envisaged. Then

$$\left(\frac{\partial U}{\partial V}\right)_{T,N} = \left(\frac{\partial A}{\partial V}\right) \left(\frac{\partial U}{\partial A}\right)_{T,N} = \frac{2}{a} \left(\frac{\partial U}{\partial A}\right)_{T,N} \quad (2)$$

where the factor $2/a$ refers to a compressible sphere of radius a . Now γ is dG/dA , which is closely equal to $dU/dA - T(dS/dA)$, both derivatives here being assumed constant with T , and deemed approximately equal to the partial derivatives. It is convenient to write the approximations as

$$\gamma = \frac{1}{\alpha} \left(\frac{\partial U}{\partial A}\right)_{T,N}$$

where $1/\alpha$ representing $1 - T(\partial S/\partial A)(\partial A/\partial U)_{T,N}$ is calculable from experimental values of γ and T . Hence with a expressed in terms of the molecular volume $1/n = 4\pi a^3/3$

$$\begin{aligned} \gamma &= \frac{1}{2\alpha} \left(\frac{3}{4\pi n}\right)^{1/3} \left(\frac{\partial U}{\partial V}\right)_{T,N} \\ &= \frac{1}{3.22\alpha n^{1/3}} \left(\frac{\partial U}{\partial V}\right)_{T,N} \end{aligned} \quad (3)$$

Values of 3.22α , from $\gamma(T)$ for several liquids,¹ are compared in Table I with the lattice value 8, eq 1. The average of the Table I values is 8.9, and the individual deviations are tolerable. Correction of the lattice value by the 11% referred to inductorily would give yet closer agreement.

The inclusion of α on the right-hand side of eq 3 merely facilitates comparison and involves no circularity of argument. It could be omitted and $(\partial U/\partial A)_{T,N}$ from eq 2 compared directly with that for the experimental $\gamma(T)$. The accord shown in the table is, as for γ itself with the lattice value,¹ to within 18% of absolute values. Discrepancies here are clearly associated with small size, but the larger molecules conform relatively well. For such sizes no major error in the theory of vapor pressures³ should thus ensue directly from the surface tension of the molecular scale cavities implied in the Onsager model employed in that theory.³ The approximate agreement of the lattice and the sphere/continuum models, in providing similar phenomenological relations for γ , is a further satisfactory result.

References and Notes

- (1) H. T. Davis and L. E. Scriven, *J. Phys. Chem.*, **80**, 2805 (1976).
- (2) L. Onsager, *J. Am. Chem. Soc.*, **58**, 1486 (1936).
- (3) D. R. Rossensky, *Nature (London)*, **227**, 944 (1970); J. G. Kirkwood, *J. Chem. Phys.*, **2**, 354 (1934).

An Approximate Treatment of Long-Range Interactions in Proteins¹

Matthew R. Pincus^{2a} and Harold A. Scheraga^{2b}

Department of Chemistry, Cornell University, Ithaca, New York 14853 (Received December 28, 1976)

An approximate method, valid beyond a critical distance, is presented for evaluating the long-range interaction energies between the residues of a protein. This approximation results in large reductions in the computer time required to evaluate the energies, compared to the usual procedure of summing the interactions over all pairs of atoms in the interacting residues. Beyond a critical distance between convenient reference atoms in each residue, the long-range nonbonded (attractive) energy may be approximated by $-B_{ij}/(R_{ij})^6$, where R_{ij} is the distance between the above-mentioned reference atoms, and the long-range electrostatic energy may be evaluated as the Coulombic interaction energy between the centers of positive and negative charge on each residue. In this approximate procedure, the interactions between residues are computed in terms of properties of the residues instead of those of the individual atoms of each residue.

Introduction

Short³- and medium⁴-range interactions dominate in determining protein structure, and empirical algorithms (which neglect long-range interactions) provide a fairly good description of the approximate ranges of the backbone dihedral angles.⁵ However, in order to obtain a molecule with the proper size and shape, it is necessary to take the long-range interactions into account⁶⁻⁹ to obtain a more accurate specification of the backbone dihedral angles.

Because of the large amount of computer time required to compute *all* pairwise interatomic interactions (including the long-range ones) in a protein, generally only a portion of the long-range interactions are computed. In particular, those beyond some arbitrary cutoff distance from any given atom are neglected.¹⁰ While the long-range interactions beyond the cutoff distance are, individually, very small, there are *many* of them in a protein molecule, and their sum need not be insignificant. Further, since the long-range nonbonded interactions beyond the cutoff distance are attractive, they could serve to compact the structure

of a globular protein; i.e., their neglect might lead to a more expanded computed structure than actually exists (unless, as in the refinement of X-ray data on proteins,¹⁰ the molecule is constrained to fit the X-ray coordinates as closely as possible). The long-range electrostatic interactions could be attractive or repulsive, depending on the configurations of the charges.

The purpose of this paper is to introduce a rapid, approximate procedure for computing these hitherto-neglected long-range interactions. Beyond a critical distance of separation, two interacting residues are treated as spheres of given radii, instead of as individual atoms,¹¹ for calculating the long-range nonbonded interactions. By considering such interactions between two spheres, instead of between all pairs of atoms, a considerable saving of computer time can be effected. Similarly, beyond a critical distance of separation, the charge distributions of two interacting residues¹¹ may be replaced by two interacting dipoles for calculating the long-range electrostatic interactions. The interaction energy between two dipoles (represented in terms of monopoles) can be calculated

more rapidly than that between all pairs of point charges on the individual atoms of the whole residues. It will be shown that these approximations provide an accurate representation of the long-range interactions beyond a critical distance, in the sense that this approximate procedure leads to energies that are similar to those computed from all pairwise interactions.¹¹ At separations less than the critical distance, all pairwise interactions¹¹ are computed without introducing this approximation. From a practical point of view, no discontinuities are encountered at the critical distance during minimization procedures.

Methods

Using the current IUPAC-IUB convention,¹² a residue is taken as the following unit:



where R is the side chain of the particular residue (R = H for glycine). In the full-atom pairwise-interaction algorithm in use in this laboratory,¹¹ the net charge on this unit is zero, except for residues whose side chains are charged; in this paper, ionizable side chains are taken in their neutral form.

A. Nonbonded Attractive Interactions. To obtain nonbonded attractive energies between residues, the following procedure was used. Two identical residues were generated with the N atom at the origin,¹¹ so that the N-C α bond of each coincided with the *x* axis and the N-H bond of each lay in the second quadrant of the *x-y* plane.¹¹ Normally, the fully extended conformation (both backbone and side chain) was used for each residue except for proline (for which $\phi = -75^\circ$, $\psi = 150^\circ$). The extended conformation was usually chosen because, in this conformation, a residue sweeps out the greatest volume when rotated in space. The choice of conformation, though, is not of much importance, as will be shown in section A of the Results section. The residues were treated as rigid bodies, with no internal rotation about single bonds. A reference atom for each residue was then chosen to be the origin for that residue, i.e., the coordinates of each residue were translated such that the reference atom was at the point (0, 0, 0). One of the two residues was then translated along the *x* axis to a desired distance away from the other residue, called the reference residue. The distance of separation between two residues is defined to be the distance between the reference atoms of each residue.

The reference atom for any given residue was chosen to be the atom judged to be closest to the "center of mass" of the residue. The "radius" of the residue was then defined as the sum of bond lengths between the reference atom and the atom most distant from it plus the van der Waals radius of that most distant atom. The distance between two residues was always equal to or greater than the sum of the residue radii. The distance that is equal to the sum of the residue radii is called the critical distance. Table I lists the reference atoms and critical distances for the 20 naturally occurring amino acid residues.

The average energy for each distance of separation was obtained in the following manner. At a given distance of separation between residues, a large number of different orientations of the two residues was generated. For each of 27 different rotational positions for the reference residues, i.e., all combinations of three rotations each about the *x*, *y*, and *z* axes, 27 different rotational positions for the second residue were generated, resulting in a total of 729 orientations in the system. For each of the 729 orientations, generated at a given distance of separation between the two residues, the sum of the total nonbonded

TABLE I: Values of B_{ij} for Attractive Nonbonded Interactions and Critical Distances between Identical Pairs of Amino Acid Residues

Residue	Reference atom	$B_{ij} \times 10^{-5}$, kcal A ⁶	Critical distance ^a (C_{ii}), A
Alanine	C α	0.330	8.74
Arginine	C γ	1.577	16.64
Asparagine	C β	0.734	11.82
Aspartic acid	C β	0.678	11.82
Cystine	C α	0.370	10.98
Glutamine	C β	1.007	13.74
Glutamic acid	C β	0.920	14.06
Glycine	C α	0.180	8.74
Histidine	C β	1.174	12.72
Isoleucine	C β	1.111	11.82
Leucine	C β	1.156	11.82
Lysine	C γ	1.451	13.80
Methionine	C β	0.906	14.56
Phenylalanine	C β	1.868	12.72
Proline	C α	0.847	9.46
Serine	C α	0.391	10.98
Threonine	C α	0.635	10.98
Tryptophan	C γ	2.387	15.44
Tyrosine	C γ	1.654	14.90
Valine	C α	0.815	10.56

^a Defined as the distance between the reference atoms of two residues that is equal to the sum of the residue radii (see text).

and hydrogen bonding energies between the residues was calculated.¹¹ In this calculation, all CH, CH₂, and CH₃ groups were treated as united atoms.¹³

The 729 (closely spaced) energies were then averaged arithmetically, and the standard deviation from the average was calculated. The average energy, U_{ii} , at each distance of separation, R_{ii} , between identical residues *i* was assumed to obey the relation

$$U_{ii} = B_{ii}(R_{ii})^{-6} \quad (1)$$

where B_{ii} is the attractive coefficient for the nonbonded interaction energy between the two residues. This coefficient was computed by a weighted least-squares best fit of U_{ii} to $(R_{ii})^{-6}$.

The coefficient for the nonbonded interaction between nonidentical residue pairs, B_{ij} , is obtained from the relation¹³

$$B_{ij} = (B_{ii}B_{jj})^{1/2} \quad (2)$$

and the critical distance between nonidentical residues *i* and *j* is equal to the sum of the radii of residues *i* and *j*.

If N_i and N_j are the numbers of atoms in the two residues, there are N_iN_j pairwise nonbonded interactions in the full-atom treatment, but only one in the approximate procedure. For N_i and N_j each of the order of ~ 10 , this effects a considerable saving in computer time.

B. Electrostatic Interactions. When the separation of two residues is large enough, the electrostatic energy between the point atomic charges of one residue and those of the other may be represented by a dipole-dipole interaction energy.¹⁴ In this case, the dipole in each residue may be treated as two point charges, one of which represents the center of positive charge and the other the center of negative charge. The vector C^+ from the origin of the residue coordinate system to the center of positive charge is defined as

$$C^+ = (1/Q^+) \sum_i q_i^+ r_i^+ \quad (3)$$

where q_i^+ is the positive charge on the *i*th atom at a position r_i^+ in the given residue, and Q^+ is the sum of all positive charges in the residue, and is equal to the absolute

value of the sum of all negative charges in the residue. The values of q_i^+ are partial atomic charges obtained by the methods described in ref 11. A similar definition gives C^- .

Coulomb's law (with a dielectric constant of 2)¹¹ is used to calculate the electrostatic energy as an interaction between the two charges on one residue with the two on the other. Thus, only four Coulomb terms need be calculated, instead of $N_i N_j$ where N_i and N_j are the number of charges on the atoms of each residue.

In the case of electrostatic interactions between two residues, the energy will depend on both the conformation of each residue and on the orientation of each one relative to the other. It is, therefore, more difficult to assign a critical distance for the electrostatic interaction between two residues. For the sake of convenience, the critical value determined for pairs of residues is taken to be the same as for the nonbonded interactions. It will be seen below that reasonable agreement between the approximate and exact methods is obtained with this arbitrary choice of critical distance. The use of the same critical distance for both nonbonded and electrostatic interactions is also convenient computationally, since only one rather than two critical distances need be stored for residue types.

C. Test of Validity. The validity of the approximate methods discussed above is tested by determining the energy of interaction between pairs of residues of a protein whose reference atoms lie beyond or at the critical distances. The long-range energy of interaction between any such pairs of residues is the sum of the nonbonded (including hydrogen bonding) and electrostatic energies; each of these is determined by both the exact (summation of pairwise interatomic energies) and by the approximate methods. The total long-range interaction energy for the protein is then the sum of the pairwise residue interaction energies calculated by either of these two ways, as described above. If the energies determined in both ways agree, when tested on a number of proteins of differing numbers of residues, the method may be taken as valid.

Results and Discussion

The importance of long-range attractive nonbonded interactions in stabilizing proteins may be illustrated by consideration of the *number* of such interactions that occur. For example, for lysozyme, a protein of 129 residues, the number of interacting residues that are separated by distances greater than or equal to their critical distances is ca. 6400 or about half the total number of interresidue interactions. Similar results are obtained for many proteins ranging in number of residues from 100 to over 300.¹⁵⁻¹⁹ In each case, the number of long-range interactions is almost half the total number of interactions. Thus, while the individual interaction energies between pairs of residues may be small, the number of such interactions is large and, hence, the long-range nonbonded energy may be significant.

A. Nonbonded Attractive Interactions. For 729 relative orientations of two identical residues at any given distance of separation, there is a range of nonbonded interaction energies. This range is quite small for large distances of separation (>15 Å), and becomes larger for smaller distances. This range of energies arises from variations in *attractive* energies; in no case did two residues approach each other closely enough to cause atomic overlaps, due to the choice of residue radii. In Figure 1, the exact and approximate nonbonded energy is plotted against the distance of separation for each of two pairs of residues. It may be noted that, for each pair of residues in Figure 1, the average energy (exact) and that calculated by using B_{ij} are quite close at all points for both residue types up

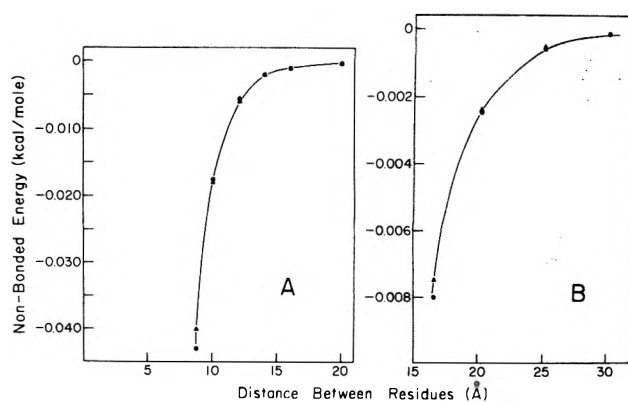


Figure 1. A plot of the average nonbonded energy of interaction between two residues as a function of their distance of separation. Filled triangles represent energies calculated from eq 1, using the value of B_{ij} for the particular residue pair. For most points, they overlap the average energies (calculated by the exact procedure) represented by filled circles. A. For a Gly-Gly pair. Each residue is in the extended conformation, and the values of α , β , and γ , the rotational angles around the x , y , and z axes, respectively, each were allowed to take on the values 0, 120, and 240°. B. For a neutral Arg-Arg pair, under the same conditions as in A, with side chain also in the extended conformation.

TABLE II: Variation of B_{ij} with Changes in Conformation and Relative Orientation for Representative Cases of Two Identical Interacting Amino Acid Residues

Residue	$B_{ij} \times 10^{-5}$ kcal Å ⁶	Rotational angle set, deg
Histidine ^a	1.174	0, 120, 240
Histidine ^b	1.055	60, 150, 300
Tryptophan ^a	2.387	0, 120, 240
Tryptophan ^a	2.489	30, 210, 315

^a All dihedral angles = 180°. ^b Backbone ϕ , ψ = -60°, -60°; side-chain dihedral angles = 180°.

to the critical distance where the discrepancy between the two values is still small. The values of B_{ij} for identical pairs of amino acids, together with the critical distances, at and beyond which this approximate procedure is valid, are presented in Table I.

To test whether the computed value of B_{ij} was independent of the choice of conformation and of the relative rotational positions, respectively, both the dihedral angles and the rigid-body rotational angles were varied for several different pairs of residues, and the value of B_{ij} was re-determined. The results obtained for two pairs of amino acid residues are shown in Table II. In each case, there is little change in B_{ij} .

Table III shows that, for three proteins^{16,20-22} chosen as examples, the approximate method gives values of the nonbonded energies that are in good agreement with those calculated by summing over all pairwise atomic interactions. This provides evidence for the validity of the approximate method. Especially in the case of lysozyme, the long-range nonbonded energies are quite substantial (-25 kcal/mol out of a total of about -200 kcal/mol), and can contribute toward compacting the entire structure. If the long-range nonbonded interactions beyond some cutoff distance were neglected, the external residues of the protein might be found to occupy positions further from the inner protein "core" in the computations. Substantial stabilization energy may be gained by allowing them to approach the "core" more closely.

B. Electrostatic Interactions. If the electrostatic interaction between two residues may be approximated by a dipole-dipole energy, it is reasonable to expect that this energy may be calculated as the electrostatic interaction

TABLE III: Comparison of the Approximation Method with the Pairwise-Atom Summation Method in Evaluating Long-Range Energies in Proteins^a

Protein	No. of residues	Total long-range nonbonded energy (atom-pairwise)	Total long-range nonbonded energy (using B_{ij})	Total long-range electrostatic energy (atom-pairwise)	Total long-range electrostatic energy (dipole)
Bovine pancreatic trypsin inhibitor ^b	58	-5.6	-5.5	-0.8	-0.5
Lysozyme ^c	129	-24.8	-25.4	-1.2	-1.8
Chymotrypsin B chain ^d	131	-14.3	-14.7	-0.2	-0.3
Chymotrypsin C chain ^d	97	-7.9	-7.8	-1.6	-1.1

^a All energies are in units of kcal/mol. ^b Reference 20. ^c Reference 16. ^d Structure generated with refined backbone dihedral angles (ref 21) and X-ray side-chain dihedral angles (ref 22).

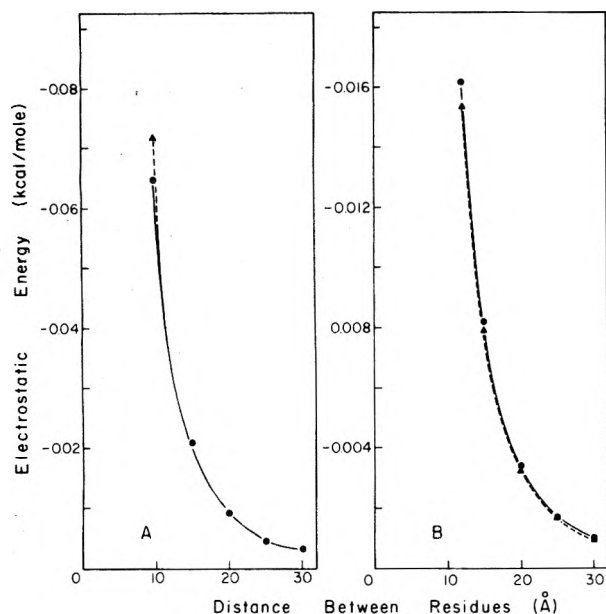


Figure 2. A plot of the electrostatic energy of interaction between two residues as a function of their distance of separation. The solid curve connecting the filled circles represents the electrostatic energy computed by the (exact) pairwise method.¹¹ The broken curve connecting the filled triangles represents the electrostatic energy calculated by the dipole method. The values of α , β , and γ were all taken as 0° in this example. A. For an Ile-Ile pair. $\phi = -153^\circ$, $\psi = 144^\circ$, $\omega = 180^\circ$, $\chi^1 = -163^\circ$, $\chi^{2,1} = 167^\circ$. B. For a neutral Asp-Asp pair. $\phi = -80^\circ$, $\psi = 95^\circ$, $\omega = 180^\circ$, $\chi^1 = -65^\circ$, $\chi^2 = 91^\circ$, $\chi^{3,2} = 180^\circ$.

energy between the centers of positive and negative charge of the two residues. In this case, it is necessary to evaluate only four distances between point charges rather than $N_i \times N_j$ where the latter two quantities are the number of atoms in residues i and j , respectively.

The validity of the approximate method for calculating the electrostatic energy was tested in two ways, first by comparing the results of the approximate method with that obtained by summing over all partial charges¹¹ for particular pairs of residues as a function of both the distance of separation between the residues and their relative orientations, and second by comparing the electrostatic energies of various proteins computed by both procedures. Two sets of residue pairs were examined, a nonpolar-nonpolar one, and a polar-polar one. Figure 2 shows the results for two pairs of amino acid residues Ile-Ile and uncharged Asp-Asp. In Figure 2, the pairs of residues were maintained in only one conformation and relative orientation; only the distance between the residues for each pair was varied. At each distance the electrostatic energy was calculated by both the full point charge method¹¹ and by the dipole method. The agreement between the two methods indicates that the approximate method is valid at and beyond the critical distance.

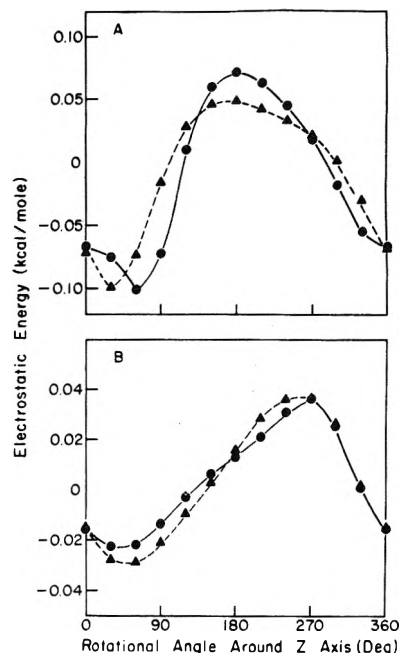


Figure 3. Comparison between the approximate method (filled triangles) and that involving summation over all pairwise interactions (exact) between atomic charges (filled circles). Two interacting residues are held at a fixed separation of their reference atoms which, in this case, was the critical distance. One residue was rotated in 30° increments around the z axis, i.e., the angle γ was varied in 30° increments, and the electrostatic energy was computed by both methods for each relative orientation. The values of α and β were taken as 0° in this example. A. For an Ile-Ile pair conformation as in Figure 2A. B. For an Asp-Asp pair conformation as in Figure 2B.

To examine further the validity of the approximate procedure at the critical distance, for the same pairs of residues, one of the residues of each pair was rotated around the z axis, and the electrostatic energy was computed by both methods as a function of rotational angle. The results, shown in Figure 3 for each residue pair, demonstrate a close correlation between exact and approximate energies at the critical distance.

A second test involved the computation of the electrostatic energies of several proteins by both procedures. The results, shown in Table III, indicate good agreement between both methods. In contrast to the long-range nonbonded energy, the long-range electrostatic energy is quite small. The probable reason for this is that, in the case of globular proteins, each residue is surrounded by a distribution of dipoles with essentially random orientations which, on the average, practically cancel leaving small residual energies. It must be noted that these sample calculations were performed on proteins whose structure is the final one, i.e., that of the already folded protein. It may happen that, in the folding of a protein, the positioning of regular structures of significant dipole moment

may in fact determine the conformations of particular residues through significant dipole–dipole interactions. The purpose of presenting the results of Table III here is merely to demonstrate that the approximate method is a valid one. Evaluation of the actual role played by long-range electrostatic effects in such processes as protein folding remains to be performed.

The computational time savings using the dipole method for the *long-range* interactions in a protein the size of pancreatic trypsin inhibitor is about 2.5. Thus, it also results in substantial reductions in computational times.

Acknowledgment. We are indebted to Drs. L. G. Dunfield and G. Nemethy for helpful comments on this manuscript.

References and Notes

- (1) This work was supported by research grants from the National Science Foundation (PCM75-08691) and from the National Institute of General Medical Sciences, National Institutes of Health, U.S. Public Health Service (GM-14312).
- (2) (a) NIH Postdoctoral Fellow, 1975–1976. (b) To whom requests for reprints should be addressed.
- (3) H. A. Scheraga, *Pure Appl. Chem.*, **36**, 1 (1973).
- (4) P. K. Ponnuswamy, P. K. Warne, and H. A. Scheraga, *Proc. Natl. Acad. Sci., U.S.A.*, **70**, 830 (1973).
- (5) For a recent discussion of empirical algorithms, see F. R. Maxfield and H. A. Scheraga, *Biochemistry*, **15**, 5138 (1976).
- (6) A. W. Burgess and H. A. Scheraga, *Proc. Natl. Acad. Sci., U.S.A.*, **72**, 1221 (1975).
- (7) S. Tanaka and H. A. Scheraga, *Proc. Natl. Acad. Sci., U.S.A.*, **72**, 3802 (1975).
- (8) M. Levitt and A. Warshel, *Nature (London)*, **253**, 694 (1975).
- (9) M. Levitt, *J. Mol. Biol.*, **104**, 59 (1976).
- (10) P. K. Warne and H. A. Scheraga, *Biochemistry*, **13**, 757 (1974).
- (11) F. A. Momany, R. F. McGuire, A. W. Burgess, and H. A. Scheraga, *J. Phys. Chem.*, **79**, 2361 (1975).
- (12) IUPAC-IUB Commission on Biochemical Nomenclature, *Biochemistry*, **9**, 3471 (1970).
- (13) (a) P. K. Warne and H. A. Scheraga, *J. Comput. Phys.*, **12**, 49 (1973); (b) L. G. Dunfield, A. W. Burgess, and H. A. Scheraga, manuscript in preparation.
- (14) J. A. Barker, *Proc. R. Soc. London, Ser. A*, **219**, 367 (1953).
- (15) P. C. Moews and R. H. Kretsinger, *J. Mol. Biol.*, **91**, 201 (1975).
- (16) C. C. F. Blake, L. N. Johnson, G. A. Mair, A. C. T. North, D. C. Phillips, and V. R. Sarma, *Proc. R. Soc. London, Ser. B*, **167**, 378 (1967).
- (17) J. C. Kendrew, H. C. Watson, B. E. Strandberg, R. E. Dickerson, D. C. Phillips, and V. C. Shore, *Nature (London)*, **190**, 666 (1961).
- (18) R. A. Alden, C. S. Wright, and J. Kraut, *Phil. Trans. R. Soc. London, Ser. B*, **257**, 119 (1970).
- (19) W. N. Lipscomb, G. N. Reeke, Jr., J. A. Hartsuck, F. A. Quiocho, and P. H. Bethge, *Phil. Trans. R. Soc. London, Ser. B*, **257**, 177 (1970).
- (20) R. Huber, personal communication.
- (21) K. E. B. Platzer, F. A. Momany, and H. A. Scheraga, *Intl. J. Peptide Protein Res.*, **4**, 201 (1972).
- (22) J. J. Birkoft and D. M. Blow, *J. Mol. Biol.*, **68**, 187 (1972).

Effect of Gallium Ions and of Preparation Methods on the Structural Properties of Cobalt–Molybdenum–Alumina Catalysts

M. Lo Jacono,[†] M. Schlavetto,^{*†} V. H. J. De Beer,[‡] and G. Minelli[†]

Centro di Studio su "Struttura ed attività catalitica di sistemi di ossidi" del CNR, c/o Istituto di Chimica Generale, Università di Roma and Istituto di Chimica Generale, Università di Roma, Roma, Italy and the Department of Inorganic Chemistry and Catalysis, University of Technology, Eindhoven, The Netherlands (Received December 30, 1976)

Publication costs assisted by Consiglio Nazionale delle Ricerche, Roma

Small amounts of gallium ions were added to γ -alumina and their influence on the structural properties of the system Co–(Mo)/ γ -Al₂O₃ was studied. It is shown that, due to the presence of Ga³⁺ ions, a "surface" spinel CoAl₂O₄ is formed with a larger amount of Co²⁺ in tetrahedral sites as compared to the spinel formed on gallium-free alumina. A decrease of the segregated Co₃O₄ is also observed. A possible effect of gallium ions on molybdenum is discussed. It is also reported that different preparation methods (single or double impregnation) lead to the formation of different surface species. Cobalt aluminate, molybdate monolayer, and Co₃O₄, depending on the Co content, are formed on doubly impregnated specimens. Cobalt aluminate and cobalt molybdate are the main species formed on singly impregnated specimens. Finally brief consideration is given to how the Co and Mo species, present in the oxide form, change in the sulfided form.

1. Introduction

In previous studies of supported oxide systems on alumina, it was shown that a "surface spinel" (MnAl₂O₄,¹ CoAl₂O₄,² NiAl₂O₄,³ CuAl₂O₄^{4a,b}) was formed, either alone or in addition to an oxide phase. Additions of trace amounts of Zn²⁺, Ga³⁺, and Ge⁴⁺ ions⁵ modify the surface properties of alumina, thus affecting the structural features of supported transition metal ions. The presence of these ions, all having a preference for the tetrahedral site, favors a normal cation distribution in the surface spinel NiAl₂O₄.⁵ Since the type of symmetry adopted by supported cobalt and molybdenum directly influences their reactivity, it was of interest to investigate the influence of Ga³⁺ ions in the

hydrodesulfurization (HDS) of Co–Mo–alumina catalysts. Within this framework we have also examined how the order of addition of transition metal ion promoters affects the structural properties of the Co–Mo/Ga₂O₃– γ -Al₂O₃ system in the oxide form, and how the Co and Mo surface species present in the oxide forms are related to those developed in the sulfided catalysts.

2. Experimental Section

2.1. Catalyst Preparation. The gallium-containing γ -alumina support (A γ Ga) was prepared by impregnating γ -Al₂O₃⁶ with gallium nitrate. The soaked mass, dried at 120 °C, was heated at 500 °C for 15 h. Two nominal Ga contents (atoms per 100 Al atoms) were prepared: 0.6 and 4 (designated as A γ Ga0.6 and A γ Ga4).

Different portions of the A γ Ga0.6 and A γ Ga4 supports were impregnated with a solution of cobalt nitrate of

[†] Università di Roma, Rome, Italy.

[‡] University of Technology, Eindhoven, The Netherlands.

TABLE I: Gallium-Containing Specimens and Their Properties

Samples	Co content, ^a wt %	Curie constant, C, erg G ⁻² mol ⁻¹ K	Magnetic moment, μ_B	Weiss temp $-\theta$, K	Co ²⁺ _{tet} , %
A γ GaCo(0.6:1)	1.12	3.11	4.99	20	42
A γ GaCo(0.6:2)	2.29	2.95	4.86	28	59
A γ GaCo(0.6:3)	3.15	2.96	4.87	35	58
A γ GaCo(0.6:4)	4.32	2.96	4.87	38	58
A γ GaCo(0.6:5)	5.29	2.95	4.86	46	(59) ^b
A-A γ GaMoCo(0.6:5:1)	1.42	3.60	5.35	30	0
A-A γ GaMoCo(0.6:5:2)	2.11	2.97	4.90	25	57
A-A γ GaMoCo(0.6:5:3)	3.31	2.97	4.90	30	57
A-A γ GaMoCo(0.6:5:4)	4.19	3.05	4.94	30	48
A-A γ GaMoCo(0.6:5:5)	4.96	3.05	4.94	36	(48) ^b
B-A γ GaMoCo(0.6:5:1)	1.17	2.86	4.80	22	68
B-A γ GaMoCo(0.6:5:2)	2.30	3.00	4.90	25	54
B-A γ GaMoCo(0.6:5:3)	3.07	3.28	5.12	23	24
B-A γ GaMoCo(0.6:5:4)	4.21	3.20	5.08	25	32
B-A γ GaMoCo(0.6:5:5)	4.80	3.28	5.12	23	24

^a Analytical, see text. ^b Due to the presence of Co₃O₄ the value is less accurate.

TABLE II: Gallium-Containing Specimens and Their Properties

Samples	Co content, ^a wt %	Curie constant, C, erg G ⁻² mol ⁻¹ K	Magnetic moment, μ_B	Weiss temp $-\theta$, K	Co ²⁺ _{tet} , %
A γ GaCo(4:1)	1.10				
A γ GaCo(4:2)	2.10	3.08	4.99	22	45
A γ GaCo(4:3)	3.05	3.06	4.95	35	47
A γ GaCo(4:4)	4.12	3.03	4.93	40	49
A γ GaCo(4:5)	5.20	2.95	4.86	43	(59) ^b
A-A γ GaMoCo(4:5:1)	0.95	3.39	5.21	22	12
A-A γ GaMoCo(4:5:2)	1.91	3.14	5.01	24	39
A-A γ GaMoCo(4:5:3)	3.12	2.98	4.89	28	(57) ^b
A-A γ GaMoCo(4:5:4)	4.44	2.48	4.48	30	c
A-A γ GaMoCo(4:5:5)	5.00	2.54	4.53	30	c
B-A γ GaMoCo(4:5:1)	0.97	2.95	4.88	10	59
B-A γ GaMoCo(4:5:2)	1.72	3.21	5.07	25	31
B-A γ GaMoCo(4:5:3)	2.77	3.20	5.07	26	32
B-A γ GaMoCo(4:5:4)	3.52	3.26	5.13	36	26
B-A γ GaMoCo(4:5:5)	4.50	3.20	5.08	31	32
CoMoO ₄ (green)	26.8	3.53	5.32	11	0
CoMoO ₄ (violet)	26.8	3.42	5.24	13	8

^a Analytical, see text. ^b Due to the presence of Co₃O₄ the value is less accurate. ^c Value not calculated due to the large amount of Co₃O₄ present.

known concentration. The material was then dried at 120 °C, ground, and fired at 600 °C for 24 h in air. Cobalt- and gallium-containing catalysts are designated as A γ GaCo(0.6:x) and A γ GaCo(4:x) with x (nominal Co content in atoms per 100 Al atoms) equal to 1, 2, 3, 4, or 5.

The Co–Mo–Ga-containing catalysts were prepared by two different methods.

Method A. The supports A γ Ga0.6 and A γ Ga4 were impregnated with an ammonium heptamolybdate solution to obtain a Mo content of 5 atom % with respect to 100 Al atoms. The paste was dried at 120 °C, ground, and fired at 500 °C for 5 h. The catalysts so obtained are designated as A γ GaMo(0.6:5) and A γ GaMo(4:5).

Cobalt was subsequently added to different portions of A γ GaMo(0.6:5) and A γ GaMo(4:5) by impregnation with a cobalt nitrate solution followed by drying at 120 °C, grinding, and firing in air at 600 °C for 24 h. The catalysts are designated as A-A γ GaMoCo(0.6:5:x) and A-A γ GaMoCo(4:5:x) with x = 1, 2, 3, 4, or 5 atoms of Co per 100 Al atoms.

Method B. The supports A γ Ga0.6 and A γ Ga4 were impregnated with an ammonium heptamolybdate solution in the same amount as in method A followed only by drying at 120 °C. Different portions of this material were again impregnated with a solution of cobalt nitrate. The mass was then dried at 120 °C, ground, and fired at 600

°C for 24 h in air. The catalysts so obtained are designated as B-A γ GaMoCo(0.6:5:x) and B-A γ GaMoCo(4:5:x) where x has the same values as before.

Sulfurization. Portions of A γ GaCo(0.6:x), A-A γ GaMoCo(0.6:5:x), and B-A γ GaMoCo(0.6:5:x) catalysts were sulfided in a silica reactor at 400 °C, for 2 h, in a flow of H₂ (90 cm³/min) and H₂S (10 cm³/min).

2.2. Physical Characterization and Chemical Analysis. Optical reflectance spectra were recorded on a Beckman DK 1 instrument, in the range 250–210 nm at room temperature, using γ -Al₂O₃ as a reference. To check the influence of grain size on the reflectance spectra, some specimens were ground for 5 and 20 h in a mechanical mortar. The same spectrum was obtained in both cases. Therefore all spectra were recorded for samples ground for 5 h.

Magnetic susceptibility measurements were carried out by the Gouy method⁷ in the temperature range 100–295 K. The specimens were contained in a sealed silica tube.

X-ray analysis was carried out with Co radiation, using a Debye–Scherrer camera (114 nm diameter) or a diffractometer (Philips).

Chemical analysis for cobalt was performed by atomic absorption techniques (Varian Techtron AA5); concentrated H₂SO₄ was used to dissolve the specimens.³ The catalysts and some of their properties are listed in Tables I and II.

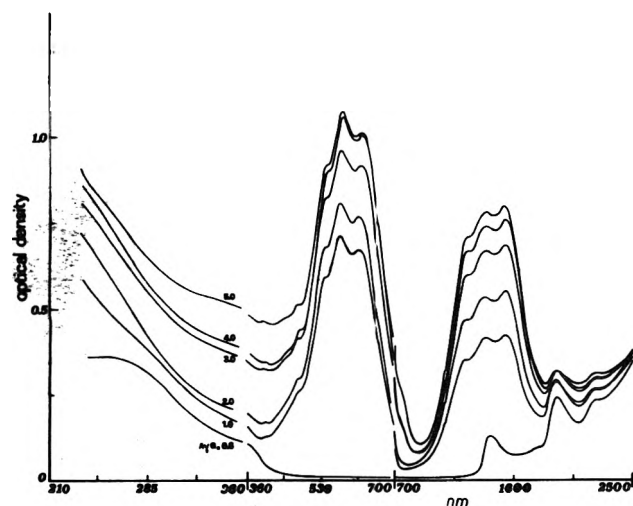


Figure 1. Reflectance spectra of $A\gamma\text{GaCo}(0.6:x)$ specimens with $x = 0-5$.

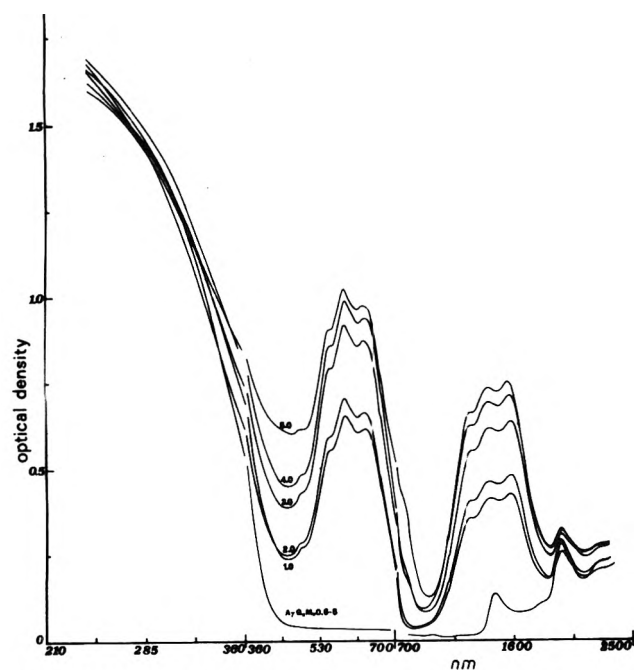


Figure 2. Reflectance spectra of $A-A\gamma\text{GaMoCo}(0.6:5:x)$ specimens with $x = 0-5$.

3. Experimental Results

3.1. *Reflectance Spectra.* Reflectance spectra were recorded for all samples. As the pattern of their spectra is essentially the same only representative series are reported. Figures 1 and 2 show the reflectance spectra of the $A\gamma\text{GaCo}(0.6:x)$ and $A-A\gamma\text{GaMoCo}(0.6:5:x)$ series, respectively. Detailed analysis of the reflectance spectra of Co^{2+} in different environments and of the assignment of optical transitions was discussed elsewhere.² Inspection of Figures 1 and 2 leads to the following conclusions:

(a) The spectra of the $A\gamma\text{GaCo}$ and $A\gamma\text{GaMoCo}$ specimens are dominated by bands due to Co^{2+} ions in tetrahedral symmetry² and their general pattern is qualitatively similar to that of the spinel $\text{Co}_x\text{Mg}_{1-x}\text{Al}_2\text{O}_4$ and of $\text{Co}^{2+}/\gamma\text{-Al}_2\text{O}_3$.²

(b) With increasing cobalt content the intensity of the absorption band at 578 nm is lower in the series $A\gamma\text{Co}_x$ (with $x \leq 3$ atom % since Co_3O_4 is present at higher x) than in the $A\gamma\text{GaCo}(0.6:x)$ series, Figure 3, as well as for the $A\gamma\text{GaCo}(4:x)$ series.

Recalling that the band at 578 nm is the most intense band for $\text{Co}^{2+}_{\text{tet}}$, one is led to the conclusion that the

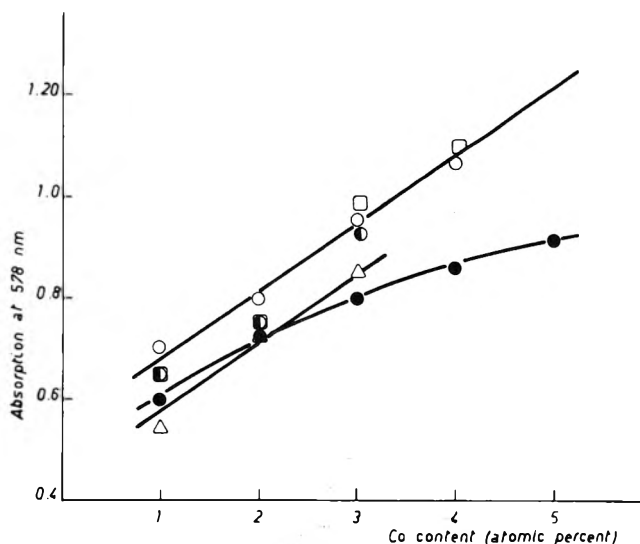


Figure 3. Intensity of the absorption band at 578 nm vs. cobalt content (atom percent): (Δ) $A\gamma\text{Co}_x$; (\circ) $A\gamma\text{GaCo}(0.6:x)$; (\bullet) $B-A\gamma\text{GaMoCo}(0.6:5:x)$; (\square) $A\gamma\text{GaCo}(4:x)$; (\blacklozenge) $A-A\gamma\text{GaMoCo}(0.6:5:x)$.

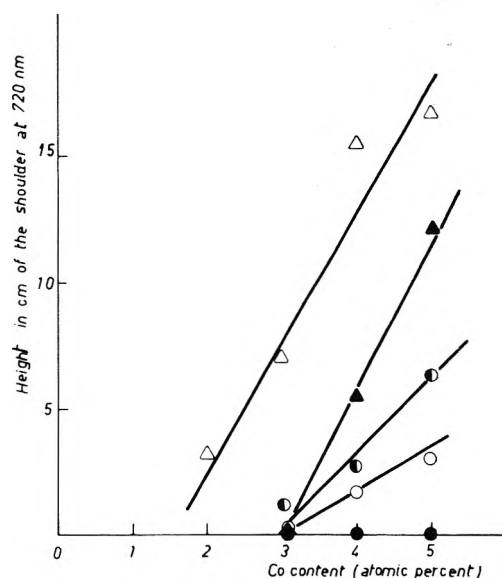


Figure 4. Intensity of the shoulder at 720 nm (Co_3O_4) vs. cobalt content (atom percent): (Δ) $A\gamma\text{Co}_x$; (\circ) $A\gamma\text{GaCo}(0.6:x)$; (\blacktriangle) $A\gamma\text{MoCo}(5:x)$; (\bullet) $A-A\gamma\text{GaMoCo}(0.6:5:x)$; (\bullet) $B-A\gamma\text{GaMoCo}(0.6:5:x)$.

amount of $\text{Co}^{2+}_{\text{tet}}$ is higher in Ga-containing specimens.

(c) Moreover, inspection of Figure 3 shows that the intensity of the band at 578 nm increases linearly with the Co content for $A\gamma\text{GaCo}(0.6:x)$ as well as for $A\gamma\text{GaCo}(4:x)$ and $A-A\gamma\text{GaMoCo}(0.6:5:x)$, while this is not the case for $B-A\gamma\text{GaMoCo}$, for which the curves become concave toward the abscissa at high Co content. This can be attributed to the presence of a new type of Co^{2+} with different symmetry. Since the extinction coefficient for octahedral Co^{2+} ions is smaller than for tetrahedral ions, the new type of Co^{2+} absorption can be attributed to ions in octahedral symmetry, probably in a new phase (the x-ray section clarifies this point).

(d) It is now useful to analyze the intensity of the shoulder at 720 nm, due to Co_3O_4 ² for different series of specimens. Figure 4 shows the change in intensity, reported as the height of the shoulder in cm, with increasing cobalt content for the series $A\gamma\text{GaCo}(0.6:x)$ and A - and B - $A\gamma\text{GaMoCo}(0.6:5:x)$; the figure also includes data for $A\gamma\text{Co}_x$ and $A\gamma\text{MoCo}(5:x)$.²

The gallium-free $A\gamma\text{Co}_x$ and $A\gamma\text{MoCo}(5:x)$ have a larger amount of Co_3O_4 , as compared to the gallium-containing

specimens $A\gamma\text{GaCo}(0.6:x)$ and $A-A\gamma\text{GaMoCo}(0.6:5:x)$ (with $x = 1-5$). Note that the samples of series $B-A\gamma\text{GaMoCo}$ do not show the presence of Co_3O_4 .

In conclusion, the reflectance spectra show that the presence of Ga^{3+} ions hinders the formation of Co_3O_4 . Moreover it favors a more normal CoAl_2O_4 spinel, i.e., a larger amount of Co^{2+} in tetrahedral sites, except for the B series in which formation of CoMoO_4 is favored (see x-ray section).

3.2. X-Ray Measurements. The phase identification via x-ray spectra for supported catalysts presents difficulties. However, the analysis of the results, as far as the presence of the surface spinel CoAl_2O_4 and/or Co_3O_4 is concerned, can be made along lines similar to those discussed elsewhere^{2,3} by comparing the intensities of different reflections, and, in more detail, the intensity profiles. The x-ray findings parallel the spectroscopic results.

It is useful to examine in more detail the x-ray spectra of $A\gamma\text{GaMoCo}$ catalysts according the method of preparation.

Method A. The x-ray pattern of $A-A\gamma\text{GaMoCo}(0.6:5:x)$ and $A-A\gamma\text{GaMoCo}(4:5:x)$ catalysts indicates only the formation of the surface spinel CoAl_2O_4 .

Method B. The formation of CoAl_2O_4 as a surface spinel is confirmed. Moreover, additional lines are visible for $\text{Co} \geq 2$ atom % and their intensity increases with cobalt content. These lines are attributable to CoMoO_4 phases; the lines at d spacing = 6.25, 3.50, 3.12, and 2.09 Å to the green CoMoO_4 ⁸ and the line at d spacing = 3.36 Å to the violet CoMoO_4 , called the "B" phase by Ricol^{9,10} and β phase by Sleight and Chamberland.¹¹ In particular, in the specimens with 0.6 atom % Ga both phases are present, while in specimens with 4 atom % Ga only the violet phase is present. Since this phase can be transformed into the green phase by grinding,^{10,12} we ground $B-A\gamma\text{GaMoCo}(4:5:x)$ for several hours. As a consequence, the line characteristic of the violet phase disappeared and the lines characteristic of the green phase appeared. Both CoMoO_4 phases were prepared to check the x-ray spectra.

Sulfided Catalysts. Sulfided $A\gamma\text{GaCo}(0.6:x)$ and $A-A\gamma\text{GaMoCo}(0.6:5:x)$ show spinel phase lines sharper than the corresponding oxidized specimens, without any additional lines. By way of contrast, the sulfided $B-A\gamma\text{GaMoCo}$ for $\text{Co} > 2$ show, besides sharper spinel phase lines, new lines at $d = 5.67, 2.98, 1.91,$ and 1.75 Å, attributable to Co_9S_8 (ASTM index). No lines attributable to MoS_2 appear; note that the lines of CoMoO_4 disappeared.

3.3. Magnetic Measurements. Tables I and II report the Curie constant C , the Weiss temperature θ , and the magnetic moment μ calculated from the Curie-Weiss law $\chi = C/(T - \theta)$, where χ is the magnetic susceptibility per mole of cobalt (actual analytical content) after correction for the diamagnetic contribution of all components.

Figure 5 reports the variation of C with cobalt content for some representative specimens and includes the data for $A\gamma\text{Co}_x$ and $A\gamma\text{MoCo}(5:x)$ ² for comparison.

From inspection of Figure 5 and Tables I and II it appears that the C values follow different trends according to whether gallium ions are present or absent and to the preparation method.

In principle, the C value is dependent on two distinct facts: (a) the presence of different phases, such as Co_3O_4 ($C \approx 1$),¹³ CoAl_2O_4 ($C_{\text{oct}} = 3.50$ ¹⁴ and $C_{\text{tet}} = 2.57$),¹⁵ or CoMoO_4 ($C = 3.54$); (b) the distribution of Co^{2+} ions among A (tetrahedral) and B (octahedral) sites of the surface spinel CoAl_2O_4 ; a higher C value corresponds to a higher $\text{Co}^{2+}_{\text{oct}}/\text{Co}^{2+}_{\text{tet}}$ ratio.

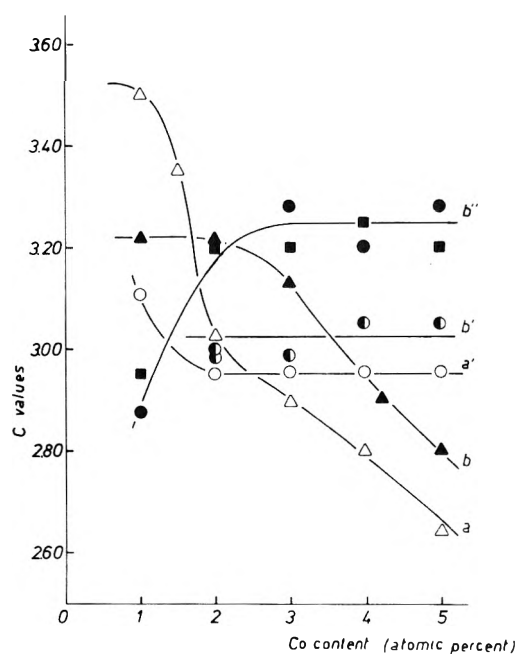


Figure 5. Curie constant, C , vs. cobalt content (atom percent): (Δ) $A\gamma\text{Co}_x$; (\circ) $A\gamma\text{GaCo}(0.6:x)$; (\blacktriangle) $A\gamma\text{MoCo}(5:x)$; (\square) $A-A\gamma\text{GaMoCo}(0.6:5:x)$; (\bullet) $B-A\gamma\text{GaMoCo}(0.6:5:x)$.

It is then appropriate to examine the magnetic results in order to establish whether the variations in C correspond to the presence of these different phases or to a variation of the $\text{Co}^{2+}_{\text{oct}}/\text{Co}^{2+}_{\text{tet}}$ ratio in the surface spinel CoAl_2O_4 . (a) Since only CoAl_2O_4 is present at low cobalt content ($\text{Co} \leq 2$, see above), the C values depend on Co^{2+} ion distribution among A and B sites of the surface spinel CoAl_2O_4 . Thus, comparison of $A\gamma\text{Co}_x$ with $A\gamma\text{GaCo}(0.6:x)$ (curve a and a' of Figure 5) indicates that the presence of Ga^{3+} ions favors a more normal spinel; in fact, a smaller C values means a higher $\text{Co}^{2+}_{\text{tet}}$ content. (b) At higher cobalt content ($\text{Co} \geq 2$), the C values strongly decrease for the sample of series $A\gamma\text{Co}_x$ (curve a) and $A\gamma\text{MoCo}(5:x)$ (curve b), due to the presence of the phase Co_3O_4 , while it remains constant (curve a' and b') for samples of series $A\gamma\text{GaCo}(0.6:x)$ and $A-A\gamma\text{GaMoCo}(0.6:5:x)$. In this last case, they reflect the distribution of Co^{2+} ions among A and B sites of spinel CoAl_2O_4 , this being the major Co species present. (c) As for the specimens of series $B-A\gamma\text{GaMoCo}$, the magnetic data (curve b'', Figure 5) shows an increase of C up to $C = 2$. This is due to the building up of the CoMoO_4 phase in which Co^{2+} ions occupy octahedral sites.

Estimate of the Degree of Inversion from Magnetic Data. An estimate of the cobalt ions distributed in octahedral and tetrahedral sites can be made for those samples in which the Co^{2+} ions can be assumed to be present as the surface spinel CoAl_2O_4 ; for this purpose we will then neglect the samples containing amounts of Co_3O_4 . For the $B-A\gamma\text{GaMoCo}$ catalyst, containing the surface spinel CoAl_2O_4 and CoMoO_4 , it is also possible to estimate the amount of tetrahedral and octahedral cobalt ions. However, we can assume that the tetrahedral cobalt is present completely as the surface spinel CoAl_2O_4 , for the octahedral cobalt we cannot determine how much is present as CoAl_2O_4 and how much as CoMoO_4 . From the experimental values of the Curie constant, C_{expt} , and taking into account these restrictions, it is possible to use the law of additivity for computing the fraction of Co^{2+} ions in octahedral and tetrahedral sites.^{3,5} The results obtained using $C_{\text{oct}} = 3.50$ ¹⁴ and $C_{\text{tet}} = 2.57$ ¹⁵ are reported in Tables I and II.

It is necessary to emphasize that the percent values given for $\text{Co}^{2+}_{\text{tet}}$ are only estimates, because of the choice of C_{oct} and C_{tet} , but the relative effect should be real.

Discussion

The presence and amounts of Co_3O_4 , CoMoO_4 , and CoAl_2O_4 are not determined solely by the chemical composition but also by the method of preparation, namely, A and B. Furthermore, the results show that the surface spinel CoAl_2O_4 is always present and its cation distribution is affected by the presence of foreign ions (i.e., in this case, Ga^{3+} ions). Moreover, segregation of the Co_3O_4 phase depends on several factors, such as the cobalt content, the method of preparation, and the presence of Ga^{3+} ions.

We discuss in order the following topics: (1) the effect of gallium ions on the cobalt and molybdenum; (2) the state of the surface according the method of preparation; (3) the sulfided specimens.

Influence of Gallium Ions on Cobalt and Molybdenum. In principle, in a spinel the M^{2+} ions can occupy tetrahedral (A) and/or octahedral (B) sites and the relative $\text{M}^{2+}_{\text{oct}}/\text{M}^{2+}_{\text{tet}}$ ratio depends on several parameters.¹⁶ In addition, recent studies⁵ on the structural and magnetic properties of Ni^{2+} ions supported on alumina showed that a small addition of Zn^{2+} , Ga^{3+} , or Ge^{4+} , all having a preference for tetrahedral sites, shifts the cation distribution in the surface spinel NiAl_2O_4 toward a more normal one.

The observed behavior was explained by invoking the polarization of anions toward tetrahedral sites. With this in mind, one would expect that the addition of cobalt ions to gallium-containing alumina, $\text{A}\gamma\text{GaCo}$ specimens, leads to a more normal CoAl_2O_4 spinel. The experimental observation matches this picture fully.

Especially in the specimens with high cobalt content, the experimental data (Figure 4) show that Co_3O_4 segregation is strongly decreased in the Ga-containing specimens ($\text{A}\gamma\text{GaCo}$ as compared to $\text{A}\gamma\text{Co}$). In order to rationalize this point, we recall that segregation of oxides in supported systems is mainly affected by two factors:¹⁴ (a) the stability of ions in the 2+ oxidation state; and (b) the diffusion pathways in the alumina lattice. It has been shown¹⁷ that for cations at tetrahedral sites the possible pathways in a spinel lattice always include a saddle position of octahedral symmetry. Now, if the crystal field around the octahedral sites is decreased when Ga^{3+} ions are added,⁵ one would expect a higher rate of diffusion of Co^{2+} ions. As a consequence, a greater amount of spinel is formed while the segregation of Co_3O_4 decreases.

The presence of Ga^{3+} may also influence the attachment of molybdate ions on the alumina surface. Molybdate monolayer formation has been extensively discussed by several authors.^{2,18-21} In our case it may be recalled that OH groups bonded to aluminum ions are about 100 times more basic than those bonded to gallium ions.²² Consequently, one would expect that molybdenum acid would react preferentially with aluminum octahedral OH giving molybdate ions attached to the surface. For a topotactic process, the molybdenum ions would occupy tetrahedral sites by extending the spinel structure immediately above the plane.^{20,21} As compared to $\text{A}\gamma\text{Mo}$, the $\text{A}\gamma\text{GaMo}$ specimens will have a somewhat larger amount of Mo^{6+} in tetrahedral sites and this fact may be relevant for catalytic reactions.

Influence of the Method of Preparation. Method A. This method consists of three successive impregnations and three calcinations according to the sequence Ga, Mo, and Co.

The first addition of Ga modifies the properties of the alumina surface.⁵ The second impregnation and calcination allows the Mo to react with the modified surface of the alumina giving a monolayer of molybdate ions attached to the alumina surface, in registry with the structure.^{2,18-21} In our case no separate phase of MoO_3 can be identified since the molybdenum content is fairly low. The cobalt, added with the third impregnation, now finds the structure of the external layers of alumina altered by the presence of Ga^{3+} and molybdate ions.

It may be noted that the presence of Ga^{3+} ions still allows the cobalt ions to react with alumina and favors a more normal spinel.

Finally, it should be emphasized that there is not a tendency to form the compound CoMoO_4 , since all the molybdenum has already reacted with the alumina surface.

Method B. Since $\text{B-A}\gamma\text{GaMoCo}$ catalysts were prepared by three impregnations but only two calcinations, the cobalt and molybdenum, react simultaneously (not in succession, as described for method A) with the alumina surface, and with each other. In fact, three reactions at 600 °C are able to occur simultaneously: (1) the reaction between Co- and Ga-containing alumina will give the cobalt aluminate, CoAl_2O_4 , and Co_3O_4 at high Co content; (2) the reaction between molybdenum and alumina will form molybdate ions attached to the alumina surface; (3) the reaction between molybdenum and cobalt¹² forms the CoMoO_4 phase.

The first reaction is dependent on the diffusion of cobalt ions into the external layers of alumina. The large surface area of alumina assists the process, by increasing the contact area between reagents.

The second reaction, considered as an acid-base reaction, should be dependent on the strength of the relative acids and bases involved and on the dispersion of molybdenum.

As far as the third reaction, the results obtained by Haber and Ziolkowski¹² for the system $\text{Co}_3\text{O}_4\text{-MoO}_3$ at 500 °C clearly indicate that the CoMoO_4 formation is rapid and dependent on the diffusion of molybdenum ions into Co_3O_4 grains. Thus, the species expected to arise as a function of Co content when the three reactions occur simultaneously can be accounted for as follows.

At low cobalt content, only the first and the second reactions occur. Apparently, the third process (CoMoO_4 formation) is also very rapid at 600 °C¹² although the strong interaction between cobalt and alumina tends to decompose the CoMoO_4 when this compound is heated with pure alumina.²³

Only at higher cobalt content does the formation of cobalt molybdate also occur, as a process taking place on the Co-rich external layers in competition with the diffusion of cobalt into the alumina. The experimental results match this picture fully. The x-ray data have shown that the formation of the CoMoO_4 phase starts to occur for a cobalt content ≥ 2 and its amount increases with increasing cobalt content. The reflectance spectra and magnetic measurements parallel the x-ray data showing that the cobalt ions, at higher cobalt content, go into octahedral sites as expected if CoMoO_4 is formed.

Sulfided Catalysts. As already reported, the effect of sulfiding is confined to the surface layers.² The process can be pictured as an exchange of surface OH^- to SH^- with a concomitant reduction of Mo^{6+} to lower oxidation states.^{2,24-27}

To throw light on the Co and Mo species which can be formed during the sulfurization, one has to take into account the species present in the oxide state.

According to literature data^{2,21,25,28} and to our results, the CoAl_2O_4 cannot be sulfided, but only their surface OH^- can be transformed into SH^- . However, if cobalt is present as separate phases (Co_3O_4 or CoMoO_4) it will undergo the Co_9S_8 transformation.^{2,21,28} Concerning molybdenum, it is currently reported that the sulfiding process of the Mo monolayer leads to an "oxysulfo" species rather than to a sulfided one.^{2,24,25} This conclusion is based on the lack of observation of MoS_2 . However, it must be pointed out that the sulfiding of B-A γ GaMoCo specimens, in which CoMoO_4 is present, produces only Co_9S_8 , the conditions being suitable for the formation of Co_9S_8 and MoS_2 . Indeed the sulfiding of pure and silica supported (Co-Mo/SiO_2) CoMoO_4 leads to the formation of cobalt and molybdenum sulfides.²⁹ Therefore, it can be argued that the growth of MoS_2 crystallites on alumina supported specimens probably occurs in two dimensions, failing x-ray detection. Another possibility could be that the crystallites are three-dimensional, but very small. Indeed, XPS studies show that MoS_2 is probably present.^{27,30}

Acknowledgment. The authors thank Professor A. Cimino for suggestions and for critically reading the manuscript.

References and Notes

- (1) M. Lo Jacono, M. Schiavello, D. Cordischi, and G. Mercati, *Gazz. Chim. Ital.*, **105**, 1165 (1975).
- (2) M. Lo Jacono, A. Cimino, and G. C. A. Schuit, *Gazz. Chim. Ital.*, **103**, 1281 (1973).
- (3) M. Lo Jacono, M. Schiavello, and A. Cimino, *J. Phys. Chem.*, **75**, 1044 (1971).
- (4) (a) M. Lo Jacono and M. Schiavello, "Preparation of Catalysts", B. Delmon, P. A. Jacobs, and G. Poncelet, Ed., Elsevier, Amsterdam, 1978, p 473. (b) Unpublished results from this laboratory.
- (5) A. Cimino, M. Lo Jacono, and M. Schiavello, *J. Phys. Chem.*, **79**, 243 (1975).
- (6) D. S. Mc Iver, H. F. Tobin, and R. T. Barth, *J. Catal.*, **2**, 485 (1963).
- (7) A. Cimino, M. Lo Jacono, P. Porta, and M. Vallgl, *Z. Phys. Chem. (Frankfurt am Main)*, **51**, 301 (1966).
- (8) G. W. Smith, *Acta Crystallogr.*, **15**, 1054 (1962).
- (9) P. Ricol, *Compt. Rend.*, **256**, 3125 (1963).
- (10) J. M. G. Lipsch and G. C. A. Schuit, *J. Catal.*, **15**, 163 (1969).
- (11) B. A. Sleight and B. L. Chamberland, *Inorg. Chem.*, **7**, 1672 (1968).
- (12) J. Haber and J. Ziolkowski, *React. Solids, Proc. Int. Symp.*, **7th**, 1972, 782 (1972).
- (13) J. R. Tomlinson, R. O. Keelling, G. T. Rymer, and J. M. Bridges, *Actes Congr. Int. Catal.*, **2nd**, 1960, 1831 (1961).
- (14) A. Cimino, M. Lo Jacono, P. Porta, and M. Vallgl, *Z. Phys. Chem. (Frankfurt am Main)*, **70**, 166 (1970).
- (15) F. Pepe, M. Schiavello, and G. Ferraris, *J. Solid State Chem.*, **12**, 63 (1975).
- (16) G. Blasse, *Phillips Res. Rep., Suppl.*, **No. 3** (1964).
- (17) F. S. Stone and R. J. D. Tilley, *React. Solids, Proc. Int. Symp.*, **7th**, 1972, 262 (1972).
- (18) J. Sonnemans and P. Mars, *J. Catal.*, **31**, 209 (1973).
- (19) T. Franzen, O. Van der Meer, and P. Mars, *J. Catal.*, **42**, 79 (1976).
- (20) W. K. Hall and M. Lo Jacono, "The 6th International Congress on Catalysis", London, 1976, paper A.16.
- (21) G. C. A. Schuit and B. C. Gates, *AIChE J.*, **19**, 417 (1973).
- (22) A. Martell and L. G. Silén, *Chem. Soc., Spec. Publ.*, **No. 17** (1964); **No. 25** (1971).
- (23) J. M. G. Lipsch, Thesis, Technological University, Eindhoven, The Netherlands, 1968.
- (24) P. C. H. Mitchell and F. Trifiro, *J. Catal.*, **33**, 350 (1974).
- (25) F. E. Massoth, *J. Catal.*, **38**, 164 (1975).
- (26) A. Cimino and B. A. De Angelis, *J. Catal.*, **36**, 11 (1975).
- (27) T. A. Patterson, J. C. Carver, P. E. Leyden, and D. L. Hercules, *J. Phys. Chem.*, **80**, 1700 (1976).
- (28) J. T. Richardson, *Ind. Eng. Chem., Fundam.*, **3**, 154 (1964).
- (29) V. H. J. De Beer, M. J. M. Van der Aalst, C. J. Machiels, and G. C. A. Schuit, *J. Catal.*, **43**, 78 (1976).
- (30) R. M. Friedman, R. I. Declerck-Grimee, and J. J. Fripiat, *J. Electron Spectrosc. Relat. Phenom.*, **5**, 437 (1974).

Analysis of Torsional Spectra of Molecules with Two Internal C_{3v} Rotors. 7.[†] Far-Infrared and Low-Frequency Raman Spectra of the Gaseous Dimethylphosphine

J. R. Durig,* M. G. Griffin, and W. J. Natter[†]

Department of Chemistry, University of South Carolina, Columbia, South Carolina 29208 (Received March 14, 1977)

Publication costs assisted by the University of South Carolina

The Raman spectrum of gaseous dimethylphosphine at a resolution of 1 cm^{-1} has been recorded between 100 and 400 cm^{-1} . The far-infrared spectrum has been recorded over the same frequency range with a resolution of 0.5 cm^{-1} . Considerable torsional data are reported and used to characterize the torsional potential function based on a semirigid model. The average effective V_3 was found to be $701 \pm 3\text{ cm}^{-1}$ (2.01 kcal/mol). The cosine-cosine coupling term, V_{33} , was found to be $240 \pm 8\text{ cm}^{-1}$ (0.68 kcal/mol) and the sine-sine term, V'_{33} , has a value of $-55 \pm 2\text{ cm}^{-1}$ (-0.16 kcal/mol). These data are compared to the corresponding quantities obtained from microwave data. Comparisons are also given to similar quantities obtained for other molecules.

Introduction

The vibrational spectrum of dimethylphosphine has been previously reported.^{1,2} Beachell and Katlafsky¹ reported the infrared spectrum of the gas and the Raman spectrum of the liquid and tentatively assigned the Raman lines at 236 and 318 cm^{-1} as the torsional motions. However, neither of these lines appeared in either the infrared or Raman spectra reported by Durig and

Saunders² and these authors concluded that these two bands arose from impurities in the earlier sample. Durig and Saunders² reported bands in the far-infrared spectra of solid $(\text{CH}_3)_2\text{PH}$ and $(\text{CD}_3)_2\text{PH}$ at 180 and 140 cm^{-1} , respectively, and assigned these bands to the CH_3 and CD_3 torsional modes. It was assumed that the frequencies for both torsional modes were essentially degenerate for both molecules and the threefold periodic barriers were calculated to be 2.14 and 2.30 kcal/mol for the CH_3 and CD_3 rotors, respectively. The barrier calculation was necessarily simplified because a proper characterization of the potential function for two interacting threefold rotors requires considerable experimental data.³⁻⁶ The availability of a

[†] For part VI, see *J. Chem. Phys.*, in press.

^{*} Taken in part from the thesis of W. J. Natter to be submitted to the Department of Chemistry in partial fulfillment of the Ph.D. degree.

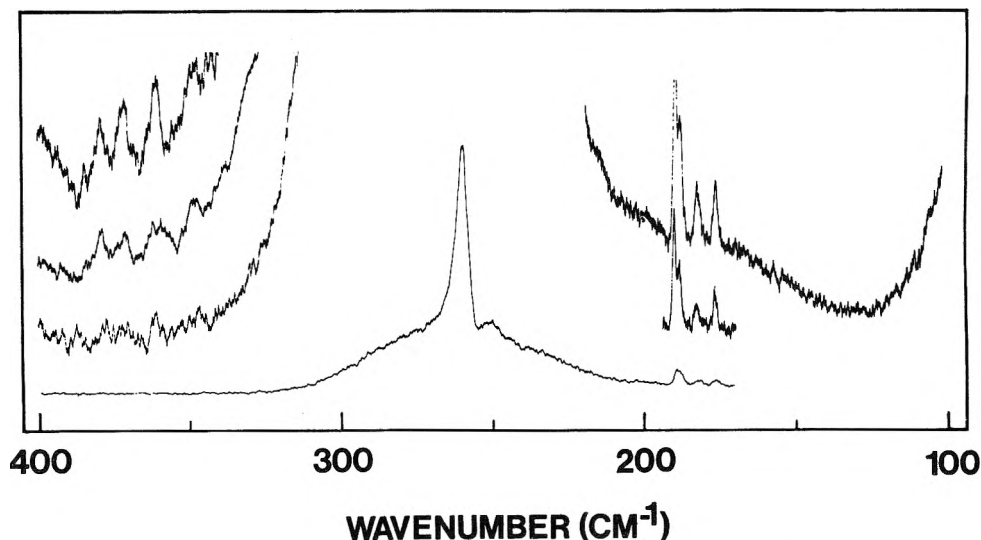


Figure 1. The Raman spectra of dimethylphosphine vapor. Spectral slit-width below 220 cm^{-1} was 1 cm^{-1} and above 330 cm^{-1} it was 4 cm^{-1} .

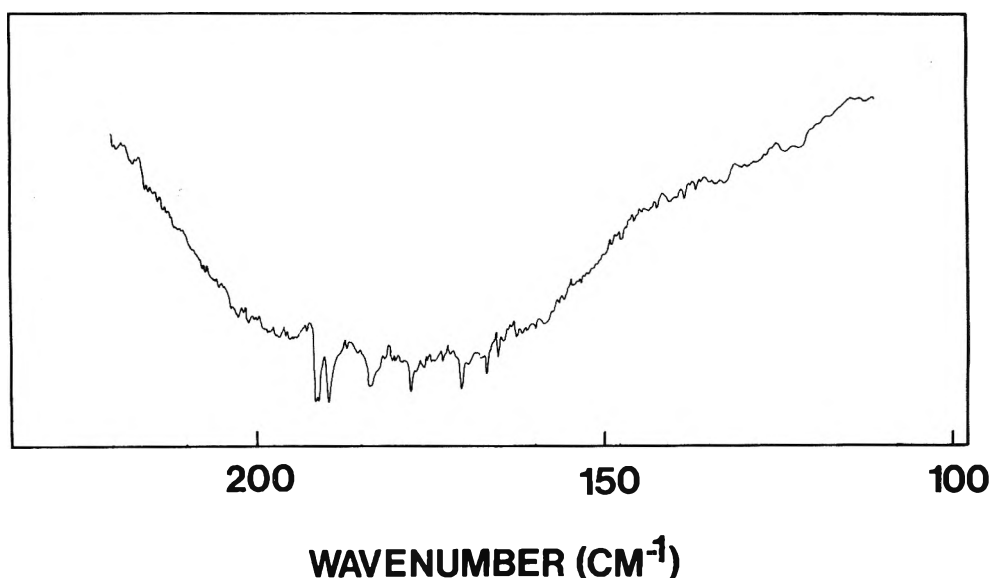


Figure 2. Far-infrared spectra of dimethylphosphine vapor with an effective resolution of 0.5 cm^{-1} . The spectrum shown is retracted eliminating absorption bands due to water.

computer-controlled Fourier transform far-infrared spectrometer, where repeated interferograms may be averaged rapidly to improve the signal-to-noise ratio and where spectral interferences may be readily subtracted, has made it possible to obtain high-quality far-infrared data for this molecule. Therefore extensive torsional data have been obtained for dimethylphosphine and are reported herein. These data have been used to characterize the torsional potential function for this molecule.

Experimental Section

The sample of $(\text{CH}_3)_2\text{PH}$ was purified by cold column fractionation techniques and handled under vacuum using Teflon greaseless stopcocks. The purified sample was stored at dry ice temperature and passed over LiAlH_4 just prior to its use to remove any water. The Raman spectra were recorded utilizing a Cary Model 82 spectrophotometer equipped with a Spectra Physics Model 171 argon ion laser operating on the 5145-\AA line. Power at the sample was typically 2 W. The samples were contained at their room temperature vapor pressure of about 1 atm in a quartz cell. The laser light was multipassed using the standard Cary accessory. Frequencies reported for sharp Raman lines in the region of $400\text{--}100\text{ cm}^{-1}$ are expected to be accurate to $\pm 1\text{ cm}^{-1}$.

The infrared spectra were obtained using a Digilab FTS-15B Fourier transform spectrometer. Spectra of the gas at 1 atm were recorded in the far-infrared region $450\text{--}80\text{ cm}^{-1}$ using a $6.25\text{-}\mu\text{m}$ mylar beam splitter and a 12-cm cell with polyethylene windows. Interferograms obtained after 3000 scans of the sample and empty cell were transformed using a box car apodization function giving 0.5-cm^{-1} resolution. Interfering water vapor bands were subtracted from the final spectrum.

Results

In the Raman spectrum (see Figure 1) there are four well-defined lines at 177, 182, 188, and 190 cm^{-1} . In the earlier Raman study² a single line was reported at 190 cm^{-1} , but the instrumental conditions were such that additional transitions would not have been observed. These and other observed transitions in the overtone region near 400 cm^{-1} are summarized in Table I. Polarization measurements were attempted but results were scarce and are not tabulated. Clearly the sharp line observed at 190 cm^{-1} was polarized, but the others in the series were of undeterminable polarization.

The far-infrared spectrum (see Figure 2) was complicated with water vapor. Numerous drying methods were employed, but the sample or the cell still contained traces

TABLE I: Observed Torsional Data and Assignment for Dimethylphosphine

Raman		Far-IR		Assignment $V'_1 V'_2 \leftarrow V_1 V_2$	Obsd - calcd
Δ , cm ⁻¹	Rel int	cm ⁻¹	Rel int		
		166.1	vw	2,0 ← 1,0	-0.93
		169.9	vw	1,0 ← 0,0	-0.52
177	vw	177.2	vw	0,4 ← 0,3	0.23
182	vw	183.0	vw	0,3 ← 0,2	-0.55
188	vw	188.6	vw	0,2 ← 0,1	-0.14
190	w	190.4	vw	0,1 ← 0,0	0.24
338	sh			2,0 ← 0,0	0.55
349	vw			2,2 ← 2,0 ^a	0.03
361	vw			0,4 ← 0,2	0.48
372	vw			0,3 ← 0,1	-0.29
379	vw			0,2 ← 0,0	0.10

^a Not used in the fit of the potential constants.

of water. Attempts were made to subtract out the water, but its absorption was such that the moderately strong water bands were still present. The observed lines reported in Table I were generally stronger than the water lines in the same region and, since the spectrum was taken at high resolution (0.5 cm⁻¹), were distinguishable from transitions arising from water.

Assignment

Initial calculations of the torsional potential function for dimethylphosphine were based solely on data observed in the Raman spectrum of the vapor. Previous experience with dimethylamine⁷ suggested that the single quantum torsional transitions observed in the Raman effect would be associated only with the higher frequency torsion (A''). Raman transitions in the single jump region were observed at 190, 188, 182, and 177 cm⁻¹. This indicated that the first two-quantum transition of the A'' torsion should occur at 378 cm⁻¹ (190 + 188 = 378). A transition observed at 379 cm⁻¹ was thus assigned. Subsequent calculations were based on expanded assignments indicated by the initial calculations.

Unfortunately, the Raman data provided no certain information on the other torsional motion of dimethylphosphine. Information on the A'' torsion only determines the general magnitude of the effective V_3 term and it does not determine the sine-sine coupling term (V'_{33}) at all. An investigation of the far-infrared spectrum of the gas phase of dimethylphosphine was undertaken to provide information on the A' torsion that would clarify the Raman spectral assignments. The far-infrared investigation was hampered by the affinity dimethylphosphine displayed toward water. It was, however, possible to observe in the far-infrared spectrum all the single quantum transitions seen in the Raman plus additional features at 169.9 and 166.1 cm⁻¹. With these data, it was possible to assign the Raman line at 338 cm⁻¹ as the 2 ← 0 transition of the A' torsion (169.9 + 166.1 = 336 cm⁻¹). The details of the entire assignment are available in Table I and the final potential function coefficients are listed in Table II.

An alternative assignment was attempted which put the 2 ← 0 of the A' torsion at 349.0 cm⁻¹. This lowered the effective V_3 by ~5% and approximately doubled the sine-sine coupling term. This alternative was abandoned since it provided no assignment for the transition at 338 cm⁻¹.

The energy level diagram for the torsional modes of dimethylphosphine is shown in Figure 3.

Discussion

The torsional problem in (CH₃)₂PH may be treated on the basis of the $C_{3v}T-C_3F-C_{3v}T$ or $C_s(e)$ semirigid model

TABLE II: Torsional Potential Constants (cm⁻¹) and Kinetic Coefficients (cm⁻¹) for Dimethylphosphine

Parameter	(CH ₃) ₂ PH $C_s(e)^a$	
	Value	Dispersion
V_{30}	940.8	5.7
V_{03}	940.8	5.7
V_{33}	240.0	8.0
V'_{33}	-55.8	2.1
$[(V_{30} + V_{03})/2] - V_{33}$	700.8	2.5
$\hbar^2 g^{44} = 2F_1$	11.455	
$\hbar^2 g^{45} = 2F'_1$	-0.509	
$\hbar^2 g^{55} = 2F_2$	11.455	
Std dev of frequency fit	0.56	

^a $C_s(e)$ is the C_s frame with equivalent tops, $V_{03} = V_{30}$.

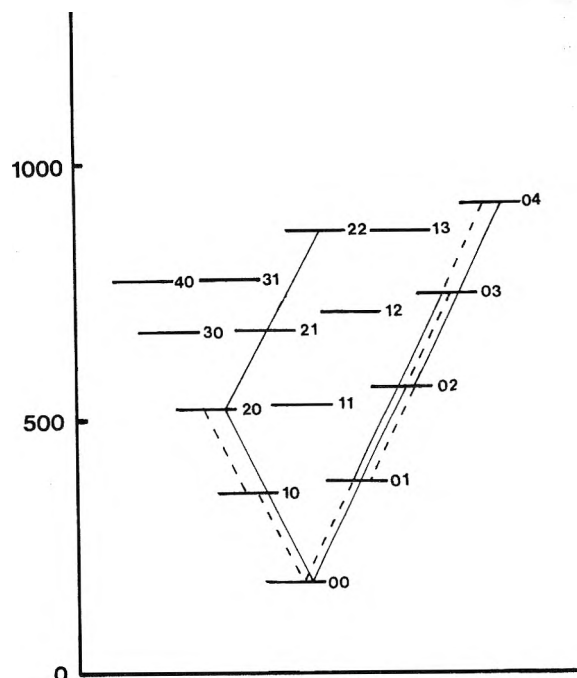


Figure 3. Energy level diagram for the torsional modes of (CH₃)₂PH, obtained from the data from Table I. Ordinate is in cm⁻¹. The numbers to the right of the energy levels denote the limiting vibrational quantum numbers ($v \bar{v}$). Any energy level consists of four sublevels where the higher ones may be partly resolved or "broadened".

(T = top, F = frame). An extensive investigation of several semirigid two-top models has recently been made by Groner and Durig^{5,6} on the basis of the internal isometric group introduced by Günthard and co-workers.⁸ They obtained the internal Hamiltonian for the $C_{3v}T-C_3F-C_{3v}T$ model as

$$\mathcal{H}_I = 1/2 [g^{44} \hat{p}_0^2 + 2g^{45} \hat{p}_0 \hat{p}_1 + g^{55} \hat{p}_1^2] + V(\tau_0, \tau_1)$$

with $V(\tau_0, \tau_1)$ in standard form as

$$\begin{aligned} V(\tau_0, \tau_1) = & 1/2 [V_{30}(1 - \cos 3\tau_0) + V_{60}(1 - \cos 6\tau_0) \\ & + V'_{60} \sin 6\tau_0 + V_{03}(1 - \cos 3\tau_1) \\ & + V_{06}(1 - \cos 6\tau_1) + V'_{06} \sin 6\tau_1 \\ & + V_{33}(\cos 3\tau_0 \cos 3\tau_1 - 1) \\ & + V'_{33} \sin 3\tau_0 \sin 3\tau_1 + V''_{33} \sin 3\tau_0 \cos 3\tau_1 \\ & + V'''_{33} \cos 3\tau_0 \sin 3\tau_1] \end{aligned}$$

The molecular symmetry requires that $g^{44} = g^{55}$, $V_{30} = V_{03}$, $V_{60} = V_{06}$, $V'_{60} = -V'_{06}$ and $V''_{33} = -V'''_{33}$. The symmetry group of this internal Hamiltonian is of order 18, $C_3 \otimes \theta_3$, and is isomorphous to the direct product of the cyclic group, C_3 , of order 3, with the dihedral group, θ_3 , of order 6. Its character table has been given by Durig et al.⁷ The

energy levels of each torsional state (v, \bar{v}) split, in the high barrier case, into the sublevels:

$$\Gamma^{00\sigma} + \Gamma^{10} + \Gamma^{11} + \Gamma^{12\sigma}$$

where σ is + or - for \bar{v} even or odd, respectively. The \bar{v} are the limiting vibrational quantum numbers of the torsional mode which is antisymmetric with respect to the symmetry plane of the molecular frame. $\Gamma^{00\sigma}$ are one-dimensional representations and Γ^{11} is two dimensional. $\Gamma^{12\sigma}$ ($\sigma = +$ or $-$) are the symbols for two complex conjugate pairs of one-dimensional representations, whereas Γ^{10} represents a complex conjugate pair of two-dimensional representations thus leading to fourfold degenerate energy levels. The selection rules have been derived and summarized by Durig et al.⁷

The kinetic coefficients g^{mn} (listed in Table II) were calculated from the structural parameters obtained from a previous microwave investigation.⁹ The initial calculations were carried out using the first four well-defined "single jump" transitions observed in the Raman effect. The fifth transition in this series ($0, \bar{v} \rightarrow 0, \bar{v} + 1$) was not observed and is presumed to be over the barrier. Additional transitions observed in the far infrared and Raman "double jumps" were included to obtain the three potential constants $V_{03} = V_{30}, V_{33}$ and V'_{33} . Efforts to expand the potential function and improve the fit were futile. $V_{60}, V_{06}, V'_{60}, V'_{06}, V''_{33}$, and V'''_{33} were therefore set equal to zero for the final calculations. V_{06} and V_{60} were found to have a very small value and thus were excluded from the fit. $V'_{60}, V'_{06}, V''_{33}$, and V'''_{33} were found to have little effect on the calculated values of the transitions and were therefore ill-determined, so they were excluded also. Durig et al.⁷ have concluded that these terms are determinable only if they are of the order of magnitude of one tenth of the effective barrier height. Final calculations were made with the values for parameters in Table II.

As shown by Groner and Durig,⁵ the parameter set commonly used for the potential function is not the best one in terms of determinability because some of the coefficients are strongly correlated. They introduced the linear combinations

$$\begin{bmatrix} V_{3s} \\ V_{3a} \\ V_{\text{eff}} \end{bmatrix} = \begin{bmatrix} 1/2 & 1/2 & 0 \\ 1/2 & -1/2 & 0 \\ 1/2 & 1/2 & -1 \end{bmatrix} \begin{bmatrix} V_{30} \\ V_{03} \\ V_{33} \end{bmatrix}$$

as determinable and less correlated parameters in place of V_{30}, V_{03} , and V_{33} . These new parameters generally have lower dispersions than the original ones. The value of the effective barrier V_{eff} is given in Table II as $701 \pm 3 \text{ cm}^{-1}$ (2.01 kcal/mol). The value of the effective barrier is about 100 cm^{-1} lower than the V_3 calculated from the microwave splittings.¹⁰ A similar difference was noted between the barriers calculated for dimethylamine⁷ and was explained on the basis of the compromise made for inversion splitting of the microwave frequencies. In the present case though, this discrepancy is believed to result from the lack of structural detail of the methyl tops. The electron diffraction study¹¹ and the microwave study of ($^{12}\text{CH}_3$)₂PH and $^{13}\text{CH}_3(^{12}\text{CH}_3)$ PH reported by Nelson⁹ strictly determined the positions of the two tops within the molecule. Any possible errors in the internal rotational reduced moments result from the CH bond distances or the $\angle\text{HCH}$ angles. Calculations of the F number for the two identical tops were made with varying CH distances within the reported error limits of $1.097 \pm 0.007 \text{ \AA}$. These resulted

in $\hbar^2 g_{44} = \hbar^2 g_{55} = 2F$ in the range of 11.455 to 11.206 cm^{-1} . Upon replacement of $\hbar^2 g_{44} = \hbar^2 g_{55}$ with the lower value, all potential constants except the cosine-cosine coupling coefficient V_{33} stayed approximately the same. This term, on the other hand, went from a value of 239 cm^{-1} for the higher kinetic term to 206 cm^{-1} for the lower one. Therefore the calculated effective barrier using this new F number ($\hbar^2 g_{44}/2 = \hbar^2 g_{55}/2$) was raised to 733 cm^{-1} , which is nearer to the 800-cm^{-1} value obtained in the microwave investigation. With the smaller F number, the microwave barrier would be lowered. The kinetic cross term $\hbar^2 g_{45}$ changed very slightly with the various CH bond distances and its effect on the calculated potential coefficients was negligible. In view of this it is reasonable to believe that small errors in the structural parameters can lead to large differences between barriers calculated with microwave splittings and those calculated from torsional transitions.

The sine-sine coupling coefficient V'_{33} calculated here differs both in sign and magnitude from that obtained in the microwave investigation. Each calculation was begun with the V'_{33} term set equal to $+29 \text{ cm}^{-1}$ which was obtained from the microwave splittings, but upon iteration the reported value of about -55 cm^{-1} was always obtained. When the parameter was held fixed at the positive value, the standard deviation of the fit was 2.5 cm^{-1} as opposed to the 0.56-cm^{-1} standard deviation obtained with the V'_{33} equal to -55 cm^{-1} . Previous investigations^{6,7} using these computer programs to calculate the barriers in two-top molecules have always had sine-sine coupling terms which agreed in sign although not always in magnitude. The programs also show there is a strong correlation between the sine-sine and cosine-cosine coupling terms while only the former can be obtained from microwave splittings. We are investigating this problem further and have no rational explanation for the difference in sign at this time.

Further structural work should be done on this molecule to determine the F number more exactly. It is believed that the small difference in the effective barrier between the microwave and vibrational results is due to structural indeterminacies.

The barrier change upon replacement of a hydrogen with a methyl group on a phosphorous atom (CH_3PH_2 ,¹² 1.96 kcal/mol and $(\text{CH}_3)_2\text{PH}$, 2.01 kcal/mol) is much smaller than that obtained with a similar replacement on a nitrogen atom (CH_3NH_2 ,¹³ 1.98 kcal/mol and $(\text{CH}_3)_2\text{NH}$,⁷ 3.01 kcal/mol). With the smaller F number this difference could be as large as 0.2 kcal/mol but still quite insignificant when compared to the corresponding amines.

Acknowledgment. The authors gratefully acknowledge the financial support given this study by the National Aeronautics and Space Administration through Grant No. NGL-41-002-003.

References and Notes

- (1) H. C. Beachell and B. Katlasky, *J. Chem. Phys.*, **27**, 182 (1957).
- (2) J. R. Durig and J. E. Saunders, *J. Raman Spectrosc.*, **4**, 121 (1975).
- (3) J. D. Swalen and C. C. Costain, *J. Chem. Phys.*, **31**, 1562 (1959).
- (4) K. D. Möller and H. G. Andresen, *J. Chem. Phys.*, **37**, 1800 (1962).
- (5) P. Groner and J. R. Durig, *J. Chem. Phys.*, in press.
- (6) J. R. Durig and P. Groner, *J. Mol. Spectrosc.*, in press.
- (7) J. R. Durig, M. G. Griffin, and P. Groner, *J. Phys. Chem.*, in press.
- (8) A. Bauder, R. Meyer, and Hs. H. Günthard, *Mol. Phys.*, **28**, 1305 (1974); **31**, 647 (1976).
- (9) R. Nelson, *J. Chem. Phys.*, **39**, 2382 (1963).
- (10) J. R. Durig, P. Groner, and Y. S. Li, *J. Chem. Phys.*, in press.
- (11) L. S. Bartell, *J. Chem. Phys.*, **32**, 832 (1960).
- (12) T. Kojima, E. L. Breig, and C. C. Lin, *J. Chem. Phys.*, **35**, 2139 (1961).
- (13) D. R. Lide, Jr., *J. Chem. Phys.*, **27**, 343 (1957).

The Fluorescent Level Inversion of Dual Fluorescences and the Motional Relaxation of Excited State Molecules in Solutions

Satoshi Suzuki,* Tsuneo Fujii, Akihiro Imai,¹ and Hideo Akahori²

Department of Industrial Chemistry, Faculty of Engineering, Shinshu University, Wakasato, Nagano, Japan (Received February 1, 1977)

The temperature dependence of the fluorescence of 1-naphthol, indole, 1-naphthonitrile, and 1-naphthylamine in propylene glycol over the temperature range 320–170 K and of 1-naphthol and indole in glycerin over the temperature range 350–200 K has been studied. These compounds all emit a broad structureless fluorescence spectrum at room temperature. Lowering the temperature blue shifts the fluorescence and structures it except for 1-naphthylamine. These observed spectral changes have been interpreted using fluorescence polarization spectra as being due to the fluorescent level inversion of dual fluorescences. From the temperature dependence of the degree of polarization, the motional relaxation of excited state molecules in solutions has been estimated. It is concluded that fluorescent level inversion may occur at temperature ranges where the solute molecules cannot translate or rotate to any appreciable extent in solution.

Introduction

The dual fluorescences caused by environmental perturbations have been reported for other compounds, since Lippert et al.^{3,4} observed dual fluorescences in *p*-dimethylaminobenzonitrile and *p*-diethylaminobenzonitrile. Indole,^{5–8} 1-naphthylamine,⁹ and 1-naphthol¹⁰ exhibit dual fluorescences in a series of dilute solutions in which the solvent polarity varies, however, doubts have been raised on the dual fluorescences of *p*-dimethylaminobenzonitrile,^{11–13} indole,¹⁴ and 1-naphthylamine.¹⁵ Suzuki et al.¹⁶ have observed fluorescent level inversion of dual fluorescences in alcoholic solutions of 1-naphthol by a change in temperature only.

These results can be interpreted in the following way. These molecules have two electronic states, ¹L_b and ¹L_a, in the region of their lowest absorption band. The ¹L_a state lies above ¹L_b in free molecules, but these states do lie close to each other. In fluid solutions at room temperature, the solvent molecules around the excited solute molecule will generally have time to reorient themselves before light emission occurs and hence they relax to their preferred equilibrium configuration which is of lower energy. In nonpolar solvents, the ¹L_a states of these molecules still lie above ¹L_b even in the preferred equilibrium configuration and hence fluorescence occurs from the ¹L_b state. In polar solvents, the interaction between dipole moments of such excited molecules and solvent molecules lowers the energy of the ¹L_a state below that of ¹L_b in their equilibrium configuration, and hence fluorescence occurs from the ¹L_a state.

At sufficiently low temperatures and high viscosities, the relaxation processes which lead to an equilibrium configuration will not occur to any appreciable extent during the lifetime of the excited state, and therefore emission will take place from an unrelaxed configuration. Such a dynamic equilibrium among various solute-solvent configurations depends on the motional relaxation during the fluorescence lifetime, and it is modified by a change in temperature and/or viscosity. It has been observed that 1-naphthol in propylene glycol emits a broad structureless fluorescence spectrum at room temperature, while it emits a structured one at low temperatures.¹⁶ These results have been satisfactorily interpreted as being due to fluorescent level inversion of dual fluorescences on the basis of the method of photoselection.^{17–20}

Favro²¹ derived the diffusion equation for anisotropic rotational Brownian motion. Chuang and Eisenthal have

solved the equation and have obtained general expressions for time-dependent fluorescence polarization.²² Labhart and Pantke^{23,24} applied these general expressions to molecules of such symmetry in which the principal axes of the diffusion tensor coincide with the possible directions of the transition moments and to a steady state experiment. From the temperature dependence of the degree of fluorescence polarization upon exciting the molecules into two perpendicularly polarized transitions, Labhart and Pantke evaluated the principal values of the rotational diffusion tensor of perylene and 9,10-dimethylanthracene in their excited states.

This paper will report on the study of fluorescent level inversion of dual fluorescences for 1-naphthol, indole, 1-naphthonitrile, and 1-naphthylamine in alcoholic solvents by varying temperature and/or viscosity and will discuss the motion of excited state molecules in solutions during the process of the fluorescent level inversion.

Experimental Section

Indole, 1-naphthol, 1-naphthonitrile, and 1-naphthylamine were purified by repeated recrystallization and then sublimed in vacuo. Propylene glycol and glycerin were stored over molecular sieves 3A and further purified by passage through silica gel. It was confirmed that no fluorescent impurity was detectable under present experimental conditions. The absorption spectra were recorded on a Hitachi EPS-3 recording spectrophotometer. The fluorescence and excitation spectra were obtained by means of Hitachi MPF-2A fluorescence spectrophotometer. The temperature was controlled by using a metal cryostat (Torisha Laboratory, Ltd.). The degree of polarization, *P*, was measured by the method of photoselection.^{17–20} The fluorescence lifetime of 1-naphthonitrile was measured by the pulse-sampling method.²⁵

Results

In Figure 1, the temperature dependence of the fluorescence for 1-naphthol in propylene glycol, and the fluorescence polarization spectra at various temperatures are shown. The absorption spectra of 1-naphthol at various temperatures are shown in Figure 2, together with the fluorescence excitation polarization spectra excited at 325 and 356 nm.

In the region of the lowest absorption band, 1-naphthol has two closely situated absorption bands:^{26–29} a ¹L_b band with a fine structure and a broad ¹L_a band at higher

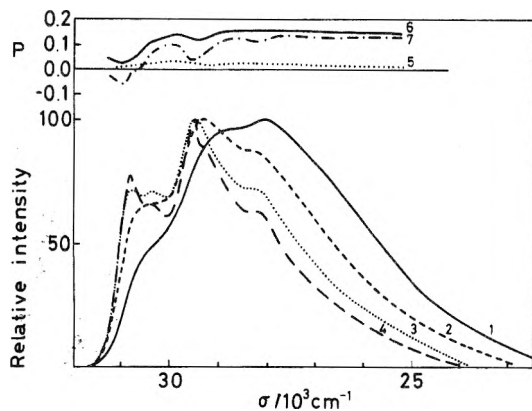


Figure 1. The temperature dependence of the fluorescence (lower) and the fluorescence polarization (upper) spectra of 1-naphthol in propylene glycol. The excitation wavelength was 297 nm: (1) 301 K; (2) 237 K; (3) 214 K; (4) 172 K; (5) 271 K; (6) 243 K; (7) 192 K.

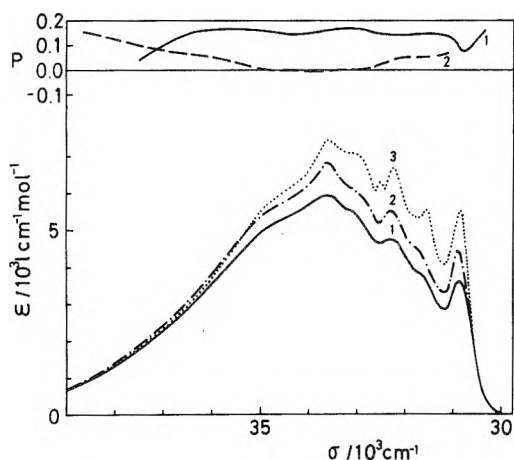


Figure 2. The fluorescence excitation polarization spectra (upper) of 1-naphthol in propylene glycol at 200 K monitored at 325 nm (---) and 356 nm (—). The absorption spectra (lower) of 1-naphthol in propylene glycol at various temperatures: (1) 293.5 K; (2) 210 K; (3) 111 K.

frequencies. The absorption spectrum shows no substantial dependence of the spectral shape on temperature. At room temperature, 1-naphthol in propylene glycol shows a broad fluorescence. When the temperature of the solution is lowered, the fluorescence blue shifts and becomes structured. These emissions differ from that of the naphtholate anion,^{30,31} proton dissociation is ruled out as the origin of this spectral change. There is a mirror-symmetry relation between the positions of the peaks of the structured emission with those of the peaks of the absorption spectrum. These findings indicate that the emitting state changes from a broad 1L_a to a structured 1L_b .

The fluorescence polarization spectrum at 271 K with an excitation wavelength of 297 nm, which corresponds to the region of 1L_a , is structureless and has slightly positive P values. As the temperature of the solution is lowered, the value of P increases and minima appear at positions corresponding to the peaks of the structured emission. This implies that the structured component increases with decreasing temperature and it has a transition moment nearly perpendicular to the 1L_a transition. In other words, the fluorescent level of 1-naphthol in propylene glycol changes from 1L_a at room temperature to 1L_b at low temperatures. The fluorescence excitation polarization spectra also support fluorescent level inversion of 1-naphthol. The fluorescence excitation polarization spectrum monitored at 356 nm, which corresponds to the maximum of broad fluorescence, has minima at wavelengths corresponding to the peaks of the 1L_b band, while

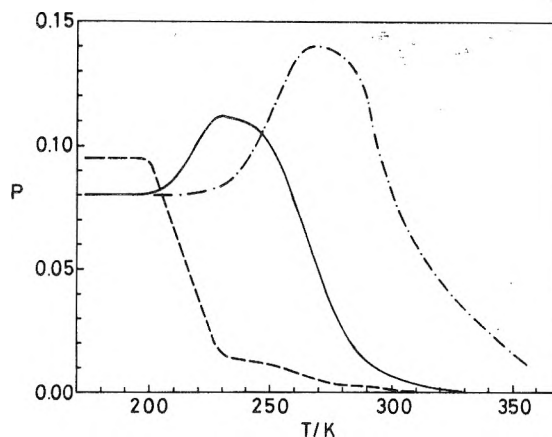


Figure 3. The temperature dependence of P for 1-naphthol monitored at 340 nm: (—) 297-nm excitation in propylene glycol; (---) 240-nm excitation in propylene glycol; (-·-·) 297-nm excitation in glycerin.

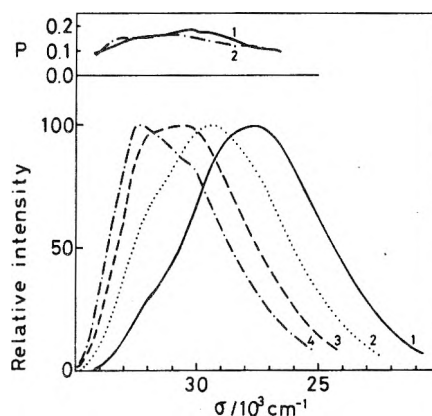


Figure 4. The temperature dependence of the fluorescence (lower) and the fluorescence polarization (upper) spectra of indole in propylene glycol. The excitation wavelength was 270 nm: (1) 301 K; (2) 190 K; (3) 170 K; (4) 112 K; (5) 251 K; (6) 170 K.

the spectrum monitored at 325 nm, which corresponds to the peak of the structured fluorescence, has slightly negative P values in the region of the 1L_a absorption band. This indicates that the structured fluorescence has a transition moment nearly perpendicular to the 1L_a transition.

Figure 3 shows the temperature dependence of P for 1-naphthol in propylene glycol observed at 340 nm when excited at 297 and 240 nm. P increases with a decrease in temperature due to the depletion of rotational depolarization when excited at 297 nm. After P reaches its maximum at about 230 K, it decreases and then becomes constant below 200 K. The decrease of P near 220 K is attributed to fluorescent level inversion, since the fluorescence spectra change markedly in the temperature range 230–210 K (see Figure 1). Once P reaches a constant at about 230 K, it then again increases to a second constant below 200 K when excited at 240 nm.

In glycerin, the fluorescence spectra of 1-naphthol show an analogous temperature dependence, except that the spectral change occurs at higher temperatures in glycerin than in propylene glycol. The temperature dependence of P for 1-naphthol in glycerin shown in Figure 3 is analogous to that in propylene glycol, but the curve is shifted toward higher temperature. This shift may be explained by the difference in viscosity between propylene glycol and glycerin (see below).

The analogous experimental results for indole in propylene glycol are shown in Figures 4–6. Indole also has two closely situated excited states in the region of its lowest absorption band.^{8,32,33} Lowering the temperature shifts the

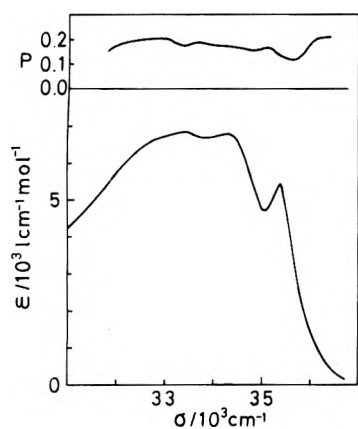


Figure 5. The fluorescence excitation polarization spectra (upper) of indole in propylene glycol at 195 K monitored at 310 nm. The absorption spectra (lower) of indole in propylene glycol at room temperature.

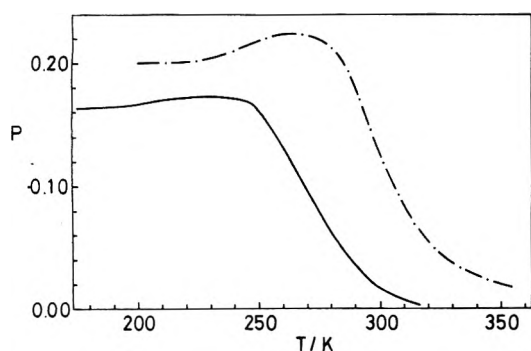


Figure 6. The temperature dependence of the degree of fluorescence polarization of indole in propylene glycol (—) and glycerin (---). The excitation wavelength was 270 nm; the wavelength monitored was 310 nm.

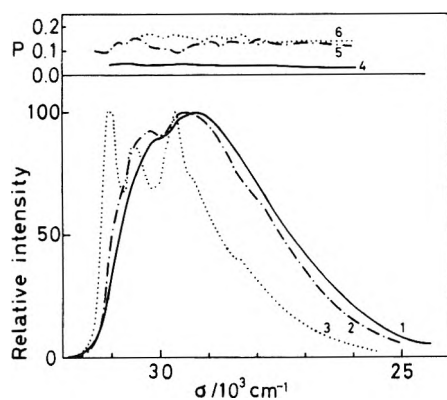


Figure 7. The temperature dependence of the fluorescence (lower) and the fluorescence polarization (upper) spectra of 1-naphthonitrile in propylene glycol. The excitation wavelength was 295 nm: (1) 291 K; (2) 226 K; (3) 132 K; (4) 263 K; (5) 208 K; (6) 208 K, 323-nm excitation.

fluorescence spectra of indole to higher frequencies. The absorption polarization spectrum monitored at 310 nm has minima at wavelengths corresponding to the peaks of the structured absorption band. The temperature dependence of P in propylene glycol and glycerin shown in Figure 6 is quite analogous to that of 1-naphthol. These findings support the fluorescent level inversion of dual fluorescences in indole as well as in 1-naphthol.

The temperature dependence of the fluorescence for 1-naphthonitrile in propylene glycol is shown in Figure 7. The fluorescence of 1-naphthonitrile is broad and structureless at 291 K. Lowering the temperature blue shifts the fluorescence and it becomes structureless. The temperature dependence of the fluorescence for 1-

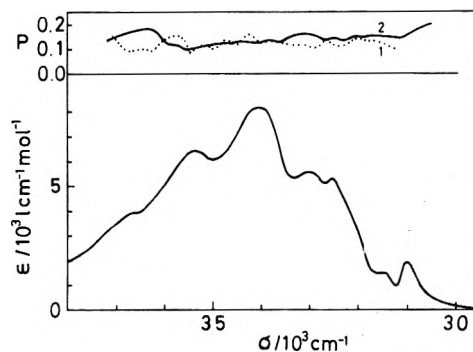


Figure 8. The fluorescence excitation polarization spectra (upper) of 1-naphthonitrile in propylene glycol at 208 K: (1) 323-nm excitation; (2) 344-nm excitation. The absorption spectra (lower) of 1-naphthonitrile in propylene glycol at room temperature.

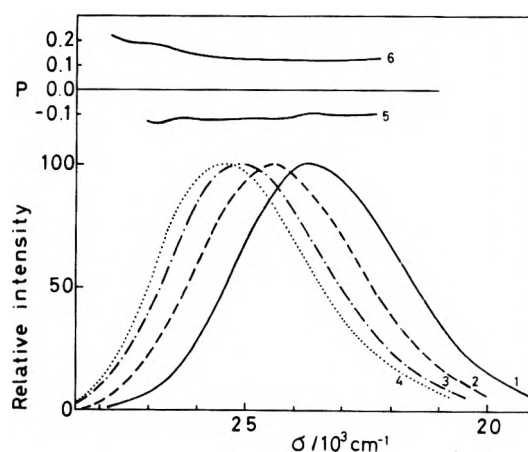


Figure 9. The temperature dependence of the fluorescence spectra (lower) of 1-naphthylamine in propylene glycol. The excitation wavelength was 310 nm: (1) 252 K; (2) 219 K; (3) 191 K; (4) 77 K. The fluorescence polarization spectra (upper) of 1-naphthylamine in propylene glycol: (5) 213 K, 255-nm excitation; (6) 130 K, 320-nm excitation.

naphthonitrile is quite analogous to that of 1-naphthol. In the fluorescence polarization spectrum at 208 K, minima appear at wavelengths corresponding to the peaks of the structured fluorescence. MO calculation shows that 1-naphthonitrile has 1L_b and 1L_a states in the region of the lowest absorption band.³⁴ This predicts the occurrence of fluorescent level inversion in 1-naphthonitrile as well as in 1-naphthol. The fluorescence and fluorescence excitation polarization spectra are shown in Figure 8, together with the absorption spectrum at room temperature. Figure 8, as well, shows that the two states participating in dual fluorescence have transition moments nearly parallel with each other.

The temperature dependence of the fluorescence of 1-naphthylamine is shown in Figure 9. The fluorescence of 1-naphthylamine also shows a large blue shift, but no fine structured fluorescence appears with a decrease in temperature. The fluorescence excitation polarization spectra are shown in Figure 10, together with the absorption spectrum at room temperature. The fluorescence excitation polarization spectrum monitored at 420 nm, which corresponds to the peak of the room-temperature component of the fluorescence, has a minimum near the shoulder at $30\,000\text{ cm}^{-1}$. This shoulder has been assigned to 1L_b ,²⁶ this indicates that the fluorescent state is indeed the 1L_a state at room temperature. Figure 11 shows the temperature dependence of P at 255- and 350-nm excitation. P reaches its maximum and then decreases to a constant on lowering the temperature. This behavior is quite analogous to that of 1-naphthol. These findings

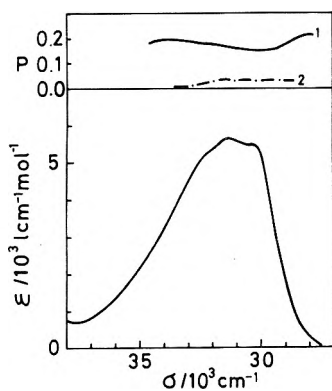


Figure 10. The fluorescence excitation polarization spectra of 1-naphthylamine in propylene glycol monitored at 420 nm: (1) 185 K; (2) 270 K. The absorption spectra of 1-naphthylamine in propylene glycol at room temperature.

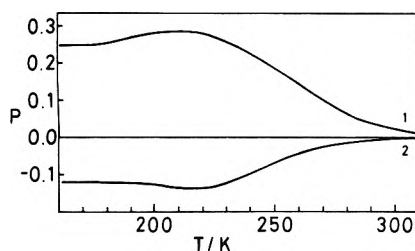


Figure 11. The temperature dependence of P for 1-naphthylamine in propylene glycol monitored at 400 nm: (1) 350-nm excitation; (2) 325-nm excitation.

suggest that fluorescent level inversion also occurs in 1-naphthylamine.

Discussion

Fluorescent Level Inversion. MO calculations on the excited electronic states of 1-naphthol predict that the lowest excited state is 1L_b and the second excited state is 1L_a lying slightly above 1L_b .^{26-29,35-37} The angles between the transition moments for the 1L_b and 1L_a transitions have been found to be 106 and 82°.^{29,36} It appears as though the two transition moments are nearly perpendicular. The polarization spectra shown in Figures 1 and 2 clearly indicate that the two components of dual fluorescences have their transition moments nearly perpendicular to each other. The π dipole moments of the 1L_b and 1L_a states have been determined by Forster and Nishimoto.³⁶ The dipole moment of the 1L_a state is greater than that of the 1L_b state; this induces a larger interaction between the dipole moments of the excited solute molecules in the 1L_a state with the polar solvent molecules compared with the case in the 1L_b state. It is concluded that the fluorescence of 1-naphthol in alcoholic solvents changes from the 1L_a state at higher temperatures to the 1L_b state at lower temperatures.

A considerable volume of data has been accumulated on the luminescence properties of indole in relation to biomolecules. Zimmermann and co-workers^{5,6} first reported the dual fluorescences of indole in ethanol at -180 °C on the basis of fluorescence polarization data. Song and Kurtin⁷ also confirmed the dual fluorescences of indole and its derivatives by means of polarized luminescence. Mataga et al.⁸ observed an unusually large red shift due to solvent perturbation on going from a cyclohexane to an acetonitrile solvent, and interpreted this large red shift as being the fluorescent level inversion of dual fluorescences. From their preliminary results, they mentioned that the fluorescence decay curve has a long and short decay component. On the other hand, De Lauder and Wahl³⁸

measured the fluorescence lifetimes of indole in various solvents and found that only a single fluorescence lifetime was obtained for the decay of indole both in polar and nonpolar solvents. They concluded that the results of their measurements do not favor the existence of emissions from two distinct excited states, and treated the results by the application of the exciplex theory proposed by Walker et al.³⁹ Eisinger and Navon⁴⁰ reported that the pronounced red shift in the fluorescence of indole in polar solvents is not attributed to an exciplex of definite composition but depends on the possibility that solvent reorientation can occur during the lifetime of the excited state. Andrews and Forster⁴¹ measured the fluorescence lifetimes, quantum yield, and polarization spectra of indole in nonpolar solvents. Their results indicate the dual fluorescences from thermally equilibrated 1L_a and 1L_b levels. They showed that the condition of thermalization will be achieved before any significant emission has occurred, and therefore a single exponential decay will be observed.

Although attempts to interpret the large red shifts of indole fluorescence in terms of solvent effects have been made,⁴¹⁻⁴⁴ it seems to be difficult to interpret all the experimental findings in terms of solvent effects only. The participation of different species has been suggested.^{14,45}

The calculated angles between the transition moments for the lower two transitions are 78 and 29°.^{32,33} The former result is consistent with the present polarization data. In conclusion, the experimental and theoretical findings on indole fluorescence, including the results of the present study, may be interpreted in terms of the fluorescent level inversion of dual fluorescences.

MO calculation shows that 1-naphthonitrile has the lowest 1L_b excited state lying slightly below the 1L_a state.³⁴ The calculated angle between the transition moments of the 1L_b and 1L_a transitions is 23°. This is consistent with the polarization spectra, which suggest that the two transition moments are nearly parallel. Comparing this with the spectral behavior of 1-naphthol, it may be concluded that the fluorescent level of 1-naphthonitrile in polar solvents changes from the 1L_a state to the 1L_b state on lowering the temperature.

In the region of the lowest absorption band, 1-naphthylamine also has closely situated excited states; the lowest and the next lowest excited states are assigned to the 1L_b and 1L_a states, respectively.^{26,28,29} The calculated angle between the transition moments of these two states is 40.8°;²⁹ this is consistent with the polarization spectrum (Figure 10). As was described previously, the temperature behavior of P for 1-naphthylamine is analogous to that of 1-naphthol, for which fluorescent level inversion was established. Mataga has ascribed the anomalous large Stokes shift of 1-naphthylamine in polar solvents to the fluorescent level inversion of dual fluorescences.⁹ From fluorescence lifetimes, El-Bayoumi et al.¹⁵ concluded that no fluorescent level inversion occurs and that the fluorescent level of 1-naphthylamine is 1L_b both in cyclohexane and in ethanol. Their results on the large increase in natural lifetimes on going from cyclohexane to ethanol (from 13 to 34 nm), however, seem to favor the fluorescent level inversion in 1-naphthylamine. It may safely be concluded that the fluorescent level inversion of dual fluorescences occurs in 1-naphthylamine as well as in the other compounds studied in this paper.

Motional Relaxation of Molecules in Solution. The principal values of the rotational diffusion tensor for perylene and 9,10-dimethylanthracene have been evaluated from measurements on the temperature dependence of the

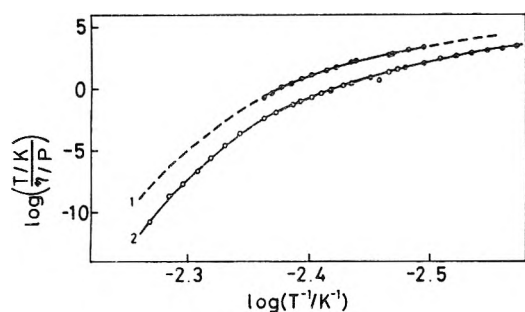


Figure 12. The $\log(T/\eta)$ plots against $\log(1/T)$ for propylene glycol (1), glycerin, and deuterated glycerin (2). The dashed curve indicates the estimated curve by extrapolation.

degree of fluorescence polarization.²³ Perylene and 9,10-dimethylanthracene have the principal axes of the diffusion tensor coinciding with the possible directions of the transition moments. The transition moments for the 1L_b and 1L_a transitions of the molecules studied in this paper do not always lie perpendicular to each other, and further the directions of these moments do not necessarily coincide with the principal axes of the diffusion tensor. It is therefore difficult to determine the three principal values for the rotational diffusion tensor of these molecules.

In the case of isotropic diffusion corresponding to spherical molecules, rotation along any axis has the same diffusion constant, D , and only one constant characterizes the rotational diffusion. Chuang and Eisenthal²² obtained the following expression for isotropic diffusion:

$$P^{-1} - 1/3 = (P_0^{-1} - 1/3)(1 + 6D\tau) \quad (1)$$

$$P_0^{-1} - 1/3 = 10/3(\cos^2 \lambda - 1)^{-1} \quad (2)$$

where τ is the lifetime and λ is the angle between the absorption and emission dipoles. P_0 corresponds to the limiting value of P in the absence of rotational diffusion, and hence P_0 can be obtained experimentally as the maximum value of P at lower temperatures. Equation 1 can be put in the form:

$$D = (P_0 - P)/5D\tau \quad (3)$$

From the observed value of P at any temperature and P_0 , one may obtain D for each temperature, provided the lifetime τ is known. The fluorescence lifetimes in ethanol⁴⁶ are as follows: τ (1-naphthol) = 7.5 ns, τ (indole) = 4.6 ns, and τ (1-naphthylamine) = 6.0 ns, and the recently measured fluorescence lifetime of 1-naphthonitrile is τ (1-naphthonitrile) = 6.5 ns.

It has been found that rotational diffusion constants are proportional to T/η over a considerable range of viscosity η .^{24,47,48} Thus one may assume that

$$D = d(T/\eta) \quad (4)$$

where the proportionality constant d does not depend on temperature. The rotational diffusion parameters for each temperature may be evaluated from the observed D . The viscosity data are taken from the literature.^{49,50} As for the region where no observed viscosity data are available, the viscosity is estimated by the extrapolation of the observed data down to lower temperatures (see Figure 12).

The resulting rotational diffusion parameters d for 1-naphthol, indole, 1-naphthonitrile, and 1-naphthylamine in propylene glycol are listed in Table I. The rotational diffusion parameter for 1-naphthol is constant over the range of about 320–240 K. Below 240 K, the error in d will increase, because P approaches P_0 . Indole and 1-naphthonitrile also have almost constant d values independent of temperature, while d for 1-naphthylamine increases with the decrease in temperature. The increase

TABLE I: The Rotational Diffusion Parameters of 1-Naphthol, Indole, 1-Naphthonitrile, and 1-Naphthylamine in Propylene Glycol

T, K	Rotational diffusion parameter $d/10^5 \text{ P s}^{-1} \text{ K}^{-1}$			
	1-Naphthol	Indole	1-Naphthonitrile	1-Naphthylamine
323	4.56	11.0		
313	4.56	7.46		
303	4.56	4.33		11.9
293	4.56	3.08	4.97	6.55
283	4.56	2.93	3.07	8.57
273	4.56	4.04	2.80	6.68
263	4.56	4.93	2.65	7.55
253	4.56	5.02	2.92	10.3
243	4.55	3.25	4.66	26.9
233	4.65	2.90	6.70	104

TABLE II: The Rotational Diffusion Parameters of 1-Naphthol and Indole in Glycerin

T, K	Rotational diffusion parameter $d/10^5 \text{ P s}^{-1} \text{ K}^{-1}$	
	1-Naphthol	Indole
353	2.16	7.66
343	2.11	7.19
333	2.29	6.68
323	2.74	6.92
313	3.75	8.12
303	4.81	8.48
293	4.80	7.10

in d of 1-naphthylamine with decreasing temperature indicates that 1-naphthylamine can rotate more easily at lower temperatures. The origin of this anomaly is not known; perhaps it is related to the amino group which has two hydrogen.

The rotational diffusion parameters for perylene and 9,10-dimethylanthracene in ethanol obtained by Labhart and Pantke are 9.0×10^5 and $18 \times 10^5 \text{ P s}^{-1} \text{ K}^{-1}$, respectively.²³ Although the indole and naphthalene derivatives that have been studied in the present paper are smaller in molecular size than perylene and 9,10-dimethylanthracene, they have smaller d values compared with those of perylene and 9,10-dimethylanthracene. This suggests that propylene glycol molecules solvate to these solute molecules and then the solvated spheres rotate as a whole. Propylene glycol solvent can self-associate through hydrogen bonding into large hydrogen-bonded networks. This prevents the rotational diffusion of solvated spheres and decreases d .

The rotational diffusion parameters obtained in glycerin are also given for 1-naphthol and indole in Table II. The d is almost constant as in propylene glycol. The d of 1-naphthol in glycerin is less than that in propylene glycol by a factor of 2, while the d of indole in glycerin is greater than that in propylene glycol. This suggests that indole and 1-naphthol differ slightly in the interaction with the solvent.

In the case of isotropic diffusion, the mean square angle $\langle \theta^2 \rangle$, determined by a molecular direction at the beginning and end of a time interval τ , is given by the following expression:⁵¹

$$\langle \theta^2 \rangle = 4D\tau \quad (5)$$

the mean square displacement $\langle x^2 \rangle$ is also obtained from the mean square angle

$$\langle x^2 \rangle = 3/2r^2\langle \theta^2 \rangle \quad (6)$$

where r is the radius of the molecule assumed to be spherical. From the observed D values, the root mean

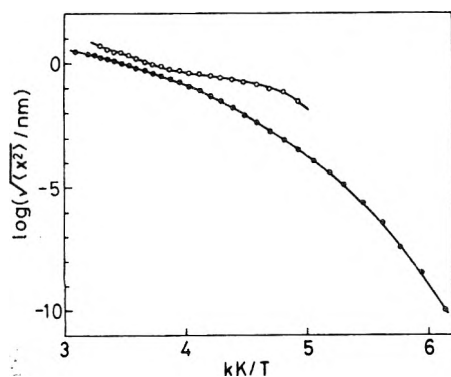


Figure 13. The $\log \langle (x^2)^{1/2} \rangle$ plots against $1/T$: (●) 1-naphthol, indole, and 1-naphthonitrile; (○) 1-naphthylamine.

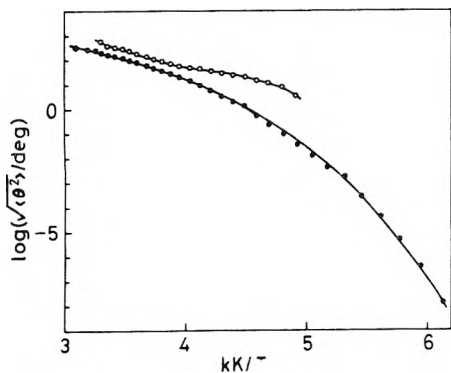


Figure 14. The $\log \langle (\theta^2)^{1/2} \rangle$ plots against $1/T$: (●) 1-naphthol, indole, and 1-naphthonitrile; (○) 1-naphthylamine.

square (rms) displacement $\langle x^2 \rangle^{1/2}$ and the root mean square rotation angle $\langle \theta^2 \rangle^{1/2}$ can be obtained.

Below the temperature where P reaches a maximum, D cannot be obtained experimentally. It has been shown that d is almost independent of temperature for 1-naphthol, indole, and 1-naphthonitrile. Assuming d for these compounds to be constant down to the temperature where fluorescent level inversion occurs, one may estimate D in the temperature region of the fluorescent level inversion, provided that T/η is known. The rms displacement and the rms rotation angle thus obtained are plotted against $1/T$ in Figures 13 and 14. The curves for 1-naphthol, indole, and 1-naphthonitrile are quite identical, but the curve for 1-naphthylamine differs considerably.

The rms displacement and the rms rotation angle at characteristic temperatures are given for 1-naphthol, indole, and 1-naphthonitrile in propylene glycol in Table III. T_1 is the temperature at which P begins to increase (the temperature at which P is $P_{\max}/20$) and T_2 is the temperature at which P reaches its maximum. T_3 is the temperature at which P becomes constant. Table III shows that the rms displacement and the rms rotation angle for the characteristic temperatures are almost the same for these molecules. The rms rotation angles at T_1 and T_2 are about 200 and 10° , respectively. This is consistent with rotational depolarization; this implies that the macroscopic viscosity is suitable for the description of rotational relaxation of such microscopic systems.

In Table IV, the rms displacement and the rms rotation angle at the characteristic temperatures are also given for 1-naphthol and indole in glycerin. These values in glycerin are nearly the same as those in propylene glycol.

It has already been shown that the dominant spectral changes due to the fluorescent level inversion begin to take place below T_2 . The rms displacement and rms rotation angle within the fluorescence lifetime at T_2 are about 0.01 nm and 10° , respectively, in propylene glycol as well as in

TABLE III: The rms Displacements and rms Rotation Angles in Propylene Glycol at Characteristic Temperatures

	T , K	$\langle \theta^2 \rangle^{1/2}$, deg	$\langle x^2 \rangle^{1/2}$, nm
1-Naphthol			
T_1^a	303	219	1.87
T_2	228	2.14	0.018
T_3	195	0.0098	0.000036
Indole			
T_1	306	295	1.95
T_2	228	2.14	0.018
T_3	190	0.0023	0.000016
1-Naphthonitrile			
T_1	300	224	1.82
T_2	220	0.93	0.0059
T_3	195	0.0098	0.000036
1-Naphthylamine			
T_1	303	572	4.89
T_2	210	0.87	0.072
T_3	185		

^a For T_1 , T_2 , and T_3 , see the text.

TABLE IV: The rms Displacements and rms Rotation Angles in Glycerin at Characteristic Temperatures

	T , K	$\langle \theta^2 \rangle^{1/2}$, deg	$\langle x^2 \rangle^{1/2}$, nm
1-Naphthol			
T_1^a	353	188	2.59
T_2	268	7.15	0.061
T_3	210	0.0070	0.000068
Indole			
T_1	343	223	1.91
T_2	263	7.63	0.043
T_3	208	0.011	0.000093

^a For T_1 , T_2 , and T_3 , see the text.

glycerin. This implies that the solute and solvent molecules cannot translate or rotate appreciably at the temperatures of fluorescent level inversion. It is therefore concluded that the fluorescent level inversion of dual fluorescences is achieved by slight relaxational motions to equilibrium solute-solvent configurations during the lifetime of excited states.

Acknowledgment. This work was supported in part by a Scientific Grant from the Ministry of Education (No. 054111). The authors thank Hiroshi Watanabe for the fluorescence lifetime measurements.

References and Notes

- (1) Present address: Industrial Apparatus Laboratory, Matsushita Electric Industrial Co., Ltd., Toyonaka, Osaka, Japan.
- (2) Present address: Heavy Apparatus Engineering Laboratory, Tokyo Shibaura Electric Co., Ltd., Tsurumi, Yokohama, Japan.
- (3) E. Lippert, W. Lüder, and H. Boos in "Advances in Molecular Spectroscopy", A. Mangini, Ed., Pergamon Press, Oxford, 1972, p 443.
- (4) E. Lippert, W. Lüder, F. Moll, W. Nägele, H. Boos, H. Brigge, and I. Selbold-Blankenstein, *Angew. Chem.*, **73**, 695 (1961).
- (5) H. Zimmermann and N. Joop, *Z. Electrochem.*, **65**, 61 (1961).
- (6) H.-V. Schütt and H. Zimmermann, *Ber. Bunsenges. Phys. Chem.*, **67**, 54 (1963).
- (7) P. Soon-Song and W. E. Kurtin, *J. Am. Chem. Soc.*, **91**, 4892 (1969).
- (8) N. Mataga, Y. Torihashi, and K. Ezurni, *Theor. Chim. Acta*, **2**, 158 (1964).
- (9) N. Mataga, *Bull. Chem. Soc. Jpn.*, **36**, 654 (1963).
- (10) S. Suzuki and H. Baba, *Bull. Chem. Soc. Jpn.*, **40**, 2199 (1967).
- (11) O. S. Khalil, R. L. Hofeldt, and S. P. McGlynn, *Chem. Phys. Lett.*, **17**, 479 (1972).
- (12) O. S. Khalil, R. H. Hofeldt, and S. P. McGlynn, *J. Lumin.*, **8**, 229 (1973).
- (13) K. Rotkiewicz, K. H. Grellmann, and Z. R. Grabowski, *Chem. Phys. Lett.*, **19**, 315 (1973).
- (14) C. M. Chopin and J. H. Wharton, *Chem. Phys. Lett.*, **3**, 552 (1969).

- (15) M. A. El-Bayoumi, J.-P. Dalle, and M. F. O'Dwyer, *J. Lumin.*, **1**–2, 716 (1970).
- (16) S. Suzuki, T. Fujii, and K. Sato, *Bull. Chem. Soc. Jpn.*, **45**, 1937 (1972).
- (17) A. C. Albrecht, *J. Mol. Spectrosc.*, **6**, 84 (1961).
- (18) A. K. Kalantar and A. C. Albrecht, *Ber. Bunsenges. Phys. Chem.*, **68**, 361 (1964).
- (19) F. Dörr, *Angew. Chem.*, **78**, 457 (1966).
- (20) F. Dörr in "Creation and Detection of the Excited State", Vol. 1, Part A, A. A. Lamola, Ed., Marcel Dekker, New York, N.Y., 1971, Chapter 2.
- (21) L. D. Favro, *Phys. Rev.*, **119**, 53 (1960).
- (22) T. J. Chuang and K. B. Eisenthal, *J. Chem. Phys.*, **57**, 5094 (1972).
- (23) H. Labhart and E. R. Pantke, *Chem. Phys. Lett.*, **23**, 482 (1973).
- (24) E. R. Pantke and H. Labhart, *Chem. Phys. Lett.*, **23**, 476 (1973).
- (25) W. R. Ware, ref 20, Chapter 5.
- (26) H. Baba and S. Suzuki, *Bull. Chem. Soc. Jpn.*, **34**, 82 (1961).
- (27) H. Baba and S. Suzuki, *J. Chem. Phys.*, **35**, 1118 (1961).
- (28) S. Suzuki and H. Baba, *Bull. Chem. Soc. Jpn.*, **37**, 519 (1964).
- (29) S. Suzuki, T. Fujii, and H. Baba, *J. Mol. Spectrosc.*, **47**, 243 (1973).
- (30) D. M. Hercules and L. B. Rogers, *Spectrochim. Acta*, **15**, 393 (1959).
- (31) D. M. Hercules and L. B. Rogers, *J. Phys. Chem.*, **64**, 397 (1960).
- (32) F. Momicchioli and A. Rastelli, *J. Mol. Spectrosc.*, **22**, 310 (1967).
- (33) E. M. Evieth, *Theor. Chim. Acta*, **16**, 22 (1970).
- (34) S. Suzuki, T. Fujii, and T. Ishikawa, *J. Mol. Spectrosc.*, **57**, 490 (1975).
- (35) K. Nishimoto, *J. Phys. Chem.*, **67**, 1443 (1963).
- (36) L. S. Forster and K. Nishimoto, *J. Am. Chem. Soc.*, **87**, 1459 (1965).
- (37) Y. Tanizaki and S. Kubodera, *J. Mol. Spectrosc.*, **24**, 1 (1967).
- (38) W. B. De Lauder and Ph. Wahl, *Biochim. Biophys. Acta*, **243**, 153 (1971).
- (39) M. S. Walker, T. W. Bednar, and R. Lumry, *J. Chem. Phys.*, **45**, 3455 (1966); **47**, 1020 (1967).
- (40) J. Eisinger and G. Navon, *J. Chem. Phys.*, **50**, 2069 (1969).
- (41) L. J. Andrews and L. S. Forster, *Photochem. Photobiol.*, **19**, 357 (1974).
- (42) A. Kawski and J. Czajko, *Z. Naturforsch. A*, **29**, 84 (1974).
- (43) A. Kawski and J. Sepiol, *Bull. Acad. Pol. Sci., Ser. Sci. Math., Astron. Phys.*, **20**, 707 (1972).
- (44) C. Cazeau-Dubroca, F. Dupuy, and M. Martnaud, *Chem. Phys. Lett.*, **23**, 397 (1973).
- (45) E. P. Kirby and R. F. Steiner, *J. Phys. Chem.*, **74**, 4450 (1970).
- (46) I. B. Berlman, "Handbook of Fluorescence Spectra of Aromatic Molecules", 2nd ed, Academic Press, New York, N.Y., 1971.
- (47) L. I. Antsiferova, N. N. Korst, V. B. Stryukov, A. N. Ivanova, N. S. Nazemets, and N. V. Rabin'kina, *Mol. Phys.*, **25**, 909 (1973).
- (48) R. E. D. McClung and D. Kivelson, *J. Chem. Phys.*, **49**, 3380 (1968).
- (49) J. A. Riddick and W. B. Bunger, "Organic Solvents", 3rd ed, Wiley-Interscience, New York, N.Y., 1970.
- (50) Landolt-Börnstein Zahlenwerte und Funktionen, II. Band, 5. Teil, Bandteil a, Transportphänomene I, Springer-Verlag, Berlin, 1969.
- (51) G. Weber in "Fluorescence and Phosphorescence Analysis", D. M. Hercules, Ed., Wiley, New York, N.Y., 1966, Chapter 8.

A Method for Calculating CNDO–MO Bonding Parameters. 1

Sankar Prasad Bhattacharyya

Department of Chemistry, Presidency College, Calcutta-700073, India

and Mihir Chowdhury*

Department of Physical Chemistry, Indian Association for the Cultivation of Science, Jadavpur, Calcutta-700032, India (Received November 10, 1976)

An analysis of the imbalance in the off-diagonal Fock matrix element in the CNDO–MO theory is made. A semitheoretical method for the estimation of the CNDO bonding parameter is developed. The use of a scheme with a nonorthogonalized and an orthogonalized basis set is discussed.

1. Introduction

It is well known that in the CNDO–MO theory, the diagonal elements of the Fock matrix (F_{ii}^{CNDO}) can be easily calculated^{1–5} by more or less standardized techniques (CNDO/1, CNDO/2, etc.) without adopting any ad hoc parametrization. Admitting that the approximations involved are of drastic nature, the numerical effect is, nevertheless, not so severe in the diagonal terms as to cause a collapse of the theory.⁶ The reasons are not difficult to understand. The F -matrix elements reflect the delicate balance between two sets of terms: the H -matrix elements representing an overall attractive potential and the G -matrix elements offering the counterbalancing repulsive potential. Since similar degrees of approximation are made in both the H and G matrix elements constituting the diagonal element of the F (CNDO) matrix, it is not strained too much, or if strained, all the diagonal terms are affected more or less equally. However, unfortunately, the same is not true for the off-diagonal $F_{ij}^{\text{AB}}(\text{CNDO})$ term ($i \neq j$, $A \neq B$). In the standard CNDO–MO method one writes

$$F_{ij}^{\text{AB}}(\text{CNDO}) = H_{ij}(\text{CNDO}) + G_{ij}^{\text{AB}}(\text{CNDO}) \quad (1)$$

$$= H_{ij}^{\text{AB}}(\text{CNDO}) - 1/2 P_{ij} g_{\text{AB}}^0$$

Thus, while terms containing bicentric overlaps ($x_i^A x_j^B$) are retained in the H matrix, they are completely removed from the G matrix by enforcing the "ZDO" principle consistently. Thus, the balance, so essential for a correct representation of the effective potential seen by the overlap charge ($x_i^A x_j^B$), is seriously disturbed. Automatically, therefore, if one attempts to estimate the $H_{ij}^{\text{AB}}(\text{CNDO})$ terms, the computed values of the $F_{ij}^{\text{AB}}(\text{CNDO})$ terms would be too negative to represent the effective potential even in an approximately correct way. This is the reason why the $F_{ij}^{\text{AB}}(\text{CNDO})$ term has to be parameterized, the standard treatment for which is the following:

$$F_{ij}^{\text{AB}}(\text{CNDO}) = H_{ij}^{\text{AB}}(\text{CNDO}) - 1/2 P_{ij} g_{\text{AB}}^0$$

$$= \beta_{\text{AB}}^0 S_{ij}^{\text{AB}} - 1/2 P_{ij} g_{\text{AB}}^0$$

$$= 1/2 (\beta_{\text{A}}^0 + \beta_{\text{B}}^0) S_{ij}^{\text{AB}} - 1/2 P_{ij} g_{\text{AB}}^0 \quad (2)$$

β_{A}^0 and β_{B}^0 are the bonding parameters of atoms A and B, respectively, and are estimated by comparing results of ab-initio LCAO–SCF calculations on the relevant diatomic species with the results obtained by making CNDO–MO calculations. The method is surely not un-

realistic but has the following awkward features:

(i) It may be difficult to find a stable diatomic species A-B which can serve as a real prototype of a system of chemically interesting molecules containing an A-B bond.

(ii) Full LCAO-SCF data on the prototype system A-B may not be available as is the case with many heavy atoms.

(iii) Extensive computations have to be performed to sort out the β_A^0 parameters giving the best fit. For some atoms (e.g., transition metals) more than one bonding parameter are needed, making the process of parameter fitting more difficult.

(iv) β_{AB}^0 , the property of a bond, is treated as an average of atomic properties β_A^0 and β_B^0 which leads to complete transferability of these parameters from molecule to molecule. Even the possibility of bond length dependence of β_{AB}^0 is not considered.

(v) The scheme is not sufficiently flexible to accommodate the use of different sets of orbital exponents or to employ different semiempirical schemes for the evaluation of electron repulsion integrals since the β_{AB}^0 parameters would have to be recalibrated in each case.

Thus, the development of a standardized, even though an approximate, scheme for calculating β_{AB}^0 parameters within a particular level of approximation is highly desirable. In the following section we have tried to develop one such semitheoretical scheme.

2. Calculation of Bonding Parameters

From consideration of the imbalance generated by the treatment of the off-diagonal Fock matrix elements in the original CNDO-MO theory, we have tried to calculate F_{ij}^{AB} terms by retaining, in addition to the usual CNDO terms, the electron repulsion integrals of the type $g_{ij,kk}$ ($k \in A$) and $g_{ij,rr}$ ($r \in B$), and neglecting the higher order terms such as $g_{ij,kl}$ or $g_{ij,rs}$, etc. This removes the major part of the imbalance and leads to β_{AB} parameters having correct order of magnitudes (i.e., of the order of β_{AB}^0). Murrell⁷ also has considered this imbalance, approached it from a different angle, and attempted to compute F_{ij}^{AB} integrals directly by retaining all terms of the $g_{ij,rr}$ type in the expression for the F_{ij}^{AB} element. Our approach is, however, different in many respects as will be evident from the following discussions. We write the modified or the imbalance-corrected F_{ij}^{AB} (CNDO) term as shown in eq 3¹³ (assuming that A and B are two neutral atoms held at normal bonding distance):

$$F_{ij}^{AB}(\text{modified CNDO}) = \langle \chi_i^A | T(1) + V_A^0(r) + V_B^0(r) | \chi_j^B \rangle + \sum_{k \in A} g_{ij,kk} P_{kk} \\ + \sum_{r \in B} g_{ij,rr} P_{rr} - 1/2 P_{ij} g_{AB}^0 = 1/2 \langle \chi_j^B | T(1) + V_A^0(r) | \chi_i^A \rangle + 1/2 \langle \chi_i^A | T(1) + V_B^0(r) | \chi_j^B \rangle \\ + 1/2 \langle \chi_i^A | V_A^0(r) + V_B^0(r) | \chi_j^B \rangle \\ + \sum_{k \in A} P_{kk} g_{ij,kk} + \sum_{r \in B} P_{rr} g_{ij,rr} - 1/2 P_{ij} g_{AB}^0 \quad (3)$$

Here P_{kk} , P_{rr} , etc. are the "basis orbital occupation numbers" for which we will use the not-too-unreasonable assumption that $P_{kk} = P_{rr} = 1$ for all k and r except for $k = i$ and $r = j$ for which we assume $P_{ii} = P_{jj} = 0$. That is, we are using the conventional picture of a chemical bond. (P_{kk} , P_{rr} , etc. for a heteroatomic system do of course vary in each iteration. Fortunately, however, the β_{AB} parameter can be shown to be relatively insensitive to such variations lending support to the use of a fixed set of β_{AB} parameters in the CNDO-MO theory. This aspect has been considered at the end of this section.)

Hence

$$\sum_{k \in A} P_{kk} = Z_A - 1 \quad \text{and} \quad \sum_{r \in B} P_{rr} = Z_B - 1 \quad (4)$$

where Z_A and Z_B are the number of valence electrons on atoms A and B, respectively, so that the bonding electron pair is assumed to be removed completely from the respective atomic regions into the bonding zone. Applying Mulliken's approximation to break up the bicentric overlap charge density $\chi_i^A \chi_j^B$ only for the evaluation of g_{ij} , g_{kk} , or g_{rr} integrals, one obtains from (3), after slight manipulation

$$F_{ij}^{AB}(\text{modified CNDO}) = 1/2 (u_i^A + u_j^B) S_{ij}^{AB} + 1/2 (u_j^B) S_{ij}^{AB} \\ + \sum_{k \in A} P_{kk} g_{ii,kk} S_{ij}^{AB} + 1/2 S_{ij}^{AB} \left(\sum_{k \in A} P_{kk} g_{jj,kk}^{BA} \right) \\ + \sum_{r \in B} P_{rr} g_{ii,rr}^{AB} + 1/2 \langle \chi_i^A | V_A^0(r) + V_B^0(r) | \chi_j^B \rangle - 1/2 P_{ij} g_{AB}^0 \quad (5)$$

In (5) u_i^A and u_j^B are the core binding energies¹⁴ of the electrons in χ_i^A and χ_j^B (AO's), respectively. Taking now the spherically averaged values of all one- and two-center electron repulsion integrals, one obtains $g_{ii,kk}^{AA} = g_{AA}^0$ for all the k 's; $g_{jj,rr}^{BB} = g_{BB}^0$ for all the r 's. $g_{jj,kk}^{BA} = g_{ii,rr}^{AB} = g_{AB}^0$ for all the k 's and r 's.

Thus, from (5) we have

$$F_{ij}^{AB}(\text{modified CNDO}) = -1/2 (I_i^A + I_j^B) S_{ij}^{AB} \\ + 1/2 (Z_A + Z_B - 2) g_{AB}^0 S_{ij}^{AB} + 1/2 \langle \chi_i^A | V_A^0(r) + V_B^0(r) | \chi_j^B \rangle - 1/2 P_{ij} g_{AB}^0 \quad (6)$$

where I_i^A and I_j^B are the ionization energies of the atomic orbitals χ_i^A and χ_j^B , respectively; i.e. $-I_i^A = u_i^A + (Z_A - 1)g_{AA}^0$ and $-I_j^B = u_j^B + (Z_B - 1)g_{BB}^0$.

To estimate the integral $\langle \chi_i^A | V_A^0(r) + V_B^0(r) | \chi_j^B \rangle$ we use the method of Ohno^{8a} (see also Brown^{8b}) with the modification that the point charge approximation is not used to evaluate the interaction of the overlapping charge density (supposed to be localized at the center of the A-B bond) with $V_A^0(r)$ and $V_B^0(r)$.¹⁵

We write, using the Mataga approximation⁹ for the estimation of two-center electron repulsion integral g'_{AB} at $r = 1/2 r_{AB}$

$$1/2 \langle \chi_i^A | V_A^0(r) + V_B^0(r) | \chi_j^B \rangle = -1/2 K S_{ij}^{AB} (Z_A + Z_B) g'_{AB}$$

where

$$g'_{AB} = e^2 / (r + a_{AB})$$

and

$$a_{AB} = 1 / (g_{AA}^0 + g_{BB}^0)$$

r_{AB} is the A-B bond length, g_{AA}^0 and g_{BB}^0 are one-center electron repulsion integrals, and Z_{Ae} and Z_{Be} are the core charges of atoms A and B, respectively; g_{AA}^0 etc. are calculated by Saturno's¹⁰ model using the exponents of ref 11. K is an empirical parameter which may be adjusted, if needed. With these approximations, eq 6 becomes

$$F_{ij}^{AB}(\text{modified CNDO}) = [-1/2 (I_i^A + I_j^B) - K/2 (Z_A + Z_B) g'_{AB} + 1/2 (Z_A + Z_B - 2) g_{AB}^0] S_{ij}^{AB} \\ - 1/2 P_{ij} g_{AB}^0 \quad (7)$$

Since I_i^A , I_j^B terms are dependent on azimuthal quantum numbers, invariance to hybridization cannot be maintained with this form of F_{ij}^{AB} term though rotational invariance is guaranteed. To correct for this, we assume that $I_i^A \approx$

TABLE I: Variation of $\beta_{AB}(I)$ Parameter in Course of the Iterations

Bond parameter β_{AB} , eV	Iteration no.								
	1	2	3	4	5	6	7	8	9
Br-F	-25.6108	-24.2358	-25.5800	-25.4770	-25.4955	-25.4963	-25.4969	-25.4971	-25.4972
I-Cl	-20.0893	-19.6887	-20.0803	-20.0580	-20.0609	-20.0611	-20.0612	-20.0611	-20.6011
I-Br	-18.1363	-18.0859	-18.1253	-18.1243	-18.1245	-18.1245	-18.1245	-18.1245	-18.1245

I_{av}^A for all i 's (av = average) and $I_j^B \approx I_{av}^B$ for all j 's, as an approximation, where for atoms with a ns, np basis

$$I_{av}^A = \frac{(2l_s + 1)I_{ns}^A + (2l_p + 1)I_{np}^A}{(2l_s + 1) + (2l_p + 1)}$$

and a similar expression for I_{av}^B is used.

Ultimately we have

$$F_{ij}^{AB}(\text{modified CNDO}) = [-1/2(I_{av}^A + I_{av}^B) - (K/2)(Z_A + Z_B)g'_{AB} + 1/2(Z_A + Z_B - 2)g_{AB}^0]S_{ij}^{AB} - 1/2P_{ij}g_{AB}^0 \quad (8)$$

$$= \beta_{AB}(I)S_{ij}^{AB} - 1/2P_{ij}g_{AB}^0 \quad (9)$$

From (1) $F_{ij}^{AB}(\text{CNDO}) = \beta_{AB}^0 S_{ij}^{AB} - 1/2 P_{ij} g_{AB}^0$.

Hence, comparing eq 1 and 2 with eq 8 and 9 we can write

$$\beta_{AB}^0 = \beta_{AB}(I) = -(I_{av}^A + I_{av}^B)/2 - (K/2)(Z_A + Z_B)g'_{AB} + 1/2(Z_A + Z_B - 2)g_{AB}^0 \quad (10)$$

Since the right-hand side of (10) depends only on the nature of the atoms, invariance requirements are fulfilled¹⁶ by $\beta_{AB}(I)$.

We will show in section 4 that with $K = 0.75$, eq 10, on the average, reproduces, for atoms with ns, np basis, Pople's β_{AB}^0 parameters for the A-B bonds fairly well, in spite of the approximate nature of the treatment. This strengthens our contention that β_{AB}^0 , just like our $\beta_{AB}(I)$, is not really a core parameter but embodies the sum total of the relevant core contributions and the contributions from the additional $g_{ij,kk}$ ($k \in A, B$) integrals which are supposed to be neglected in the CNDO-MO theory. We must point out that use of eq 1 introduces no actual change in the basic framework of the CNDO-MO theory. It only gives us an insight into the nature of the β_{AB}^0 parameters and presents an approximate method of guessing these quantities.

Variable β -CNDO-MO Method. Equation 10 can be rewritten a bit more elaborately as

$$\beta_{AB}^0 = \beta_{AB}(I) = 1/2(u_{av}^A + u_{av}^B + \sum_{k \neq i}^A P_{kk} g_{AA}^0 + \sum_{r \neq j}^B P_{rr} g_{BB}^0) - (K/2)(Z_A + Z_B)g'_{AB} + 1/2(Z_A + Z_B - 2)g_{AB}^0 \quad (10a)$$

where u_{av}^A and u_{av}^B are defined in the same way as I_{av}^A and I_{av}^B . In a diatomic system A-B if some of the electronic charge migrates from A \rightarrow B during the iterative stages of the SCF process the $\sum_r^B P_{rr} g_{BB}^0$ term increases in magnitude; but this increase is almost balanced by a parallel decrease in the $\sum_k^A P_{kk} g_{AA}^0$ term. The difference of the two opposing contribution which would be reflected in the β_{AB}^0 parameter is expected to be small, which would justify the conventional nonvariable β_{AB} approximation introduced by Pople. To check these ideas, we have tested our variable β -CNDO method through actual numerical

calculations on three heteronuclear diatomic species, viz. BrF, ICl, IBr. The details of the approximations used are reported in the part 2 of this series of papers. The results of the calculations, reported in Table I, show the pattern of variation of $\beta_{AB}(I)$ parameter during the iterations. They always tend to converge to the starting value. The energies are a bit lower in the fixed β calculations while the ionization energies (Koopman) are highly insensitive to this change in the approximation (see part 2). The results support the use of the nonvariable β approximation. Since our β_{AB} parameter would always be evaluated with reference to a prototype diatomic species A-B, this conclusion is a general one, and supports the use of a fixed β_{AB} value.

3. Bond Parameters for Use with an Orthogonalized Basis

Let χ_i^A and χ_j^B be the STO's on the atomic centers A and B, respectively. Then $\langle \chi_i^A | \chi_j^B \rangle = S$. If we assume that S^2 and higher order terms are negligible, χ_i^A and χ_j^B can be replaced by two symmetrically orthogonalized orbitals ψ_i^A and ψ_j^B (to first order in S): i.e.

$$\psi_i^A = \chi_i^A - 1/2 S \chi_j^B$$

$$\psi_j^B = \chi_j^B - 1/2 S \chi_i^A$$

It is easy to see that the G -matrix elements defined in the approximately ortho-normal basis ψ_i^A, ψ_j^B and subjected to the usual CNDO approximations retain a term by term identity with the corresponding CNDO G -matrix elements defined in the nonorthogonalized basis χ_i^A, χ_j^B , to a first order approximation.

Thus

$$\langle \chi_i^A | \chi_i^A | \chi_j^B | \chi_j^B \rangle \approx \langle \psi_i^A | \psi_i^A | \psi_j^B | \psi_j^B \rangle$$

and

$$\langle \chi_i^A | H^{\text{core}} | \chi_i^A \rangle \approx \langle \psi_i^A | H^{\text{core}} | \psi_i^A \rangle$$

Regarding F as the effective Hamiltonian operator for the diatomic system A-B, where A and B are neutral atoms, we have

$$\langle \psi_i^A | F | \psi_j^B \rangle = \langle \chi_i^A | F | \chi_j^B \rangle - 1/2 S_{ij}^{AB} [\langle \chi_i^A | F | \chi_i^A \rangle + \langle \chi_j^B | F | \chi_j^B \rangle] \quad (11)$$

For the case considered, it is not unreasonable to assume that

$$\langle \chi_i^A | F | \chi_i^A \rangle \approx -I_i^A$$

and

$$\langle \chi_j^B | F | \chi_j^B \rangle \approx -I_j^B \quad (12)$$

In the previous section we have shown that (e.g., eq 7)

$$\langle \chi_i^A | F | \chi_j^B \rangle = F_{ij}^{AB}(\text{modified CNDO}) = [- (I_i^A + I_j^B)/2 - (K/2)(Z_A + Z_B)g'_{AB} + 1/2(Z_A + Z_B - 2)g_{AB}^0]S_{ij}^{AB} - 1/2 P_{ij} g_{AB}^0 \quad (7)$$

TABLE II: Comparison of $\beta_{AB}(I)$ and $\beta_{AB}(II)$ Parameters with β_{AB}^0 ^a

Bond type	$-\beta_{AB}(I)$ ($k = 0.75$), eV	$-\beta_{AB}(II)$ ($k = 1$), eV	$-\beta_{AB}^0$ (Pople), ^b eV	r_{AB} , ^c Å
C-H	18.93	10.60	15.00	1.09 (CH)
F-F	32.06	24.70	39.00	1.418 (F ₂)
Cl-Cl	22.35	26.02	22.33	2.00 (Cl ₂)
Cl-F	27.15	20.44	28.16	1.628 (ClF)
C-C	17.63	11.10	21.00	1.34 (C ₂ H ₄)
Br-Br	21.20	13.90	21.23	2.28 (Br ₂)
Br-F	26.10	19.32	30.10	1.755 (BrF)
Br-Cl	21.28	14.93	22.26	2.138 (BrCl)
I-Br	19.43	13.21	19.52	2.50 (IBr)
C-N	19.45	13.58	23.00	1.718 (CN)
N-H	21.08	12.58	17.00	1.02 (NH ₃)
C-O	22.06	15.63	26.00	1.13 (CO)
C-B	15.67	9.50	19.00	1.64 (CB ₄)
N-N	21.85	15.63	25.00	1.10 (N ₂)
N-O	24.45	17.84	28.00	1.15 (NO)
N-F	29.32	19.87	32.00	1.36 (NF ₃)
N-B	17.72	11.50	21.00	1.28 (BN)
O-O	27.15	20.18	31.00	1.20 (O ₂)
O-F	30.44	22.18	35.00	1.42 (OF ₂)
O-B	20.20	13.34	24.00	1.36 (BO)
B-F	22.75	15.50	28.00	1.26 (BF)
S-S	18.13	11.82	18.15	2.05 (S ₂ H ₂)
P-P	15.95	9.35	15.05	2.25 (P ₂ S ₂)
P-S	16.91	10.57	16.61	2.10 (P ₂ S ₃)
Si-Si	12.76	7.23	13.06	2.32 (Si ₂ Cl ₆)
Al-S	13.64	8.56	15.72	2.03 (AlS)

^a For definition of the symbols see text. ^b For second row or heavier atoms Pople's bonding parameters (β_{AB}^0) have been generally obtained by an extrapolation technique (see ref 4). ^c The bond lengths (r_{AB}) are taken from Sutton's bond length tables. The corresponding species are also indicated.

Hence, inserting (7) into (11) and using (12), we have

$$\begin{aligned} \langle \psi_i^A | F | \psi_j^B \rangle &= [-(K/2)(Z_A + Z_B)g'_{AB} + 1/2(Z_A \\ &+ Z_B - 2)g_{AB}^0] S_{ij}^{AB} - 1/2 P_{ij} g_{AB}^0 \\ &= \beta_{AB}(II) S_{ij}^{AB} - 1/2 P_{ij} g_{AB}^0 \end{aligned}$$

So

$$\beta_{AB}(II) = -(K/2)(Z_A + Z_B)g'_{AB} + 1/2(Z_A + Z_B - 2)g_{AB}^0 \quad (13)$$

$\beta_{AB}(II)$ can be regarded as the bond parameter to be used when approximately orthogonalized basis orbitals are employed. Indeed, to first order this is the only change that has to be made for using an orthogonalized basis set. For the estimation of the $\beta_{AB}(II)$ parameters we have used $K = 1$.

Comparison of $\beta_{AB}(I)$ and $\beta_{AB}(II)$ with β_{AB}^0 . In Table II we present some of our $\beta_{AB}(I)$ and $\beta_{AB}(II)$ parameters along with the β_{AB}^0 parameters of Pople et al. for comparison. It is seen from Table II that the calculated parameters, $\beta_{AB}(I)$, are of the same order of magnitude as β_{AB}^0 . $\beta_{AB}(I)$ parameters, however, are consistently larger than the $\beta_{AB}(II)$ parameters, while $\beta_{AB}(II)$ parameters are always $\ll \beta_{AB}^0$. Depending upon the nature of the bond, the deviations of $\beta_{AB}(I)$ from β_{AB}^0 may be either positive, negative, or nearly zero for a fixed choice of $K (= 0.75)$. However, we should note that K can always be adjusted so as to produce "zero deviation" for any particular type of bond. We should also note the fact that our bonding parameters for use with the orthogonalized orbitals are

TABLE III: Bond Length Dependence of $\beta_{AB}(I)$ and $\beta_{AB}(II)$ Parameters

Bond type	Bond length r_{AB} , Å	$-\beta_{AB}(I)$, eV	$-\beta_{AB}(II)$, eV
N-H	1.02	21.08	12.58
N-H	1.25	21.09	12.18
N-H	1.50	21.03	11.73
N-H	1.75	20.99	11.27
C-H	1.09	18.93	10.64
C-H	1.25	18.88	10.39
C-H	1.50	18.78	9.99
C-H	1.75	18.65	9.60
P-P	1.5	15.39	9.57
P-P	1.8	15.68	9.51
P-P	2.0	15.83	9.45
P-P	2.25	15.95	9.35
P-P	2.50	16.04	9.22

numerically smaller than those for use with the nonorthogonal (NO) basis is in keeping with the analysis of Jug¹² who tried to estimate these parameters from a different approach. Pople assumed a "NO" basis set in his CNDO-MO theory and hence the comparison of $\beta_{AB}(I)$ with β_{AB}^0 is more meaningful. The maximum difference observed (Table I) among the calculated $\beta_{AB}(I)$ and the calibrated β_{AB}^0 parameters is of the order of 4 eV. Within the usual limit of accuracy of the calculated molecular properties obtained by CNDO-MO calculations, this difference may be considered quite insignificant. We note that the reported $\beta_{AB}(I)$ parameters for a number of bonds between two second row atoms agree quite well with those suggested by Santry and Segal. This, perhaps rationalizes the Segal-Santry extrapolation technique to some extent. The $\beta_{AB}(II)$ parameters for these bonds are surprisingly close to the β_{AB} parameters used by Santry.⁵ This agreement may, however, be coincidental.

Transferability of $\beta_{AB}(I)$ and $\beta_{AB}(II)$ Parameters. To test the transferability of calculated parameters from molecule to molecule we have reported β_{AB} parameters of a number of bonds over a range of bond lengths, r being the only factor which might affect transferability in our model (Table III). For N-H and C-H bonds $\beta_{AB}(I)$ parameters are seen to be very nearly independent of bond lengths. $\beta_{AB}(II)$ parameters for the same bonds show a weak bond length dependence. The β_{AB} parameter for the P-P bond is seen to decrease to some extent as r is reduced and vice versa. In some cases $\beta_{AB}(I)$ parameters are even found to increase slightly on decreasing the bond length. This weak bond length dependence is thus a new feature of our theory, and has some bearing on the optimization of bond length. This is being studied at present.

Conclusion

Our analysis shows that a formulation for computing bonding parameters to be used in CNDO-MO type calculations is possible. We feel that it is always better to calibrate formulae for generating these parameters from a rationalized approach than to calibrate the parameters individually. We have already extended this approach to transition metal complexes. Results of model calculations will be published shortly.

Acknowledgment. Sincere thanks are due to the University of Calcutta for the award of a Research Fellowship (UGC) to one of us (S.P.B.).

References and Notes

- (1) J. A. Pople, D. P. Santry, and J. Chem. Phys., **43**, S129 (1965).
- (2) J. A. Pople and G. A. Segal, J. Chem. Phys., **43**, S136 (1965).
- (3) J. A. Pople and G. A. Segal, J. Chem. Phys., **44**, 3289 (1966).
- (4) D. P. Santry and G. A. Segal, J. Chem. Phys., **47**, 158 (1967).
- (5) D. P. Santry, J. Am. Chem. Soc., **90**, 3309 (1968).
- (6) B. J. Nicholson, Advan. Chem. Phys., **18**, 249.
- (7) J. N. Murrel and A. H. Harget, "Semi-Empirical Self-Consistent Field Molecular Orbital Theory of Molecules", Wiley-Interscience, New York, N.Y., 1971, Chapter 6, pp 145-156.
- (8) (a) K. Ohno, Theor. Chim. Acta, **2**, 219 (1964); (b) R. D. Brown and K. R. Roby, *ibid.*, **18**, 175, 299 (1970).
- (9) N. Mataga and K. Nishimoto, Z. Phys. Chem., **12**, 335 (1957).
- (10) A. F. Saturno, Theor. Chim. Acta, **11**, 365 (1968).
- (11) (a) E. Clementi and D. L. Raimondi, J. Chem. Phys., **38**, 2686 (1967). (b) E. Clementi, D. L. Raimondi, and W. P. Reinhardt, J. Chem. Phys., **47**, 1300 (1967).
- (12) K. Jug, Theor. Chim. Acta, **16**, 95 (1970).

$$(13) \langle x_i^A | T(1) + V_A^0(r) + V_B^0(r) | x_j^B \rangle = \langle x_j^B | T(1) + V_A^0(r) | x_i^A \rangle + \langle x_i^A | V_B^0(r) | x_j^B \rangle$$

Also

$$\langle x_i^A | T(1) + V_A^0(r) + V_B^0(r) | x_j^B \rangle = \langle x_i^A | T(1) + V_B^0(r) | x_j^B \rangle + \langle x_i^A | V_A^0(r) | x_j^B \rangle$$

Averaging leads to eq 3.

$$(14) T(1) + V_A^0(r) | x_i^A \rangle = u_i^A | x_i^A \rangle$$

$$T(1) + V_B^0(r) | x_j^B \rangle = u_j^B | x_j^B \rangle$$

(15) Estimation of this integral by direct quadrature is possible, as discussed by Murrel,⁷ but to keep the spirit of semiempiricism intact, we have adopted an approximate technique. However, a semiempirical constant has to be introduced.

(16) In the discussion given by Murrel this aspect has not been considered.

A Method for Calculating CNDO-MO Bonding Parameters. 2. Preliminary Applications

Sankar Prasad Bhattacharyya

Department of Chemistry, Presidency College, Calcutta-700073, India

and Mihir Chowdhury*

Department of Physical Chemistry, Indian Association for the Cultivation of Science, Jadavpur, Calcutta-700032, India (Received November 10, 1976)

A semitheoretical parametrization technique developed in part 1 is tested by performing some actual CNDO-MO calculations. The results obtained are satisfactory so far as molecular ionization potentials, nuclear quadrupole coupling constants, etc. are concerned.

1. Introduction

Recently, we have developed a semitheoretical model¹ for estimating the bonding parameters (β_{AB}) needed for performing CNDO-MO calculations. In the present paper we discuss some of the results of a preliminary application of this model. In the reported calculations, we have adopted the following schemes for obtaining our CNDO-MO parameters.

(a) One-center (A) electron repulsion integrals (g_{AA}^0) are calculated by adopting Saturno's² model; i.e., with $(r_{12})^{-1} = (r_1 + r_2)^{-1}$.

(b) Two-center (A, B) electron repulsion integrals (g_{AB}^0) are calculated by using the Mataga³ approximation; i.e., with $r_{12}^{-1} = (r_1 + r_2 + R)^{-1}$.

(c) Bond parameters $\beta_{AB}(I)$ suitable for use with a nonorthogonal nS, nP basis are calculated by using eq 1,

$$\beta_{AB}(I) = -(I_{av}^A + I_{av}^B)/2 - [(Z_A + Z_B)/2]K'g'_{AB} + (Z_A + Z_B - 2)g_{AB}^0 \quad (1)$$

while bond parameters $\beta_{AB}(II)$ suitable for use with an orthogonalized basis are calculated by eq 2. K' and K''

$$\beta_{AB}(II) = -K''[(Z_A + Z_B)/2]g'_{AB} + (Z_A + Z_B - 2)g_{AB}^0 \quad (2)$$

are adjustable parameters of the theory. We have shown that $K' = 0.75$ reproduces, on the average, Pople's β_{AB}^0 parameters (within ± 4 eV); K'' has been taken to be equal

to unity in all the applications reported. There is a further possibility of varying K' and K'' with the specific nature of the bond (σ, π , etc.). We, however, have used a single value of K' and K'' for all bonds in the present work. The possibility of using a variable β_{AB} CNDO-MO method as discussed in part 1 of this series of papers has also been tested on a few heterodiatomics and compared with fixed β_{AB} CNDO-MO results.

The results of calculations are reported for two series of compounds: (i) the diatomic halogens and interhalogens ($F_2, Cl_2, Br_2, I_2, ICl, IBr, BrCl, BrF, ClF$); (ii) a few small hydride molecules ($NH_3, PH_3, AsH_3, NH_4^+, PH_4^+, CH_4, SiH_4, GeH_4$).

2. Details of the Approximations Used

(A) *Halogen and Interhalogens.* Calculations were performed in two sets (I and II) each having a few distinctive features.

Set I: (a) CNDO/2 parameterization was adopted for the diagonal terms of the Fock matrix. (b) STO's with Clementi and Raimondi's⁴ optimized exponents were used. Since $\xi_{ns} \neq \xi_{np}$, we used $\xi_{av} = 1/4(\xi_{ns} + 3\xi_{np})$ for the calculations of the g_{AA}^0 and overlap integrals. (c) For basis orbitals with $n \geq 3$, the g_{AA}^0 integrals were arbitrarily increased by +1 eV, as Saturno's model seemed to underestimate these integrals for orbitals with high n values. It seems that the angular correlation forces are diminished in these orbitals. (d) For the off-diagonal core matrix elements, we used

TABLE I: Results of Calculations Performed Using the Approximations of Set I^a

Molecule A ⁺ -B ⁻	Charge on A	Charge on B	1st IP, eV	2nd IP, eV	3rd IP, eV	NQCC of A in AB, MHz		NQCC of B in AB, MHz
F-F	0	0	15.87 (π_g) (15.63) ^c (π_g)	16.32 (σ_g) 17.35 (σ_g)	18.26 (π_u) (18.46) (π_u)			
Cl-Cl	0	0	11.08 (π_g) (11.50) (π_g)	13.93 (σ_g) (14.11) (π_u)	14.05 (π_u) (15.94) (σ_g)	-105.95	(-109.74) ^d	-105.95
Br-Br	0	0	10.22 (π_g) (10.71) (π_g)	12.53 (π_u) (12.52) (π_u)	12.74 (σ_g) (14.44) (σ_g)	751.28	(769.75) ^e	751.28
I-I	0	0	9.38 (π_g) (9.65) (π_g)	11.39 (π_u) (11.28) (π_u)	11.65 (σ_g) (12.79) (σ_g)	-2285.5	(-2292.71) ^f	-2285.5
Cl-F ^b	+0.042	-0.042	12.13 (π_g)	14.99 (σ_g)	17.21 (π_u)	-105.85		
Br-F	+0.092	-0.092	11.39 (π_g)	13.81 (σ_g)	16.34 (π_u)	795.60		
Br-Cl	+0.037	-0.037	11.02 (π_g)	12.33 (σ_g)	12.87 (π_u)	771.68		-102.10
I-Cl	+0.072	-0.072	9.97 (π_g)	12.65 (σ_g)	12.84 (π_u)	-2361.50		-82.50
I-Br	+0.047	-0.047	9.81 (π_g)	11.92 (π_u)	12.01 (σ_g)	-2334.40		718.6

^a Bracketed quantities represent experimental values; see also Table II. ^b Available experimental quantities for the interhalogens are reported in Table II. ^c Reference 7. ^d Reference 8. ^e Reference 9. ^f Reference 10.

TABLE II: Results of Calculations Performed Using the Approximations of Set II^a

Molecular	Charge	Charge	1st IP, eV	2nd IP, eV	3rd IP, eV	NQCC of A in AB, MHz		NQCC of B in AB, MHz
Cl-F	+0.16	-0.16	13.14 (π_g) (12.7) ^b (?)	18.67 (σ_g)	19.12 (π_u)	-122.68	(-146.0) ^d	
Br-F	+0.23	-0.23	12.14 (π_g) (11.90) ^b (?)	17.05 (σ_g)	17.77 (π_u)	924.86	(1089) ^e	
Br-Cl	+0.08	-0.08	11.10 (π_g) (11.10) ^b (?)	14.75 (π_u)	15.97 (σ_g)	815.56	(876.8) ^f	-94.91 (-103.6) ^f
I-Cl	+0.11	-0.11	10.26 (π_g) (10.56) (π_g)	13.84 (π_u) (12.16) (π_u)	13.94 (σ_g)	-2449.98	(-2930) ^g	-90.83 (-82.5) ^g
I-Br	+0.06	-0.06	9.89 (π_g) (10.23) ^h (π_g)	12.89 (π_u) (11.64) (π_u)	14.17 (σ_g)	-2345.66	(-2731) ^h	693.78 (722) ^h

^a Bracketed quantities are the experimental values. ^b Reference 11. ^c Reference 12. ^d Reference 13. ^e Reference 14. ^f Reference 15. ^g Reference 16. ^h Reference 17.

$$H_{ij}^{AB} = \beta_{AB(II)} S_{ij}^{AB} \quad (3)$$

with $\beta_{AB(II)}$ given by eq 2.

Set II: (a) CNDO/1 parameterization was used in the diagonal Fock matrix elements. (b) Instead of ξ_{av} , ξ_{ns} exponents were used. (c) Saturno's values of the g_{AA}^{AB} integrals were used without any readjustment. (d) $H_{ij}^{AB} = \beta_{AB(I)} S_{ij}^{AB}$ was used. (e) Only five diatomic interhalogens were studied.

B. Hydrides. Calculations were performed in two sets of approximations (III and IV).

Set III: The techniques adopted are identical with those adopted in set I except that CNDO/1 formulation was used in the diagonal terms.

Set IV was identical with set III except that $\beta_{AB(I)}$ parameters were used in the place of $\beta_{AB(II)}$.

3. Discussion of Results

(A) Halogens and Interhalogens. In the Tables I and II, we have reported the computed net atomic charges, the ionization potentials (IP's) (in a frozen orbital approximation), and the nuclear quadrupole coupling constants (NQCC's). The NQCC's were calculated from the CNDO density matrices by using Sichel and Whitehead's⁵ model. The first ionization potentials (IP1) were satisfactorily predicted in most cases. The IP's predicted by set I calculations are somewhat lower and those by set II higher than the experimental counterparts. Both the sets of calculations, however, predict correctly the experimentally noted trends in the variations of the NQCC of an atom (X) with changes in the chemical environments (e.g., from X-X to X-Y or from X-Y to X-Z). It seems that a differential treatment of the σ and π types of bonding interactions ($H_{ij}^{AB}(\sigma)$ or $H_{ij}^{AB}(\pi)$) and of the $\langle \chi_\sigma^A | V_B^0(r) | \chi_\sigma^A \rangle$, $\langle \chi_\pi^A |$

TABLE III: Results of Modified CNDO-MO Calculation on Some Hydride Molecule (Sets III and IV)

Molecule	Set III		Set IV	
	IP1, eV	IP2, eV	IP1, eV	IP2, eV
NH ₃	11.56 (a ₁) (10.88) ^a (a ₁)	14.45 (e) (16.4) ^a (e)	12.06 (a ₁)	17.96 (e)
PH ₃	10.99 (a ₁) (10.59) ^a (a ₁)	12.66 (e) (13.5) ^b (e)	11.55 (a ₁)	15.81 (e)
AsH ₃	10.55 (a ₁) (10.58) ^c (a ₁)	12.10 (a ₁) (12.90) ^c (e)	11.15 (a ₁)	15.11 (e)
CH ₄	12.81 (t ₂) (13.00) ^d	25.37 (a ₁) (24.2) ^d	16.79 (t ₂)	36.49 (a ₁)
SiH ₄	11.39 (t ₂) (12.20) ^e	19.00 (a ₁)	15.30 (t ₂)	25.64 (a ₁)
GeH ₄	11.36 (t ₂) (12.30) ^e	19.35 (a ₁)	15.50 (t ₂)	25.95 (a ₁)

Inversion Barriers		
NH ₃ (C _{3v} → D _{3h})	14.9 kcal/mol (5.75 kcal/mol) ^f	17.9 kcal/mol
PH ₃ (C _{3v} → D _{3h})	19.1 kcal/mol (37 cal/mol) ^g	22.8 kcal/mol

Protonation Energies		
NH ₃ → NH ₄ ⁺ (C _{3v}) (T _d)	282.02 kcal/mol (201 kcal/mol) ^h	515.00 kcal/mol
PH ₃ → PH ₄ ⁺ (C _{3v}) (T _d)	252.30 kcal/mol (187 kcal/mol) ^h	463.30 kcal/mol

^a Reference 18. ^b Reference 19. ^c Reference 20. ^d Reference 21. ^e Reference 22. ^f Reference 23. ^g Reference 24. ^h Reference 25.

$V_B^0(r) | \chi_\pi^A \rangle$ etc. is necessary to effect further improvement in the actual values of the computed NQCC's. Inclusion of *nd* orbitals may also be important.

(B) Hydrides. In Table III, the computed IP's (first and second) are compared with the available experimental

TABLE IV: Comparison of Fixed β - and Variable β -CNDO-MO Results on Some Model Systems

Molecule AB	Variable β -CNDO-MO results			Fixed β -CNDO-MO results		
	Total electronic energy at conveyance, eV	1st IP, eV	2nd IP, eV	Total electronic energy, eV	1st IP, eV	2nd IP, eV
Br-F	-999.297	11.6211	15.1673	-999.365	11.6251	15.1707
I-Cl	-761.464	10.1524	14.4912	-761.486	10.1504	14.4934
I-Br	-659.366	10.0276	12.9486	-659.373	10.0268	12.9495

quantities. It is seen that calculations of set III generally lead to ionization potentials which are smaller than the experimental values. This effect is more prominent in the second ionization potentials. Set IV, however, gives ionization potentials that are somewhat larger than the experimental quantities. However at the CNDO level of accuracy the agreement seems to be fair.

We have also reported computed inversion barriers ($C_{3v} \rightarrow D_{3h}$) of NH_3 and PH_3 and their protonation energies in Table II. It is seen that the computed values of the protonation energies improve significantly on incorporating a two-center nonorthogonality correction in the off-diagonal core matrix elements in our model. The inversion barriers predicted are rather unsatisfactory and this is known to be a weak feature of the CNDO-MO theory. We are at present studying the effects of varying orbital exponents and two-electron (one- and two-center) integrals on the computed barrier heights. The results obtained so far indicates a strong dependence of the computed barrier heights on these factors.

(C) *Comparison of Variable and Fixed β_{AB} CNDO-MO Results.* We pointed out in paper 1 that β_{AB} parameters might vary in course of iterations. However such variations were shown to be small, as expected. In this paper, we have compared the electronic energies and ionization potentials (frozen orbital approximation) of BrF, ICl, and IBr, computed by these two methods. One-center electron repulsion integrals were calculated by Saturno's method for all cases reported in this section. The valence shell ionization energies needed for the estimation of the diagonal core matrix elements were slightly different from those used in set I and II (e.g., $I_{2s}^F = 38.01$ eV and $I_{2p}^F = 17.6$ eV) ξ_{av} was used. In short, the same types of approximations were adopted in both methods for estimating all the parameters except β_{AB} . These results are reported in Table IV. They indicate that the electronic energies are slightly lower in the fixed β_{AB} -CNDO approximation while the computed ionization potentials are highly insensitive to the type of approximation used. This gives further support for using the fixed β_{AB} approximations introduced by Pople.

Conclusion

The scheme of parametrization studied in this paper seems to be a fairly good one for obtaining molecular properties such as IP's, NQCC's, protonation energies, etc.

The performance of this method in the computation of bond lengths, bond angles, bond energies, etc. is being studied at present with special emphasis on transition metal complexes. Obviously the extension of this scheme to transition metal complexes require some modifications. The details of these studies will be reported shortly.

Acknowledgment. S.P.B. wishes to acknowledge his sincere thanks to the University of Calcutta for the award of a Research Fellowship (UGC) and both the authors express their indebtedness to the University Computer Centre for providing computation facilities.

References and Notes

- (1) S. P. Bhattacharyya and M. Chowdhury, *J. Phys. Chem.*, preceding article in this issue.
- (2) A. F. Saturno, *Theor. Chim. Acta*, **11**, 365 (1968).
- (3) N. Mataga and K. Nishimoto, *Z. Phys. Chem.*, **12**, 335 (1957).
- (4) (a) E. Clementi and D. L. Raimondi, *J. Chem. Phys.*, **38**, 2686 (1963); (b) E. Clementi, D. L. Raimondi, and W. P. Reinhardt, *ibid.*, **47**, 1300 (1967).
- (5) J. M. Sichel and M. A. Whitehead, *Theor. Chim. Acta*, **11**, 263 (1968).
- (6) J. M. Sichel and M. A. Whitehead, *Theor. Chim. Acta*, **11**, 220 (1968).
- (7) D. C. Frost, C. A. McDowell, and D. A. Vroom, *J. Chem. Phys.*, **46**, 4255 (1967).
- (8) R. Livingston, *J. Chem. Phys.*, **19**, 1434 (1951).
- (9) H. G. Dehmelt, *J. Chem. Phys.*, **19**, 1434 (1951).
- (10) See the NQCC's referred to by Sichel and Whitehead in ref 5.
- (11) A. P. Irsa and L. Friedman, *J. Inorg. Nucl. Chem.*, **6**, 77 (1958).
- (12) D. C. Frost and C. A. McDowell, *Can. J. Chem.*, **38**, 407 (1960).
- (13) D. A. Gilbert, H. Roberts, and P. A. Garishold, *Phys. Rev.*, **76**, 1723 (1944); **77**, 742 (1950).
- (14) D. F. Smith, M. Tidwell, and D. V. P. Williams, *Phys. Rev.*, **77**, 420 (1950).
- (15) D. F. Smith, M. Tidwell, and D. V. P. Williams, *Phys. Rev.*, **79**, 1007 (1950).
- (16) C. H. Towness, F. R. Merritt, and B. D. Wright, *Phys. Rev.*, **73**, 1334 (1948).
- (17) T. S. Jaseja, *J. Mol. Spectrosc.*, **5**, 445 (1960).
- (18) R. Moccia, *J. Chem. Phys.*, **40**, 2176, 2186 (1964). The first ionization potential of NH_3 as given by A. Joubury and Turner (*J. Chem. Soc.*, 4434 (1964)) is 10.88 eV.
- (19) The value reported is an average of three independent determination by UV photoelectron spectroscopy. (a) G. R. Branton, D. C. Frost, C. A. McDowell, and I. A. Stenhouse, *Chem. Phys. Lett.*, **5**, 1 (1970); (b) A. W. Potts and W. C. Price, *Proc. R. Soc. London, Ser. A*, **326**, 181 (1972); (c) J. P. Maier and D. W. Turner, *J. Chem. Soc., Faraday Trans. 2*, **68**, 711 (1972).
- (20) W. R. Cullers and D. C. Frost, *Can. J. Chem.*, **40**, 390 (1962).
- (21) M. Krauss, *J. Chem. Phys.*, **38**, 54 (1963).
- (22) H. Neuert and H. Clasen, *Z. Naturforsch. A*, **7**, 410 (1952).
- (23) J. D. Swaken and J. A. Ebers, *J. Chem. Phys.*, **38**, 1914 (1962).
- (24) J. M. Lehn and Munsch, *Chem. Commun.*, 1327 (1969). This is an ab-initio result and not an experimental result.
- (25) C. V. Hodges and J. L. Beaucham, *J. Inorg. Chem.*, **14**, 2887 (1975), see Table III of this reference.

COMMUNICATIONS TO THE EDITOR

The Photoperoxidation of Unsaturated Organic Molecules. 17. The Thermal Regeneration of Acceptor

Publication costs assisted by the University of South Florida

Sir: Following previous reports¹ to the effect that endoperoxides of certain substituted polyacenes thermally regenerate molecular oxygen and the parent hydrocarbon, Wasserman and co-workers have demonstrated that in the case of 9,10-diphenylanthracene peroxide,² rubrene peroxide,² and 1,4,5-trimethylnaphthalene peroxide,³ the thermally generated oxygen is in the singlet ($O_2^1\Delta_g$) state.

Insofar as the thermal regeneration process 2 is the reverse of $O_2^1\Delta_g$ acceptor addition (process 1) interest



attaches to the activation energy E_2^\ddagger given by eq I where

$$E_2^\ddagger = E_1^\ddagger + \Delta H_f^\circ(M) + \Delta H_f^\circ(O_2^1\Delta_g) - \Delta H_f^\circ(MO_2) \quad (I)$$

ΔH_f° refers to the standard formation enthalpy of the parenthesized species given in Table I for 9,10-diphenylanthracene (DPA) and rubrene. These provide lower limits of $E_2^\ddagger \geq E_1^\ddagger + 40$ kcal/mol for the peroxides of both compounds which, in the case of DPA, exceed the value of 28.6 ± 0.2 kcal/mol estimated² for $O_2^1\Delta_g$ regeneration. In view of this discrepancy and the apparent lack of data for rubrene peroxide we have investigated the thermal regeneration of parent hydrocarbon from DPA and rubrene peroxides in several solvents.

Solutions of the peroxides were prepared by the self-sensitized photoperoxidation of the hydrocarbon at known concentration (typically 10^{-4} M) by selective excitation in the long wave absorption band. These were placed in a cell designed to permit withdrawal of 2-mL aliquots while minimizing solvent evaporation losses and the cell placed in a constant temperature bath (Messgerate-Werk Landa) preheated to the appropriate temperature. The aliquots withdrawn at time intervals of a few minutes were cooled by dilution and refrigeration and thermal regeneration of the parent hydrocarbon followed spectrophotometrically. In all cases regeneration was first order and the rate constants were estimated from eq II where OD_0 and OD_∞

$$\ln \left\{ \frac{OD_\infty - OD_0}{OD_\infty - OD_t} \right\} = k_2 t \quad (II)$$

denote initial and final optical densities monitored in the long wave acceptor absorption band. The percentage regeneration was estimated from OD_∞ and the optical density of the original acceptor solution at the same wave length prior to photoperoxidation.

Table II summarizes the temperature dependance of rate constants k_2 obtained in terms of Arrhenius parameters A_2 and E_2^\ddagger . As shown in Figure 1 the data for DPA in toluene and decalin are in good agreement with those reported by Wasserman et al.² from $O_2^1\Delta_g$ regeneration in toluene, benzene, and methylene chloride. The percentage regeneration of DPA and of rubrene also correspond well

TABLE I: Standard Formation Enthalpies

	ΔH_f° , kcal/mol
9,10-Diphenylanthracene	73.8 ± 0.8^a
9,10-Diphenylanthracene peroxide	49.0 ± 5.0^b
Rubrene	148.0 ± 5.0^c
Rubrene peroxide	123.0 ± 5.0^c

^a A. Magnus and F. Becker, *Z. Phys. Chem.*, **196**, 378 (1951). ^b G. R. Somayajulu and B. J. Zwolinski, personal communication. ^c J. D. Cox and G. Pilcher, "Thermochemistry of Organic and Organometallic Compounds", Academic Press, New York, N.Y., 1970, p 250.

TABLE II: Rate Data for Thermal Decomposition of Peroxides

Peroxide	Solvent	E_2^\ddagger , kcal/mol	log A	% regeneration of	
				Acceptor	$O_2^1\Delta_g$
Rubrene	Decalin	32.6 ± 1.2	14.1 ± 0.6	30	5
	<i>o</i> -C ₆ H ₄ Cl ₂	33.0 ± 1.2	14.1 ± 0.6	30	5
	Benzene ^a				36
DPA	Decalin	30.6 ± 1.1	13.9 ± 0.7	95	5
	Toluene	31.1 ± 3.0	14.3 ± 1.4	95	5
	Toluene ^a	27.8 ± 0.2	12.1 ± 0.1		99

^a Reference 2.

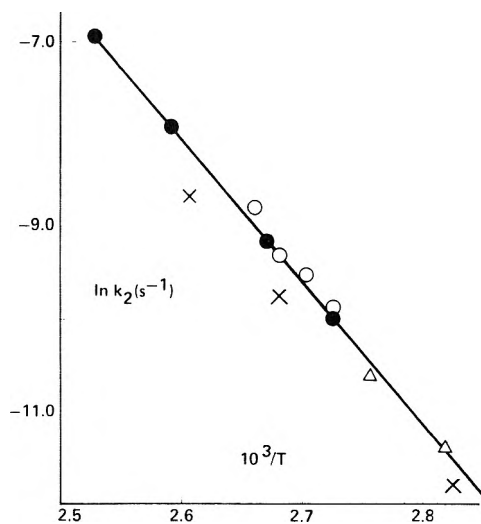


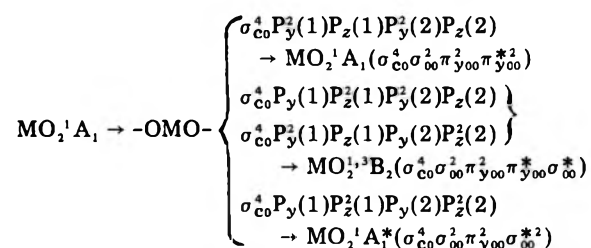
Figure 1. Temperature dependence of rate constant k_2 (s^{-1}) for thermal dissociation of 9,10-diphenylanthracene in decalin (●), toluene (○, this work and X, ref 2), benzene (▲, ref 2), and methylene chloride (△, ref 2). Data line represents least-squares fit for data in decalin.

with the percentage regeneration of $O_2^1\Delta_g$ from the corresponding peroxides.

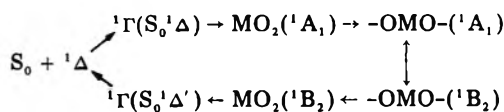
The data indicate that either the tabulated heats of formation are attended by greater limits of uncertainty than those quoted,⁴ that the heats of solution of the hydrocarbon exceed those of the corresponding peroxide by some 10 kcal/mol, or that thermal regeneration of acceptor and $O_2^1\Delta_g$ is not the reverse of $O_2^1\Delta_g$ acceptor addition.

In view of the findings that (a) the activation energies for $O_2^1\Delta_g$ regeneration (Table II) are close to those reported for primary peroxide bond fission in anthracene peroxide⁶ (29.8 kcal/mol) and ascaridole⁷ (31.4 kcal/mol), (b) the thermal regeneration of DPA from the endoperoxide is reduced to 35% in alcoholic solvents, and (c) the 30% regeneration of rubrene from rubrene peroxide is essen-

Scheme A. Orbital Correlations for Homolytic Fission and Re-Formation of the Peroxide Bond



Scheme B. Possible Peroxide Formation-Dissociation Sequence



tially temperature independent indicating that different reaction channels follow a single primary event, it is of interest to examine the possibility that $\text{O}_2^1\Delta_g$ regeneration by aryl-substituted endoperoxides also involves primary $-\text{O}-\text{O}-$ bond fission.

If symmetry is conserved during the homolytic peroxide bond cleavage normal to the yz plane the tetrapotic (σ , π) process⁸ forms one of the four diradical pairs shown in Scheme A. The $\text{P}_y(1)$ and $\text{P}_z(1)$ atomic orbitals of oxygen atom (1) (and corresponding orbitals of atom (2)) are distinguishable only by their electron occupancies since they are rotationally equivalent and recombination in the four diradical pair states produces the four lowest electronic states of the peroxide ${}^1\text{A}_1(\text{S}_0^1\Delta)$, ${}^3\text{B}_2(\text{S}_0^3\Sigma)$, ${}^1\text{B}_2(\text{S}_0^1\Delta')$, and ${}^1\text{A}_1^*(\text{S}_0^1\Sigma)$ which correlate with dissociation products shown parenthetically. Of these states, the formation of ${}^3\text{B}_2$ is eliminated if the diradical pair remains spin correlated, and ${}^1\text{A}_1^*$ is the least accessible energetically. Since the re-formation of ${}^1\text{A}_1$ ground state restores the 40 kcal/mol energy barrier calculated for dissociation, the thermal regeneration of $\text{O}_2^1\Delta_g$ via primary peroxide bond fission must utilize the remaining channel through the peroxide ${}^1\text{B}_2$ state which should lie at least 10 kcal/mol above the diradical pair state. The resulting peroxide formation-dissociation sequence shown in Scheme B does not violate the principle of microscopic reversibility since the complex states⁹ ${}^1\Gamma(\text{S}_0^1\Delta)$ and ${}^1\Gamma(\text{S}_0^1\Delta')$ have different

transformation properties. However the description of $\text{O}_2^1\Delta_g$ regeneration in terms of sequential barrier crossings of 30 and 10 kcal/mol, respectively, will provide an overall activation energy of 30 kcal/mol only if the former process is rate determining and irreversible. Since it is not immediately obvious why the diradical pair state should re-form the peroxide ${}^1\text{B}_2$ state endothermically rather than its ${}^1\text{A}_1$ ground state, any further discussion should await experimental confirmation of the thermodynamic data from which the reaction energy profile is constructed.

It is of interest to note, however, that the presence of aryl substituents at the site of O_2 attachment, which appear to be necessary for $\text{O}_2^1\Delta_g$ regeneration, would stabilize the linked triaryl-methoxy groups in the diradical intermediate with respect to exoxidation or solvent H-atom abstraction which account for the thermolysis products of alkyl- and unsubstituted endoperoxides of anthracene and tetracene.¹⁰

Note Added in Proof: Drs. H. H. Wasserman and T-Y. Ching (private communication) find that $E_2^* = 30.8 \pm 0.8$ kcal/mol and $\log A_2 = 14$ for the regeneration of DPA from its peroxide in benzene, in excellent agreement with the data tabulated. We are grateful to these authors for permission to quote these data.

References and Notes

- (1) E.g., K. Gollnick, *Adv. Photochem.*, **6**, 1 (1968).
- (2) H. H. Wasserman, J. R. Scheffer, and J. L. Copper, *J. Am. Chem. Soc.*, **94**, 4991 (1972).
- (3) H. H. Wasserman and D. L. Larsen, *J. Chem. Soc., Chem. Commun.*, 253 (1972).
- (4) In this connection it is noted that $\Delta H_f^\circ(\text{DPAO}_2)$ is estimated by the method of triatomic additivity⁵ although thermochemical data for rubrene are based on experimental heats of combustion.
- (5) G. R. Somayajulu and B. J. Zwolinski, personal communication.
- (6) J. W. Breitenbach and A. Kastell, *Monatsh. Chem.*, **84**, 645 (1953).
- (7) J. Boche and O. Rungquist, *J. Org. Chem.*, **33**, 4285 (1968).
- (8) W. G. Dauben, L. Salem, and N. J. Turro, *Acc. Chem. Res.*, **8**, 41 (1975).
- (9) D. R. Kearns, *J. Am. Chem. Soc.*, **91**, 6554 (1969).
- (10) K. Gollnick and G. O. Schenck, "1,4-Cycloaddition Reactions", J. Hamer, Ed., Academic Press, New York, N.Y., 1967, p 255.

Department of Chemistry
University of South Florida
Tampa, Florida 33620

B. Stevens*
R. D. Small, Jr.

Received May 2, 1977

Journal of Chemical and Engineering Data

JULY 1977, Vol. 22, No. 3

TABLE OF CONTENTS

The Vapor Pressure of Tetrakis(2,2,6,6-tetramethylheptane-3,5-dionato)uranium Ray G. Bedford* and Ethan B. Huss	239
The P-V-T Behavior of Acetone in the Dense Gaseous Region Ralph M. Keller, Jr., and Leonard I. Stiel*	241
Dissociation Constants of <i>p</i> -Amino- and <i>p</i> -Guanidino-Substituted Phenylalanines Christopher W. Owens,* Els ten-Krooden, and Andrew K. Grzybowski	244
Isobaric Vapor-Liquid Equilibrium Data for the System <i>n</i> -Hexane-2-Propanol John M. Rotter and Harold N. Knickle*	246
Thermodynamic Properties of Ternary Mixtures. 2. The Excess Volumes of Mixing of Ternary Mixtures of Cyclohexane, Aromatics, and Halomethanes R. P. Rastogi,* Jagan Nath, and Shiva Saran Das	249
Vapor-Liquid Equilibria in the Ternary Systems Water-Formic Acid-Acetic Acid and Water-Acetic Acid-Propionic Acid Jalme Wisniak* and Abraham Tamir	253
A Crude Oil-Natural Gas System Vapor-Liquid Equilibrium Ratios (Data at 250 °F and System Containing 20% C ₇₊) C. Floyd Wiesepepe, H. T. Kennedy, and Paul B. Crawford*	260
Refractive Indices and Molar Refractions of Liquid Mixtures Major S. Dhillon* and Harinder S. Chugh	262
Vapor-Liquid Equilibria of the Binary and Ternary Systems Containing <i>n</i> -Hexane (1)-Benzene (2)- <i>tert</i> -Butyl Alcohol (3) at 760 mmHg Pressure S. Govindaswamy, AN. Andiappan,* and SM. Lakshmanan	264
A Fluorescence Method for the Measurement of the Partition Coefficients of Naphthalene, 1-Methylnaphthalene, and 1-Ethylnaphthalene in Water Frederick P. Schwarz* and Stanley P. Wasik	270
Determination of Temperature Dependence of Solubilities of Polycyclic Aromatic Hydrocarbons in Aqueous Solutions by a Fluorescence Method Frederick P. Schwarz	273
Solubilities of Gases in Aqueous Solutions of Amine Eizo Sada,* Hidehiro Kumazawa, and M. A. Butt	277
Viscosity of Nitrobenzene- <i>n</i> -Pentane and Nitrobenzene- <i>n</i> -Heptane Systems Eizo Sada,* Katsuroku Takahashi, and Mitsuhiro Hamada	279
The Equilibrium Phase Properties of the Nitrogen-Isopentane System Thamra R. Krishnan, Harish Kalra, and Donald B. Robinson*	282
Vapor-Liquid Equilibrium of Petroleum Fractions Single Fraction and Binary Systems Hamed H. Hamza* and Paul G. Mikolaj	285
Thermodynamic Properties of Alcohol-Amine Mixtures: Excess Enthalpies of Methanol-Triethylamine and Ethanol-Triethylamine Abhai Chand and David V. Fenby*	289
Excess Enthalpies and Volumes for Mixtures of <i>o</i> -Dichlorobenzene with Some Aromatic Hydrocarbons at 298.15 K Reiji Tanaka and George C. Benson*	291
Vapor-Liquid Equilibria of the Ternary System Methyl Borate-Methyl Alcohol-Carbon Tetrachloride Larry E. Schindler, Charles A. Plank,* Phoebus M. Christopher, and Walden L. S. Laukhuf	294
Enthalpies of Solution of Selected Electrolytes in Sulfolane and in Acetonitrile Young-Sang Choi and Cecil M. Criss*	297

The Diffusion Coefficient of Ferricyanide Ions in Aqueous Potassium Chloride Solutions with and without Polyethylene Oxide Addition	Bruin Roffel* and Jan J. van de Graaf	300
Experimental Measurements of Phase Equilibrium Properties for Systems Containing <i>n</i> -Heptane, Benzene, <i>N</i> -Methylpyrrolidone, and Monoethanolamine. Representation by the NRTL Equation	Jean-François Fabries, Jean-Louis Gustin, and Henri Renon*	303
Ionic Equilibria in Mixed Solvents: Formation of Calcium Lactate	Buddhadev Sen* and James J. Gibbons	309
Elevation of the Boiling Point of Water by Salts and Saturation: Data and Correlation	David Meranda and William F. Furter*	315
Solubility of Hydrogen Sulfide and Carbon Dioxide in a Sulfinol Solution	Ezra E. Isaacs, Frederick D. Otto, and Alan E. Mather*	317
Vapor-Liquid Equilibria at 25 °C for Nine Alcohol-Hydrocarbon Binary Systems	Shuen-Cheng Hwang and Robert L. Robinson, Jr.*	319
Solubility of Nitrogen, Argon, Methane, and Ethane in Ethylene Oxide	James D. Olson	326
Densities of the Molten Salt System Cesium Bromide-Cuprous Bromide	Gert J. Lamprecht	329
Vapor-Liquid Equilibria of the Cyclohexane-Cyclohexanone System at 323.15 and 348.15 K	Tomas Boublik and Benjamin C.-Y. Lu*	331
Some Physicochemical Properties of the Binary Mixtures Heptane-Propanone and Heptane-Ethyl Acetate	F. Vanden Kerchove* and M. De Vlijder	333
Isopiestic Determination of the Activity Coefficients of Some Aqueous Rare Earth Electrolyte Solutions at 25 °C. 3. The Rare Earth Nitrates	Joseph A. Rard, Loren E. Shlers, David J. Heiser, and Frank H. Spedding*	337
Activity Coefficients and Henry's Constants by the Pseudocritical Method	Joseph Joffe	348

NEW COMPOUND SECTION

Synthesis of Some New Exocyclic Olefins via Phosponium Ylides	Ram S. Tewari,* Komal C. Gupta, and Purshottam S. Kendurkar	351
Thiazo Compounds. Derivatives of 4,5-Dihydro-7,8-dimethoxybenzothiazepin-3-one 1,1-Dioxides	Panayotis Catsoulacos* and Charalabos Camoutsis	353
Preparation and Spectral Properties of Benzylidene Diacetates	Fillmore Freeman* and Elaine Marie Karchefski	355
Synthesis of Potential Specific Inhibitors of Certain Amino Acid Decarboxylases	Zafar H. Isralli* and Edward E. Smissman	357
Chemical Shift Nonequivalence of Prochiral Groups in the ¹ H Nuclear Magnetic Resonance Spectra of Some 3-Alkyl Derivatives of Phthalic Anhydride and Tetrachlorophthalic Anhydride	Norman F. Bray,* Reuben L. Baumgarten,* and Edward Edelson	359
Synthesis and Properties of Substituted α -Phenylcinnamionitrilesulfonamides	James T. Stewart,* Richard D. Dowling, and Otis J. Bouwsma	362
Fluorometric and Mass Spectral Data for 2-(9-Acridinyl)ethyl <i>N</i> -Substituted Carbamates and Their 10- <i>N</i> -Oxides	James T. Stewart,* Richard E. Gammans, and Otis J. Bouwsma	364

There is no supplementary material for this issue.

* In papers with more than one author, the asterisk indicates the name of the author to whom inquiries about the paper should be addressed.

Special Centennial Tapes

4 Historic Symposia! 24 Speakers! Custom Packaging! Special Prices!

Milestones in Physical Chemistry

8 Speakers — 315 Figures
Length: 5 Cassettes — 8 Hours
PRICE: \$45 (postpaid)

The Speakers:

- G. T. Seaborg — 40 Years of Transuranium Elements
- D. Hodgkin — Structure of Molecules in Crystals
- G. Porter — Chemistry in Microtime
- P. J. Flory — Thermodynamics of Polymer Solutions
- W. O. Baker — Chemistry of the Solid State
- L. C. Pauling — Perspectives in Chemical Bonding & Structure
- H. Eyring — Reaction Rate Theory
- J. H. Van Vleck — Evolution of Theoretical Chemistry in America

Structure and Quantum Chemistry + Evolution of Magnetic Resonance

8 Speakers — 210 Figures
Length: 4 Cassettes — 6 Hours
PRICE: \$35 (postpaid)

The Speakers:

- J. A. Pople — Orbital Studies of Molecular Structure & Stability
- H. G. Drickamer — Pressure & Electronic Structure
- F. H. Stillinger — Quantum Chemistry & Eccentric Behavior of Liquid Water
- R. Zwanzig — Molecular Hydrodynamics
- H. S. Gutowsky — 30 Years of Relaxation
- J. S. Waugh — Alchemy of Nuclear Spins
- H. M. McConnell — Spin Labels
- F. A. Bovey — NMR of Macromolecules

Evolution of Kinetics

8 Speakers — 140 Figures
Length: 4 Cassettes — 6 Hours
PRICE: \$35 (postpaid)

The Speakers:

- B. S. Rabinovitch — Perspectives on Vibration Energy Relaxation in Unimolecular Reactions
- W. A. Noyes, Jr. — Photochemical Kinetics
- R. A. Marcus — Trends in Theoretical Chemical Kinetics
- K. F. Freed — Radiationless Processes in Polyatomic Molecules
- G. B. Kistiakowski — Early Years of Gas Phase Chemical Kinetics
- J. C. Polanyi — Recent Studies of Infrared Chemiluminescence & Fluorescence
- S. Claesson — Diffusion Rates & Chemical Reaction Kinetics
- J. Jortner — Intramolecular Dynamics in Excited Molecular States

— SPECIAL PRICE —

BUY ALL THREE SETS —
ONLY \$85 (postpaid)

SAVE \$30!

ORDER FROM:

American Chemical Society
1155 Sixteenth St., N.W.
Washington, D.C. 20036
ATTN: DEPT. AP

Name _____

Address _____

City _____

State _____

Zip _____

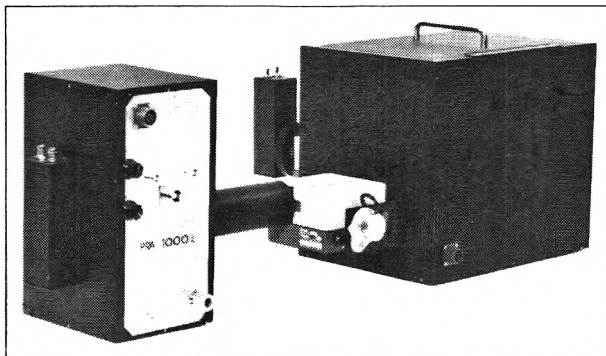
(allow 4 to 6 weeks for delivery)

New Pulsed Nanosecond Fluorometer Systems

The PULSED NANOSECOND FLUOROMETER SYSTEMS are ideal for use in single photon counting, fluorescence studies, trace analysis, fluorescent labelling and detection and in any other applications where low level luminescence dictates high sensitivity and selectivity of emission measurements

Excellent signal to noise ratio, low level of stray light and efficient optics permits examination of substances with low fluorescence quantum yield

The measurements are not restricted to exponential decays and time resolution is not limited by the rise time of the PMT but by a statistical time dispersion of about 0.3ns. Lifetimes as short as .5ns can be readily detected



The SYSTEMS are available with various electronics packages, PMT's, monochromator, sample chamber, excitation source and power supplies. The modular construction lends itself to numerous options which can be added as needed. Computer software program for deconvolution is also available.

PRA offers complete service with these systems, installation, on-site testing and training in use of the instrument. PRA, with its expertise gained through five years of research in designing these systems, will be happy to consult with you as to your requirements.

These SYSTEMS can be seen at the ACS Exhibit in Chicago from August 29-September 2 at Booth 107.

For further information, please contact:

PRA Photochemical
Research
Associates
Inc.

(519) 679-6181

University of Western Ontario
Chemistry Building
London, Ontario, Canada N6A 5B7
Telex 064 7597

REPRINTS REPRINTS REPRINTS

to aid you in
your work.

1973
(ChemTech)

Visual Aids for Technical Presentations

Garret R. Hyde \$2.00

1973
(Chemical Reviews)

Intramolecular Hydrogen Transfer in Mass Spectra. I. Rearrangements in Aliphatic Hydrocarbons and Aromatic Compounds

Joan T. Bursey, Maurice M. Bursey, David G. I. Kingston \$5.00

1973
(Chemical Reviews)

Lanthanide Shift Reagents for Nuclear Magnetic Resonance Spectroscopy

Anthony F. Cockerill, Geoffrey L. O. Davies, Raymond C. Harden, David M. Rackham \$4.00

1973-1975
(ChemTech)

Enzyme Engineering

W. R. Vieth,
K. Venkatasubramanian
Part I through IV \$5.00
Combined I through IV .. \$6.50
Part V alone \$2.00

1975
(Accounts of Chemical Research)

Special Issue on the Chemistry of Vision

Edited by Eva L. Menger—
(\$1.50 each on ten or more)
..... \$3.00

1973
(Accounts of Chemical Research)

The Chemical Composition of the Lunar Surface

Anthony L. Turkevich \$2.00

1975
(Analytical Chemistry)

Pharmaceuticals and Related Drugs

Richard E. Huettemann, Mary L. Cotter and Charles J. Shaw
..... \$3.50

1969 (Journal of
Agricultural & Food Chemistry)

Symposium on Natural Food Toxicants

19 papers from the Atlantic City Symposium in 1968. 128 pages.
Paper \$3.00

1971 (Journal of
Agricultural & Food Chemistry)

Symposium on Characterization of Proteins

18 papers from the Chicago meeting in 1970. 125 pages.
Paper \$3.50

Prepayment is required. Make check or money order payable to the American Chemical Society

Send to: **Business Operations, Books and Journals Division, ACS**

1155 16th Street, N.W., Washington, D.C. 20036

Name _____

Address _____

City _____

State _____

Zip _____